HEAT TRANSFER TO SPRAYS

AND FLOWING GASES

HEAT TRANSFER TO SPRAYS AND FLOWING GASES

by

KENNETH GORDON POLLOCK, B.Eng.

A Thesis

Submitted to the Faculty of Graduate Studies

in Partial Fulfilment of the Requirements

for the Degree

Doctor of Philosophy

McMaster University

October, 1967

Doctor of Philosphy (1967)
(Chemical Engineering)

McMaster University,
Hamilton, Ontario.

TITLE : Heat Transfer to Sprays and Flowing Gases

AUTHOR : Kenneth Gordon Pollock, B.Eng. (McMaster University)

SUPERVISOR : Dr. T.W. Hoffman

No. of PAGES : xiii, 307, Z-5l

SCOPE AND CONTENTS

An experimental investigation of an Atomized Suspension Technique system was carried out in an experimental apparatus of semi-pilot plant scale. The complex gas flow patterns which occur in such systems as the result of the interaction of natural convection and forced convection prevented a quantiative analysis of the system.

The problem was then approached by dividing the overall process into a number of idealized studies; these were, convection in the entrance region, radiation to a gas, radiation to a cloud of droplets.

A theoretical model was developed to predict heat-transfer rates and gas temperature profiles in the entrance region ($x/D < 2$) of a cylindrical column. The model was verified experimentally.

A theoretical gas-radiation model was developed using the zoning technique of Hottel. Experimental gas-temperature measurements qualitatively verified the model.

An investigation of the established immersion cell technique for

the determination of drop-size distributions in sprays indicated that this technique could not be used with any confidence in systems where the spray is moving at low velocities.

Several experimental devices and techniques were developed throughout the course of this study.

ACKNOWLEDGEMENT

The author wishes to express his sincere gratitude and deep appreciation to all those people who have contributed their talents and abilities throughout the entire course of this investigation. He is particularly indebted to:

His research director, Dr. T.W. Hoffman, for his guidance, encouragement, understanding and fellowship throughout the trials and tribulations of this investigation.

His wife, Barbara Ann, for her encouragement, understanding and patience throughout these many years.

The author also wishes to acknowledge his appreciation for the financial support provided by the Pulp and Paper Research Institute of Canada. Fellowships were granted to this author by the National Research Council of Canada, the Consolidated Mining and Smelting Company and the Shell Oil Company of Canada.

TABLE OF CONTENTS

APPENDICES

LIST OF TABLES

LIST OF FIGURES

1. INTRODUCTION

1.1 General

The chemical industry to-day is in general experiencing a growing trend towards the use of higher temperatures and pressures and finer states of subdivision. There is considerable economic justification for following these trends since operational improvements such as higher reaction rates, greater heat transfer rates and smaller equipment can be realized. Also, investigations of the fundamentals of both evaporation and chemical treatment have indicated the importance of greater transfer area, greater driving force and intimate mixing of the phases present.

The greater transfer area is obtained by utilizing finer initial states of subdivision such as occur with atomization. The increased driving force is realized by employing larger temperature and/or concentration gradients in the process. Intimate mixing can be effected by controlling the fluid flow patterns which exist in the processing equipment.

These trends can be readily seen in the evolution from fixed to fluidized catalytic beds where the solids-gas mixture is often considered to be a pseudo-liquid. The next step in the evolution is the transported bed[P1, W1] where the solid particles are suspended and carried along in the gas stream. Here the solids-gas mixture may

be considered as a pseudo-gas.

A logical extension of these trends towards higher temperatures, finer states of subdivision, and intimate mixing of the phases present has resulted in the development and patenting of a process known as the Atomized Suspension Technique[G1], hereafter abbreviated to A.S.T.. As in the case of the transported bed the solids-gas or liquid-gas mixture is considered to be a pseudo-gas. The process is versatile enough to be applied to evaporation systems and solid-gas reactions and consequently to their combination in one continuous operation.

Detailed descriptions of the A.S.T. and its potential applications are available in the literature and will not be discussed here[G1, G2, G3, L1, L2, P2, P3, P4, R1]. A brief summary of the main features will be given, however, to familiarize the reader with its mode of operation.

In the A.S.T. process a solution, suspension, or slurry is sprayed into the top of a cylindrical tower (1 to 5 ft. diameter; 10 to 20 ft. high), the walls of which are maintained at an elevated temperature (1300 to 1600^{o}F). Unlike the normal spray drying process, no external gas is supplied to the tower. Consequently, only the vapours produced from the evaporation of the finely-divided droplets are available as a conveying medium. Early experiments with A.S.T. [P2, H1] appeared to corroborate the original hypotheses[G1, G3] that turbulence in the vapour phase was avoided because of the low vapour velocities (1 - 3 ft./sec.) present at the outlet of the column. Hence it was thought that the atomized suspension was in streamline flow and passed through successive well defined zones of evaporation,

drying, and, if desired, chemical treatment or pyrolysis as it proceeded down the tower. The solids could then be collected in external separators while the vapour would proceed to a condenser or steam converter.

The Atomized Suspension Technique is presently being used on an industrial scale. As yet, however, the interactions of and the principles underlying the various phenomena which occur in the process have not been completely determined. These phenomena include the following:

(i) atomization

(ii) droplet or particle dynamics

(iii) high temperature heat transfer

(iv) evaporation from clouds of droplets

(v) kinetics of chemical reactions

(vi) turbulence and its effect on the above phenomena.

The most recent and comprehensive investigation of the A.S.T. was carried out by Hoffman[H1] at McGill University. He attempted to analyse the heat and mass transfer phenomena which occur in this complex system and then to validate his results and conclusions by observations from an exploratory experimental program. The experimental results indicated that the theoretical analysis was reasonable. However because of equipment limitations no detailed quantitative verification of the theoretical model was possible.

The present study was undertaken to experimentally verify, quantitatively, and to modify if necessary, Hoffman's analysis of

the heat and mass transfer phenomena occurring in the A.S.T. process.

1.2 Atomized Suspension Technique (A.S.T.)

1.2.1 Description

To appreciate the past and present work which was motivated by the A.S.T. process the reader will be given a slightly more detailed look at some of the phenomena which occur therein.

It was previously mentioned that a solution, suspension or slurry was first sprayed into the top of a hot-walled cylindrical tower. The spray, formed by a conventional atomizing device,* jets at high velocity into the column or tower where large aerodynamic drag forces cause the droplets to rapidly decelerate to their terminal velocities. The so called "nozzle zone" is defined by the distance which the spray travels before reaching terminal velocity.

This nozzle zone is characterised by :

1. large scale turbulence which results from back-mixing of the gas; this flow reversal is caused by the inherent pumping or entraining action of the spray jet (B1, H2, H3, K2, L3, R3, S2, T1) which sucks gas from the lower region of the column ,
2. high evaporation rates as the result of the large surface area of the liquid, the high relative velocities between gas and liquid and the intense

---

* The mechanics of spray formation and the size distributions of the resultant sprays will not be discussed here. The interested reader should consult some of the following references (C1, D1, H13, M1, P6, R2, S1).

surface deformation which occurs during the atomization process[G2, P5].

The occurrence of high heat transfer rates in the nozzle zone makes the analysis of this region very important for the determination of the total heat transfer. However, the turbulence and back-mixing make a prediction of the droplet dynamics almost impossible. Furthermore, because of their small size (average size is 25 to 50 microns) the droplets, after deceleration, will follow the gas flow patterns[D2, K1, S3]. When the gas flow reverses, the small drops are flung against the wall, thereby further complicating the heat transfer analysis. It is obvious that the complexities of this region could represent the severest limitations of the entire analysis. Hoffman[H1, H4] has discussed some of the complexities and limitations of the nozzle zone analysis.

In all zones below the nozzle zone the cloud of droplets moves at its terminal velocity with respect to the gas phase. If the drops which are generated are less than 50 microns in diameter, the terminal velocities are small when compared to the gas velocity of 1-3 ft/sec. and can be safely neglected when computing droplet velocities in these regions. Note that only if the assumption of streamline flow is valid[G3], will the evaporation zone, and any subsequent zones be well defined.

The following heat transfer mechanisms occur to varying degrees in all regions of the A.S.T. tower.

Radiation from the walls to the gas.

Radiation from the walls to the droplets or particles.

Radiation from the gas to the droplets or particles.

Convection from the walls to the gas.

Convection/Conduction from the gas to the drops or particles.

It will be necessary to determine the relative magnitudes of these processes in the regions of the system under study since the main objective of this investigation is the prediction of the magnitude and distribution of the heat flux from the walls.

1.2.2 Design

To distribute the energy supply* properly along the length of the column it is necessary to predict the heat flux distribution on the tower walls. This distribution will be a function of the evaporative - load distribution throughout the unit. Hoffman[H1] has emphasized how important an understanding of the flow mechanics and basic heat transfer processes are for the prediction of the evaporative load and hence wall heat-flux distribution.

---

* The energy supply may be oil or natural gas burners, pulverized coal, or as in this study electrical heaters which permit the best control of the wall heat flux.

The evaporative - load distribution can be determined by experimentally measuring the evaporation of the spray as it moves through the column. Alternatively the evaporation history of the spray can be calculated from the model of the process. A partial check of the model can then be made by measuring the gas temperatures throughout the column and comparing them to the predicted temperatures. This was the technique employed by Hoffman[H1, H4] and was also utilized in the present study.

1.3 Thesis Organization

This thesis is comprised of two major sections. The first section deals with the experimental study of spray evaporation in a 10 ft. x 8 in. diameter column of a design similar to the commerical A.S.T. unit. The results of this study along with the work which was published in the literature since the commencement of the investigation indicated that the complexities and interactions occurring during the evaporation process could not be analysed in a column of this geometry.

This situation suggested that experimental and theoretical analyses would have to be performed on the various fundamental transfer mechanisms in rather idealized systems. The ultimate aim would be to provide sufficient information to allow analysis of the more complex system. Consequently a second smaller cylindrical column was designed to remove some of the complexities and thus be more amenable to a quantitative analysis of certain aspects of the transfer mechanisms in an A.S.T. system. The second section of the thesis deals with the experimental and theoretical investigation of the heat transfer processes which occur in this smaller column.

2. LITERATURE REVIEW

2.1 Introduction

This investigation is concerned with the analysis of the distribution and magnitude of the heat flux arising in a cylindrical column the walls of which are at high temperature and which contains a cloud of evaporating droplets or solid particles. This study was initiated as the direct consequence of the results and conclusions of Hoffman's work at McGill[H1, H4 - H6]. The literature review therefore will not repeat the survey made by Hoffman[H1] but will add to and amplify it where necessary.

To this writer's knowledge, Hoffman's analysis and experiments represent the only investigation of the fundamental phenomena and the inherent interactions which occur in a hot-walled enclosure into which a liquid is sprayed and evaporated. Several investigators have isolated particular phenomena for detailed study but have not considered the process in its entirety.

The literature review is divided into separate sections. Each section discusses the present understanding of either a particular phenomenon which occurs in an A.S.T. system or an experimental technique which must be utilized in the experimental investigation of the system.

2.2 Radiation

Electromagnetic radiation from the walls of a cylindrical enclosure to a spray or cloud of droplets descending through it will supply thermal energy to the droplets with the subsequent vapourization of some of the liquid. The vapours produced usually will absorb thermal radiation over certain wave length regions of the infra-red spectrum. (Since this particular study will consider only water as the evaporating liquid the analysis and statements will pertain specifically to the water-vapour (steam) - water-droplet system.) To determine the radiant heat-flux distribution on the walls of the enclosure it is necessary to ascertain the magnitude of the absorption of this thermal energy both by the droplets and by their vapours.

The cloud in this case will consist of droplets in the size range 5 - 100 microns. This range is comparable to the wave lengths occurring in the infra-red spectrum (1 - 20 microns).

2.2.1 Gas Radiation

The problem of calculating the radiant heat exchange in an enclosure containing an absorbing medium has received considerable attention in the recent literature. Several approaches to the problem exist. The most rigorous approach, that of Elsasser[E2], involves the use of the exact expression for the net attenuation of a beam of monochromatic energy in an absorbing and emitting medium:

$$dI_\nu = k_\nu \cdot (I_{b\nu} - I_\nu) \cdot dm \qquad (2.2\text{-}1)$$

where I is the intensity of radiation

k is the absorption coefficient

and subscript

ν indicates a particular vibration frequency
b indicates ideal (black body) radiation

For an isothermal, homogeneous medium this equation can be integrated to yield

$$I_\nu = I_{b\nu} \cdot (1 - \exp(-k_\nu m)) + I_{\nu o} \cdot (\exp(-k_\nu m)) \qquad (2.2\text{-}2)$$

The exponential factors in equation (2.2-2) are used to define the monochromatic transmission and absorption of the medium:

$$T_\nu = \exp(-k_\nu m) \qquad (2.2\text{-}3)$$

$$\alpha_\nu = 1 - \exp(-k_\nu m) = 1 - T_\nu \qquad (2.2\text{-}4)$$

These exponential relationships are derived assuming Beer's law for the attenuation of intensity of monochromatic radiation through a medium of absorption strength k_ν and mass path length, m, (where m is the product of the radiating component density, ρ, and the distance travelled by the beam, r).

The emission or absorption of radiation by a gas does not extend continuously over the whole wave length or frequency spectrum as is the case for a solid body. Instead the emission or absorption of radiation is restricted to specific regions of the spectrum. A complete description of molecular spectra

is beyond the scope of this thesis; however, it should be mentioned that the basic physics of absorption and emission by gases indicates that these processes occur at either discrete frequencies (line absorption or emission) or over a narrow range of frequencies (band absorption or emission).

Bevans and Dunkle[B2] review the basic physics of absorption and emission of thermal radiation by gases and develop the exact equations for the prediction of total emissivity and absorptivity for the entire spectrum. The equations are in the form of a sum of line and band absorptions and transmissions based on the band approximations of Elsasser[E2] and the statistical analysis of Goody[G4]. As the authors point out, the application of this exact method to a real physical situation is impractical.

Bevans and Dunkle[B2] then go on to develop the so-called band approximation which is the first step away from the rigorous approach. Now instead of integrating over the entire wave length or frequency spectrum the discrete nature of gaseous absorption or emission is utilized and band absorptivities and transmissivities are defined for finite wave length intervals. The width and location of these intervals depends upon the particular gas being considered. For a given gas the total α's and T's are thus a function of the sum of the corresponding band values.

The authors[B2] point out that the theoretical analyses of Elsasser[E2] and Goody[G4] along with the experimental

measurements of Howard et al[H9] indicate the non-exponential behavior of band absorption. This implies that the original assumption, made by Schack[S4] and Hottel[H8] and those who have followed those early workers, of exponential attenuation for monochromatic radiation is not valid when absorption over a finite wave length interval is being considered. Howard's data for carbon dioxide and water vapour[H9] indicate that the band absorption for the so-called weak bands is a function of the square root of the optical density (pressure x distance for isothermal gases). For the so-called strong bands they found that the band absorption is a logarithmic function of the optical density.

For a specific gas at a given temperature and pressure, various bands do not all behave according to only one of these two functional relationships. Consequently the absorption calculated for some bands is a mixture of the absorption calculated from the logarithmic and square root relationships. The total absorption by the gas is the sum of the absorption occurring in each of the bands.

To calculate the radiation interchange in an enclosure with this band approximation it is necessary to first of all determine the band absorptivities for the regions of the spectrum over which the gas is absorbing. A number of papers have been published on the quantitative spectral and band absorption of water at various optical path lengths and temperatures[B8, G6, F2, J2, L4, L5, O2, P9]. Edwards et al[E6]

have correlated the results of several workers for water vapour at temperatures from 300°K to 1100°K for the absorption bands centred at 1.38, 1.87, 2.7, 3.2 and 6.3 microns (B6, B7, F1, H9, N3). Using an exponential, wide-band model the authors (E6) predict band absorption as a smooth function of optical density, pressure and temperature. Goldman and Oppenheim (G8) correlated their experimental data for water vapour as a function of optical density and pressure at 1200°K using the spectral band-model of Goody (G7). The calculated total emissivities agreed well with Hottel's experimental data (H8). Ludwig and Ferriso (L6) used the same approach as Edwards (E6) and found excellent agreement with Hottel's data over a range of 0.1 to 10,000 cm.-atm. Ferriso (F4) experimentally determined band absorptivities for water vapour in the range 300°K to 3000°K. These data and the data of 80 other workers were correlated using the Goody model for all the absorption bands between 1 and 22 microns. The concepts of band absorption, calculation techniques, and many excellent references are available in Penner's text (P7).

Bevans (B3) has proposed correlations for the total emissivities and absorptivities of water vapour as a function of temperature and optical density. The equations are based on the relationships obtained by Howard et al (H9). Predicted emissivities agree within 3% of the experimental published data (H8, E3) over a temperature range of 800 - 3600°R. These

correlations are shown as equations (2.2-5), (2.2-6) and (2.2-7)

$$\varepsilon = K_1 \cdot (p \cdot \ell) + (K_2 \cdot (p \cdot \ell))^{\frac{1}{2}}$$

$$0.01 \leq p \cdot \ell \leq 0.1 \text{ atm-ft.} \qquad (2.2\text{-}5)$$

$$\varepsilon = (K_2 \cdot (p \cdot \ell)^{\frac{1}{2}} + K_3 \cdot \log(K_4 \cdot (p \cdot \ell))$$

$$0.1 < p \cdot \ell \leq 1.0 \text{ atm.-ft.} \qquad (2.2\text{-}6)$$

$$\varepsilon = K_3 \cdot \log(K_4 \cdot (p \cdot \ell))$$

$$1.0 < p \cdot \ell \leq 20. \text{ atm.-ft.} \qquad (2.2\text{-}7)$$

where $p \cdot \ell$ is the product of path length and partial pressure of the water vapour. The various K's are temperature dependent.

Edwards [E4] pointed out that the range of applicability of each correlation is uncertain and transition from one to another is abrupt with a resultant discontinuity in the first derivative. Consequently the correlations will be inaccurate in the region of the discontinuity since the measured absorption increases smoothly with path length. Edwards [E4] showed that the assumption of exponential decay over one band leads to acceptable results over an 8-fold range of $p \cdot \ell$. It was also found that a power law approximation for the strong bands gave better results than the logarithmic function.

To apply the band approximation to an enclosure it is also necessary to determine the spectral emittance and reflectance of the surfaces involved. This data is not abundant but a recent paper[B4] describes methods for obtaining this information.

The most frequently used approximation for absorption of thermal radiation by gases is the so-called gray radiation model. This approximation is based on the assumption that the radiation properties of the surfaces and gases involved are frequency independent. This assumption is a result of the inadequate knowledge of the spectral behavior of these characteristics and is a necessity born from ignorance.

Bevans and Dunkle[B2] have compared the exact calculation, band and gray radiation approximations in a cubical enclosure containing a non-absorbing medium. They found that the band approximation yielded results which were very close to those of the exact calculation. The gray radiation model was in error by approximately 50%.

Edwards[E5] has shown how to estimate band absorption data from Hottel's total emissivity data[H8] in the absence of band absorption correlations. Using Hottel's water vapour data[H8] the gray gas approximation was found to yield results 43% higher than when the band approximation was used.

The computations which have been made indicate that the band energy approximation yields more accurate results than the gray radiation approximation. However the labour and

time required for the calculations militate against the adoption of this more accurate method for general engineering problems. As a consequence, a large number of workers have used the gray radiation approximation when studying radiant heat transfer and its interaction with other heat transfer processes.(A6, C8, E8, E9, G5, H14, H15, H16, S5, S6, V1, V2, V4, V5, V6)

In recent years there has been a growing trend toward the use of the basic radiative transport equations originally derived and used by the astrophysicists(C9, K5). This approach uses the concept of a mass absorption coefficient rather than the "emissivity" of the engineering approach. The resulting equations are difficult to handle but they do allow the geometry ($p \cdot \ell$) to be separated from the material property effects. This method also has the advantage that it is possible to formulate a differential energy balance on an arbitrary control volume. Thus the effect of radiation can be used directly in the equations of fluid mechanics. Viskanta(V1, V6) has given a comprehensive treatment of this approach. His literature survey is extensive and includes the work of many Russian authors. Nichols(N1, N2) also uses the radiative transport equations coupled with the fluid mechanics equations to predict the temperature profile in the entrance region of an annular passage through which an absorbing gas (steam) is flowing. The band approximation, used with absorption occurring over six finite bands, predicted profiles that agreed

well with experimental measurements.

The radiative transport approach is laborious and time consuming and in the opinion of this author is not warranted in most engineering problems.

As indicated previously the gray radiation model is the least accurate approach but the loss in accuracy is compensated for by the relative ease with which it can be used. To analyse an enclosure containing an absorbing medium Hottel[H8] indicates that the shape of the gas must be allowed for. This allowance is made by defining a mean beam length "L". "L" is the radius of a hemisphere of gas, at the same temperature and pressure as the gas in the enclosure, which produces on unit differential area at the centre of its base, the same heat flux density as the gas in question produces on its container walls. For a transparent gas the mean beam length is often referred to as the geometric mean beam length[D9] and is found to be

$$L^{o} = \frac{(4)\ (\text{volume of gas})}{\text{area of enclosure}} \qquad (2.2\text{-}8)$$

Recently several authors have published papers on the evaluation of mean beam lengths for absorbing gases, taking into account the absorption over discrete wave length intervals. [D9, 03, T6]. Dunkle[D10] has extended the mean beam length concept to pairs of surfaces rather than complete enclosures.

Once a mean beam length has been calculated the total emissivity of an isothermal gas can be determined as a function of path length by fitting Hottel's data[H8] to an equation

of the form

$$\varepsilon = 1 - e^{-kL} \qquad (2.2\text{-}9)$$

This relationship assumes an exponential decay law with the absorption coefficient "k" being independent of path length, wave length and temperature.

Hottel and co-workers (H2, H8, H12, S11) have shown the inadequacies of this approach. They indicate that since the gas emissivity versus pL relation takes different forms in different ranges of pL, representing effects of different spectral regions, and that since ε increases continuously with pL, the gas emissivity, for an isothermal gas at a fixed total pressure, can always be represented in the form

$$\varepsilon = \sum_{i}^{N} a_i \, (1 - e^{-k_i L}) \qquad (2.2\text{-}10)$$

where $\sum a_i = 1$

One may think of a_i as the weighted sum of the wave length regions in which the effective absorption coefficient is k_i. Alternatively "a" and "k" may be thought of simply as the numbers which make the exponential series fit a given function. The a's and k's are not intrinsic properties of the gas but depend upon the conditions and dimensions of the system under consideration.

For a first approximation N = 2 and the real gas can be considered as consisting of one transparent gas (k = 0) and one gray gas of absorption coefficient "k" operating over the

appropriate "a_i" fraction of the spectrum. Hottel[H7] indicates how these a's and k's are evaluated in terms of the mean beam length of the enclosure.

The total gas emissivity is temperature dependent because of the Plank's Law Shift in the energy spectrum and because the absorption coefficients are temperature dependent. Thus in a non-isothermal system, the emissivity will vary from one point to another. However, observation of emissivity data suggest that "k" is much less sensitive to temperature than the value of "a". Hence the entire influence of temperature on emissivity has been forced[H7] into the weighting factor a_i while the k_i's are kept constant.

Hottel has shown[H8] how to determine gas absorptivities from emissivity data. The absorptivity of a gas, however, varies with pL, gas temperature, and surface temperature. Hottel and Sarofim[H12] have indicated that the absorptivity can be calculated from a series relationships in a similar manner to the emissivity calculation. In this case the k_i's which are applicable to ε_i at some average gas temperature are used and the weighting factors are determined at the temperature of the surface. This is obviously a simplification since absorptivity does vary slowly with gas temperature at a constant surface temperature.

The radiation interchange in an enclosure containing an absorbing medium can be analysed by making an energy balance on an infinitesimal gas volume and an infinitesimal surface

area and then integrating over the gas volume and surface area of the enclosure. The resulting integro-differential equations can be solved analytically only for simple geometries such as spheres and infinite parallel plates. Even for simple geometries an analytical solution is possible only if one neglects conductive and convective transport and assumes that the gas is gray[S18, U1].

Hottel and Cohen[H7] and several workers following them have analysed the radiation interchange in an enclosure containing an absorbing medium by dividing the walls of the enclosure and the contained gas into a number of finite zones each of which is small enough to be considered isothermal. Their size and number depend upon the accuracy desired. Now instead of an integro-differential equation the energy balances on each zone yield a set of algebraic equations, one for each unknown temperature or heat flux in the system. A solution of a set of these equations yields the desired distribution of temperature and flux throughout the enclosure.

To solve the algebraic equations it is necessary to evaluate first the direct radiant interchange between the various zones making allowance for absorption by the gas between the zones and for diffuse reflection at the surface of the enclosure. The direct radiant interchange between zones is determined by calculating "direct-geometric view factors" or "reception factors" as a function of $k\delta$; where k is the absorption coefficient and δ is a characteristic dimension of the zone. (Direct geometric view factors for cartesian and

cylindrical systems are available in the literature[E1, H6, H7].) Total-interchange factors can then be calculated from the direct-geometric view factors[H7] to account for the reflective flux from all surface zones.

Hottel and Cohen[H7] indicate that when employing this method, the a's and k's are assumed constant over the enclosure. However as indicated previously, the a's should be evaluated at the temperature of that part of the system which contributes the most to the total heat transfer. If this is done, these authors conclude that although moderate variations may occur in "a" and "k" the error is minimized, for the major temperature variation is still allowed for. These parameters affect only the interchange factors; the emissive power (σT_i^4) is allowed to vary at will in the energy balance equations.

Hoffman[H1, H6] has determined direct-geometric view factors for a cylindrical geometry as a function the absorption coefficient times the cylinder diameter. The gas zones are right circular cylinders with height equal to column diameter. Erkku [E1] also determined these factors for a cylindrical geometry but his gas zones were annular rings. When Erkku's factors were added together and compared to Hoffman's, the agreement was found to be better than 0.5% in all cases. Since each zone is considered to be isothermal, Erkku's factors allow for a radial variation in gas temperature while Hoffman's do not.

The results obtained with the zoning technique and the representation of a real gas as the sum of a number of gray gases should lie between those of the more rigorous band approximation and the less exact gray radiation model. A quantitative analysis of the accuracy is beyond the scope of this dissertation.

2.2.2 Particle Radiation

Hoffman[H1, H6] discusses the problem of radiation to a cloud of droplets suspended in a non-absorbing medium. As he indicates, the attenuation of radiation occurs as the result of absorption, reflection and scatter. He indicates that the magnitude of the scattering is difficult to determine because the scattering is a function of drop size, wave length and index of refraction when the circumference of the drop is less than 100 times the wave length of the radiation. For larger droplets, the scattering can be determined by a simpler approach using geometric optics. Droplets in the 5 to 100 micron size range have a circumference considerably less than 100 times the wave length encountered in the infra-red spectrum. In addition, the Mie theory which predicts the magnitude and direction of the scattering applies to single particles and does not allow for the multiple scattering which occurs in a dense cloud of droplets or particles.

Several authors have investigated both theoretically and experimentally the problem of multiple scattering. The majority of the theoretical work has utilized the radiative

transport approach of the astrophysicists. Because of the complexity of the problem the analyses usually consider a semi-infinite medium rather than a medium contained in an enclosure of finite dimensions.(C2, C3, D4, K3, L8, V1, V3). A limited number of experimental investigations of scattering characteristics of solid particle clouds have been carried out(M6, K4, K6, S8). Approximate scattering relationships are available but they apply only to particles which are relatively large compared to the wave length of the radiation striking them(K3, P8, S7, V3). As yet no information is available which would allow the determination of the scattering characteristics of a cloud of droplets flowing through a cylindrical enclosure. This lack of information necessitates the use of geometric optics to determine the scattering cross-section of the droplets. Hoffman(H1) has indicated that the application of geometric optics is valid as the ratio of the droplet circumference to the wave length of the radiation approaches 100.

If the absorptivity of the droplets, α_p, is close to one then very little radiation will be reflected from the cloud and absorption will be the principal cause of attenuation. If the absorptivity is much less than one then reflection and refraction at the gas - liquid interfaces become important. Hoffman(H1) has indicated how these latter effects can be accounted for using the ray tracing analysis of Thomas(T2) and Simpson(S15).

Thomas[T2], using geometric optics and assuming Beer's law showed that the fraction of incident monochromatic energy which is absorbed by a droplet can be approximated by

$$f_\lambda = \beta(1 - \exp(-1.75\, k_\lambda r)) \qquad (2.2\text{-}11)$$

The index of refraction is assumed to be 1.33. The coefficient β equals 0.95 for large $k_\lambda r$ by virtue of large r; if $k_\lambda r$ is large by virtue of k_λ being large, Thomas indicates that reflection will be decreased and f_λ will approach unity. In any case, the error for large values of $k_\lambda r$ will not exceed 5%.

To determine the absorptivity of a water droplet for infra-red radiation one must know the variation of absorptivity with wave length. Friedman and Churchill[F3] have indicated that, because of the nature of band absorption (k_λ is not a continuous function of λ) and the fact that the average absorption over a finite wave length interval is not an exponential function, k_λ cannot be determined from film transmission measurements made with an instrument of finite resolution.

Elsasser[E2] showed that the erratic coefficient k_λ can be approximated by a smoothed coefficient γ_λ which allows the monochromatic transmission measurements to be expressed as

$$T_\lambda = \operatorname{erfc}\,(\gamma_\lambda r)^{\frac{1}{2}} = \frac{1}{\Delta\lambda}\int_{\lambda - \frac{\Delta\lambda}{2}}^{\lambda + \frac{\Delta\lambda}{2}} (\exp(-k_\lambda r)\, d\lambda \qquad (2.2\text{-}12)$$

Here $\Delta\lambda$ is assumed to be sufficiently large so that there is no contribution to the transmittance at the centre of the interval from lines outside the interval.

Chin and Churchill[C4] have shown that the integral in equation (2.2-12) over a small wave length range for any function of $k_\lambda r$ can be transformed into a function of $\gamma_\lambda r$.

Following the approach of Friedman and Churchill[F3], the average absorption fraction of a droplet in the neighborhood of λ is defined as

$$\alpha_\lambda = \frac{1}{\Delta\lambda}\int_{\lambda-\frac{\Delta\lambda}{2}}^{\lambda+\frac{\Delta\lambda}{2}} f_\lambda \, d\lambda \qquad (2.2\text{-}13)$$

Then, using Chin and Churchill's transformation[C4] and equations (2.2-11) and (2.2-13) the average absorption fraction of a droplet can be expressed as

$$\alpha_\lambda = \beta\left[1 - 1/\Pi\int_0^1 \frac{\exp(-1.75\gamma_\lambda r/t)}{[t(1-t)]^{\frac{1}{2}}}\,dt\right] \qquad (2.2\text{-}14)$$

where t is a dummy variable of integration.

This equation can not be evaluated analytically.

Friedman and Churchill[F3] show how these relationships can be applied to the transmissivity data for JP-4 jet fuel to determine the per cent of incident black body radiation which is absorbed by a spray of this fuel.

The above relationships should be used to determine the absorptivity of water droplets from experimentally determined transmissivity data. A search of the literature revealed

several sources of transmission data for liquid water in the wave length range of 2 to 15 microns. The data are consistent in defining the wave length intervals over which absorption occurs but inconsistent in the magnitudes of the transmission for the various bands. Table 2.2-1 indicates the wave length range, cell thickness, and cell material for the references which have been investigated.

More work is required in this area before droplet absorptivities can be determined with any confidence.

TABLE 2.2-1 : References for Water-Film Transmission Measurements

REFERENCE	WAVE LENGTH RANGE (microns)	CELL THICKNESS (microns)	CELL MATERIAL
A1	2.5 - 12	4	AgCl
B9	5 - 13	25	Thallium Bromide - Iodide
G9	2 - 15	100, 25	AgCl
L7	2 - 15	-	Type II Diamond
P10	2 - 42	10, 30	C_aF_2
P11	2.5 - 11	27	B_aF_2
P12	6.6 - 11	25	B_aF_2
S9	2 - 13	17, 51	Thallium Bromide - Iodide

Hoffman indicates[H1, H6] that as a first approximation, if Beer's law is assumed, one can calculate an average absorption coefficient from absorptivity measurements made at

one particular film thickness; i.e.,

$$\alpha = 1 - e^{-kL} - 1 - T \qquad (2.2\text{-}15)$$

Alternatively one can use the transmissivity data at two film thicknesses to calculate an average absorption coefficient which is considered to be active over fraction "a'" of the spectrum in the same way that one fits gas emissivity data at two mean beam lengths[S15]. Using the transmissivity data of Sternglanz[S9], which were integrated by this author, Ross[R7] found that the average absorption coefficient k varied from 300 to 1000 cm^{-1} over the source temperature range 720 to 1600°R.

Once an average k has been calculated the absorptivity for any size droplet can be calculated from

$$\alpha = a' (1 - \exp(-kr) \qquad (2.2\text{-}16)$$

With this relationship Hoffman[H1, H6] has shown that the absorption coefficient of the cloud, k_{CLOUD}, can be approximated in terms of an average absorptivity for the cloud, the cloud density, and the volume-to-surface mean diameter of the cloud, i.e.,

$$k_{CLOUD} = \tfrac{3}{2} (\alpha_{ave}) (\rho_s/\rho_L)(1/d_{vs})(1-E_f)/E_f \qquad (2.2\text{-}17)$$

where E_f is the fractional evaporation of the spray after it is formed. External gas addition can be easily included.

When the cloud of droplets is in an absorbing medium the droplets and gas will operate in parallel to attenuate the radiation. Hoffman[H1] shows that since Beer's law has been

assumed the absorption coefficients can be added in the exponential, i.e.,

$$I = I_o \cdot \exp(-(k_{CLOUD} + k_{GAS}) \cdot L) \qquad (2.2\text{-}18)$$

In the light of this discussion, it should be apparent that relationships of the form of equation (2.2-18) will not yield accurate results, but that the analysis is expected to be adequate considering the limited data which are presently available.

2.3 Drop Size Measurements

Hoffman and Gauvin[H6] have indicated the dependence of the absorption coefficient of the cloud on the volume-to-surface mean diameter, d_{vs}*, of the spray. This diameter is calculated from the drop-size distribution of the spray. Thus to determine the variation of the absorption coefficient of a spray as it evaporates and to evaluate the approximations made in the analysis of the absorption characteristics of a spray[H1, H6], it is necessary to determine the drop-size distribution of the spray as it descends through, and evaporates in, a high temperature environment.

Several techniques are available for determining the drop-size distributions of sprays. An excellent survey of the literature prior to 1957 is given by Putnam et al[P6]. These authors point out that the most generally used technique of removing a sample from the spray by some mechanical device suffers from the major disadvantage of a biased sample. They also indicate however that if the proper care is taken during the sampling procedure this method is easier to use and permits a more accurate analysis than photographic methods. Hassen[H13] who studied sprays by collecting solidified droplets of wax also

---

* $d_{vs} = \frac{\Sigma n_i d_i^3}{\Sigma n_i d_i^2}$ where n_i is the number of drops in size interval i having an average diameter d_i.

emphasizes the necessity of knowing how the drop size analyses depend upon the determination method.

Photographic techniques have the advantage that the spray is not disturbed by a sampling device, however the quality of the droplet images is poor because so few of the drops are actually in sharp focus in the narrow depth of field. That is, at magnifications which produce sufficiently large images for analysis, the depth of field becomes very small. Droplet velocities must also be determined to permit conversion of the spatial distribution obtained on the photograph to the temporal distribution in the spray. Thompson et al[T7] in a recent paper have discussed the application of hologram techniques for particle-size analysis. The technique appears promising, being limited only by the film which the images are recorded on. Unfortunately the equipment required is sophisticated and expensive but future development work may permit this technique to be generally adopted for spray analysis.

Light dispersion is another technique which does not interfere with the spray, however as Dobbins[D8] indicates one can only obtain information about the average drop size and not the distribution of the spray. This technique also assumes that the index of refraction is constant throughout the system, which of course will not be the case if the spray is in a medium where large temperature gradients exist.

At this time mechanical sampling techniques, such as freezing[A2, H13], droplet impaction[M3], dyes or stains [G10, M4], or immersion cells[R5], to mention just a few, appear to be the easiest to use. Tate[T4] has suggested that Rupe's[R5] immersion cell technique is one of the best

ways of obtaining a representative sample from the spray. Several workers have claimed to have successfully used this technique (A3, D5, H4, M5, T4).

Briefly, the immersion technique consists of collecting a sample of the spray in a small glass-bottomed cell which is filled with a suitable fluid. The collected drops are allowed to settle to the bottom of the cell where they are subsequently photographed.

A suitable fluid is one which

i) has a density which will permit the sampled drops to settle through the liquid and rest on the bottom without flattening;

ii) is completely immiscible with the liquid being sampled;

iii) has a low enough surface tension to permit small droplets to penetrate the surface;

iv) has a viscosity which is low enough to allow penetration without break-up yet high enough to restrict convection currents within the cell;

v) has a low vapour pressure so that no bubbles form and the fluid does not evaporate when placed in a hot gas stream;

(v) has good light transmission characteristics so that the droplets can be photographed.

Rupe found that Stoddard solvent had all the desired characteristics. Dlouhy[D2] found that Varsol (Imperial Oil Company) was a petroleum fraction with essentially the same properties.

Rupe also found that if the glass bottom was coated with a non-wetting agent the discrepancy between the size of the recorded image and the droplet would be less than 2%.

The geometry of the cell must be such that the collection efficiency is as high as possible if a representative sample is to be obtained. The shutter mechanism which is necessary if the cell is to be exposed to the spray for short periods of time must also be designed so as to minimize the interference with the spray[T4].

Large droplets at high velocity will shatter when striking the collection fluid interface[T4]. Rupe[R6] has shown however that droplets less than 180 microns will not shatter if their velocity is less than 30 ft./sec. Darnell and Marshall[D6] showed that at six inches from the atomizing source drops less than 200 microns would be essentially at their terminal velocity. Hence for sprays with a maximum size of 200 microns there is no danger of shatter if a sample is taken at least 6 inches from the nozzle.

It is interesting to note here that Manning and Gauvin[M5], who photographically determined drop velocities close to an atomizing nozzle, found for example that 30 micron drops had a velocity of the order of 150 ft/sec. at a distance of three inches from the nozzle.

Darnell and Marshall's[D6] correlation indicates that at this distance thevelocity of these drops should be less than 1% of their initial velocity. This would require initial velocities in the order of 10,000 ft./sec. which are physically impossible. The reason for the discrepancy was not determined because the original work of Darnell and Marshall was not available; therefore their correlations should be used with care.

To obtain a representative distribution for the spray, Tate[T4] suggests collecting samples of 3000-4000 drops. Tate and Marshall[T5]

indicate that a sample of this size should not deviate from the true distribution by more than 2%. On the other hand, Dlouhy and Gauvin[D5], claim to obtain reproducible size distributions in a spray dryer with sample sizes of 150 - 300 drops. Based on an extrapolation of Tate and Marshall's figures, Dlouhy's distributions could be expected to deviate from the true distribution by approximately 10%.

Large samples have a tendency to result in droplet coalescence in the cell because of the relative proximity of the drops. To minimize this tendency Tate[T4] suggests that the droplet-area fraction of the cell (i.e., the fraction of the total cell area occupied by the collected droplets) should be of the order of 0.05.

Recognizing these advantages and disadvantages, this author has attempted to use the immersion cell technique to determine the drop-size distributions of an evaporating spray.

2.4 Gas Temperature Measurement

When measuring gas temperatures in a particulate system it is necessary to shield the temperature sensing device from the droplets or particles otherwise the indicated temperature will be a function of the droplet or particle temperature. Also, if the enclosure is at a much different temperature than the gas it is necessary to shield the measuring device to prevent measurement errors due to radiation interchange between the device and the walls of the enclosure.

Hoffman and Gauvin[H4] measured gas temperatures in a cloud of water droplets which had been sprayed into an 8 inch diameter column with wall temperatures in excess of 650°C. The measuring device was a Pt - Pt 10% Rh thermocouple made from 0.010 inch diameter wire. The thermocouple was contained within 3 concentric cylindrical shields with the inner shields connected to a vacuum line. The thermocouple probe assembly was vertically oriented in the column and the vacuum was sufficient to draw the gas across the thermocouple at a maximum velocity of approximately 100 ft./sec.[H1]. (The gas velocity at the inlet to the probe must not be high enough to cause small droplets to enter the device.)

These authors reported that no radial temperature variation was detected and that the maximum temperature oscillation was ±2°C. Themelis and Gauvin[T8] measured gas temperatures with a similar probe in a 4.4 inch diameter column with iron oxide particles as the particulate phase. No radial temperature variation was noted in this study either, although the walls were maintained at temperatures in excess of 600°C. These results would indicate that the original assumption of streamline flow

in an A.S.T. reactor is not valid[G1, G3].

The fact that the Grashof number, which is a measure of the ratio of buoyancy forces to viscous forces was large[T8] in these systems would suggest that the natural and forced convection forces would interact. Interaction would result in turbulence which would tend to transport the hot gases from the wall region into the centre of the column and vice versa. This would have the effect of increasing the temperature gradients in the stagnant layer adjacent to the wall. It would also tend to reduce the temperature gradients in the gas in the core of the column.

To determine the convective heat transfer at the wall in systems where natural and forced convection can be expected to interact Brown[B13] measured the gas temperature profiles in an air stream. His measurements were made in the same column that Themelis[T8] used but the complications of temperature measurement in a particulate system were eliminated by studying the profiles in single-phase flow.

Brown was able to measure the gas-temperature profile at the wall by accurately positioning an unshielded Pt - Pt 10% Rh thermocouple at various radial locations relative to the wall. Temperatures were measured at several radial locations, within 0.100 inches of the wall where the profile was approximately linear. Temperatures were also measured, on a coarser radial grid, right to the centre line of the column.

Brown's thermocouple was constructed of 0.0005 inch diameter wire to reduce the radiation error as much as possible. These wires were

joined to the 0.010 inch wires of Ceramo (Thermo Electric Company) stainless sheathed thermocouple wire. Brown calculated that the maximum radiation error to this small thermocouple was 11°F and the maximum conduction error only 2°F.

Ross[R7] in his study of forced convection heat transfer to a stationary droplet in a high temperature environment used a thermocouple of the same dimensions as Brown's. Ross's analysis however indicated that the radiation error was of the order of 1 or 2°F for the case of an enclosure temperature of 1800°R and a gas temperature of 700°R. Ross also showed that the 0.010 inch support wires may attain a temperature of the order of 100°F above that of the gas. He indicated however that there was negligible conduction to the thermocouple from the latter support wires.

Short and Sage[S16] have analysed the conduction error in a 0.001 inch butt-welded thermocouple. The conduction error is caused by the gradients which exist in the thermocouple wire when it is exposed to large gas temperature gradients (6000°F/in.). They calculated that for these large gradients and this particular wire diameter, the error in the measured gradient would be approximately 5%. Thus for a thermocouple of Brown's design the conduction error would be considerably less for two reasons:

1. The wire diameter was half that of Short and Sage's which reduces the cross-sectional area available for conduction by a factor of 4; and
2. The thermocouple ball could be oriented with respect to the larger support wires so as to maintain essentially isothermal conditions

along the wire from the weld to the supports.

Thus, it would appear that Brown's thermocouple should be capable of recordingtrue gas temperatures at all radial positions in the column.

Brown[B13] found that for the range of Reynolds numbers studied (271 - 6,900) large temperature gradients existed from the wall to the centre line of the column. The gas temperature measurements of Hoffman[H1] and Themelis[T8] were made in a particulate system where the droplets or particles might tend to moderate the radial temperature gradients. However, Brown's results suggest that the observed flat temperature profiles[H1, T8] are rather suspect. Brown's thermocouple was much more sensitive than those of Hoffman and Themelis and this suggests that the relatively large shielded probes, aspirating relatively large volumes of gas, were not capable of accurately measuring radial temperature gradients.

2.5 Gas Flow Patterns

In Hoffman's investigation[H1] of the fundamental mechanisms of heat transfer in the A.S.T. system a cloud of droplets was produced by a conventional atomizing nozzle. These nozzles inject the atomized fluid into the system at a high velocity, thus creating an expanding jet of fluid. Spalding[S2] has shown by a momentum and mass balance that a jet emerging into a relatively stagnant atmosphere will entrain or induce gas from the surrounding atmosphere into the boundaries of the jet. As Hoffman points out, if the jet is produced in a closed column the gases which are entrained by the jet must come from the lower regions of the column. Thus in the region where the jet is decelerating and for some distance beyond it there will be a backflow of gas into the upper regions of the column. This backflow will cause large scale turbulence in the jet deceleration (nozzle zone) region and makes prediction of the convective heat transfer from the wall difficult if not impossible.

The backflow of gases and the inherent large-scale turbulence also make the determination of the droplet dynamics in this region impossible because as Dlouhy[D2] and Kessler[K1] indicate, the drops can be expected to follow the turbulent fluctuations of the gas stream. A recent theoretical analysis of particle/gas amplitude ratios in a turbulent stream[H11] indicates that water droplets less than 10 microns in diameter which are entrained in a turbulent air stream, can be expected to follow the velocity fluctuations in the gas stream up to frequencies of 700 c.p.s. The corresponding frequency limit for a 100 micron drop is however only 7 c.p.s. Thus it can be expected that the gas

stream turbulence will not affect the cloud uniformly.

Since small droplets follow large-scale, low-frequency, turbulent eddies, a knowledge of the gas flow patterns is important because they will influence the flow paths of the droplets, the residence time of the droplets in the turbulent region, and the extent of droplet deposition on the walls of the enclosure. Consequently, the gas flow pattern will affect the rate and degree of evaporation of the spray.

Several workers have attempted to determine the gas flow patterns in a so-called ducted jet system. Arni[A2] attempted to measure the velocity profiles in the nozzle region of a spray dryer with a hot wire anemometer. His results however are specific for the geometry of a particular dryer and cannot be generalized. Thordarsen[T3], also working in a spray dryer, qualitatively observed the gas flow patterns by photographing the trajectories of small balsa particles. Buckan and Warlton[B10] attempted to estimate the flow patterns in a dryer by comparing measured gas temperature profiles with those predicted by a plug flow and a complete mixing model.

Many investigators have tried to quantitatively predict the entrainment characteristics of a free jet. (See reference B11 for a bibliography.) For a ducted jet however, Thring and Newly[T1] were one of the first to quantitatively analyse the entrainment characteristics. Their analysis was only approximate and a more comprehensive theory of confined jet systems was developed by Curtet[C5, C6]. Craya and Curtet[C7] had previously collaborated to enunciate a criterion governing the similarity of fully-turbulent, incompressible, confined jet flows.

The similarity parameter was named the Craya-Curtet number by Becker et al[B1] and denoted Ct. This parameter is a unique function of the mass and momentum ratio of the jet flow to the induced flow. It can be calculated from the following equation.

$$Ct = \frac{U_k}{((U_s^2 - U_{fo}^2)(\frac{r_s}{r_w})^2 + \frac{1}{2}U_{fo}^2 - \frac{1}{2}U_k^2)^{\frac{1}{2}}} \qquad (2.5\text{-}1)$$

where r_s is the radius of the circular nozzle

r_w is the radius of the cylindrical duct

U_{fo} is the uniform initial velocity of the free stream, $r_s < r < r_w$

U_s is the uniform nozzle velocity $0 \leq r < r_s$

and U_k is calculated from

$$U_k = (U_s - U_{fo})(\frac{r_s}{r_w})^2 + U_{fo} \qquad (2.5\text{-}2)$$

When $U_s = U_{fo}$, $Ct = \infty$ and hence the resultant flow is uniform.

When $U_{fo} = 0$ $\quad Ct = \dfrac{r_s/r_w}{(1 - \frac{1}{2}(\frac{r_s}{r_w})^2)^{\frac{1}{2}}}$

and Ct approaches zero if $r_s/r_w \ll 1$

For a given ratio of r_s/r_w, Ct is a unique criterion for dynamic similarity.

In order to quantize the recirculation and gas velocity profiles in a ducted or confined jet, Becker et al[B1, B11] measured velocity and concentration profiles as well as velocity and concentration fluctuations. Concentration refers to the concentration of an aerosol of oil droplets which was introduced in the jet to permit the free stream and jet gases

to be discriminated. The concentration was determined by using a sol scattered light technique developed by Rosensweig et. al.[R4]. This technique made it possible to determine the probability of finding the nozzle fluid at a point in question[B12]. The velocity measurements were made with thin-lipped impact tubes.

The above studies[B1, B11, B12] indicated that recirculation occurs when Ct < 0.75. Hottel and Sarofim[H12], when considering the effect of gas flow pattern on radiative transfer in cylindrical furnaces, showed that for values of Ct of 0.51, 0.18 and 0.033 the recirculation rates, as a fraction of the total gas flow rate, were 0.075, 1.44, and 10.91 respectively.

The quantiative results will thus permit the recirculation rate to be predicted for A.S.T. and similar systems where no free stream flow exists to feed the expanding jet. (U_{fo} = 0 and Ct approaches 0.). It should be noted, however, thatthe gas flow patterns have been determined for an isothermal system and temperature gradients in the gas could be expected to have a significant effect.

2.6 Natural Convection Effects

As previously mentioned, one would expect some interactions between natural and forced convection forces in a hot-walled enclosure where the gas flow rate was very low. In A.S.T. and similar systems where the spray and vapour descend vertically through a high temperature environment the buoyancy forces at the wall act in the opposite direction to the forced flow. The heat transfer literature usually refers to this as heat transfer in opposed flow. Several authors have theoretically and experimentally investigated opposed flow heat transfer. Recently Brown[B13] and Brown and Gauvin[B14] critically discussed these previous investigations in the light of their own study.

It has been shown[A4, S17] that when the buoyancy forces are of the same order of magnitude as the forced flow or inertia forces, $N_{Gr} \sim N_{Re}^{2}$. In regions where the two opposing forces have significant interaction some authors[A5, S13, S14] correlate the heat transfer rate against the flow rate with natural convection as a parameter (i.e., N_{Nu} vs. N_{Re}, with some measure of natural convection as a parameter; e.g., N_{Gr} or N_{Ra}). These workers report that for the N_{Re} range investigated, the heat transfer rate increased with an increase in the natural convection forces. Other authors have correlated N_{Nu} vs. N_{Gr} or N_{Nu} vs. $N_{Gr}.N_{Pr}$ [B13, B14, B15, E10] and found no effect of N_{Re} on the heat transfer rate for the range of variables studied, i.e., natural convection forces completely controlled the rate of convective heat transfer.

Brown and Gauvin[B14] have predicted that the influence of natural convection on forced convection would be less than 10% if the

Grashof number was less than a critical Grashof number, N_{Gr}', obtained from the following relationship:

$$N_{Gr}' = 0.423 \quad [N_{Re}^2/N_{Nu}] \qquad (2.6\text{-}1)$$

That is, if the Grashof number in the system exceeds that calculated by equation (2.6-1) one should expect the free convection to increase the heat transfer rate above that predicted from pure forced convection correlations. These authors have shown that in the region where interaction is expected to occur, if $N_{Gr} < 3 \times 10^5$ the N_{Nu} calculated from experiments was less than that predicted from pure free convection. In the N_{Gr} range from about 3×10^5 to 10^6 the calculated Nusselt numbers increased to a value about 45% above the free-convection line. Brown and Gauvin explain these results in terms of two effects. At low N_{Gr}, the opposed buoyancy forces will act to decrease the velocity gradient and consequently the heat transfer rate at the wall. As N_{Gr} increases above 3×10^5 the interaction between the forced and natural convection forces causes sufficient turbulence to increase the heat transfer rate at the wall above that predicted for pure free convection.

The heat transfer rates, temperature profiles and temperature fluctuations which Brown[B13] measured for a single-phase system suggest that Hoffman's[H1] original assumption of uniform flow was not valid. In fact with the experimental conditions employed by Hoffman one would not only expect the heat transfer rate to be affected by the natural convection forces but one would also expect to find a large volume of hot gases flowing upward adjacent to the wall. These upward flowing gases would transport heat from below into the relatively cold upper regions of the column. This thermal energy, supplied by the upward

bulk flow of gas, would cause the rate of evaporation of the spray to be increased.

Thus it is obvious that a knowledge of the magnitude of the natural convection forces and their interaction with a forced flow field is necessary if one is to quantitatively analyse the heat transfer processes occurring in an A.S.T. system.

PART I

3. EXPERIMENTAL EVALUATION OF A.S.T. MODEL

3.1 Introduction

The attempted experimental verification of the original model of the A.S.T. process[H1] was undertaken in semi-pilot-plant-scale equipment. The equipment and procedures which are described in the following pages represent the final designs and techniques which have resulted from an extensive preliminary experimental development program.

The results of this study gave direction to the investigations which followed and which are described in Part II of this dissertation.

3.2 Scope

The first study made in this program was initiated to experimentally evaluate Hoffman and Gauvin's analysis[H4, H5, H6] of the fundamental mechanisms of heat transfer which occur in an A.S.T. system.

The theory which was available in the literature at the time of initiation of this project suggested that natural convection effects in A.S.T. systems might be expected to interact with the forced flow of the vapours produced during the evaporation process. If the natural convection forces were large enough, the gas flow patterns in the system would be complex and the original analysis would have to be modified. However, the preliminary experimental measurements which were made in A.S.T. systems did not detect the presence of large natural convection effects. Consequently since the analysis of the system was applied to an operating industrial process which could benefit from an understanding of the phenomena occurring therein, it was decided to study a system which was operating under conditions similar to those which exist in the commercial A.S.T. system.

A modification to the industrial A.S.T. process was made to eliminate one of the major complexities which limited the original analysis. This modification consisted of removing the nozzle zone (region where the spray is generated) from the high temperature enclosure where the spray or cloud was evaporated. By removing the nozzle zone, the large scale back-mixing with its inherent turbulence was no longer present in the evaporation section; i.e., when the cloud reached the high temperature environment it was flowing freely in a well-controlled manner and consequently the droplet dynamics were expected to be

predictable. With the spray generated externally it was necessary to introduce a carrier gas into the system to transport the spray to the hot evaporation zone. This carrier gas also served to supply some of the gas required by the expanding spray jet and hence further reduced the turbulence level in the column. The introduction of a carrier gas, however, does represent a departure from the A.S.T. process where the only gases present are those from the vapourized liquid and the atomizing device (if a pneumatic nozzle is used). This departure was considered to be warranted in view of the simplification in the flow patterns which would be effected.

Essentially this experimental program consisted of conveying a water spray, in a low-velocity (velocities up to 8 ft./sec. were used) steam or air stream, into a 8-in. diameter by 10-ft. long vertical column (evaporator or reactor*), the walls of which could be heated to any temperature up to approximately 1600^{o}F. The column was provided with access ports to allow temperature measurements and spray samples to be obtained at various axial and radial positions. Experiments were performed with and without spray, i.e., with gas flow only.

The experimental equipment can be divided into sections according to functions, viz. the spray generator, gas flow and control system, evaporator column, and instrumentation for temperature and drop measurements. The following description provides the details of the experimental equipment and procedures.

---

*This column is referred to as a reactor only because the evaporation step is usually followed by a chemical reaction in the industrial process utilizing the Atomized Suspension Technique. Only the evaporation process is being studied here.

3.3 Experimental Equipment

3.3.1 Evaporator

The experimental apparatus is shown diagrammatically in Figure 3.3-1. The evaporator consisted of a 8-in. diameter by ⅛-in. wall by 10-ft. high column located in the centre of an electrical furnace. The column was flanged both top and bottom; the bottom flange was bolted to a support stand so that expansion (about 1½-in.) arising out of the large temperature changes could occur. A cone equipped with a ball-valve was also bolted to the bottom flange; a 2-in. line conveyed the steam to a water-cooled, shell-and-tube condenser (11 sq. ft.). The top flange permitted attachment of the spray-generating and calming sections.

The column had 2-in. diameter sampling ports located at one foot intervals along its length, as shown in Figure 3.3-1. The sampling ports were 17-in. long and extended through the firebrick cladding which housed the electrical heaters. The ports were flanged to allow drop sampling and temperature measuring devices as well as contoured plugs to be locked into position. The stainless steel plugs were machined to fit flush with the evaporator wall to form a continuous surface when a port was not being used to gain access to the column.

The furnace was heated by three banks of ribbon heaters, (each rated at 36 k.v.a. at 575 V), mounted concentrically on an 18-in. diameter porcelain support. The heating units were encased in a 36¾-in. diameter bricked, split-jacket shell shown

in Figure 3.3-3. The unit was designed by Trent Incorporated - Philadelphia and constructed by Pioneer Electric Eastern Limited - Toronto.

The heaters were independently controlled by three Honeywell Model 105R12 PYR-O-VOLT current proportioning controllers. The input to each of these controllers was an e.m.f. signal generated by a $\frac{1}{8}$-in. stainless steel sheathed chromel-alumel thermocouple welded to the outside wall of the column as shown in Figure 3.3-2. The output signal of each controller was sent to a Honeywell Model 6191 Magnetic Amplifier which controlled one of the three delta-connected saturable core reactors. (Electron Manufacturing Company, Chicago, Illinois) supplying power to the heating elements. The reactors were delta-connected to the 575 V. 3-phase mains to permit each heater to be independently controlled.

The power input to the evaporator could be measured by utilizing current transformers (P. Gossen & Co. (Germany) Type STW-2) and low voltage wattmeters (Canadian Research Institute, 6250 ohm.). These measurements indicated that the maximum heat flux that could actually be attained was 105 k.v.a. which represented approximately 17,000 B.t.u./(hr.)(ft.^{2}) on the walls of the 8-in. column.

Figure 3.3-2 shows the location of the chromel-alumel thermocouples which provide the input signal for the controllers. Also indicated in this figure are the locations of the $\frac{1}{16}$-in. diameter, stainless-steel sheathed, chromel-alumel thermocouples used only for temperature monitoring. All the indicating

thermocouples were spot welded onto 1-in. square by $\frac{1}{16}$-in. stainless steel plates in order to minimize conduction error. The plates were then welded onto the outside wall of the evaporator.

The thermocouples located at the extremes of the column indicated the magnitude of the departure from isothermal conditions caused by heat losses through the ends. The centrally located thermocouples served to check the isothermal condition of the column both axially and radially.

The millivolt signals from the indicating thermocouples were monitored by Honeywell multi-point recorders.

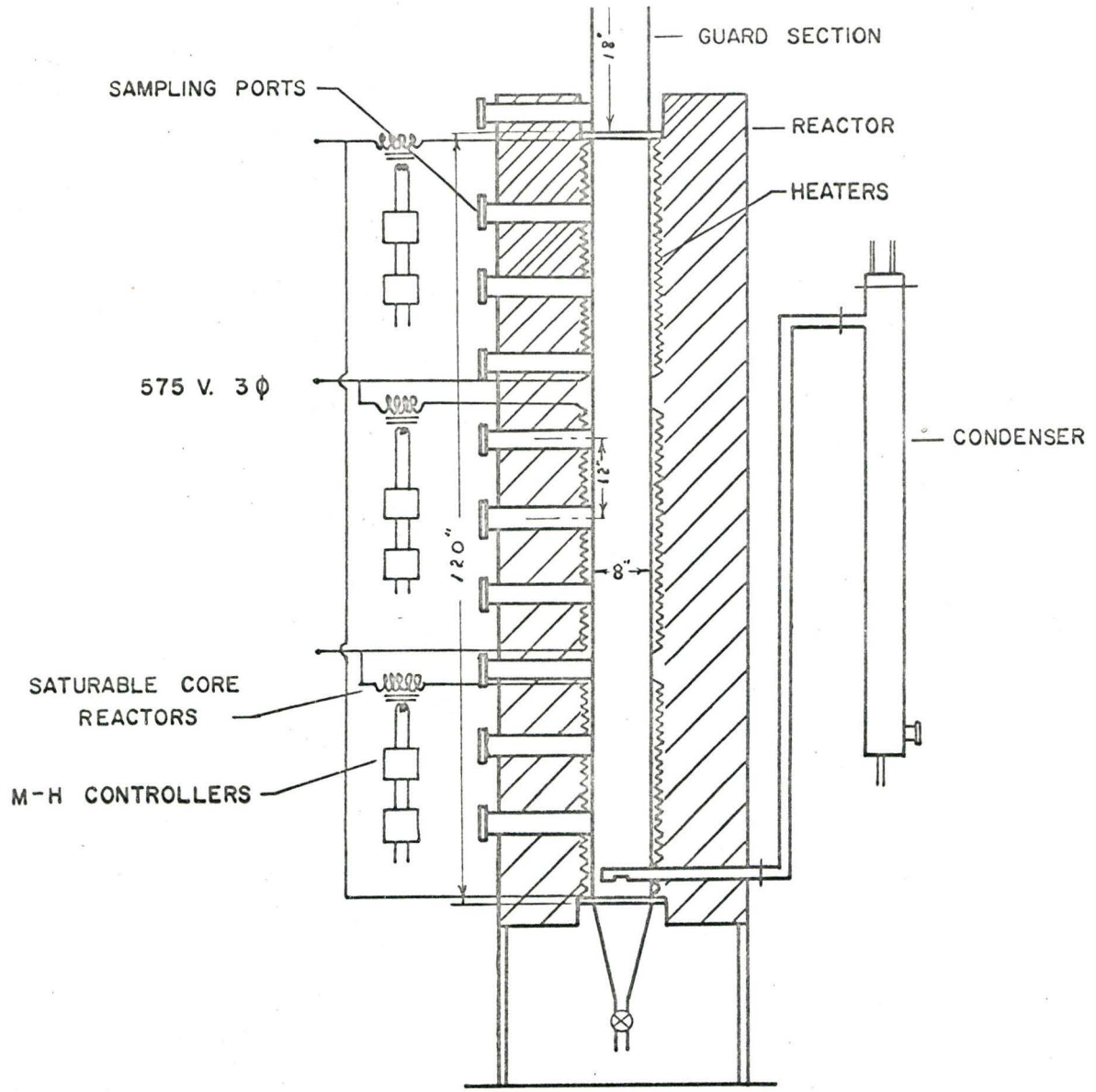

FIGURE 3.3-1

Experimental Apparatus

THERMOCOUPLE LOCATIONS

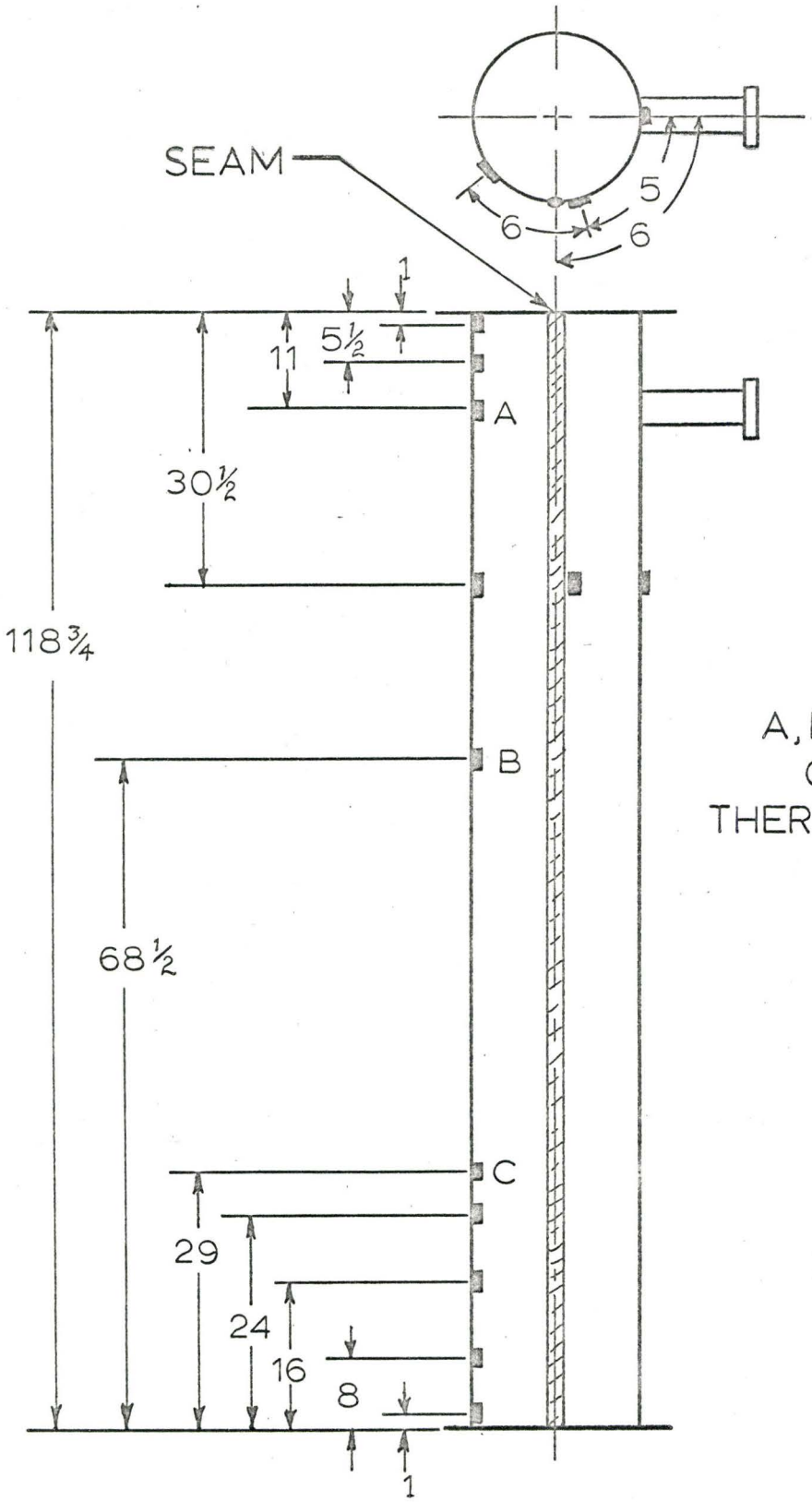

A, B & C are CONTROL THERMOCOUPLES

DISTANCES IN INCHES

FIGURE 3·3 – 2

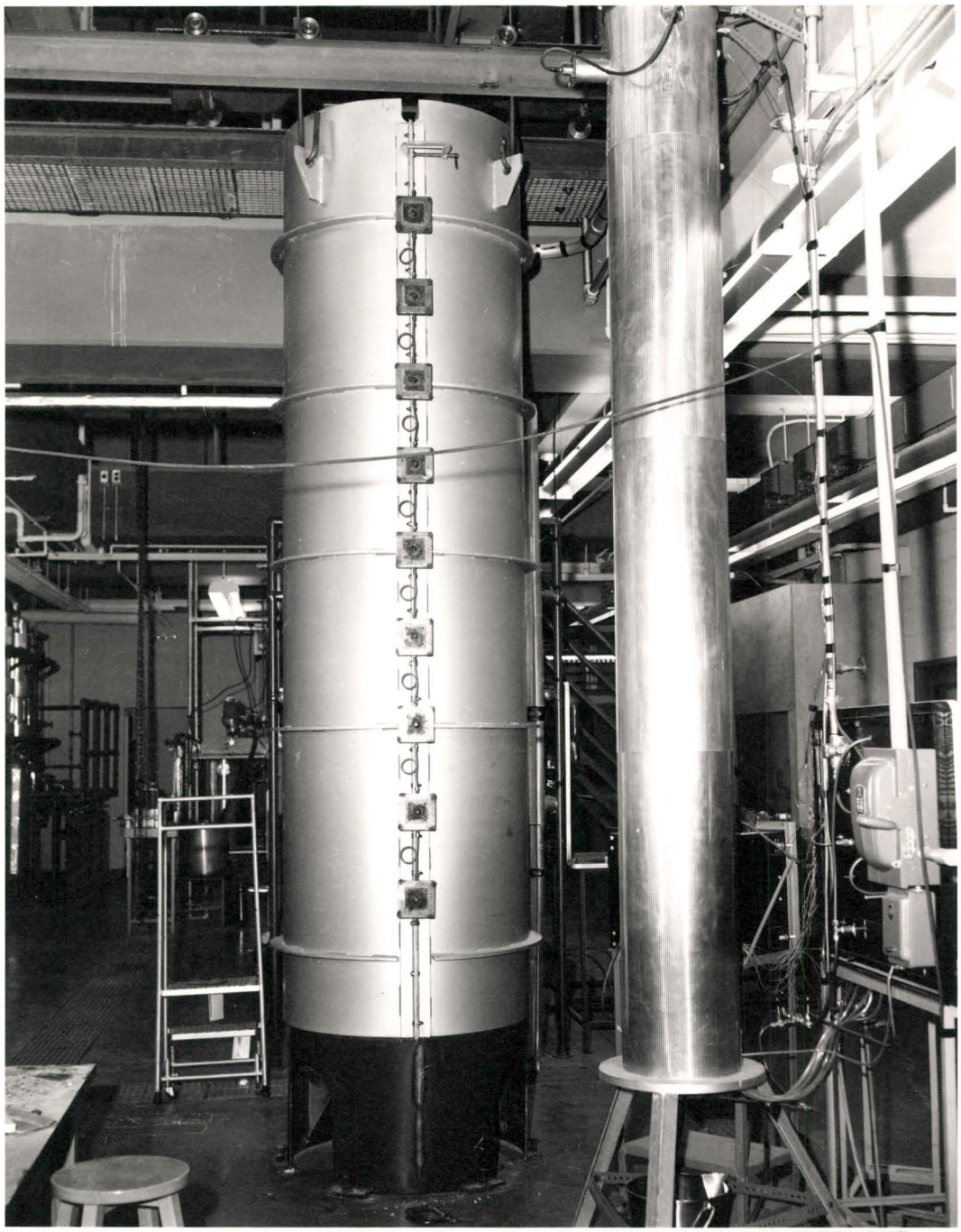

FIGURE 3.3-3 : Split-Jacket Heater Shell

3.3.2 Spray Generator and Calming Sections

Figure 3.3-4 is a schematic diagram of the spray generation and calming sections which form a superstructure above the actual column. All sections had the same internal dimension - 8-in. The 2-ft. by $\frac{1}{16}$-in. wall stainless steel calming section which was bolted onto the furnace had a sampling port which was identical to those on the furnace to permit determination of the gas temperature and drop-size distribution of the spray immediately prior to entering the high temperature environment. Two viewing ports with glass plugs were oriented at 120° to permit visual observation of the spray. The top of this section had a $\frac{1}{16}$-in. protruding lip to intercept any liquid descending along the wall. This lip was drained continuously through 4 - $\frac{3}{8}$-in. stainless-steel tubes which directed the flow of liquid into a tygon-tubing collection system, thus permitting the run-off to be continuously monitored.

A 5 ft. x $\frac{1}{16}$-in. wall stainless steel section was bolted to the above unit. This section helped isolate from the furnace section the large scale turbulence which was inherent during atomization, and enabled the particulate flow stream to become uniform. Welded to the bottom of this section were 8 - $\frac{1}{16}$-in. stainless steel wires which directed any liquid on the wall into the run-off lip of the adjacent section. Two viewing ports with glass plugs, orientated at 120° were located at the top of the section where the atomization occurred.

Two 18-in. long by ¼-in. wall aluminum sections were bolted to the stainless steel calming section. The lower section had two bored-through ⅜-in. brass Swagelok fittings located 3 in. from the bottom and diametrically opposed. These fittings allowed the air and water supply lines to be connected to and to support the pneumatic atomizing nozzle. Eight 100-mesh circular screens, which aided in establishing a uniform gas flow and in damping out the large fluctuations arising from the expanding gas jet at the top of the column, were supported on a shoulder located 1½-in. from the top of the lower aluminum section. A chromel-alumel thermocouple in a ⅜-in. stainless steel tube was inserted into the column directly below the screens through a bored-through ⅜-in. Swagelok fitting.

A 3-in. long by ¼-in. wall aluminum entry section was bolted to the upper 18-in aluminum section. Twelve 100-mesh circular screens were supported on a shoulder in the centre of this section. An 81-hole distribution plate was located above the screens to distribute the gas flow which entered through a 1½-in. aluminum pipe directly above the distribution plate.

The top four sections of the column were wrapped with a 1-in. thick layer of fibre glass insulation to reduce heat loss.

COLUMN SCHEMATIC

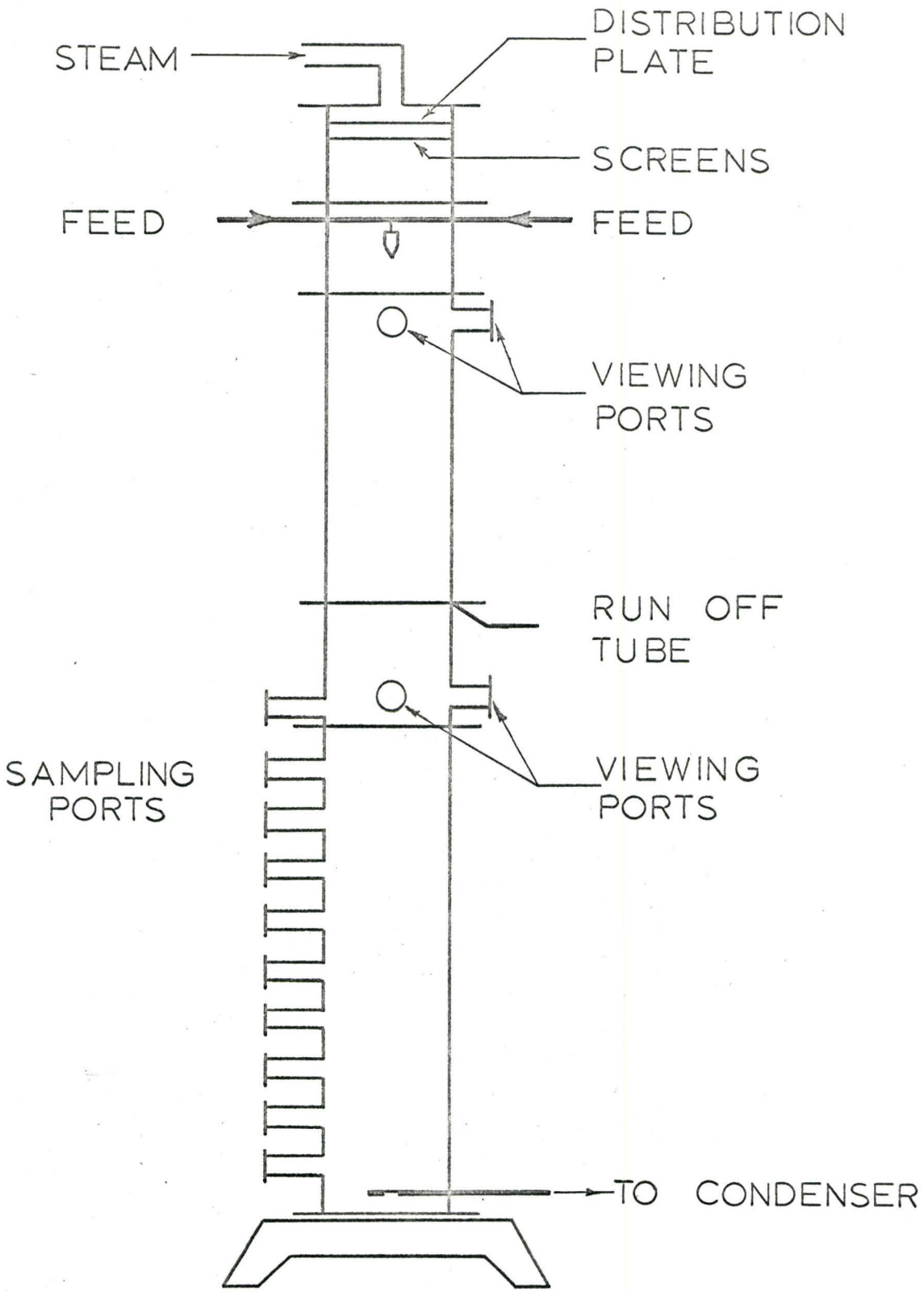

FIGURE 3·3 – 4

3.3.3 Flow System

Figure 3.3-5 is a schematic diagram of the entire flow system. Details of the important components are given in Table 3.3-1.

(i) Gas Flow

Steam or air could be supplied to the column (F) and pneumatic nozzle (E) by proper positioning of positive shut-off valves (V1, V2 and V3, V4) respectively. Saturated steam was obtained from a 100 lb. laboratory supply line (N) and air was obtained from a 100 lb. supply line (O).

Steam to the column passed through entrainment separator (C) with the flow rate determined by globe valve (V6). The steam then flowed through an absolute orifice (D) with the upstream pressure monitored by pressure gauge (P3). During start-up the steam flowed directly to the condenser (I), thus by-passing the column. After start-up the valves (V7, V8) were positioned so as to direct the flow through superheater (H1) into the column. The inlet steam temperature was monitored by thermocouple (T1).

Air to the column passed through two filters (A) with the flow rate controlled by globe valve (V5). The air then flowed through orifice (B) where the upstream pressure was monitored by pressure gauge (P2) and the differential pressure drop across the orifice was measured with a U-tube, mercury manometer made from high-pressure glass tubing. From this point the flow system was the same for both air and steam.

FLOW SCHEMATIC

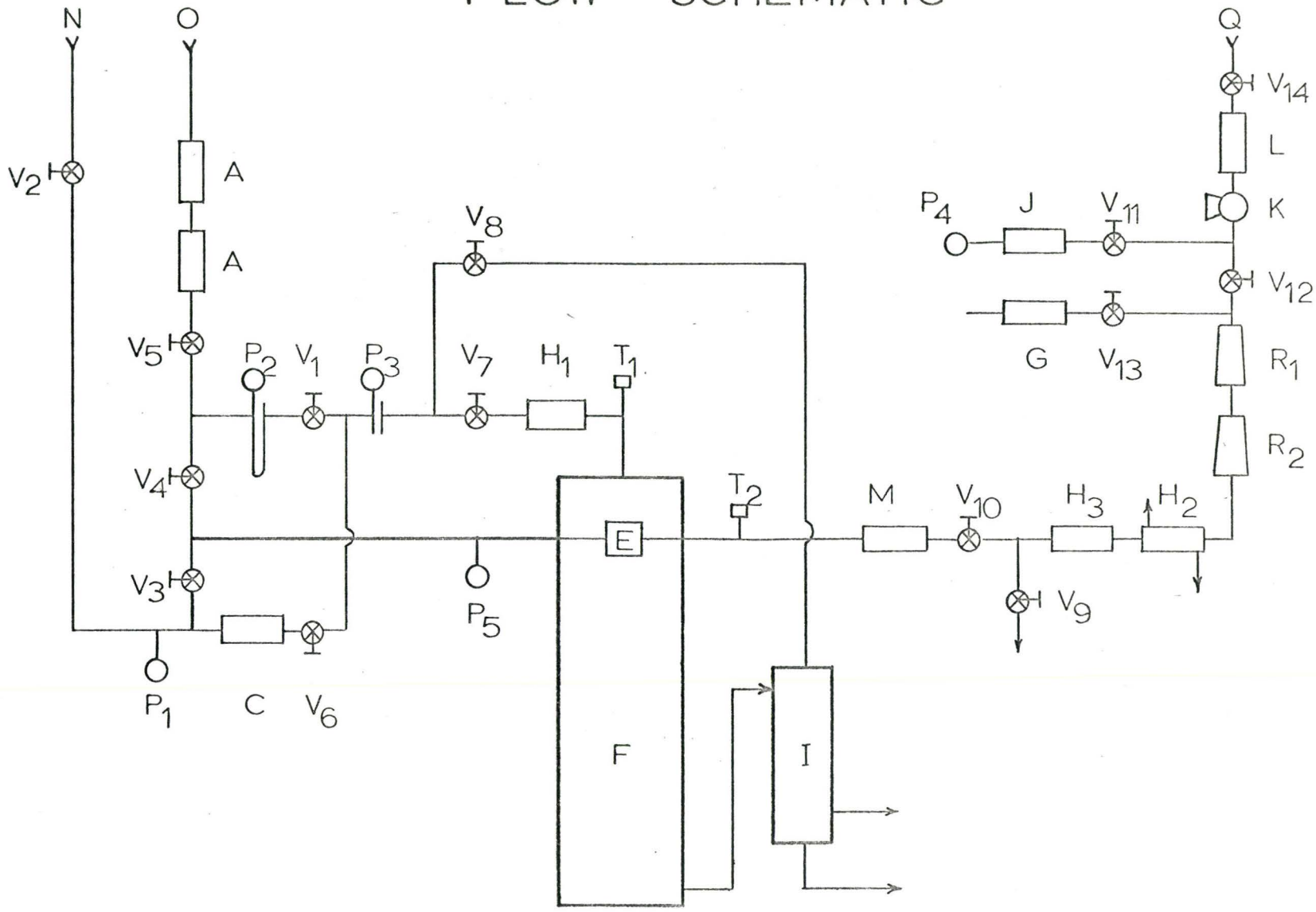

FIGURE 3·3 – 5

TABLE 3.3-1 : FLOW COMPONETS

No.	COMPONENT	SPECIFICATIONS
A	Filter	Norgren Manual-Drain Filter Type 12-002
B	Orifice	Brass Flanges - Flange Taps - 1-in. C.T. Line Removable Stainless Steel Plate - 0.636-in. Bore (Designed according to Taylor Inst. Co., - Technical Data Calc'n Manual No.1) Calibration in Appendix A
C	Entrainment Separator	Centrifix Corporation - ($\frac{3}{4}$-in. pipe fittings)
D	Orifice	Brass Flanges - Flange Taps - 1-in. Pipe Line Removable Stainless Steel Plate - 0.370-in. Bore (Designed as Absolute Orifice)- Calibration in Appendix A
E	Atomizer	Spraying Systems Co. - Pneumatic-Round Spray Type $\frac{1}{4}$ J Nozzles #11, 12A, 12, and 22B.
F	Column	See Previous Description in Text.
G	Feed Tank	5000 p.s.i. High Pressure Stainless Steel Tank 4 ft. x 6 in. I.D. x $\frac{3}{8}$-in. walls - Flanged Both Ends.
I	Condenser	Baffled, 1 Shell - 2 Tube Pass, Stainless Steel Vertical Condenser; 6 tubes (70-in. x $\frac{1}{2}$-in., 18 gauge stainless steel) per pass; total area - 11 sq. ft.
J	Surge Tank	12-in. x 6-in. I.D. x $\frac{1}{8}$-in. wall cast iron pipe with welded ends and $\frac{3}{4}$-in. pipe nipples on each end.
K	Pump	Robbins and Meyers Moyno Tubular Pump Type CDQ-150 p.s.i. Maximum Operating Pressure Driven by $\frac{3}{4}$ H.P. 1725 r.p.m. 60 cycle 3Ø motor speed controlled by Zero-max variable Speed Reducer - Model 24 - 100-in. lb. torque; 0-$\frac{1}{4}$ input r.p.m.
L	Filter	Nupro Type FR Brass Body, Inline Removable Filter - $\frac{1}{4}$-in. Swagelok fittings - 15 micron Stainless Steel Filter
M	Filter	Nupro Type F 316 Stainless Steel Body, inline Removable Filter - $\frac{1}{4}$-in. Swagelok fittings - 15 Micron Stainless Steel Filter

TABLE 3.3-1 (Continued)

No.	COMPONENT	SPECIFICATION
N	Steam Supply	100 lb. saturated steam from 1½-in. supply line
O	Air Supply	100 lb. building air from 1-in. supply line
H1	Heater	15-in. x 2-in. I.D. x ⅛-in. wall stainless steel, baffled cylinder. Cylinder is supported inside a Kanthal Type 7-30 cylindrical electrically heated furnace. Power Supply - Lovatt Engineering RC step down transformer - 240 V primary - 20 V sec. - 1500 VA. Power Control - Superior Electric - 126 - V2, 0-230 Volt variable transformer
H2	Heater	30-in. x 1-in. O.D. Double-Pipe Heat Exchanger Feed Line - ¼-in. Copper Tubing. Heating Medium - Steam from 100-lb. Mains.
H3	Heater	22-ft. x ¼-in. 316 Stainless Steel Tubing - formed in a 2-in. diameter coil. Coil is supported inside a Kanthal REH 10-60 cylindrical electrically heated furnace. Power supply - Hammond Class A Step Down transformer - 270 V primary - 65V secondary - 2700 VA. Power Control - 2 Superior Electric 2 PF 136, 2.8 K.v.a. variable transformers.
R1	Rotameter	Fisher - Porter variable area flow meter Type FP - ¼ - 25 - G 5/81 with Glass Ball Float. Calibration in Appendix A.
R2	Rotameter	Fisher - Porter variable area flowmeter Type FP - ½ - 21 - G 10/80; Float 16 USUT - 40 Calibration in Appendix A.

Air to the nozzle passed first through the filters - (A) while steam entered the nozzle directly from the mains. The atomizing gas pressure was monitored by pressure gauge (P5).

(ii) Liquid Flow

(a) Continuous operation - City water from the mains flowed through in-line filter (L) and into the inlet of a variable - speed positive displacement Moyno pump (K). Pressure fluctuations were removed from the feed system by a surge tank (J). The pressure in the liquid feed system was monitored by pressure gauge (P4) on the surge tank. With gate valves (V12, V13) in the proper position the water flowed through rotameters (R1) and (R2) and feed - preheaters (H2) and (H3). During start-up the feed could be directed to a drain by proper orientation of toggle valves (V9) and (V10). After start-up the feed was passed through in-line filter (M) into the atomizing nozzle (E). The feed temperature was monitored by thermocouple (T2) located in the line close to the nozzle.

(b) Batch operation - Proper orientation of valves (V12) and (V13) permitted high pressure tank (G) to supply the liquid feed to the system. The tank was pressurized with nitrogen from a commercial gas cylinder.

Gas and vapour passed from the reactor into water cooled condenser (I) and the condensate was monitored to determine the total mass flow through the system.

3.3.4 Drop Sampling Probe

The drop sampling probe, shown in Figures 3.3-6 and 3.3-7 was designed to permit samples of the spray to be removed from the column. The probe could be inserted through one of the sampling ports on the column and a sample of the spray collected in a stainless-steel, glass bottomed, liquid-filled sample cell (j)* which fits into well (i) in the probe head (h).

The principle of operation is based on that originally proposed by Rupe[R5] and used by Dlouhy[D2], Manning[M5], Hoffman[H1], Tate[T4] and others. This immersion-cell technique utilized a water-saturated solvent, varsol (Imperial Oil, Sarnia, Ontario), which is only slightly miscible with water and which has a density less than water. Droplets entering the cell therefore settle to the bottom and are maintained in their spherical state by coating the glass bottom with a non-wetting agent SC-87 (General Electric Company). The glass bottom allowed shadow-photographing of the droplets under magnification (40X).

The sample cell used in this study was a ¼-in. by ¼-in. diameter stainless steel cylinder; shown as (j) in Figure 3.3-7. The glass bottom was a 0.050-in. by 0.225-in. diameter optically flat glass disc (Corning Glass Works - Glass 7740) which was cemented to the cell with teflon cement (John Crane Company). The droplets settled onto a 0.050-in. by 0.185-in. diameter optically flat disc which was placed in the bottom of the cell prior to sampling. This disc could be easily removed for cleaning and coating

---

* Small letters here refer to letters on probe components shown in Figure 3.3-7.

of the surface.

The cell (j) was exposed to the spray for a known period of time by activating the shutter (g) with two electromagnets (b). The electromagnets were activated by an electronic timer. (Automatic Timing and Controls Inc. - series 5231). Leads and activation switch can be seen in Figure 3.3-6.

The probe head (h) is a streamlined cylindrical stainless steel shell designed to intercept the radiation originating at the reactor walls. Without this shielding the absorbed radiant energy would cause the temperature of the collection fluid in the cell (j) to increase and result in loss of fluid through evaporation. The heat absorbed by the shield was removed by a circulating heat transfer medium which entered and left the shell through tube system (a).

Plug (f) was machined and contoured to fit flush with the column wall. The probe head could be positioned relative to the plug and locked into position with locking device (c). (The locking device is not shown in Figure 3.3-6).

Stainless steel rods (e) joined the plug to flange plate (d); this plate, matched the flanges on the sampling ports and allowed the probe to be locked into position in the column.

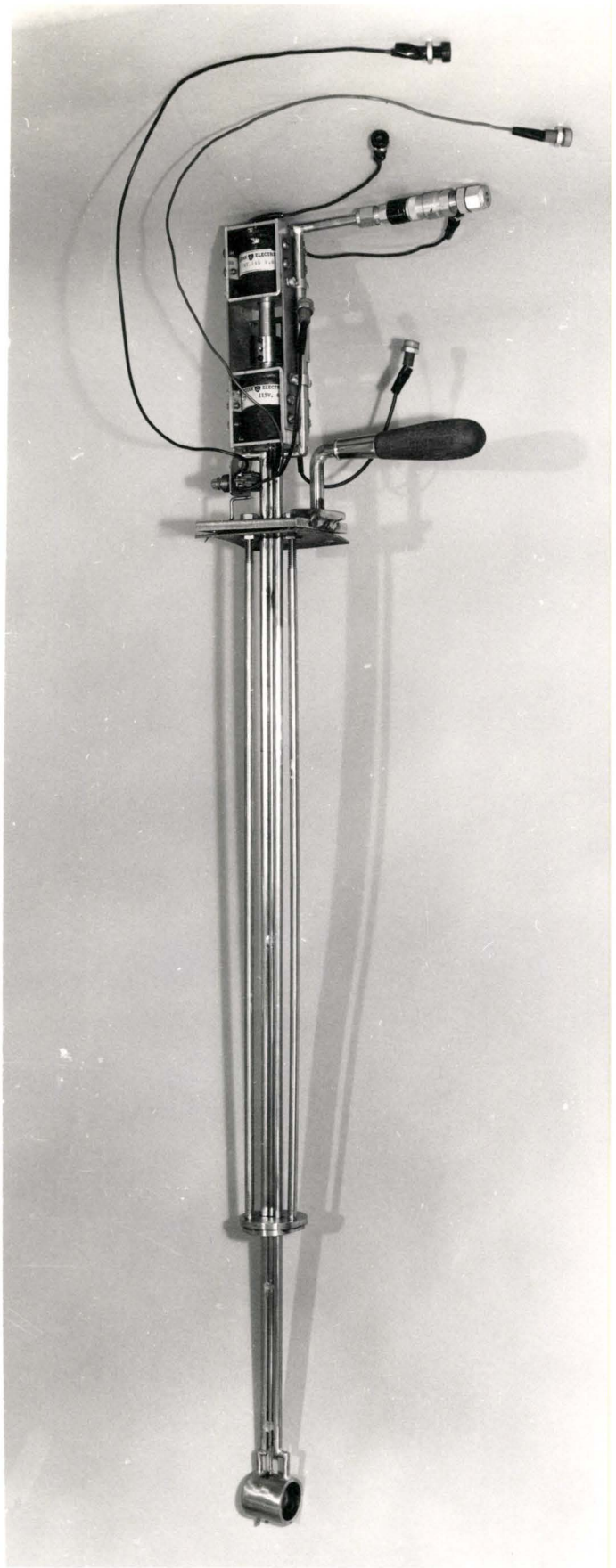

FIGURE 3.3-6 : Drop Sampling Probe

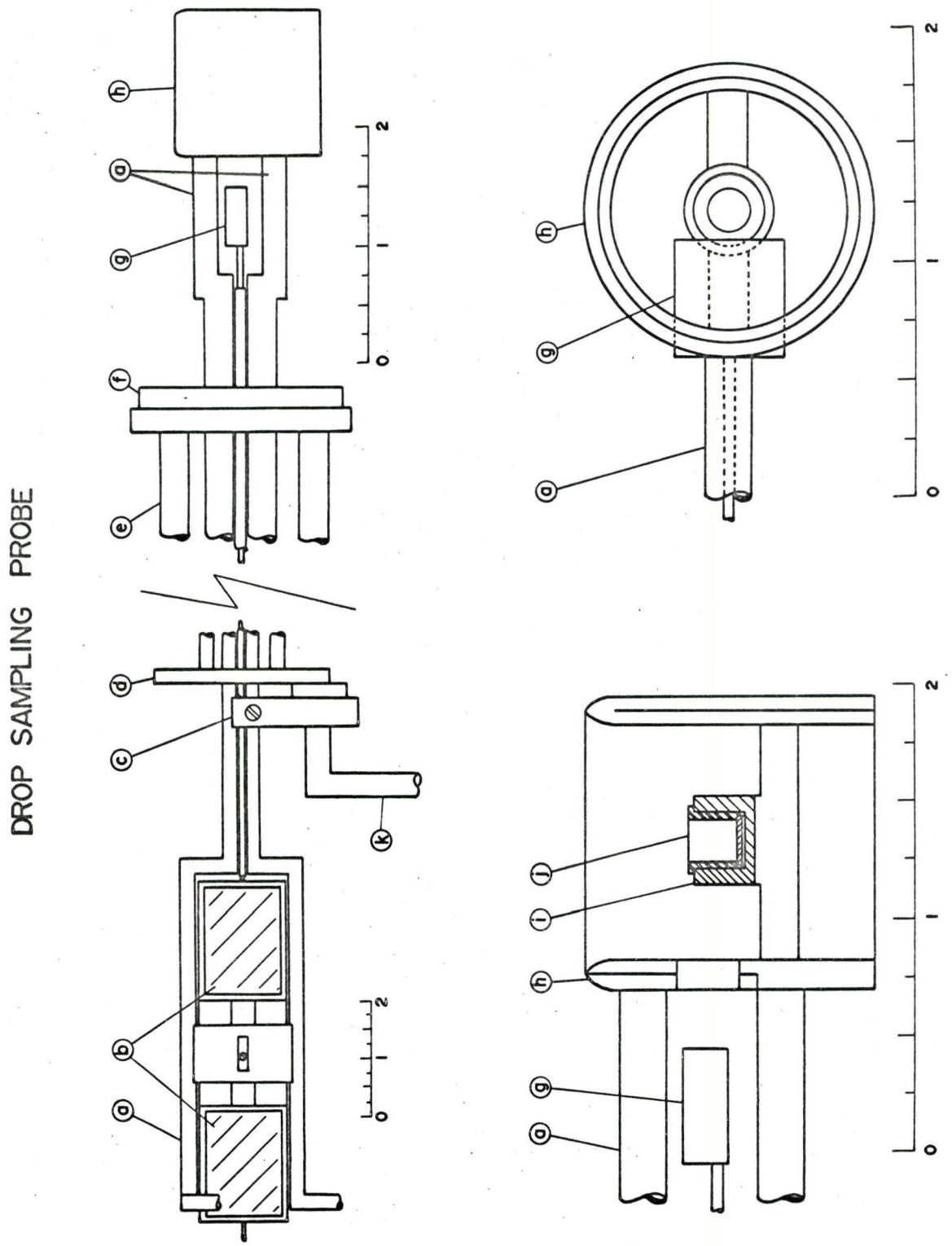

FIGURE 3.3-7

3.3.5 Temperature Probe

(i) Aspiration probe - The aspiration probe shown in Figure 3.3-8 was designed to permit gas temperatures to be measured in a particulate stream flowing in a high-temperature environment. Gas was drawn in across the 0.001-in. Pt-Pt 10% Rh thermocouple which was supported inside three concentric tubes. These tubes prevented the droplets from contacting the thermocouple and also shielded the thermocouple from the radiation emitted at the column walls. A circular plate covered with thin platinum foil was located in front of the suction orifice to prevent radiation from streaming directly into the probe.

The probe tip, shown in Figure 3.3-9 was designed according to the criterion established by Wadleigh and Oman [W2]. These workers measured the gas-phase composition of a high velocity two-phase flow. The basic idea was to cause the gas to negotiate a path of high curvature which would result in "shedding" of the liquid droplets which were being transported by the gas. Suction on the annulus around the centre tube suppressed the flow of "boundary layer" liquid into the centre tube and helped to establish a sharply-curved gas-flow pattern into the centre tube.

Gas was drawn across the thermocouple at mass flows in the order of 0.1 gm./min. by applying suction to the innermost tube. This tube was connected to a 2.1 sq.ft. compact heat exchanger (American Standard - Ross Type - SSCF) with high vacuum rubber tubing. The exchanger was connected to a glass

receiver bulb to which a vacuum was applied from a general laboratory vacuum line. The vacuum was measured with a mercury manometer. Calibration of the probe against the unshielded probe indicated that a vacuum of approximately 4 cm. of mercury should be applied to the receiver bulb. No suction was applied to the inner annulus but steam was observed to flow from the annulus at all time during operation of the probe.

The probe was calibrated under normal column operation (with gas flow only) against the "bare" thermocouple described in the next section. Results are given in Appendix A.

(ii) Bare or Unshielded Thermocouple. This probe is shown alongside the aspiration probe in Figure 3.3-8. The probe was inserted into the column in the same manner as the aspiration probe and the drop sampling probe.

Figure 3.3-10 is a scale drawing of the important features of the probe.

(A) indicates the geometry of the probe tip, while (B) shows the actual thermocouple detail. The stainless steel sheathed thermocouple (c) runs through a $\frac{3}{8}$-in. stainless steel tube (a) and is welded into position at the end of the tube. The stainless steel rod (b) is also welded to tube (a) and serves to locate the probe at the furnace wall. Pt and Pt 10% Rh wires of 0.0005-in. diameter (e) are welded to the corresponding 0.010-in. diameter wires (d) from standard, $\frac{1}{16}$ O.D., stainless steel sheathed, double conductor, Pt - Pt 10% Rh, thermocouple wire. (Thermo-Electric Company). A 0.001 - 0.002-in. ball is

formed at the end of the 0.0005-in. wires by welding the wires with the flame from a microtorch. The ball is located within 0.005-in. of the end of the rod, the distance being measured by a cathetometer (Griffin and George - Model No. P369). The probe tip was constructed following the design of Brown[B13]. The probe could be located relative to the furnace wall within ±0.001-in. by means of the positioning mechanism shown in (c) of Figure 3.3-10. Flange plate (f), to which support plate (h) is bolted, permits the unit to be locked into position in the column. Yoke (g) and adjusting screw (i) were used to position the thermocouple relative to the wall by inserting mild steel "Jo" blocks of varying size between the flange plate (f) and the tip of the screw. The "Jo" or spacer blocks which rest on plate (h) were machined to a tolerance of 0.001-in..

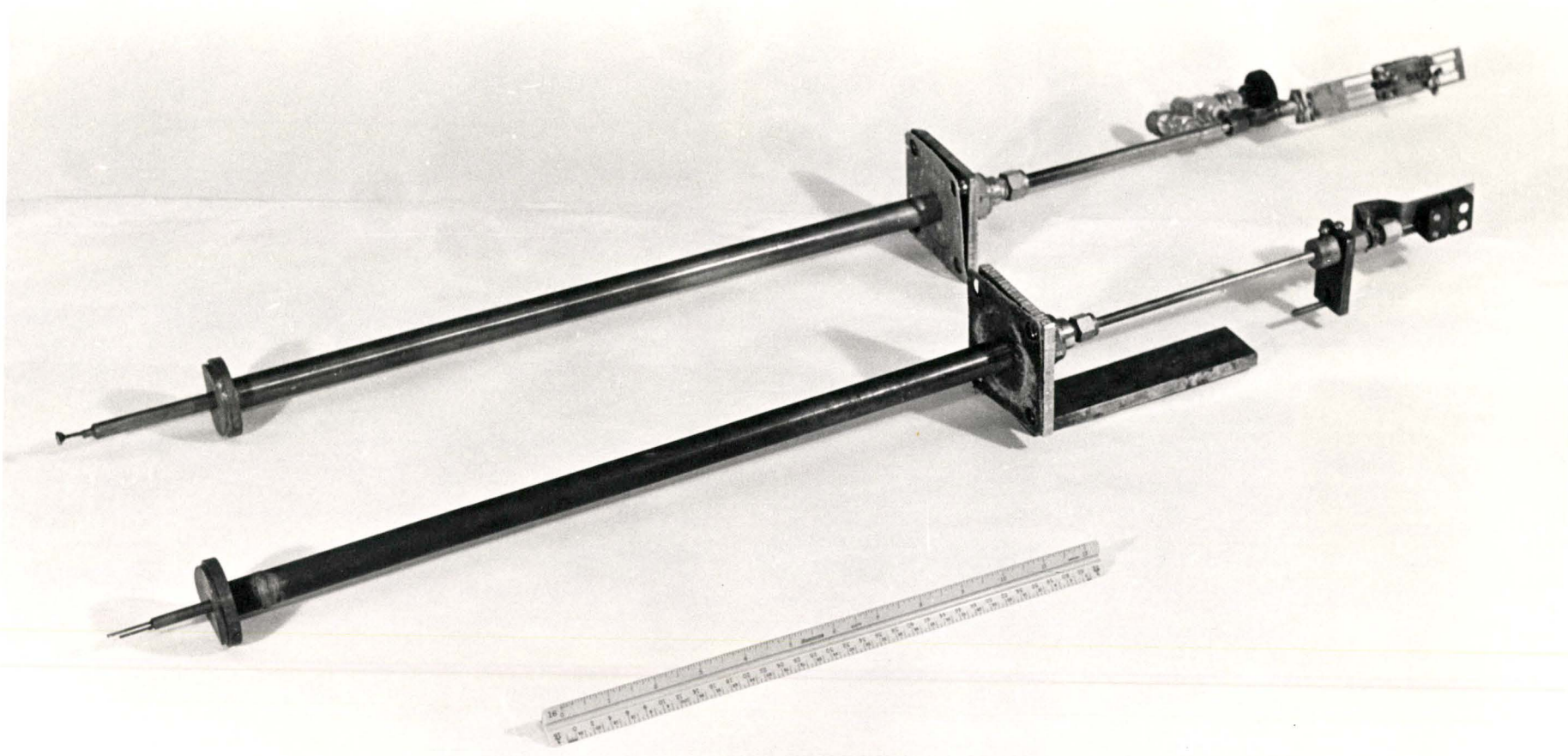

FIGURE 3.3-8 : Gas-Temperature Probes

TIP OF ASPIRATION PROBE

FIGURE 3.3-9

BARE TEMPERATURE PROBE

(A) PROBE TIP

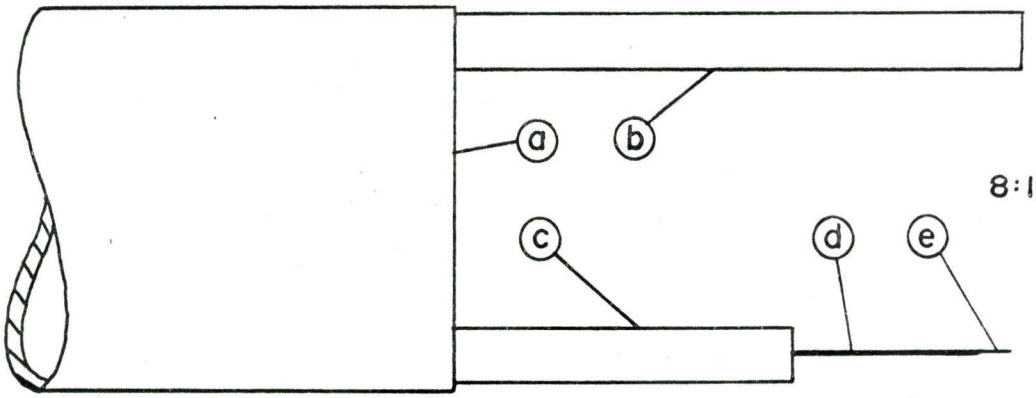

(B) THERMOCOUPLE

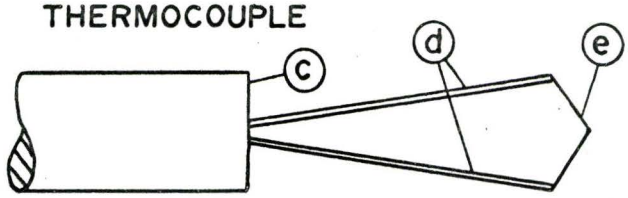

(C) POSITIONING MECHANISM

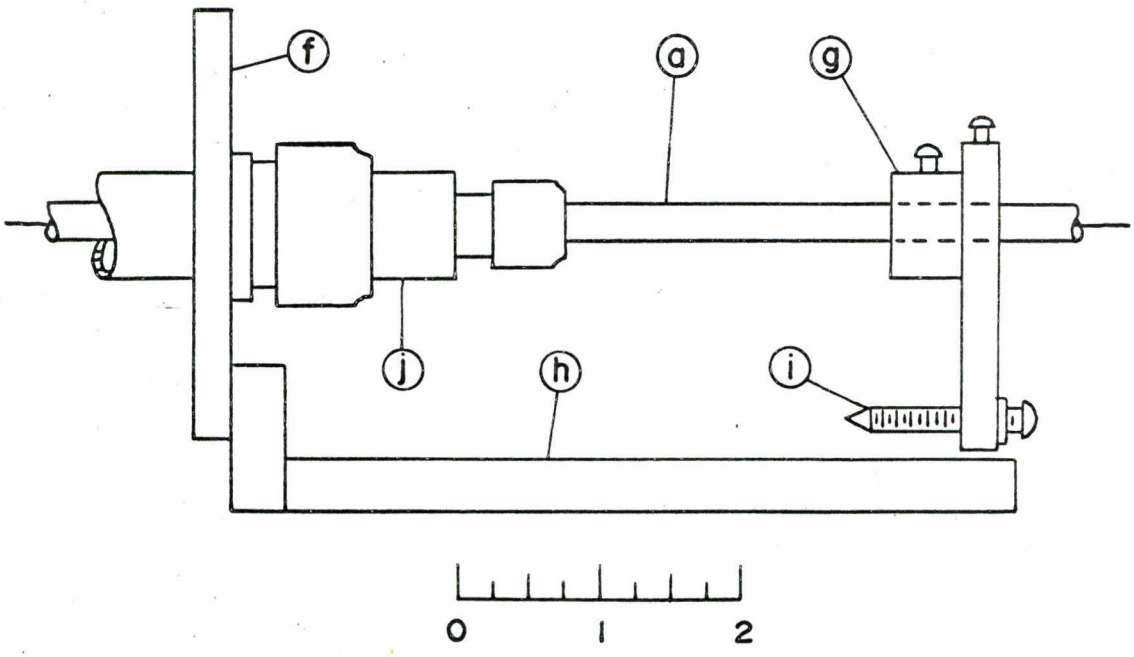

FIGURE 3.3-10

ASPIRATION PROBE

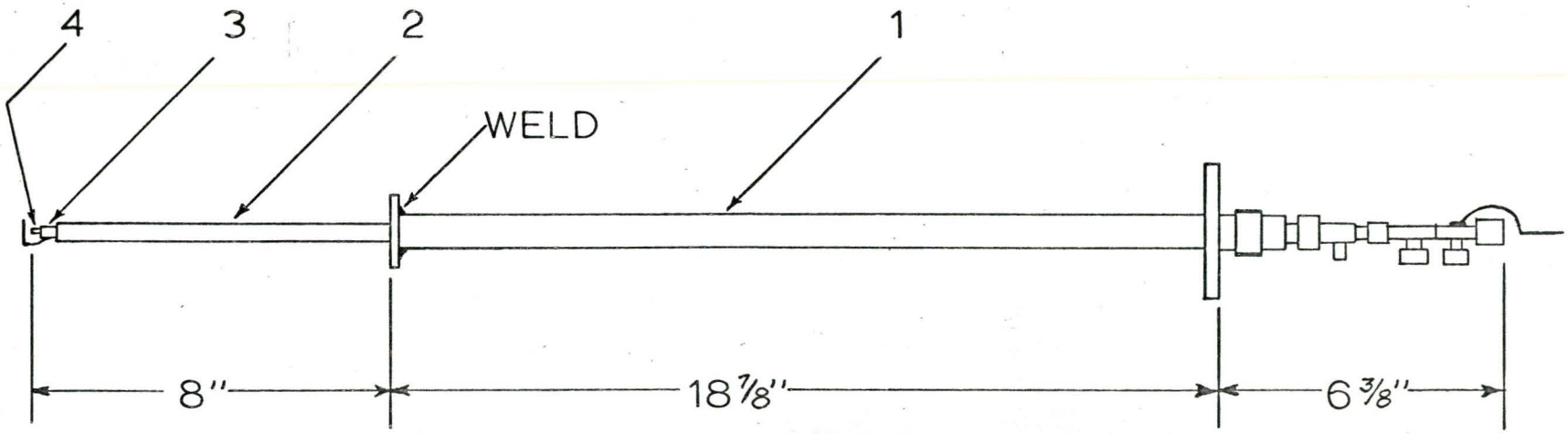

STAINLESS STEEL TUBING

1 — 3/4" x .049" WALL x 20" LONG
2 — 3/8" x .035" WALL x 29 2/32" LONG
3 — 1/4" x .035" WALL x 30 9/32" LONG
4 — .109" O.D. x .085" I.D. x 31 2/32" LONG

FIGURE 3·3 – 10a

3.3.6 Temperature Recording Equipment

(i) Single pen recorder. Millivolt signals from the probes were recorded on a Honeywell variable span single pen recorder. The signal obtained at each point in the traverse was recorded for approximately 30 sec. to ensure that any low frequency oscillation in the average temperature would be monitored. Initially the signals were fed directly to the recorder but as the wall temperature of the reactor increased the fluctuations became of such a magnitude that estimation of the average signal became exceedingly difficult. Also, when the magnitude of the fluctuations was large the recorder pen could not follow the signal because of the relatively long recorder response time.* Consequently, an electronic damping circuit was designed as shown in Figure 3.3-11.

(ii) Filter Circuit. The circuit was designed to dampen out the relatively high frequency (1 to 10 c.p.s.) fluctuations. by means of the capaciter C1. The capacitance of the circuit could be readily increased if the fluctuations increased in magnitude. Variable resistor R3 attenuates the input signal exactly by a factor of two thus eliminating the problem of an unknown offset caused by the capacitance.

When using the filtering or damping network the attenuation of the input signal was frequently checked by sending a known millivolt signal to the circuit and recorder from a

---

* With a span of 0-8 mv the recorder was only able to follow a 2 c.p.s. 1 millivolt fluctuation to within 80% of the full fluctuation.

Honeywell Model 2733 portable potentiometer. (This same potentiometer was also used to calibrate the single pen recorder.) Because the input signal was attenuated, the recorder span could be doubled over that used for the unattenuated signal and hence the reading accuracy was maintained.

For the highest wall temperatures the span was the largest and hence the reading accuracy the poorest. The largest span used for an attenuated signal was 0-4 millivolts. The recorder chart could easily be read to ± $\frac{1}{10}$ division which represents ± 0.004 mv at this span. Since the signal is attenuated this difference represents an actual uncertainty of ± 0.008 mv. At a temperature level of 600°F this uncertainty in the chart reading represents an uncertainty of ± 2°F in the gas temperature. This degree of uncertainty is considerably less than the uncertainties arising from the fluctuations themselves.

Low frequency (<0.1 c.p.s.) fluctuations in the average temperature gave rise to wavy traces on the recorder chart. The average millivolt signal was estimated from the trace by eye with an estimated accuracy of ± 0.5 divisions. With the signal attenuated by ½ and a 0-4 mv span this represents an uncertainty in the thermocouple temperature of ± 7°F.

(iii) Random Signal Voltmeter. For several runs the thermocouple millivolt signal was also monitored by a random signal voltmeter (Flow Corporation Model 12A1) which indicated the root mean square of the voltage fluctuation. The low frequency fluctuations caused the r.m.s. signal to slowly vary

and consequently it was necessary to take an eye-average over a 30 to 60 second period.

FILTER CIRCUIT

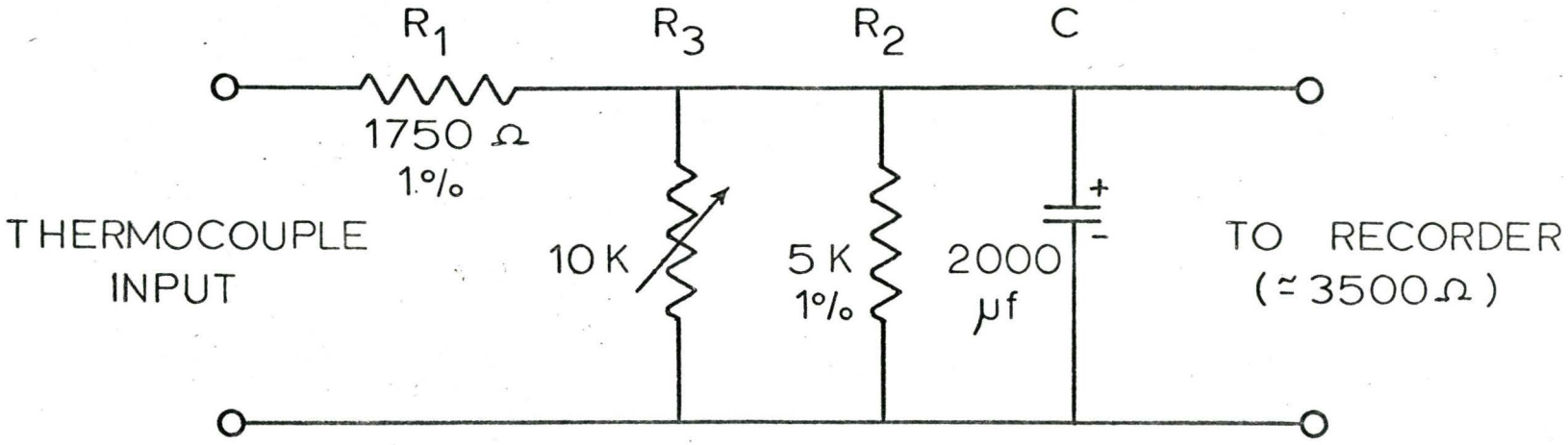

FIGURE 3·3 – 11

3.4 Experimental Procedure

3.4.1 General Operation

Power was applied to the heaters and the column brought up to the desired operating temperature over a one hour period. When operating with steam as the gaseous medium it was necessary to by-pass the column until the supply lines had warmed up. Heater H1 was usually employed to add an additional 4 or 5°F of superheat to the steam.

(i) Gas Flow only. In the case of experiments performed in a gaseous medium with no spray, the air or steam was introduced into the system and the column allowed to equilibrate to the particular power level over a 15-20 min. period. Gas temperature profiles in the column could then be measured with either the shielded or unshielded probes previously described.

(ii) Gas and Liquid Flow. For experiments with sprays, the carrier gas was supplied to the column before atomization was begun. If the feed was to be introduced at an elevated temperature, heaters H2 and H3 were activated. The feed was directed to a drain until the desired temperature was obtained. A period of 20 - 30 min. was allowed to ensure that steady-state conditions had been reached. Temperature profiles with the aspiration probe and drop sampling could then be initiated. If the feed supply originated from the high-pressure tank, it was also possible to determine the relative fractions of steam and feed in the run-off from the upper walls of the column by measuring the concentration of a soluble manganese salt which had been introduced into the feed tank. Details of this procedure are given in Section 3.4.4.

3.4.2 Drop Sampling

(i) Preparation of Sample Cell. The glass bottom of the sample cell was carefully cleaned after which a 0.05-in. thick optically flat glass disc was placed in the cell. The disc was also carefully cleaned and coated with a non-wetting agent (General Electric, SC-87 Dri-Film) before being inserted into the cell. The cell was then placed in a brass holder shown in Figure 3.4-1 which rested on an aluminum heater block. (The block was heated by two Chromalox C 203 75 watt cartridge heating elements.)

(ii) Sampling. Just prior to taking a drop sample the cell was filled with varsol or Dow Corning 200 Silicone oil from a hypodermic syringe. The collection fluid had been warmed to approximately 140°F and saturated with water prior to injection into the cell. The cell was then placed in the probe, which had been preheated by insertion into a small muffle furnace, and covered with the shutter. The probe was inserted into the column at the desired radial and axial location and the shutter activated to expose the cell to the spray. Upon removal of the unit from the furnace the cell was replaced in the cell holder and covered with a glass slide which was held in place with two spring clips.

(iii) Photography. The brass cell holder containing the loaded cell was inserted into a special heated block which was mounted on a substage microscope (Officine Galileo Model 125418) (The block was heated with two Chromalox C202 30-watt cartridge heating elements.) The cell was illuminated from above with a 6-volt, 30-watt Mazda lamp which was focused on the cell with a 55 mm. condensing lens.

The cell was viewed through the optics of a 35 mm. single lens reflex camera (Asahi Pentax SLI). which was mounted on the lens barrel of the microscope. The objective and eyepiece of the microscope gave an image magnification of 40x* on the ground glass screen of the camera. At this magnification approximately $\frac{1}{20}$ of the cross-sectional area of the cell was visible. By the time the cell had been mounted on the microscope the drops collected in the cell had settled through the collection medium and were resting on the glass disc in the bottom of the cell.

The cell was carefully traversed by moving the microscope stage; the drop images were recorded on 35 mm. film (Ilford FP-3).

The film was developed in fine grain developer (Acufine) under controlled conditions; the droplet images were subsequently enlarged 4x and printed on single weight paper, (Leonar Megatype).

(iv) Counting. The enlarged droplet images were sized and recorded on a Particle-Size-Analyser (Carl Zeis Model TGZ3). This device determines the size of the image on the photographic paper by matching a variable light spot to each droplet image. The relative size of the spot was recorded on a panel of mechanical counters. The results from the counting operation were then entered on punched cards and processed by an IBM 7040 computer to yield the desired average diameters of the sample.

The minimum size of the light spot was 1 mm. and hence at a total magnification of 160x the smallest detectable drop had

---

* The exact magnification was determined by photographing a microscope calibration slide (Bausch and Lombe).

a diameter of 6 microns. Thus no droplets below this size were measured. However, since the target efficiency of the cell was expected to be low for these small droplets, not many should be collected in any event. These droplets consitute a very small fraction of the weight of the spray.

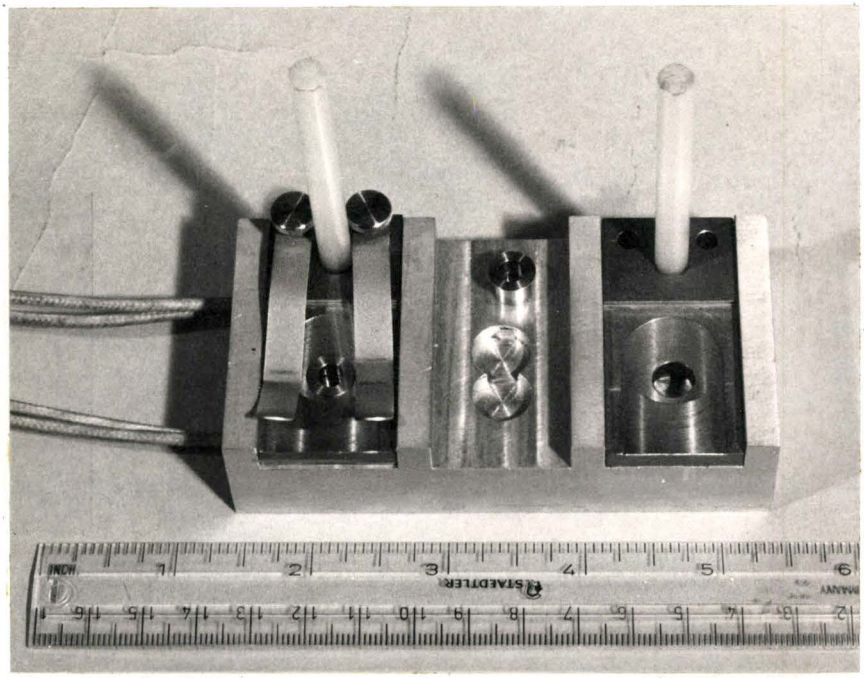

CELL AND CELL HOLDER

FIGURE 3.4-1

3.4.3 Gas Temperature

(i) Particulate System. The aspiration probe previously described was used to measure the gas temperature when the spray was present. The probe was locked into position in the sample port and a radial traverse made by sliding the probe mechanism through the Swagelok fitting on the outer flange. The radial location of the thermocouple was determined from index marks on the outer tube.

Before starting the radial traverse, suction was applied to the probe. The probe was then allowed to equilibrate to the column conditions.

Temperatures were usually recorded at the following radial locations, measured from the wall opposite the entry port:

0.3, 0.5, 0.7, 1.0, 1.5, 2.0, 2.5, 3.0, 4.0, 5.0, 6.0, 6.5, 6.7, 7.0, 7.2, 7.5 in.

The millivolt signal was recorded on a Honeywell single pen recorder as described in Section 3.3.6

(ii) Gas flow only. The bare or unshielded probe, described in 3.3.5, was used to measure gas temperature gradients at the wall and to calibrate the aspiration probe. The probe was locked into position and the stainless steel tube carrying the thermocouple wire was extended into the column until the stop-rod touched the wall of the evaporator. A 0.100-in. spacer block was then placed on the support plate, flat against the end; the yoke and set screw were adjusted so that the tip of the screw just touched the block in this "zero" position. After recording

the millivolt signal on the single pen recorder the probe was withdrawn slightly and a larger spacer block was inserted. The probe was again inserted until the screw tip just touched the spacer block. This process was repeated until a radial traverse over half the column had been completed. Temperatures were usually measured at distances of 0, 0.005, 0.010, 0.020, 0.030, 0.040, 0.050, 0.070, 0.100, 0.200, 0.300, 1.000, 2.00, 3.00, 4.00-in. from the wall. These readings had to be corrected for the distance the stop protruded beyond the thermocouple.

For several traverses the millivolt signals from the thermocouple were also monitored by an r.m.s. meter (Flow Corporation) in order to determine the root mean square of the gas temperature fluctuations.

3.4.4 Run-off Determination

When the spray was formed in the confines of the 8-in. diameter column a large fraction of the liquid impinged on and ran down the wall to the catch-trough from where it flowed out of the column and was monitored.

Since there was some heat loss from the system some of the steam must have condensed on the walls of the atomization chamber and this would be measured as run-off. Therefore, it was necessary to identify the relative fractions of condensate and feed in the run-off if the true gas and spray flow to the evaporator were to be known.

In order to determine the relative fractions in the run-off a colourimetric analysis technique was employed. The technique consisted of;

1. placing a known quantity of $MnSO_4.H_2O$ in the high pressure feed tank.
2. pressurizing the feed tank with nitrogen and opening the feed line to the nozzle.
3. collecting the run-off in glass stoppered erlenmyer flasks and allowing it to cool.
4. pipetting a 50 ml. sample from the collected liquid into a 125 ml. erlenmyer flask
5. adding 10 ml. of 85% phosphoric acid and an excess of KIO_4
6. warming the solution to oxidize the manganese from the +2 to the +7 state.*
7. cooling the solution and diluting it to 100 ml. in a volumetric flask

---

* Balanced redox reaction for this case is:

$$2Mn^{++} + 5\ IO_4^- + 3H_2O \rightleftharpoons 2MnO_4^- + 6H^+ + 5IO_3^-$$

8. filling a 23 ml. optical cell of a Fisher Electrophotometer (Model A) with the coloured solution and determining the transmittance using a 525-B filter.

9. comparing the transmittance reading with the calibration curve previously constructed (see Appendix A) to determine the concentration of MnO_4^- present and hence the concentration of Mn^{++} prior to oxidation.

10. determining the concentration of feed and steam in the run-off from a knowledge of the original concentration of Mn^{++} in the feed.

3.5 Results and Discussion

3.5.1 Gas Temperature Measurement

(i) Single Phase System

Figure 3.5-1 to 3.5-4 represent typical gas temperature profiles which were measured with the unshielded thermocouple for both steam and air flows at Reynolds numbers of 10×10^3 based on inlet conditions. Figure 3.5-1 and 3.5-3 illustrate that the radial temperature gradients exist from the wall to the centre-line of the column. Figure 3.5-2 and 3.5-4 indicate the gas temperatures which were measured at distances less than 0.100 in. from the wall. Close to the wall the temperature gradients are linear as one would expect, since the mechanism of energy transport in the boundary layer close to the wall is molecular conduction. The temperature gradients are also observed to decrease with distance from the entrance as the bulk temperature of the gas is increased.

The most important aspect of the gas-temperature profiles at the wall is that the extrapolated wall temperature does not agree with the temperature indicated by the thermocouples which were welded to the exterior of the column. The discrepancy in the two temperatures is much greater than either the temperature drop across the stainless steel wall ($\doteq 10^{\circ}F$) or the thermocouple conduction error analysis of Short and Sage[S16] would indicate. A careful check of the control thermocouples did not disclose any errors in their millivolt output. The wall temperatures were also

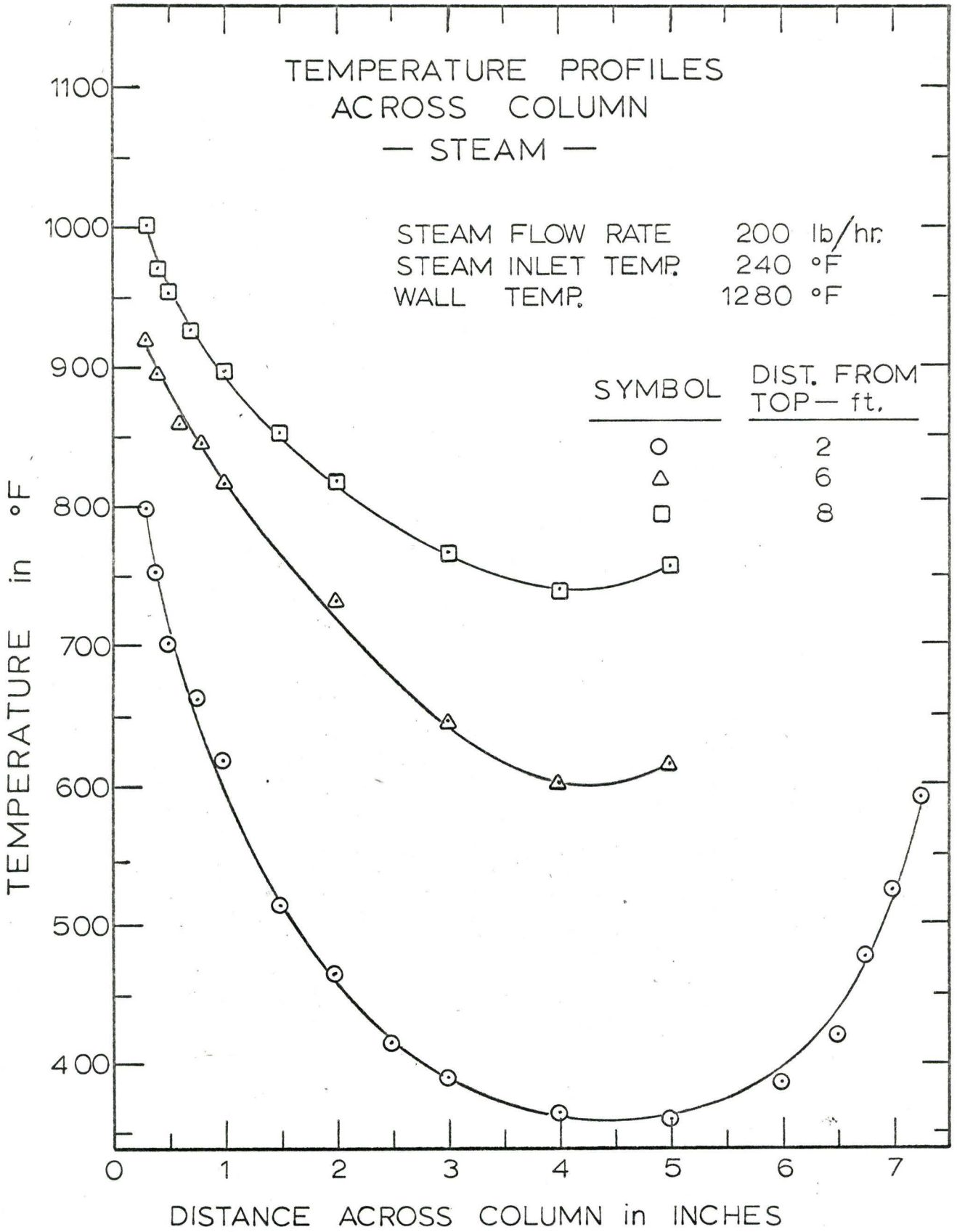
TEMPERATURE PROFILES
ACROSS COLUMN
— STEAM —
STEAM FLOW RATE 200 lb/hr.
STEAM INLET TEMP. 240 °F
WALL TEMP. 1280 °F
SYMBOL
DIST. FROM TOP — ft.
2
6
8
TEMPERATURE in °F
1100
1000
900
800
700
600
500
400
0
1
2
3
4
5
6
7
DISTANCE ACROSS COLUMN in INCHES

FIGURE 3·5—1

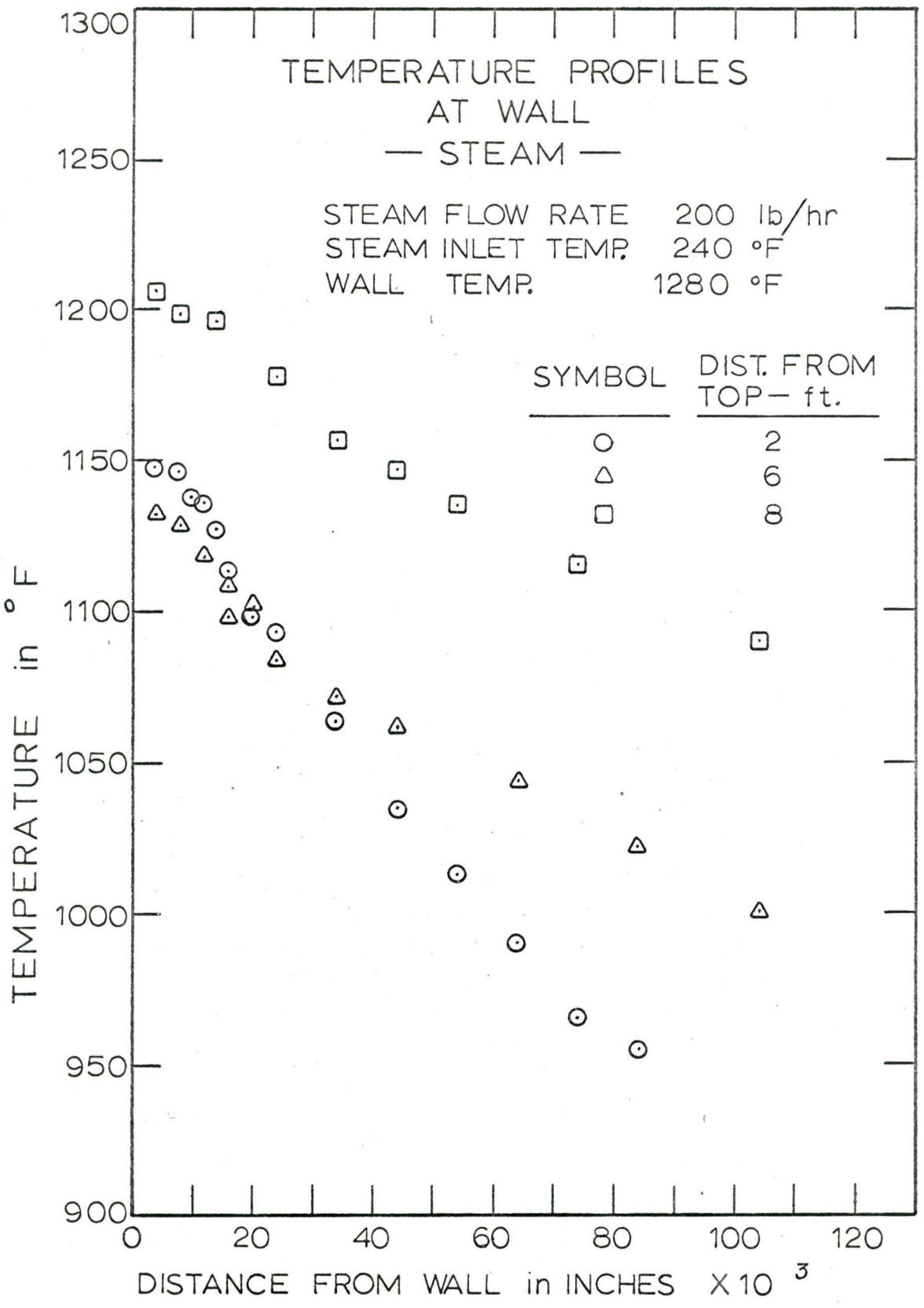
TEMPERATURE PROFILES
AT WALL
— STEAM —
STEAM FLOW RATE 200 lb/hr
STEAM INLET TEMP. 240 °F
WALL TEMP. 1280 °F
SYMBOL
DIST. FROM TOP — ft.
2
6
8
TEMPERATURE in °F
1300
1250
1200
1150
1100
1050
1000
950
900
0
20
40
60
80
100
120
DISTANCE FROM WALL in INCHES X 10 3

FIGURE 3·5 —2

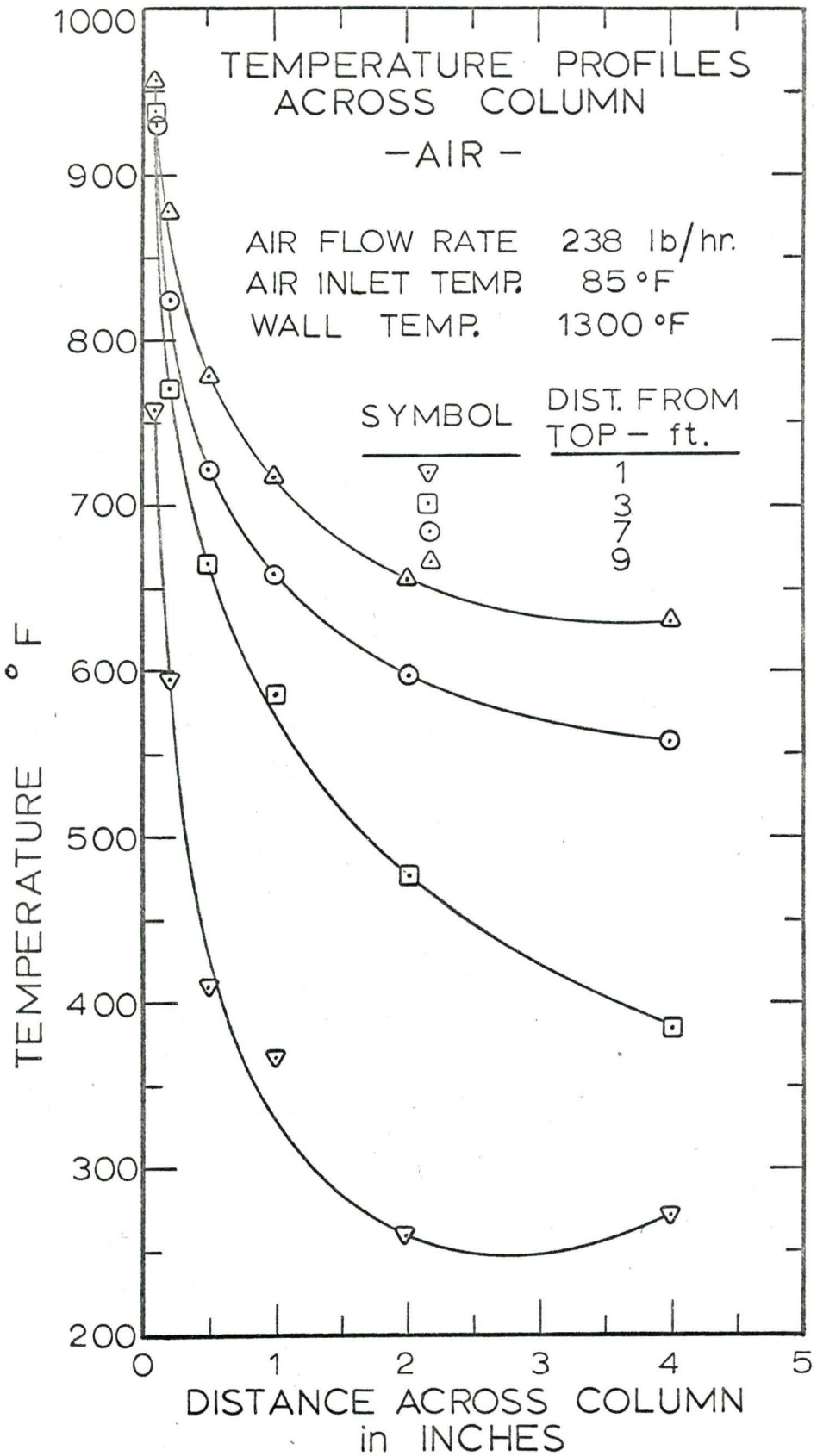
TEMPERATURE PROFILES
ACROSS COLUMN
-AIR-
AIR FLOW RATE 238 lb/hr.
AIR INLET TEMP. 85 °F
WALL TEMP. 1300 °F
SYMBOL
DIST. FROM TOP - ft.
1
3
7
9
TEMPERATURE °F
1000
900
800
700
600
500
400
300
200
0
1
2
3
4
5
DISTANCE ACROSS COLUMN in INCHES

FIGURE 3·5-3

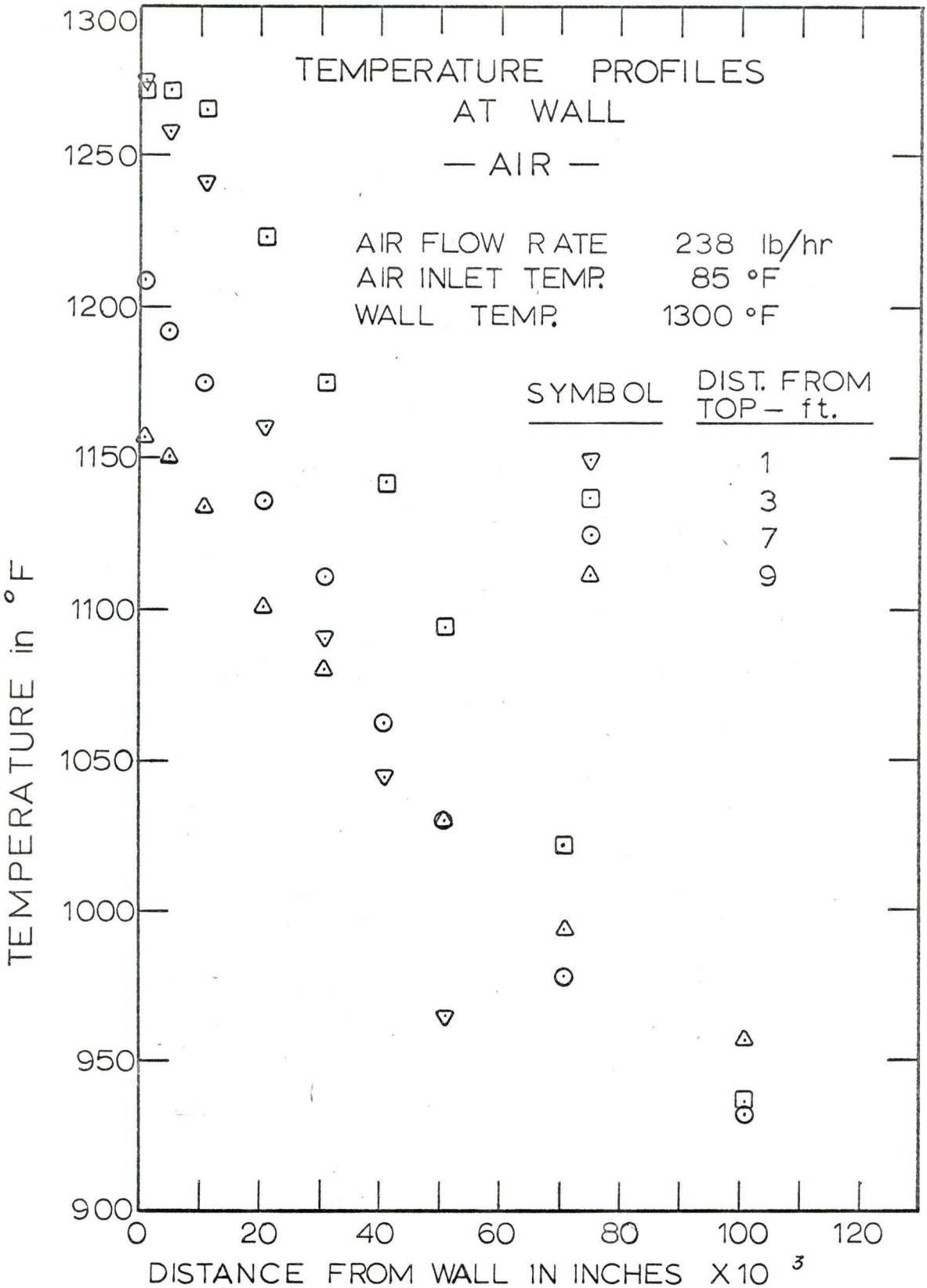
TEMPERATURE PROFILES
AT WALL
— AIR —
AIR FLOW RATE 238 lb/hr
AIR INLET TEMP. 85 °F
WALL TEMP. 1300 °F
SYMBOL
DIST. FROM TOP — ft.
1
3
7
9
TEMPERATURE in °F
1300
1250
1200
1150
1100
1050
1000
950
900
0
20
40
60
80
100
120
DISTANCE FROM WALL IN INCHES X 10 3

FIGURE 3·5 —4

measured by sighting through the sample ports with a two-wavelength pyrometer. The agreement between the temperatures measured with the pyrometer and those measured with the wall thermocouples was within expected measurement errors.

Since the geometry of the probe tip was the same as that used by Brown[B13] it would seem that his profiles adjacent to the wall should exhibit the same effect. It is not possible to check his data since he used the extrapolated gas temperature profile to calculate his wall temperature and did not indicate the temperatures which were recorded by the thermocouples on the outer wall. He does report however that his results were obtained at "nominal wall temperatures" of 100, 500 and 950°C. An examination of his extrapolated wall temperatures reveals in some cases that the extrapolated temperature deviates from the "nominal temperature" by as much as 50°C. This deviation could indicate that the probe was not measuring the correct temperature close to the wall, but without more information no positive conclusion can be drawn.

Brown correlated his results in terms of N_{Nu} versus N_{Gr_D}, i.e. no effect of N_{Re} was noticed. The Nusselt numbers calculated from the measured temperature gradients in this work agree with those of Brown within ± 25%. At this level of agreement it was not possible to detect differences in the convective heat-transfer rates, although the rates calculated in this work would be expected to be less than those of Brown because absorption of thermal radiation by the steam would tend to decrease the temperature gradient at the wall.

The temperatures on Figure 3.5-1 to 3.5-4 are indicated as points but they represent average temperatures at each particular location. The temperatures were calculated from the damped thermocouple-millivolt signal which was recorded for 30 sec. to 1 min. The damping was sufficient to allow a relatively constant reading over the entire time interval. At the first two positions adjacent to the wall and over the centre 6 in. of the column the recorder traces were straight lines and the uncertainty of the measurements was ± 2°F as indicated in Section 3.3.6. For the remaining radial positions the maximum deviation of the trace was ± 1 division on the recording paper. This represents an actual millivolt uncertainty of ± 0.08 mv. which corresponds to ± 15°F.

The root-mean-square temperature fluctuations, at the radial traverse location closest to the wall (0.002 in.) were found to vary from approximately ± 7°F at the lowest axial location to ± 18°F near the top of the column. This increase in the magnitude of the temperature fluctuations would appear to indicate that the turbulence level was higher in the upper regions of the column than in the lower regions. This would be expected if the natural-convection forces were large enough to cause a flow reversal at the wall. This upward flow of gases would tend to increase in volume and velocity as the gas moved upward along the wall. The resultant effect on the forced-flow might be expected to manifest itself in an increased level of turbulence caused by the interaction between the two flow fields. The maximum r.m.s. fluctuations, which occurred near the top of the column were of the order of ± 170°F.

Near the top of the column (Ports 1 and 2) this maximum occurred at distances of 0.5 to 1-in. from the wall.

The calculation in Appendix C.2 indicates that for the particular thermocouple employed in these measurements, the indicated millivolt fluctuation can be expected to be within 98% of the millivolt fluctuation corresponding to a temperature fluctuation in the gas stream.

(ii) Particulate System

The curves in Figure 3.5-5 are typical temperature profiles taken with the aspiration probe for a particulate and a single-phase flow under the same experimental conditions. The estimated flow of spray was 15 lb./hr. The indicated temperatures are the eye-averaged temperatures taken from the millivolt trace on the single pen recorder. These average temperatures have a deviation of $\pm$ 25°F near the wall, gradually decreasing to $\pm$ 10°F at the centre line. The peak-to-peak fluctuations were a maximum near the wall and found to be of the order of $\pm$ 75°F.

The effect of introducing the spray into the system can be seen in the decreased gas temperatures across the diameter of the column. The indicated profiles are intended only as a qualitative illustration of the effect of introducing a large heat sink into the system in the form of a cloud of droplets.

The temperatures for the particulate system differ from those measured by Hoffman and Gauvin[H4] in two ways

1. The temperature gradient is observed to extend to the centre-line of the column.

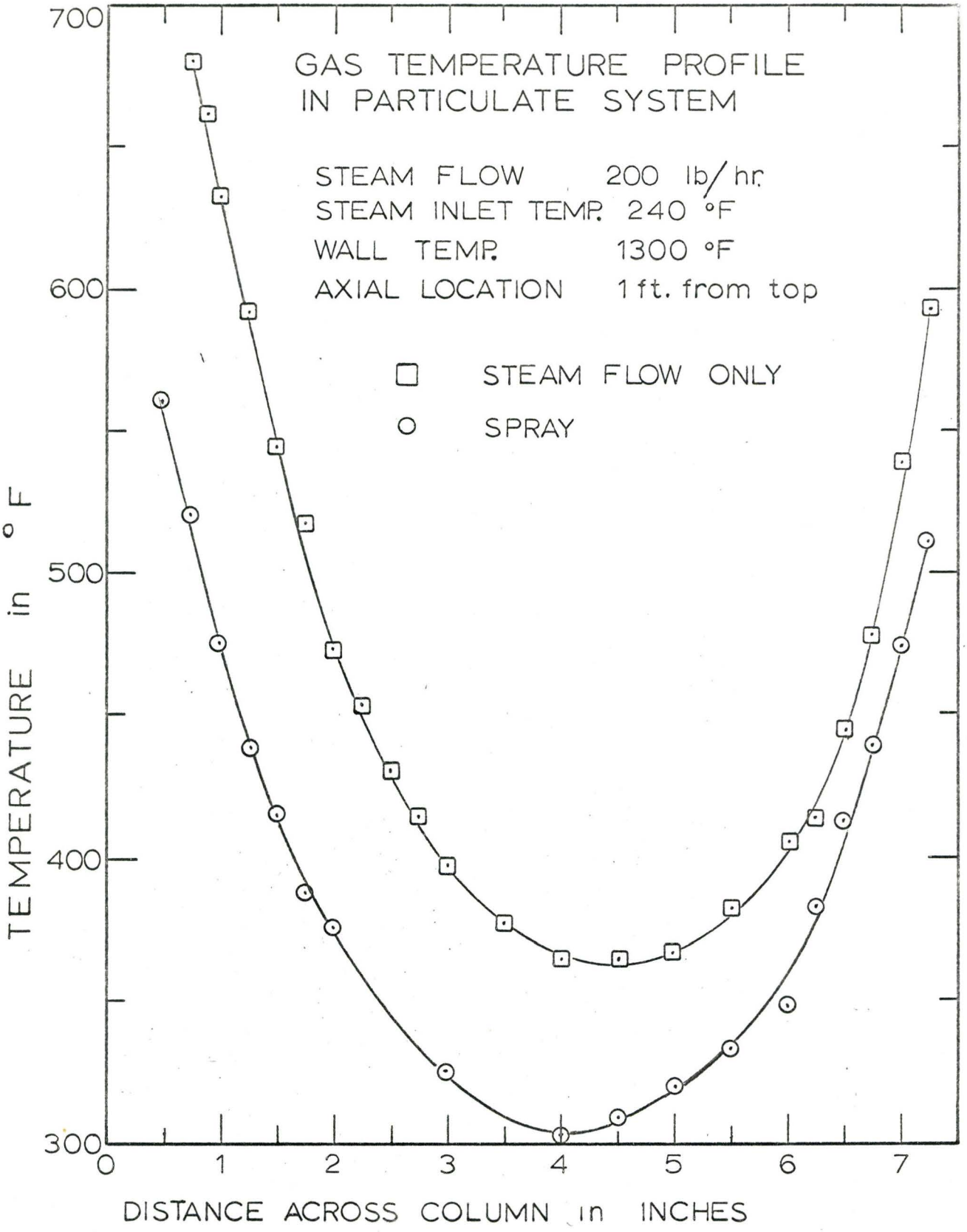
GAS TEMPERATURE PROFILE
IN PARTICULATE SYSTEM
STEAM FLOW 200 lb/hr.
STEAM INLET TEMP. 240 °F
WALL TEMP. 1300 °F
AXIAL LOCATION 1 ft. from top
STEAM FLOW ONLY
SPRAY
TEMPERATURE in °F
700
600
500
400
300
0
1
2
3
4
5
6
7
DISTANCE ACROSS COLUMN in INCHES

FIGURE 3·5 –5

2. the magnitude of the fluctuations is approximately 10 to 20 times greater than that which they reported.

These results are in keeping with those of Brown[B13] and this work for a single-phase system.

Since visual observation indicated that the spray was uniformly distributed over the column cross-section and since the inlet steam temperature was only 240°F, the measured gas temperatures are higher than expected. At such a short distance into the evaporator one would expect that the high heat transfer rates between the gas and the spray, which occur as a result of the large surface area presented by the spray, would maintain the gas at a relatively low temperature.

The relatively high temperatures for both the particulate and single phase systems, as well as the large temperature fluctuations, would suggest that hot gases were flowing up along the walls because of large buoyancy forces even though the inlet Reynolds number for this gas flow is 1.18×10^4.

Equation (2.6-1) predicts that free convection will influence forced convection if $N'_{Gr} > 1.5 \times 10^6$. A conservative estimate of the Grashof number for this experiment is 1×10^9, indicating that natural or free convection is very important. Thus one might expect to find large volumes of hot gas rising to the top of the column, causing turbulence and increased evaporation rates of the spray.

3.5.2 Determination of Flow of Spray to the Evaporator

The concentration of M_n^{++} in the run-off was determined as indicated in the procedure. This technique allowed the determination of the absolute and relative amounts of the liquid which proceeded through the system.

Table 3.5-1 indicates the per cent of the spray generated by a 22B pneumatic nozzle which was actually transported to the evaporator section under various flow conditions.

Comparison of Test 1 and 2 indicates that for approximately the same feed rate, the magnitude of wall impingement increases as the pressure of the atomizing gas increases. This is to be expected since the spray angle increases with increasing pressure thus giving the spray a greater radial velocity component.

Tests, 3, 4, 5 and 6 indicate that increasing the flow rate of carrier gas (steam) decreases the wall impingement. The impingement is decreased because the higher carrier-gas flow rates more nearly satisfy the gas volume requirements of the expanding jet. Consequently less gas is required from the lower regions of the column and the degree of back-mixing with its inherent turbulence is reduced. The decreased back-mixing means fewer drops will be flung to the walls as they attempt to follow the turbulent eddies and the large-scale gas flow patterns.

A comparison of tests 6 and 7 indicates that at the same carrier gas flow rate, the column loading can be increased by increasing the feed rate although the per cent of the feed which

TABLE 3.5-1 : Run-Off Analysis

Test No.	Feed Rate (cc/min)	Atomizing Pressure (p.s.i.g.)	Carrier Gas Flow (lb./hr.)	Total Runoff* (cc/min)	Feed in Runoff** (cc/min)	Feed Through Column*** cc/min	lb./hr	% of Feed Going to Evaporator
1	198	25	0	257	86	112	14.8	56
2	208	52	0	270	147	55	7.3	26
3	210	52	162	330	130	80	10.6	38
4	235	52	162	355	151	84	11.1	36
5	202	52	285	295	118	84	11.1	42
6	208	52	285	300	114	94	12.4	45
7	378	60	285	470	258	120	15.9	32
8	378	60	162	500	300	78	10.3	21

* The reported run-off rates are the average of at least three measurements. The precision of all these readings is ± 5 cc/min.

** The feed in the run-off was determined from the average of three separate samples. The precision was always better than ± 5 cc/min.

*** The absolute or relative errors are not indicated because the results were only interpreted qualitatively.

flows through the column is decreased. The per cent is decreased because at the higher flow rates the spray has a higher kinetic energy and a greater fraction of the spray will strike the walls before the terminal velocity is reached.

Tests 7 and 8 further substantiate the trends observed in tests 2 through 6.

These tests were made without regard to the resultant drop-size distribution. With a constant liquid feed rate, as the pressure of the atomizing gas is increased, the average drop size decreases, hence producing a lower d_{vs}. Thus although test 1 has a larger spray throughput than test 2, the drop-size distribution would be much wider and the average drop size would be larger. Also, tests 7 and 8 would have a wider distribution and larger average drop size than tests 3 through 6 because of the relative increase in liquid feed rate compared to the increase in atomizing pressure.

The results in Table 3.5-1 follow the expected trends and illustrate that the $M_nSO_4 \cdot H_2O$ colorimetric tracer technique enabled the actual spray throughput to be determined.

3.5.3 Drop-Size Determinations

Preliminary tests with the sampling probe indicated that drop samples of reasonable density could be obtained with cell exposure times of 0.2 - 0.7 seconds. During these tests the samples were taken from the column under ambient conditions, i.e., the column was not heated.

When the column was hot (1300^{o}F) it was not possible to obtain dense enough samples from any axial location in the column even with exposure times in excess of 2 seconds. The reason for this apparent absence of droplets was not obvious since

1. the spray was observed (through the viewing ports) to be flowing axially as a well-controlled two-phase mixture in the column above the evaporator
2. calculations indicated that no more than 15% of the spray should be evaporated when the cloud descends as far as the first sampling station on the evaporator.

Furthermore it can be easily shown (Appendix C) that for a mass flow rate of 5 lb./hr. and a volume mean diameter of 50 microns, if the exposure time of the cell is one second and the spray is uniformly distributed across the column, the number of drops in the sample should exceed 5000. If a correction for the target efficiency of the samples were included, the number of droplets actually caught in the cell would not be reduced to the extent that the observations suggest.

3.6 Conclusions

The temperature measuring device used in the single-phase system was not capable of measuring the correct magnitude of temperature in the steep temperature gradients adjacent to the wall. An examination of Brown's data[B13] revealed that his device may have suffered from the same defect. Also, a comparison of the results obtained with these two probes did not reveal an effect of radiation on the temperature profile and hence convective heat transfer rate.

It is essential that the effect of the measuring device upon the temperature of the gas be eliminated if convective heat transfer rates are to be determined with a reasonable degree of confidence.

Gas temperature measurements, made with a fine wire aspiration - thermocouple probe in a particulate system, indicated that radial temperature gradients existed from the wall to the centre-line of the column.

A mathematical simulation of the process requires that the column be divided into a number of finite, isothermal zones. In the original model[H1] the assumption was made that no radial gradients existed in the column and consequently the zones were taken to be right-circular cylinders. These results show that this assumption is not valid and that the model of the system must include an allowance for the radial gradient. Erkku[E1] has calculated the necessary "radiation reception factors" which would permit the column to be zoned in both the axial and radial directions.

The large temperature fluctuations, the high temperature level, and the apparent absence of a dense spray in the upper regions of the evaporator suggest that the natural-convection interaction with the forced-convection flow field is significant. It appears that large volumes of hot gas were rising next to the wall and then mixing and descending with the main flow in the column above the evaporator thus giving rise to large-scale recirculation. This supply of hot gases would cause considerable evaporation of the spray as it descended as far as the first sample port, thus accounting for the apparently low cloud density.

The temperature measurements made with and without the spray indicated that, as expected, the spray does represent a large heat sink which causes a large decrease ($\sim 100^{\circ}F$) in the gas temperature.

The recirculation volume and gas-flow patterns were unknown at the time and consequently a quantitative analysis of the heat transfer phenomena occurring in the system was not possible. A quantitative analysis of the heat transfer would be possible only if

1. the velocity profiles in the column were known, or
2. the natural convection effects causing the flow reversal and resultant interaction were greatly reduced or eliminated.

The actual volume of the liquid feed which entered the evaporator as a cloud of droplets could be successfully determined by a tracer-colorimetric-analysis technique.

PART II

SCOPE

The results from Part I of this study indicated that the large natural-convection forces which occur in A.S.T. systems interact with the forced flow and cause increasedturbulence and complicated flow patterns. These effects increase immensely the difficulty of the analysis of the system; in fact a comprehensive analysis is not possible until the flow patterns and turbulence level have been quantitatively determined.

Rather than embark upon a study of the gas flow patterns in an opposed forced convection-natural convection system, it was decided that a greater insight into the overall process could be gained by dividing the overall problem into a number of separate idealized studies. It was hoped that the results from these studies could then be applied to the complete system to yield a more quantitative description of the phenomena occurring therein.

In keeping with this decision then, Part II of this work was divided into three studies

(i) Convection from the walls to the gas

(ii) Radiation and convection from the walls to the gas

(iii) Radiation to a cloud of evaporating droplets

To permit these phenomena to be studied it was necessary to reduce as much as possible, the complicated effects of natural convection. Since the Grashof number, which is a measure of the magnitude of natural-convection forces, is dependent on the length of the heat-transfer surface

to the 3rd power, the magnitude of the natural convection forces could be reduced by a factor of 1000 by reducing the length by a factor of 10. To achieve a reduction of this magnitude, the length of the evaporator was decreased from 10 ft. to 1 ft., keeping the same column diameter.

Since the length of the column was 1 ft. and the diameter 8-in., the length-to-diameter ratio of the entire hot zone was only 1.5. This meant that the convective heat transfer from the wall was occurring in the so-called entrance region, where the gas-temperature profile is not fully developed, i.e. the thermal boundary layer is still growing and has not yet reached the centre-line of the column. A search of the literature indicated that no experimental or theoretical analyses had been made for convective heat transfer at these small length to diameter ratios. Consequently, it was necessary to develop a theoretical prediction for the heat transfer by convection at small L/D ratios and to verify these predictions by experiment.

The results from the study of convection were then combined with the theoretical analysis of gas radiation to indicate the effect of the two mechanisms of heat transfer on the gas-temperature profiles in the column.

After it was shown that the convection and radiation heat transfer to a gas could be predicted with reasonable accuracy, these same calculation techniques were to be applied directly to the problem of evaporating sprays in a high-temperature environment. The assumption concerning absorption and reflection of radiation from droplets (asymptotic solution of the Mie

Theory) could be tested by carrying out experiments in which the gas temperature and drop-size distribution could be compared with that predicted.

The second part of this dissertation is divided naturally into three sections. The first section (Ch. 4) discusses the convective heat-transfer analysis, the second section (Ch. 5) discusses the radiation analysis including the convection results and the third section (Ch. 6) reports on the experimental and calculational problems associated with the study of radiation to sprays in a high-temperature environment.

4. Convection in the Entrance Region

4.1 Introduction

This chapter discusses the theoretical analysis of the convective heat transfer from the walls of a cylindrical column and the experimental program to verify this analysis. The column was 8-in. I.D. with heat applied only over a 1 ft. length to reduce the magnitude of the natural convection forces in the system. Consequently, the entire hot zone, which had a maximum L/D* ratio of 1.5, was in the so-called thermal entrance region where the gas-temperature profile was still developing.

Available correlations in the literature did not extend to these small L/D ratios and did not apply readily to a variable wall temperature boundary condition. Consequently it was necessary to solve numerically the basic heat transfer equations (subject to certain simplifying assumptions) to permit prediction of the convective heat transfer in this system.

The experimental verification of these predictions was made by measuring the gas-temperature profiles in the column by a similar technique to that used in Part I.

4.2 Background

The problem of predicting the convective heat transfer which occurs in flow systems of various geometries has been studied for some time. This discussion does not attempt to give a comprehensive review of the

---

* L/D represents the ratio of the length of the heat transfer surface from the beginning to the diameter of the cylindrical surface.

entire field but is restricted to the problem of predicting the magnitude of the convective heat transfer in the entrance region of a cylindrical column. The discussion is further restricted to fluids which are in fully-developed turbulent rather than laminar flow.

Subject to the limitations noted below, the energy equation describing the heat transfer in a cylindrical tube in which the velocity profile is fully-developed and axial-symmetric is

$$U' \frac{\partial t}{\partial x} = \frac{1}{r} \frac{\partial}{\partial r} \left[r (a + \varepsilon_h) \frac{\partial t}{\partial r} \right] \qquad (4.2\text{-}1)$$

To write (4.2-1) in this form, the following assumptions were made.

1. The mean value of the radial velocity, V, is zero.
2. The fluid properties are constant
3. Viscous dissipation is negligible
4. Axial diffusion of heat is negligible compared to axial bulk convection*
5. The radial transport of heat due to turbulent diffusion can be accounted for by introducing the thermal diffusivity ε_h.

Sparrow et al[S19] reduced the axial-symmetric energy equation (4.2-1) to a dimensionless form which was linear in temperature and independent of the continuity and momentum equations. In other words, the authors neglected the effect of heat transfer on the velocity profile and vice-versa. They assumed that the velocity profile was fully

---

* Schneider[S22] has indicated that this assumption is valid for $N_{Re}\ N_{Pr} > 100$.

developed and hence not a function of axial distance. If these assumptions were not made, the energy equation would have to be solved simultaneously with the momentum equation. These "coupled" equations would then be non-linear and the problem of determining the solution becomes formidable.

The authors separated the temperature field into two regions; a fully-developed and an entrance region. The wall boundary condition in both regions was that of constant heat-flux at the wall. The temperature was assumed uniform at the entrance to the heat-transfer section and the eddy diffusivity for heat transfer was assumed to be equal to the eddy diffusivity for momentum transfer, i.e., $\varepsilon_h = \varepsilon_m$.

In the fully-developed region the energy equation becomes an ordinary-differential equation which was solved by standard techniques on a digital computer.

In the entrance region the energy equation was solved by using a separation of variables technique on the partial-differential equation. With this assumption, the radial dependence of the fluid temperature was described by an O.D.E. of the Sturm-Liouville type. The solution was given in terms of eigen-functions and their corresponding eigen-values.

The authors give the first six eigen-functions and eigen-values for a number of Reynolds number and Prandtl numbers.

The predicted Nusselt numbers, (hD/k), as a fuction of the dimensionless distance along the tube (x/D), did not extend to x/D's < 2 because the series solution was truncated at 6 terms; to predict the heat transfer at smaller values of x/D, a larger number of terms must

be included in the series solution of the energy equation.

Sleicher and Tribus[S20] also solved the energy equation, subject to the same limitations imposed by Sparrow et al[S19], by the same mathematical techniques. They determined only the first three eigen-functions and eigen-values by solving the appropriate equations on an analog computer and consequently they too were unable to predict the heat transfer at small values of x/D. These authors indicated how their results could be used to predict the heat transfer for the following boundary conditions at the wall;

1. constant heat flux
2. uniform temperature
3. arbitrary wall-temperature profile.

Both Sleicher and Tribus[S20] and Sparrow et al[S19] found that, when x/D was large enough so that the temperature profile was fully-developed, their predicted Nusselt numbers agreed with the empirical correlation originally proposed by Dittus and Boelter[D14]:

$$N_{Nu} = 0.023\, N_{Re}^{0.8}\, N_{Pr}^{0.4} \qquad (4.2\text{-}2)$$

Both of these analyses assumed constant properties which enabled the energy equation to be solved independently of the momentum equation; i.e. the effect of temperature on the velocity profile was neglected. Consequently the analytical results are expected to predict the convective heat transfer only for the case of low heat flux or small wall temperature-to-bulk gas temperature ratios. These analyses used the fully-developed, adiabatic, velocity and momentum diffusivity profiles from Deissler's analysis[D11].

In a later paper, Siegel and Sparrow[S21] compared the Nusselt numbers calculated with a uniform wall-temperature and constant heat-flux boundary condition at x/D's > 2. They showed that the N_{Nu} calculated for the two different boundary conditions approached one another at large N_{Re} and large x/D. However for a Reynolds number of 10,000 and an x/D of 2 the two predictions differed by 9%. Thus in the N_{Re} range used in this present study (10×10^3 to 20×10^3) and at x/D's < 2, Siegel and Sparrow's analysis indicates that the N_{Nu} predicted from the constant heat-flux boundary condition can not be used to predict the heat transfer for a uniform wall-temperature boundary condition.

Deissler[D11] also solved the energy equation in the entrance region. He did not solve the equation numerically but obtained an analytical solution by employing an integral boundary-layer analysis; i.e. he assumed that the temperature and velocity profiles in the boundary layer were of the same shape as those which exist in fully-developed flow and then calculated the increase of the thermal boundary layer with distance from the entrance.

Deissler's analysis also neglected the effect of temperature on the velocity profile but he did allow for property variation with temperature in the energy equation. He assumed Cp and N_{Pr} were constant and described the viscosity and thermal conductivity by the following relationship.

$$\frac{\mu}{\mu_w} = \frac{k}{k_w} = \left(\frac{T}{T_w}\right)^{0.68} \qquad (4.2\text{-}3)$$

Deissler's analysis is thus more applicable to systems which have an appreciable heat flux because of this allowance for property variation although at large heat fluxes the velocity profile is expected to be appreciably affected.

Deissler's analysis, at low heat flux, is compared to that of Sparrow et al [S19] in Figure 4.2-1. It will be noted that even under low heat-flux conditions where the property effects are not important, Deissler predicts a lower rate of heat-transfer in the entrance region. This predicted lower heat-transfer rate may be caused by the original assumption of a boundary layer with known velocity and temperature profiles. The experimental data of Magee [M8] and Hall and Price [H18] agree more closely with the predictions of Sparrow et al than those of Deissler. These workers [M8, H18] did not measure gas temperature profiles but determined the heat transfer coefficients from a heat balance at the wall.

Hall and Price employed a 1-in.-diameter column which was constructed of 30, 1-in. long separate heaters; each one had a thermocouple mounted on the outer wall. They were thus able to determine the average heat-transfer rate for each of these sections. Although they report a heat-transfer coefficient at an x/D of ½, this value is the average over the first section, ($0 \leq x/D \leq 1$). It should be noted that although the heat-flux distribution could be varied along the column, the heat flux was constant over any one section.

Magee measured heat-transfer rates in a 0.129-in. and 0.250-in. I.D. Hastelloy tube with a constant heat-flux at the wall. The wall

temperature was never measured at an x/D < 0.93 and the correlation of his results does not extend below an x/D of 2. Both of the above workers applied electrical energy directly to the walls of the tube.

Wolf[W4, W5] used Deissler's analysis but changed the exponent on the temperature ratio used to predict the property variation (equation 4.2-3). His predicted heat-transfer rates differ very little from those of Deissler.

Magee[M11] has solved the energy equation by writing the P.D.E. in finite-difference form and solving the resulting equations on a digital computer. He made the same assumptions as Sparrow et al but allowed for property variation in the energy equation. He used Deissler's expression for the radial variation of the momentum diffusivity (ε_m) and neglected the distortion of the velocity profile due to the dependence of viscosity on temperature. He employed a constant wall-flux boundary condition and at low fluxes found that his predicted and measured heat transfer rates agreed with the predictions of Sparrow et al.

Magee also measured the static pressure at various axial locations in the entrance region and correlated his results in terms of the friction factor, (f), with the following expression

$$f/2 = f'/2 \cdot (T_w/T_b)^{k-0.16} \qquad (4.3\text{-}4)$$

where $k = 0.701 - 0.168 \ln (x/D)$

and f' = standard "Nikuradse" friction factor.

This friction factor correction, which allowed for entrance effects, was obtained for values of x/D > 5.

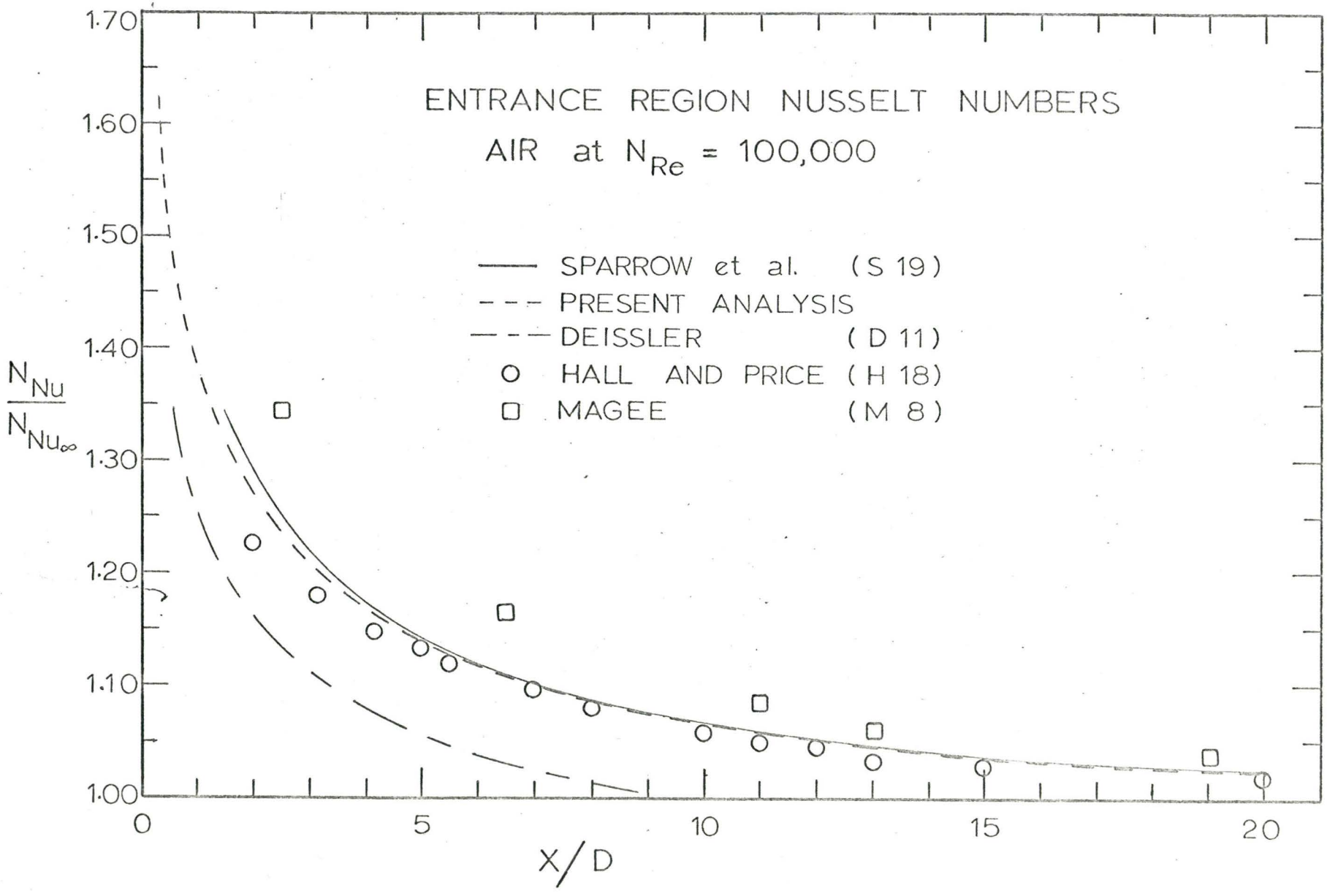
ENTRANCE REGION NUSSELT NUMBERS
AIR at N_{Re} = 100,000
SPARROW et al. (S 19)
PRESENT ANALYSIS
DEISSLER (D 11)
HALL AND PRICE (H 18)
MAGEE (M 8)
$\frac{N_{Nu}}{N_{Nu_\infty}}$
1.70
1.60
1.50
1.40
1.30
1.20
1.10
1.00
0
5
10
15
20
X/D

At high heat fluxes, characterized by a large wall-to-bulk temperature ratio, (T_w/T_b), Magee correlated the results of his theoretical analysis for the entrance region by the following equation

$$N_{Nu} = 0.205 \cdot N_{Re}^{0.8} \cdot N_{Pr}^{0.4} \cdot (T_w/T_b)^{-0.4} \left[1 + 0.6\, D/x \cdot (T_w/T_b)^{0.4} \right] \qquad (4.3\text{-}5)$$

where the physical properties were evaluated at the fluid bulk temperature. His experimental results for air were predicted by this correlation at low heat fluxes but at high heat fluxes the experimental results were 10 - 25% higher than the correlation predicted. This discrepancy at the higher heat fluxes may be due to the effect of temperature on the velocity profile; i.e., natural-convection forces are altering the shape of the velocity profile and increasing the turbulence level.

Perkins and Worsoe-Schmidt[P15] determined heat-transfer rates to turbulently flowing nitrogen at temperature ratios, (T_w/T_b), up to 7.5 in an electrically heated inconel tube. They correlated their heat-transfer results in a similar manner to Magee and suggested the following correlation

$$N_{Nu} = 0.024\, N_{Re}^{0.8}\, N_{Pr}^{0.4} \cdot (T_w/T_b)^{-0.7} \left[1 + (x/D)^{-0.7}\, (T_w/T_b)^{0.7} \right] \qquad (4.3\text{-}6)$$

where properties are evaluated at the bulk temperature. This equation correlates their results within ± 20% for $1.2 \leq x/D \leq 40$. For $x/D > 40$ the "entrance effect" term is removed from the correlation (4.3-6).

It should be noted that these workers[M8, P15] and others (see bibliographies in reference M8, P15, D12) working at high heat

fluxes (large T_w/T_b) have correlated their results by using a modified forced-flow correlation. While these correlations may predict the heat transfer it should be remembered that they are not based upon a true physical analysis of the system; i.e., they have not considered the influence of natural convection which could be expected to influence the heat transfer under these high wall-to-bulk temperature differences. Consequently care should be exercised when using these correlations to ensure that one is not extrapolating beyond the range of the correlation.

None of the above workers has measured the temperature and velocity profiles in the gas stream. They obtained their heat-transfer results by heat-flux and wall-temperature measurements. Johnk and Hanratty[J3] actually measured gas-temperature profiles for air, in turbulent flow, in the entrance region of a smooth pipe, at a constant low heat flux (approximately 70 B.T.U./hr. sq.ft.). Their measured heat-transfer coefficients agree fairly well at a N_{Re} of 50,000 with the analysis of Sparrow et al[S19].

While no direct comparison to Deissler's analysis[D11] was made, Johnk and Hanratty's results indicate that the heat-transfer rates predicted by Deissler are too low in the entrance region. Their temperature profiles indicate that in the heat-transfer entry region there is a portion of the temperature profile close to the wall which is described by the fully-developed relation as Deissler assumed. However their results also indicate that there is not a sharp transition between the fully-developed profile near the wall and the uniform temperature region in the centre as Deissler assumed. They further showed that the position

where the temperature profile was completely developed was much further downstream than Deissler assumed. These discrepancies between Deissler's assumptions and Johnk and Hanratty's measurements might help to explain the low predictions of Deissler.

Johnk and Hanratty calculated ε_h from their experimental temperature profiles. Their results indicated that ε_h varied with axial distance over the first twelve pipe diameters from the entrance, after which it became constant at any one radial position. However the change with axial distance occurred only at dimensionless radial locations (r/r_w) less than 0.8, i.e., at all positions closer to the wall the value of ε_h was independent of axial position. Consequently the fully-developed ε_h versus radius relationship, which was used by Sparrow et al [S19] in the entrance region, should not lead to a significant error in the predicted temperatures because

1. in the region where the temperature gradient is large ε_h is not a function of x/D
2. in the region where ε_h changes with x/D the temperature gradients are very small.

Johnk and Hanratty report that their results can not be used with any accuracy at $x/D < 3$ because of inaccuracies in their temperature measurements close to the wall. This, along with the fact that their results were obtained under constant heat-flux conditions does not allow their results to be used in this investigation for the prediction of heat transfer in the entrance region.

The literature does not yield a heat-transfer correlation which can be used with any confidence at values of $x/D < 2$ with a constant or

experimentally measured wall-temperature profile. Consequently in the next section the energy equation is solved for the above mentioned conditions with the limiting assumption of constant properties.

4.3 Theoretical Analysis

4.3.1 Introduction

This chapter presents an analysis of the heat transfer occurring in the thermal entrance region for the turbulent flow of a gas through a heated cylindrical tube. The governing equations are reduced to forms similar to those used by Sparrow et al [S19], and then made non-dimensional. With the assumption that the energy and momentum equations are independent (i.e., the distortion of the velocity profile due to viscosity variation can be neglected in the energy equation), a finite-difference approximation to the dimensionless energy equation is made, and solved on a digital computer.

4.3.2 Governing Equations

(i) Assumptions and Restrictions

1. The flow is steady, turbulent and subsonic.
2. Time-averaged velocities and temperatures can be used in the energy equation.
3. The flow is axial-symmetric (angular dependence can be neglected).
4. The mean value of the radial velocity is zero.
5. Viscous dissipation can be neglected.

6. Axial diffusion of heat (molecular and turbulent) is much less than axial bulk convection of heat and can be neglected.

7. The velocity profile is fully developed.

8. The fluid properties are constant.

9. The turbulent mechanism for heat transfer is the same as the turbulent mechanism for momentum transfer, i.e., $\varepsilon_h = \varepsilon_m$.

(ii) Energy Equation

A diagram of the co-ordinate system used is shown in Figure 4.3-1.

Figure 4.3-2 indicates the energy balance made on a differential-control-volume in the cylinder. This balance yields the following parabolic partial-differential equation.

$$\rho Cp\ U' \frac{\partial t}{\partial x'} = \frac{1}{r} \frac{\partial}{\partial r} (rk \frac{\partial t}{\partial r}) + \frac{1}{r} \frac{\partial}{\partial r} (r\rho Cp\ \varepsilon_h \frac{\partial t}{\partial r}) \qquad (4.3\text{-}1)$$

which can be rearranged and simplified to

$$U' \frac{\partial t}{\partial x'} = \frac{1}{r} \frac{\partial}{\partial r} [r(a + \varepsilon_h) \frac{\partial t}{\partial r}] \qquad (4.3\text{-}2)$$

(iii) Dimensionless parameters

The following dimensionless variables will now be defined.

$$x = x'/r_w \quad ; \quad R = r/r_w \ ;$$

$$U = U'/\sqrt{T_w/\rho_w}; \quad T = (t - t_i)/(t_w - t_i);$$

$$RO = r_w \sqrt{T_w/\rho_w}\ /\mu_w/\rho_w \ ;$$

$$G = (a + \varepsilon_h)/\mu_w/\rho_w = \frac{1}{N_{Pr}} + \varepsilon_h/\mu_w/\rho_w$$

DIAGRAM OF THE CO-ORDINATE SYSTEM USED

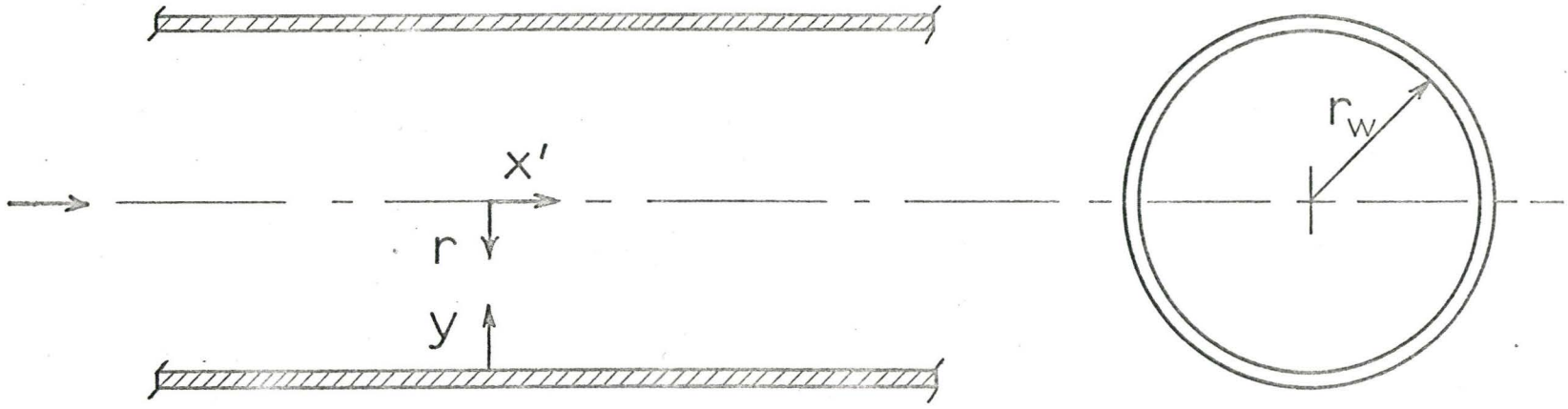

FIGURE 4·3-1

ENERGY BALANCE ON A CONTROL VOLUME

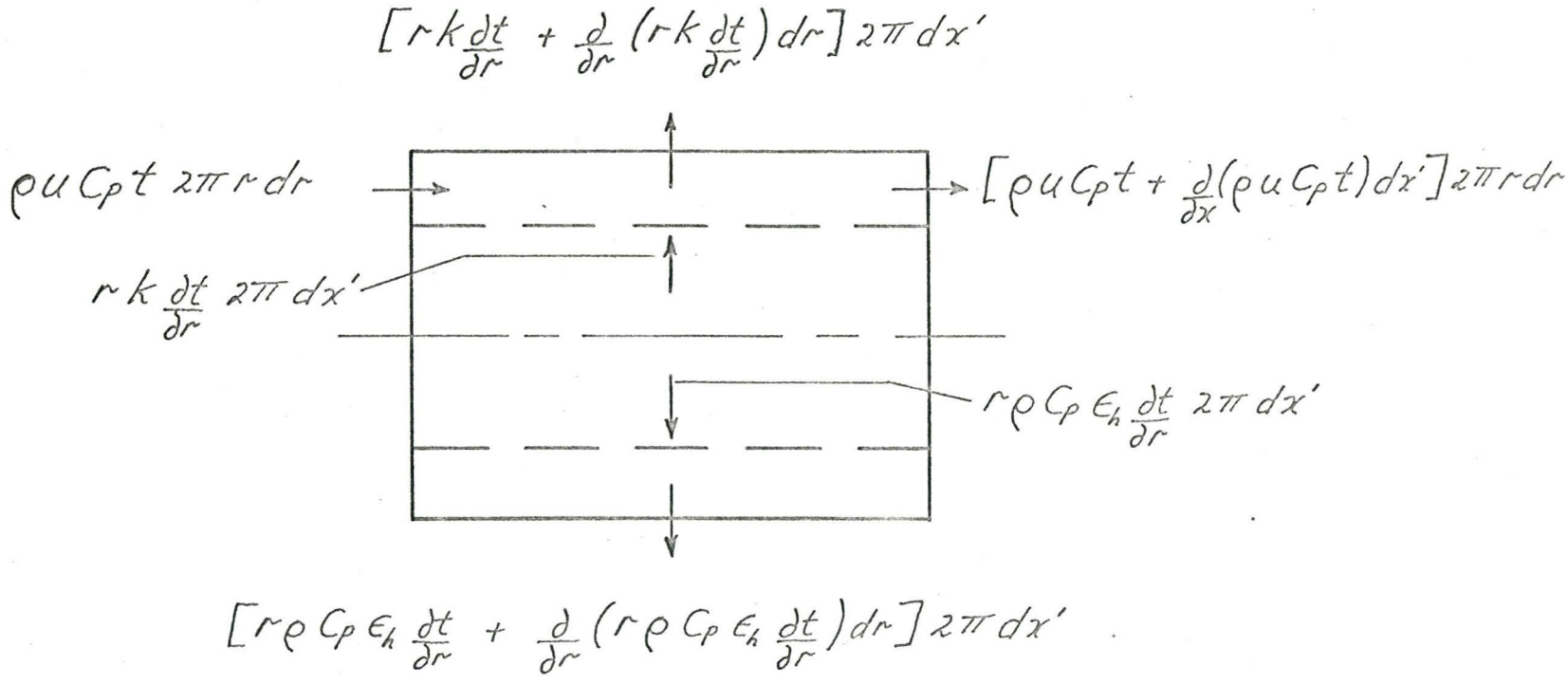

FIGURE 4·3–2

Inserting these variables into equation (4.3-2) and simplifying yields

$$RO \cdot U \frac{\partial T}{\partial x} = \frac{G}{R} \frac{\partial T}{\partial R} + \frac{\partial G}{\partial R} \frac{\partial T}{\partial R} + \frac{\partial^2 T}{\partial R^2} \qquad (4.3.-3)$$

for the non-dimensional energy equation.

(iv) Boundary Conditions

1. $T(R,0) = T_i(R)$ (inlet gas temperature profile known)
2. $T(1,x) = T_w(x)$ (wall temperatures known)
3. $\frac{\partial T}{\partial R}(0,x) = 0$ (axisymmetrical temperature profile)

(v) Dimensionless Velocity Distribution

The dimensionless velocity profile given by Deissler[D13] for fully developed, turbulent, adiabatic flow was used in this analysis. Deissler's definition of dimensionless distance from the wall is given as

$$y^+ = y \sqrt{T_w/\rho_w} \; / \; \mu_w/\rho_w .$$

The previously defined, dimensionless velocity, U, can be calculated now from the following equations

$$U = \int_0^{y^+} dy^+ \; / \; [1 + (0.124)^2 U y^+ (1 - \exp(-0.124)^2 U y^+))] \qquad (4.3.-4)$$

for $y^+ < 26$.

$$U - 12.85 = \frac{1}{0.36} \ln (y^+/26) \qquad (4.3-5)$$

for $y^+ \geq 26$.

(vi) Dimensionless Eddy Diffusivity for Heat Transfer

The dimensionless eddy diffusivity profile given by Sparrow et al [S19] was used in this analysis; using the previously defined dimensionless variables and assuming $\varepsilon_h = \varepsilon_m$ the equations are

$$G = \frac{1}{N_{Pr}} + (0.124)^2 \, U \, y^+ \, [1-\exp(-(0.124)^2 \, U \, y^+] \qquad (4.3\text{-}6)$$

for $y^+ < 26$

and

$$G = \frac{1}{N_{Pr}} + 0.36 \, y^+ \, [1 - y^+/RO] - 1 \qquad (4.3\text{-}7)$$

for $y^+ > 26$

The minus one term appearing on the right side of equation (4.3-7) is retained for $26 \leq y^+ \leq RO/2$ and is deleted for larger values of y^+.

(vii) Gas Properties

The gas properties for air and steam were evaluated at some representative temperature using the correlations given in Appendix B.

(viii) Finite-Difference Equations

Equation (4.3-3) was approximated by a finite-difference equation (see Appendix D.2) and solved on a digital computer. The finite-difference mesh system used in this work is shown in Figure 4.3-3 where the mesh-point locations are labelled. A

variable step-size in the radial direction, similar to that used by Houghton[H19], was used throughout. This yielded a large number of mesh points close to the surface where the temperature gradients are large and a relatively small number of mesh points further from the surface where the gradients are small. A constant step-size was used in the axial direction except for the first axial increment at $x = 0$. This increment was further subdivided into a number of equal steps because of the steepness of the axial gradient close to the wall in this region.

The finite-difference equation could be solved using either explicit or implicit procedures. Explicit methods allow the solution to proceed directly but very small step-sizes were required in the "marching direction" (axial direction in this problem) to ensure a stable solution. In the implicit technique a set of simultaneous algebraic equations must be solved at each step[L10]. The implicit technique is stable even with relatively large steps. Since large sets of algebraic equations can be readily handled using matrix techniques and a digital computer, the implicit technique was employed in this work.

The Crank-Nicholson implicit method[L10] was used to approximate the derivatives in the radial direction and a forward-difference approximation[L10] was used for the derivatives in the axial direction. Details and computer listings may be found in Appendices D.1 and Z.1 respectively.

FINITE – DIFFERENCE MESH SYSTEM

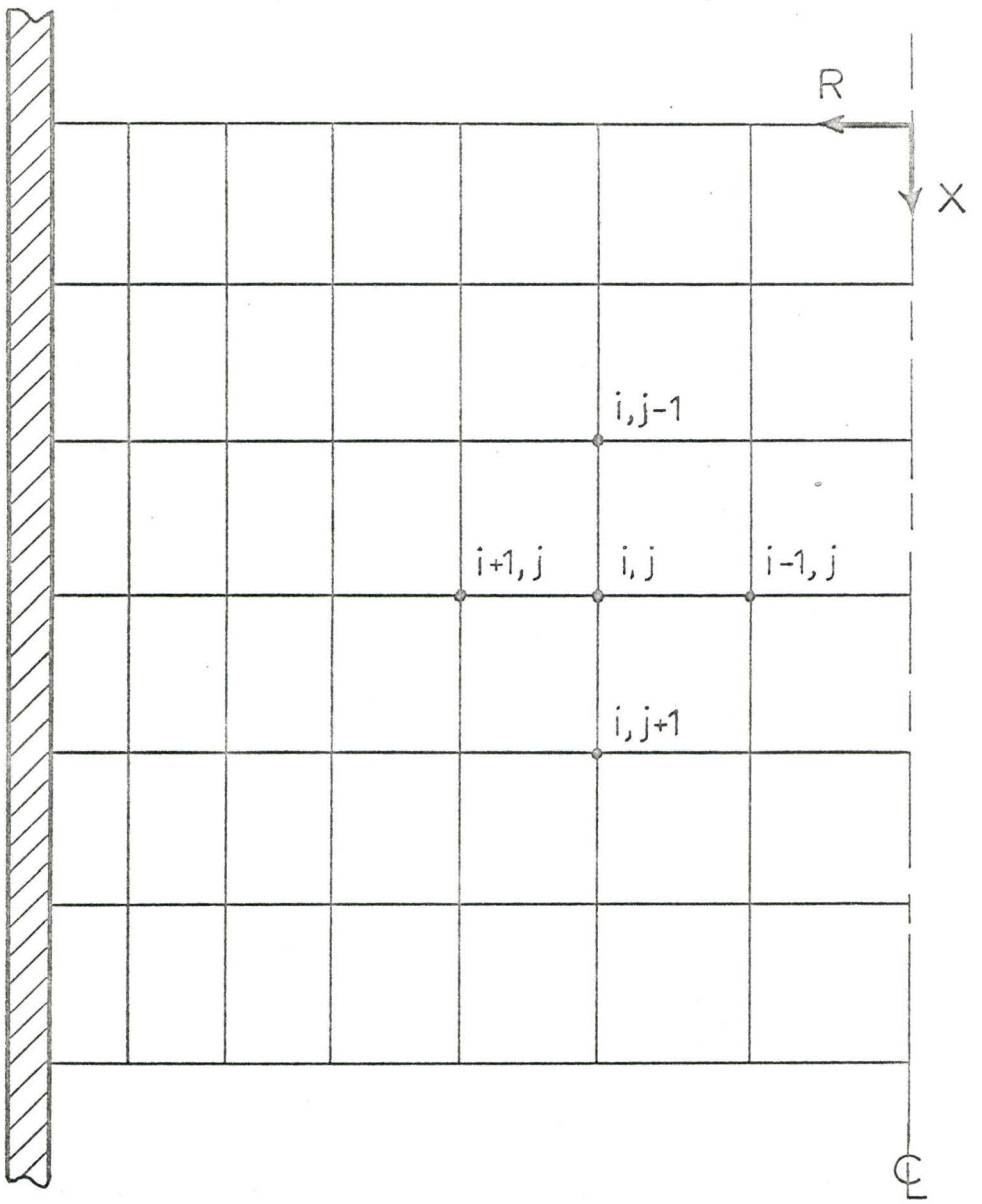

FIGURE 4·3 – 3

4.3.3 Exactness of the Model

The question of whether a numerical solution is a good approximation of the exact analytic solution is normally a very difficult one to resolve except in the trivial case where the analytic solution is available. In cases where general analytic solutions are not known, some indication of the "accuracy" of the numerical results may be obtained by comparing them with any available asymptotic solutions and with experimental results obtained where the physical situation corresponds to the equation and its boundary conditions. An additional criterion very often used is the application of the convergence test, i.e., to decrease the finite-difference mesh size in order to check whether any further change of calculated values occurs. Any terms in the complete differential description of the phenomena which have been neglected for ease of computation should be examined to ensure that the exclusion of such terms is a truly valid assumption. These topics will be covered in the ensuing discussion.

(i) Convergence Test

Extensive convergence tests were carried out by varying the step-sizes in both the axial and radial directions. It was found that Nusselt numbers calculated with 40 mesh points in the radial direction (calculation of mesh points shown in Appendix D.1) did not differ by more than 2% from the Nusselt numbers calculated with 60 mesh points. The computation time for 40 mesh points was in the order of 4 minutes when the calculations were carried to an x/D of 60. For 60 mesh points this time was approximately doubled.

Consequently 40 radial mesh points were used in all computations. The Nusselt numbers calculated with an axial step-size, $\frac{\Delta x}{r_w}$, of 0.0125 did not differ by more than 1% from the Nusselt numbers calculated with a step-size of 0.00625. The computation time was increased by approximately 30% for a step-size of 0.00625 over that required for a step-size of 0.0125. Consequently an axial step-size of 0.0125 was used in all computations which calculated the Nusselt number in the entrance region. When calculating Nusselt numbers at large values of x/D, (>15), a coarser axial grid could be used, i.e., the axial step-size could be increased to 0.125 without changing the predicted Nusselt numbers. This was possible because at relatively large values of x/D the temperature gradient in the axial direction is very small.

(ii) Comparison with Asymptotic Solutions and Other Mathematical Analyses

Table 4.3-1 compares the Nusselt numbers calculated in this work with those of other investigators. The Nusselt numbers calculated for this comparison were for an inlet temperature of 90°F and a wall temperature of 150°F, which corresponds to a low, constant heat-flux boundary condition. The relationships of the other investigators, which were used to calculate the comparative Nusselt numbers, were all developed for the case of a constant heat-flux boundary condition. As Siegel and Sparrow[S21] indicate, however, the Nusselt numbers for the two boundary conditions should be in close agreement at large values of x/D.

Sparrow's values were calculated from the following equation

$$N_{Nu_\infty} = 0.0245\, N_{Re}^{0.77}, \quad \text{for } N_{Pr} = 0.7 \qquad (4.3\text{-}8)$$

Magee's values were calculated from equation (4.3-5) with the entrance parameter omitted.

The Nusselt numbers shown in Table 4.3-1 indicate that the predictions of this analysis are in excellent agreement with those of Sparrow and Magee. This is to be expected since, under the conditions of comparison, the same form of the energy equation was used and the assumptions and boundary conditions were essentially the same.

TABLE 4.3-1 : Nusselt Number Comparison - Theoretical - Large x/D

N_{Re}	Sparrow(S19)	Mageee(M11)	This Analysis
10^5	173.5	173.5	174.2
5×10^4	101.7	99.0	101.2
2×10^4	50.2	47.9	51.0
10^4	29.5	27.0	30.4

The ratio of N_{Nu}/N_{Nu_∞} predicted in this analysis is compared in Table 4.3-2 to that calculated by Sparrow et al in the entrance region. The excellent agreement indicates that the solution of the finite-difference approximation yields a suitable solution to the energy equation but does not indicate the validity of the assumptions used in developing the particular form of the energy equation .

TABLE 4.3-2 : Nusselt Number Comparison - Theoretical - Entrance Region

	$N_{Re} = 10^5$		$N_{Re} = 5 \times 10^4$	
x/D	Sparrow et al	This work	Sparrow et al	This work
2	1.285	1.263	1.293	1.266
4	1.178	1.164	1.178	1.164
6	1.125	1.116	1.123	1.114
8	1.093	1.087	1.090	1.085
10	1.071	1.067	1.068	1.065

(iii) Comparison with Experimental Results

A comparison of the asymptotic, predicted Nusselt numbers with the empirical correlation of Perkins and Worsoe-Schmidt[P15], equation (4.3-6), and with the Dittus-Boelter equation[D14] is made in Table 4.3-3. The latter equation, given as

$$N_{Nu} = 0.023 \; N_{Re}^{0.8} \; N_{Pr}^{0.4} \; , \qquad (4.3\text{-}9)$$

was also determined empirically and has been available as a standard design-equation for years.

TABLE 4.3-3 : Nusselt Number Comparison - Experimental - Large x/D

N_{Re}	Perkins[P15]	Dittus-Boelter[D14]	This Analysis
10^5	199	199	174.2
5×10^4	114	113	101.2
2×10^4	56	55	51.0
10^4	32.4	31	30.4

The above correlations were reported to predict the experimental results within ± 20%. Thus the predicted Nusselt numbers from this analysis are seen to be in satisfactory agreement with experiment at large values of x/D where the temperature and velocity profiles are fully developed.

(iv) Testing the Validity of the Assumptions

Perhaps the most questionable assumption made in this and other analyses is that of negligible axial diffusion in the entrance region where the axial temperature gradients are large compared to those which exist beyond the entrance region.

To check this assumption the energy equation was solved by solving the finite-difference approximation with the axial diffusion term included. The same assumptions were made and the same dimensionless variables were used as in the case of no axial diffusion (equation 4.3-3). It was also assumed that the eddy diffusivity in the axial direction was the same as that in the radial direction at any fixed point in the system. Thus the dimensionless energy equation can be written as

$$RO{\cdot}U\ \frac{\partial T}{\partial X} = \frac{G}{R}\ \frac{\partial T}{\partial R} + \frac{\partial G}{\partial R}\ \frac{\partial T}{\partial R} + G\ \frac{\partial^2 T}{\partial R^2} + G\ \frac{\partial^2 T}{\partial x^2} \qquad (4.3.-10)$$

where it has also been assumed that G is not a function of axial distance; therefore $\frac{\partial G}{\partial x} = 0$. The required boundary conditions are

1. $T\ (R,0) = T_i(R)$
2. $T(1,x) = T_w(x)$

3. $\frac{\partial T}{\partial R}$ $(0,x)$ $= 0$

4. $\frac{\partial T}{\partial x}$ (R,∞) $= 0$

Equation (4.3-9) is elliptic in form and requires that boundary conditions be given at all boundaries of the region to which it is applied. Because of the small axial step-size which must be used in the entrance region, available computer memory did not permit the boundary condition at $x = \infty$ to be utilized. Instead, the temperature profile which was calculated from the solution of the parabolic equation at a particular x/D was used as the downstream boundary condition. It is realized that the calculated temperature profiles would not be necessarily the true profiles but, by comparing the profiles obtained with boundary conditions obtained at different axial distances, the relative importance of axial diffusion could be determined.

The details of the finite-difference equation and its solution are given in Appendix D.2.

Figure 4.3-4 compares the temperature profiles obtained from the parabolic and elliptic forms of the energy equation. The elliptic equation was solved by using the temperature profile obtained from the solution of the parabolic equation at an x/D of 0.00625. Also shown is the temperature profile obtained from the elliptic equation with the boundary temperature profile at an x/D of 0.0313. Since the two profiles calculated from the elliptic equation at different boundary conditions are in close agreement it seems reasonable to assume that the effect of axial diffusion is

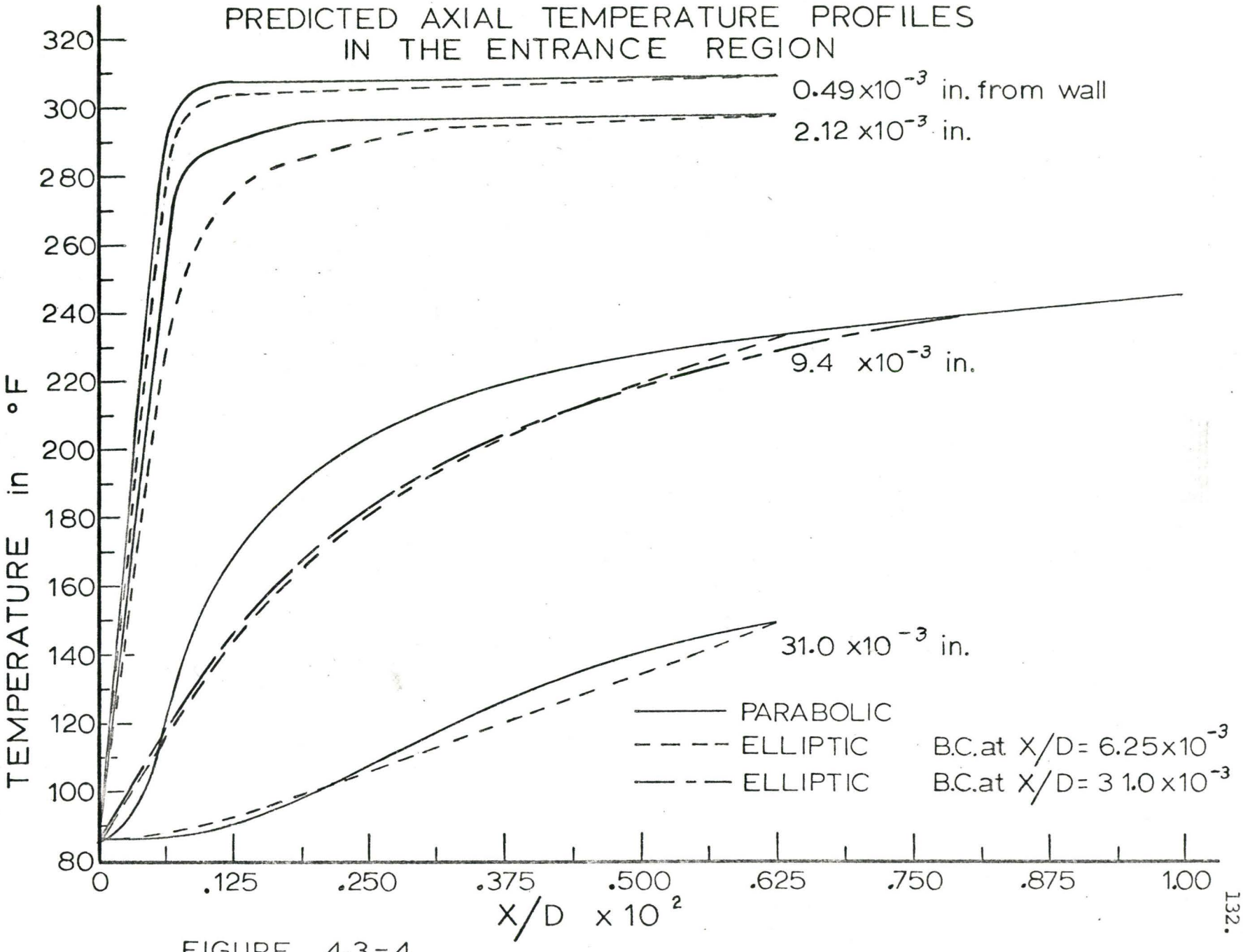
PREDICTED AXIAL TEMPERATURE PROFILES
IN THE ENTRANCE REGION
0.49x10⁻³ in. from wall
2.12 x10⁻³ in.
9.4 x10⁻³ in.
31.0 x10⁻³ in.
PARABOLIC
ELLIPTIC B.C.at X/D= 6.25x10⁻³
ELLIPTIC B.C.at X/D= 3 1.0x10⁻³
TEMPERATURE in °F
320
300
280
260
240
220
200
180
160
140
120
100
80
0
.125
.250
.375
.500
.625
.750
.875
1.00
X/D x 10²

FIGURE 4.3-4

restricted to a very small distance from the entrance. As a further check, the elliptic equation was solved using temperature profiles calculated from the parabolic solution at values of x/D of 0.069 for the initial profile and 0.156 for the downstream profile. No difference was observed between the profiles calculated by the parabolic and elliptic forms of the energy equation over this axial region.

(v) Conclusions

The agreement between the results of this analysis and other theoretical analyses as well as the agreement with empirical correlations of experimental data indicates that a satisfactory solution of the energy equation has been obtained using the finite-difference approximations. The fact that the effect of axial diffusion is restricted to a region where $x/D < 0.01$ indicates the validity of neglecting the effect of axial diffusion in the energy equations under these particular flow conditions. For the case of low Prandtl number fluids, flowing under low Reynolds number conditions, the effect of axial diffusion would have to be re-evaluated.

4.4 Experimental Equipment

4.4.1 Introduction

In this experiment, the atomization and flow-calming sections were placed on top of a short section (8-in. diameter by 14-in. high) of a heated pipe. Spray samples could be obtained before and after the section through sample ports; axial and radial temperature-traverses of the droplet-laden stream could be made over the entire section through the use of a specially-designed port and probe. The details are given below.

4.4.2 Evaporator

The evaporator section was a 14-in. long by 8-in. I.D. stainless steel pipe with ¼-in. walls. The inside walls were sand blasted and painted with "blackening" paint (Pyromark Paint, Tempil Corporation) to insure that the emissivity was as high as possible. The evaporator was flanged at both ends and the wall was reduced to a thickness of $\frac{1}{16}$-in. for a distance of $\frac{7}{8}$-in. at each end to reduce conduction heat-losses out the ends. A drawing of the furnace section is shown in Figure 4.4-1. The column also had two ¼-in. wide by $\frac{5}{32}$-in. deep grooves located $2\frac{5}{8}$-in. from each end which helped to isolate the end-heaters on the column and thus further facilitated the attainment of isothermal conditions on the furnace walls.

To further compensate for heat losses through the flanges two 0.440-in. diameter circular-heating-elements were clamped into grooves cut in the underside of each flange. The 1500 watt incoloy elements had a radius of curvature of $4\frac{13}{32}$-in. and were custom made by the Canadian Chromalox Company (Catalogue No. T1 3545 WLOF Tubular Element).

EVAPORATOR SECTION

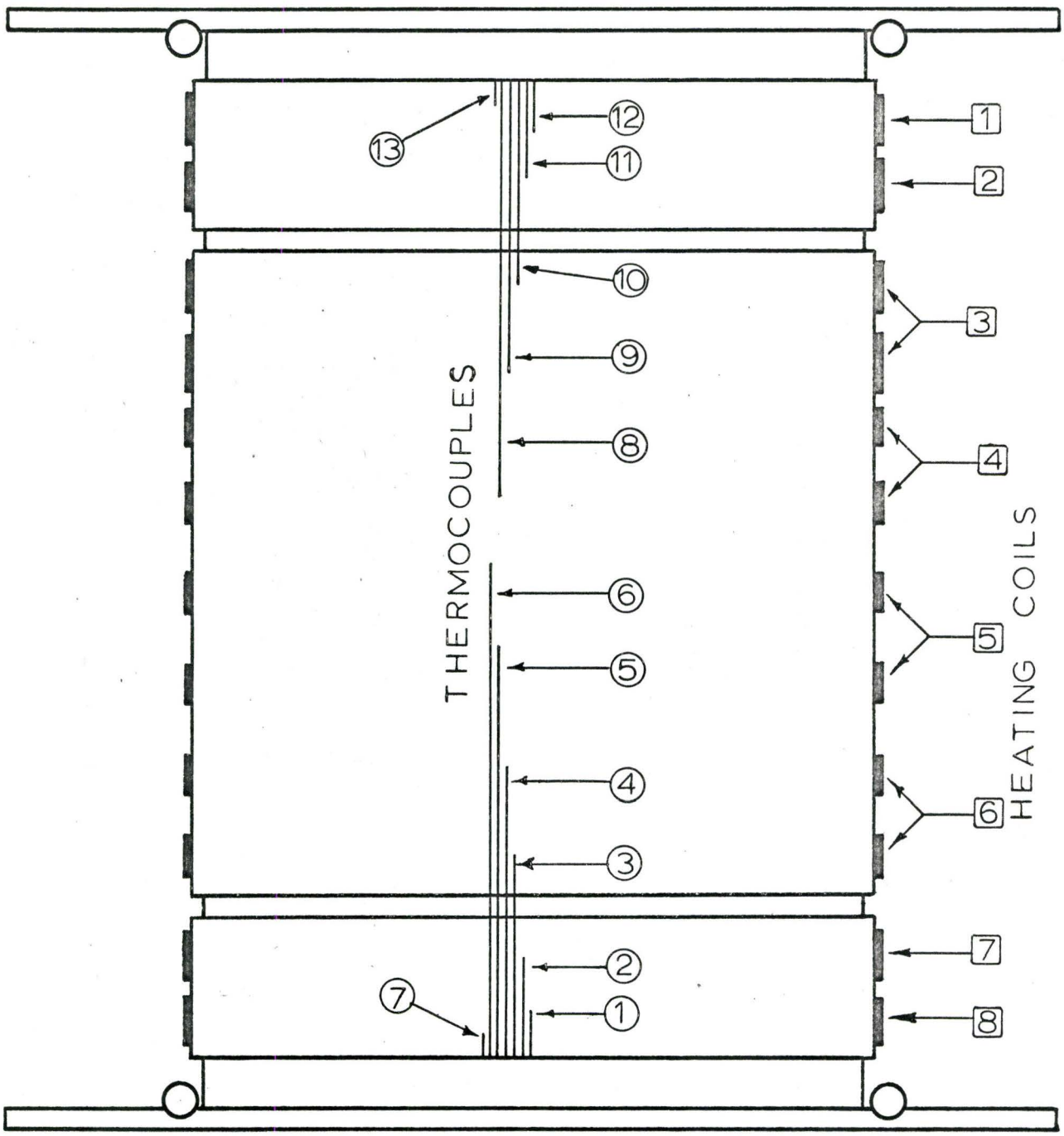

FIGURE 4·4—1

Power was supplied to these elements by two 2.8 k.v.a. variable transformers (Superior Electric, 2PF-136).

Heat was supplied to the column via Kanthal A-1 heating strip which was wound directly onto the column on a ¼-in. thick layer of refractory cement (Kaiser Refractories, Hiloset). The strip was then covered with a ¼ to ½-in. thick layer of the same cement. A photograph of the furnace section just prior to installation is shown in Figure 4.4-2. The outer cement layer and strip extensions for electrical connections can be seen in the Figure.

The strip size and spacing varied over the column in order to satisfy the requirements of the expected heat-load distribution and to utilize the available power supply and control equipment. The heater numbers are shown in Figure 4.4-1. The various strip sizes and power-supply specifications are given in Table 4.4-1. Note that the heaters were wound only over the centre 12 inches of the column.

Stainless steel sheathed $\frac{1}{16}$-in chromel-alumel thermocouples were used to monitor the wall temperature. The thermocouple wires were peened into $\frac{1}{16}$-in. axial grooves of various lengths as shown in Figure 4.4-1. The thermocouple junctions were peened into 0.026-in.-dia. x $\frac{1}{32}$-in. deep holes which were drilled at the end of each groove.

This particular orientation of the thermocouples served to reduce conduction error along the thermocouple wires and to allow all the leads to be strongly supported in one position.

The thermocouples are numbered in Figure 4.4-1 and Table 4.4-2 gives the location of each thermocouple relative to the shoulders located $\frac{7}{8}$-in. from each end.

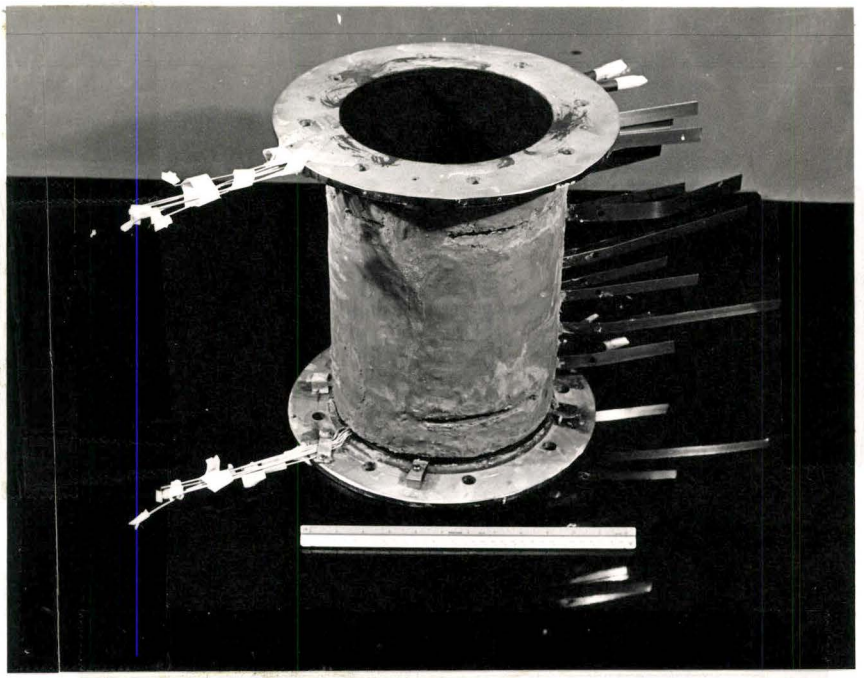

HEATER SECTION

FIGURE 4.4-2

TABLE 4.4-1 : HEATER SPECIFICATIONS

HEATER NUMBER	DIMENSIONS (inches)	OHMS/Ft.	TOTAL° MEASURED OHMS	MAXIMUM* POWER (k.v.a.)	CONTROL UNIT**
1,8	5/8 x .028	0.0387	0.20	2.5	Type 236, 2.5 kva, 9 amps 240 v. input
2,7	5/8 x .028	0.0387	0.20	1.5	Type 226, 1.7 kva, 6 amps 240 v. input
3	3/4 x .015	0.061	0.31	2.5	Type 236, 2.5 kva, 9 amps 240 v. input
4,5,6	1/2 x .015	0.0872	0.48	1.0	Type 226, 1.7 kva, 6 amps 240 v. input

° Element resistance measured in situ with a wheatstone Bridge. All measurements made to ± 0.01 ohms.

* For all heaters the controlled voltage from a variable transformer went to the primary winding of a Hammond Type E 240 v. - 24 v. step down transformer. The maximum power was the power rating of the transformer

** Heaters were all controlled by controlling the voltage to the primary of the step-down transformer with a "Powerstat" variable transformer (Superior Electric).

As well as the thermocouples indicated in the Figure, an additional thermocouple was peened to the wall adjacent to the underside of each flange.

TABLE 4.4-2 : Thermocouple Location

Thermocouple Number	Distance from Top Shoulder (inches)	Thermocouple Number	Distance from Bottom Shoulder (inches)
13	1/8	7	1/8
12	5/8	1	5/8
11	1¼	2	1¼
10	2½	3	2½
9	3⅝	4	3⅝
8	5⅛	5	5⅛
		6	6⅛

The thermocouples were all connected to bakelite terminal strips which were mounted on special brackets fastened to the flanges. Chromel-alumel 20-gauge lead wire connected the terminal blocks simultaneously to a panel of banana plugs and an 18 point multiswitch (Honeywell). This configuration allowed the millivolt signals from the thermocouples to be continuously monitored by a Honeywell 12-point, adjustable span recorder and simultaneously measured by a Honeywell Model 2733 portable potentiometer which was connected to the common lead of the multiswitch.

The evaporator was mounted between two 27-in. long stainless

steel cylinders of the same inside diameter. A schematic of the assembled unit can be seen in Figure 4.4-3. Each of the adjacent sections had two diametrically-opposed horizontal sampling ports located 3-inches from the flanged ends which were bolted to the furnace. The ports were of the same dimensions as those on the 10 foot furnace described in 3.3.1. This allowed the sampling probe to be inserted above and below the hot-zone without making any alterations to the probe.

The upper section had a run-off lip on the top flange which was identical to the run-off lip on the section adjacent to the 10-ft. column described in Section 3.3.2.

The lower section had two diametrically opposed 14-in.-long x 1-in. wide vertical slots located 5-in. below the top flange. The slots were designed to allow a vertically extended thermocouple probe, described in 4.4.4, to be inserted into the column. With this construction, both radial and axial gas-temperature profiles in the evaporator section could be measured. This remote entrance to the evaporator was used in order to eliminate distortion of the wall-temperature profile which would arise if sampling ports were mounted on the actual furnace section.

An analysis of the heat losses from the evaporator when operating at 2000^{o}R with air as the flowing medium, indicated that approximately 7000 B.T.U./hr. would be lost by radiation and 3000 B.T.U./hr. by conduction to the first 8-inches of each of the adjacent sections. In order to remove this heat and thus

COLUMN SCHEMATIC

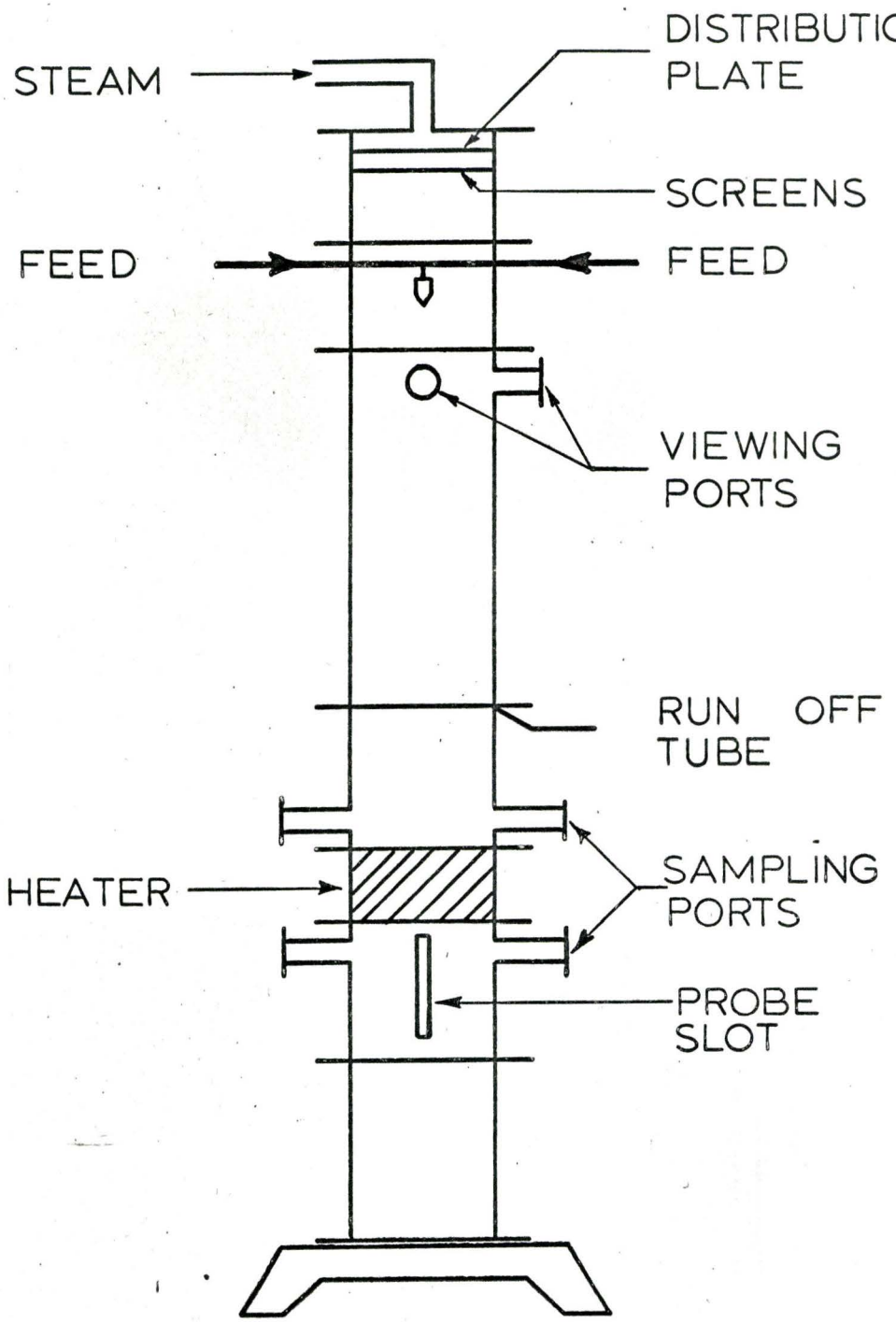

FIGURE 4·4—3

restrict the high temperature zone to the actual evaporator section, cooling coils were spot-brazed to the walls of each of the adjacent sections close to the flanges. The coils were constructed of $\frac{3}{8}$-in. O.D. copper tubing and extended a distance of 5-in. from the flanges. Good thermal contact between the column and the coils was attained by covering the coils with "Thermon - S" heat transfer cement (Macdonald Manufacturing Company). Figure 4.4-4 is a photograph of the bottom section.

The lower section was bolted to a 30-in. long aluminum pipe which in turn was bolted to a three-legged support stand. Thirty-four feet of $\frac{3}{4}$-in. O.D. copper tubing were coiled inside this lower section to form a condenser when steam was the flowing medium. The condenser had a capacity in excess of 7×10^5 B.T.U./hr. with city water as the condensing medium.

The support stand was constructed with a removable funnel bottom. When operating with steam the funnel served to direct the condensate into a simple collection system. When operating with air the funnel was removed in order to eliminate the exit constriction and thus permit large air flows while keeping the column close to atmospheric pressure.

The calming sections, which were bolted to the upper section containing the run-off lip, were the same ones which were bolted to the large furnace and which were previously described in 3.3.2.

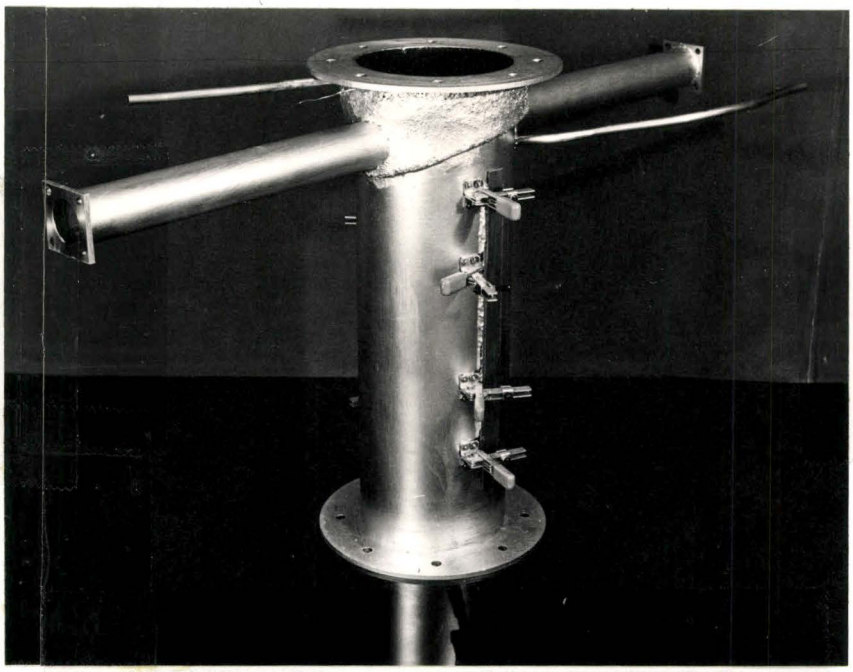

LOWER COLUMN SECTION - SHOWING ACCESS SLOT

FIGURE 4.4-4

4.4.3 Cooling Coil System

The $\frac{3}{8}$-in.O.D. copper-tube cooling coils which were spot-brazed to the column walls were connected into a closed, pressurized system. The water coolant was circulated through the system by a positive - displacement gear pump (Sihi CAO 3101). The pump was capable of delivering 14 U.S.G.P.M. at a head of 40-ft. and was driven by a $\frac{3}{4}$ hp., 1140 r.p.m. electric motor (General Electric).

A 40-in. long x 4-in. diameter stainless steel hold-up tank, shown in Figure 4.4-5, acted as a receiver and flash tank for the hot coolant. A $\frac{1}{2}$-in. control valve (Research Controls Inc. Type 755 ATO) was mounted on top of the tank and the desired operating pressure was selected and controlled by a pressure controller (Honeywell Type PP97A 1043-2, 2-50 lb.).

Under most operating conditions the heat losses from the unlagged circulation system reduced the coolant temperature sufficiently to prevent flashing in the tank and consequently no make-up water was required during the experiment. When flashing did occur, make-up water was added to the system by copper tube connections from the building supply lines.

4.4.4 Temperature Probe

Two temperature probes were constructed to measure gas-temperature profiles. Figure 4.4-6 is a photograph of these probes which were designed with the same insertion and manoeuvring mechanisms.

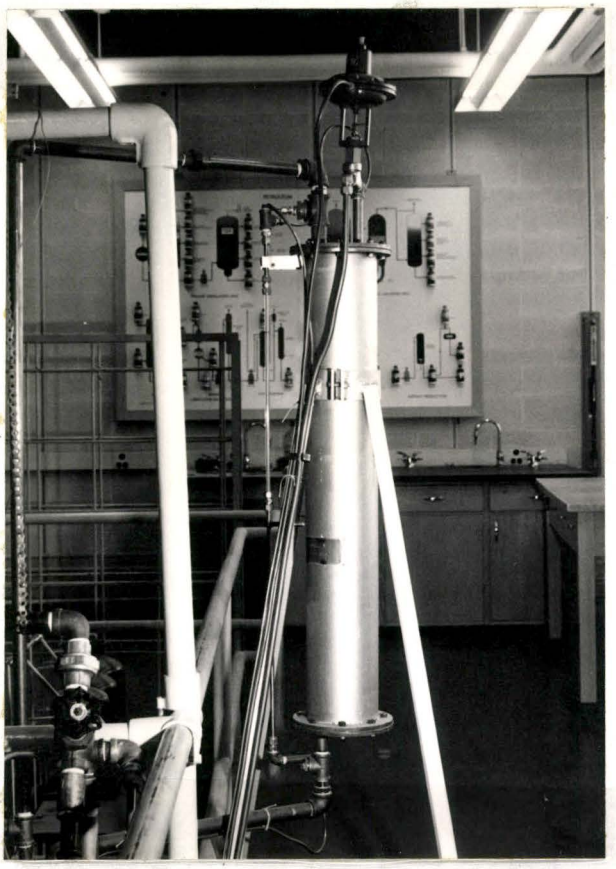

FLASH TANK

FIGURE 4.4-5

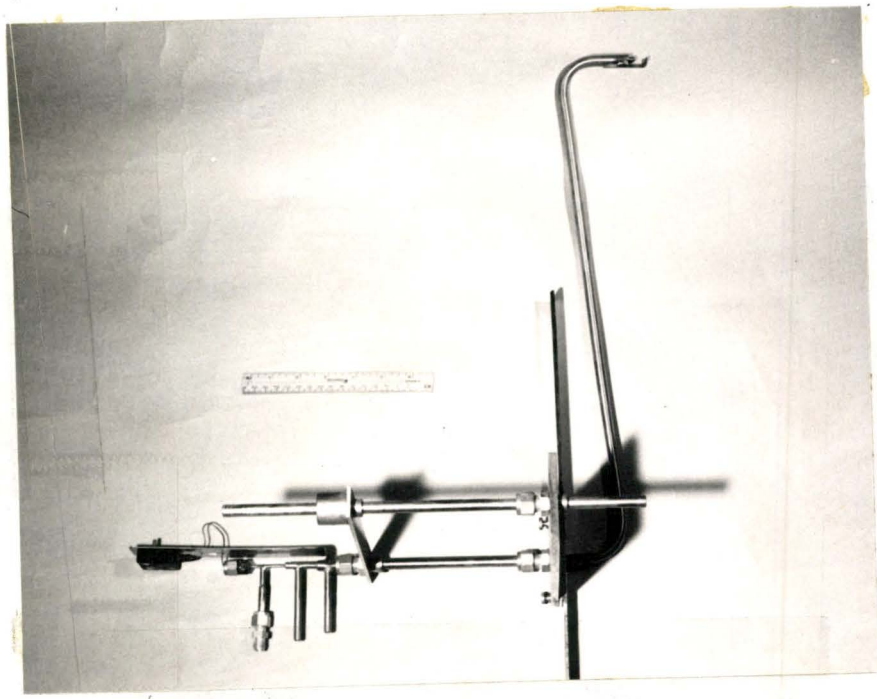

ASPIRATION PROBE

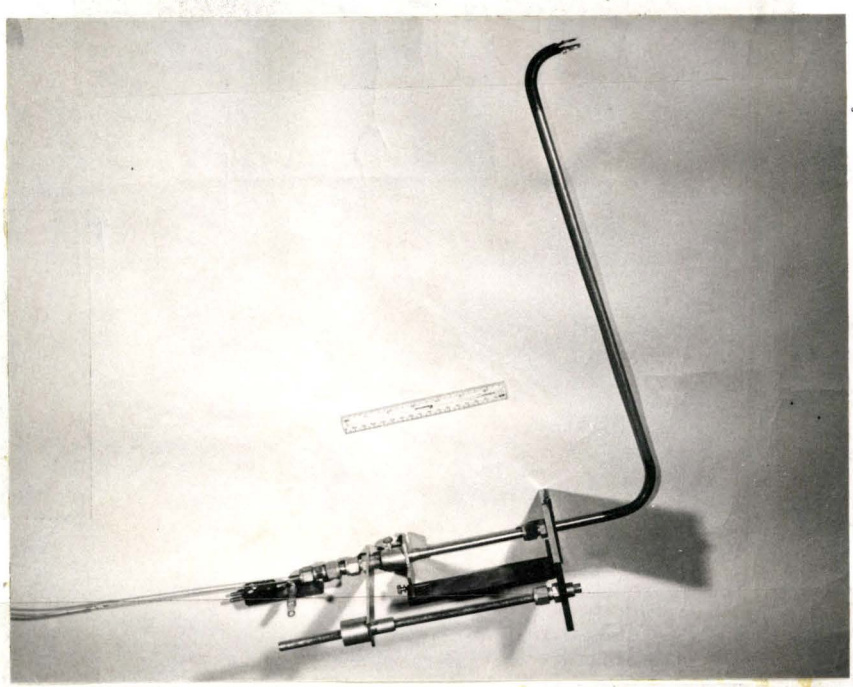

UNSHIELDED PROBE

FIGURE 4.4-6 TEMPERATURE PROBES

As in the case of the thermocouple probes described in Section 3.3.5, the thermocouple wire plus any additional suction tubes were encased in a $\frac{3}{8}$-in. O.D. stainless steel tube. This outer tube was used to position the probe relative to the column walls by sliding it through a bored-out Swagelok fitting. The fitting was screwed into a 7 x 3 x $\frac{1}{4}$-in stainless steel mounting plate (as shown in Figure 4.4-6).

The mounting plate served three purposes.

1. The "Jo" block support plate as described in Section 3.3.5 was bolted to it.

2. The 14 x 1 x $\frac{1}{8}$-in. axial positioning plate was attached to it by means of two thumb screws.

The axial positioning plate was stainless steel and machined to give a slip-fit when inserted into the entrance slot located below the evaporator. There were six of these plates each with a 0.65-in. diameter hole located such that by fastening each plate in the sequence to the mounting plate and then moving the thermocouple over a 2-in. axial travel, the entire length of the evaporator could be traversed. The hole in the plates permitted the plate to be slipped over the thermocouple tip and down the tube to its fastening position on the mounting plate.

3. A guide bushing was located 6-in. from the thermocouple access fitting and on a line exactly 90° to the axial positioning plate. This guide bushing received a $\frac{3}{8}$-in. stainless steel rod which was fastened to a permanently mounted yoke plate located at the tail end of the stainless steel thermocouple tube. The yoke, rod and bushing formed a positioning assembly which ensured that the thermocouple probe would be oriented vertically, in the column.

The aspiration and unshielded thermocouple probe-tips, as well as the suction-assembly, were basically of the same design as described in Section 3.3.5. However the unshielded probe required a modification to permit accurate radial positioning at the wall of the furnace.

Initial experiments with the unshielded probe indicated that, because of a small degree of flexibility in the positioning assembly, the physical contacting of the stop rod with the wall was not a sensitive enough technique. Consequently an air-jet positioning procedure was developed.

A length of stainless steel hypodermic tubing (0.072-in. diameter by .010-in. walls) was attached with high-temperature solder to the stop rod and extended through the $\frac{3}{8}$-in. diameter tube. The tube tip was drawn to a diameter of approximately 0.03-in. and the end carefully machined perpendicular to the axis of the tube. The tail end of the tube was connected via tygon-tubing to a valve on the laboratory 20 lb. air supply; a glass U-tube manometer was connected in parallel. (The U-tube was filled with Miriam oil, S.G. 1.75 and was open to the atmosphere)

With the air supply turned on enough to give a predetermined deflection of the manometer, the probe was moved to the proximity of the wall. When the probe was within 0.002-in. of the wall the pressure increase in the tube caused the manometer fluid to further deflect. The probe was calibrated on a milling-machine bed prior to operation in the column so that when the probe tip was within 0.001-in. of the wall a known manometer deflection was produced.

The thermocouple junction was carefully positioned relative

to the end of the air tube and the actual distance from the end was measured with a cathetometer as described in Section 3.3.5.

4.4.5 Velocity Probe

In order to ensure that the gas flow was fully-developed in the reactor section, velocity profiles were measured by inserting a 24-in. long "hot-wire" probe through a special guide plug which was fastened in the horizontal sampling ports.

The probe had an 8 ohm., 0.00015-in. diameter tungsten wire sensing element and was connected to a Hubbard Model IHR constant - temperature anemometer. The probe was calibrated (Appendix A) in air at the centre-line of a calibrated nozzle[R7].

4.4.6 Flow System

The flow system was the same as that indicated in Section 3.3.3 with the exceptions that

1. the hot-zone of the column was now 1 ft. rather than 10 ft. long.
2. the exit gases flowed directly out of the bottom of the column rather than through an external condenser.

4.5 Experimental Procedure

4.5.1 General Operation

The general operation of the equipment was the same as in Part I except that the column was brought up to the desired temperature level over a 2 to 3 hour period. This increase in the time required to reach steady-state operation was necessary to avoid severe wall-temperature overshoot since the power level was now manually rather than automatically controlled.

4.5.2 Gas Temperature

(i) Particulate System

The same procedure was followed as described in Section 3.4.3.

(ii) Gas flow only

The same radial traversing and signal recording technique was used as described in Section 3.4.3. The only difference in the procedure here was in the technique of locating the probe at the wall and of positioning the probe axially.

(a) Axial positioning - The first step in this procedure was to slip an axial positioning plate over the thermocouple and lock it into position on the mounting plate with two thumb screws. The thermocouple probe was then inserted into the column through the entrance slot and the axial positioning plate was locked into position with four toggle-action clamps (Lapeer Manufacturing Company Knu-Vise V-100). The probe was allowed to equilibrate in the column for approximately 5 minutes and then was adjusted

axially to the exact desired position.

The axial location was determined by measuring the distance between the bottom flange of the furnace and the bottom edge of the "Jo" block support plate with a cathetometer. (Griffin and George Limited. Model S31-950). This distance could be determined within ± 0.01 inches. The distance between the bottom of the support plate and the thermocouple junction was also measured to ± 0.01 inches and hence the measurement error in the thermocouple location was ± 0.02 inches. An approximate allowance was made for longitudinal thermal expansion of the evaporator and no allowance made for expansion of the probe. However, using a linear coefficient of expansion of 11×10^{-6} inch/inch ^{o}F(Ell), the maximum longitudinal change, which occurred at the top of the evaporator at a wall temperature of $1400^{o}F$, was only 0.20 inches.

Once the probe was positioned axially, a radial traverse was made. The clamps were then removed from the positioning plate and the thermocouple assembly removed from the column. The positioning plate was then unlocked, removed and another plate locked into position. This procedure was repeated until traverses had been made at all the predetermined axial locations.

Radial traverses were usually made with the thermocouple junction located at distances of 1.5, 4.2, 7.1, 10.1 and 13.1 inches from the top flange of the evaporator.

(b) Radial positioning - With the probe located in the desired axial position the valve in the air line to the positioning jet was slowly opened until there was a differential of $1\frac{5}{8}$-in. in the manometer fluid. This differential was the so-called

"initial differential" for which the probe was calibrated. The probe was then slowly pushed into the column until the manometer level just started to change. The probe was then left in this position for 3 to 4 minutes to equilibrate with the high temperature gases close to the wall. The probe was then eased slightly closer to the wall until the manometer deflection indicated that the end of the jet was within 0.001-in. of the wall. The probe was then withdrawn slightly and again eased into position and the manometer reading noted. The yoke and indicating screw on the stainless steel tube were then brought to the zero position in the same way as for the straight unshielded probe which was used in the large column. After the probe was zeroed at the wall, the air to the jet was turned off and after 2 to 3 minutes the radial traverse was made in the same manner as described in Section 3.4.3.

4.5.3 Gas Velocity

With air flowing in the column and after the electronic circuits of the anemometer had stabilized, the hot-wire probe was inserted through one of the horizontal sampling ports. The column was then traversed by positioning the probe at ½-in. intervals from the plug face for a distance of 6½-in. into the column. An additional point in the traverse was made ¼-in. from the wall.

At each point in the traverse, the amplified milliamp signal from the wire was monitored on the milliammeter of the

anemometer for 1 to 2 minutes after which time an eye-averaged reading was recorded. Also at 1-inch intervals in the traverse, the magnitude of the milliamp fluctuations, caused by velocity fluctuations, was monitored on the r.m.s. meter of the anemometer.

The milliamp and r.m.s. signals were then converted to velocities and turbulence intensities respectively by utilizing the previously determined hot-wire calibration curves.

4.6 Results and Discussion

4.6.1 Velocity and Turbulence Measurements

The velocities measured with the hot-wire probe in an isothermal air stream are shown in Figure 4.6-1. The solid line represents the equation determined by Deissler[D13] from experimental velocity measurements in a turbulent air stream[D15, L11]. The measurements were taken at the horizontal sampling stations both above and below the evaporator; they were taken over a Reynolds number range of 1.16×10^4 to 2.08×10^4. For any one set of conditions, the slope determined from a least-squares analysis of the data was not significantly different from the predicted slope, at the 95% level of confidence.

The intensity of turbulence (ratio of the r.m.s. velocity fluctuation at a point to the average velocity at a point) was also measured for the same conditions. The results are shown in Figure 4.6-1a. The magnitude of the measured intensities was in the range expected for fully-developed turbulent flow in a tube[B16, S23].

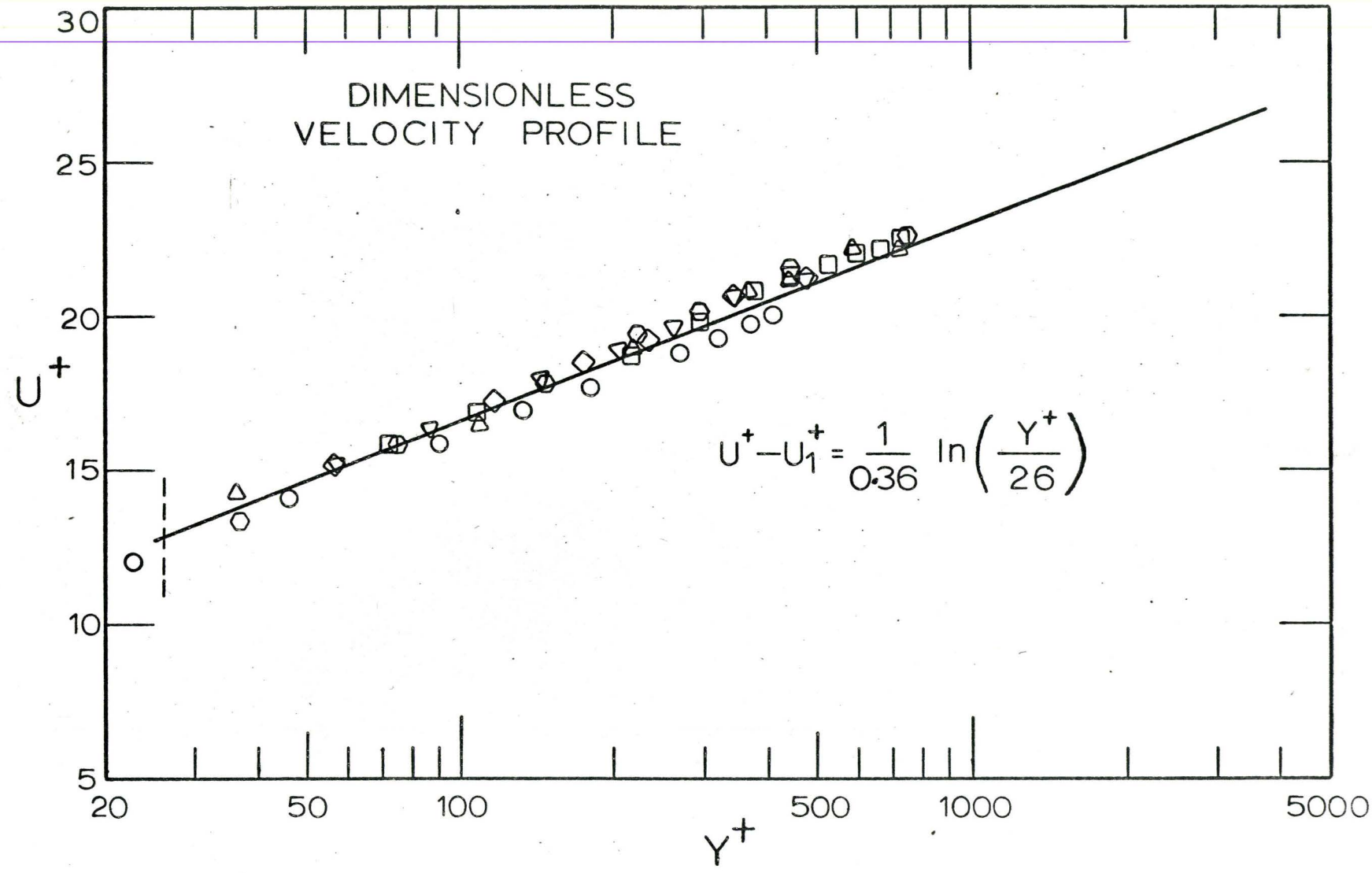
DIMENSIONLESS
VELOCITY PROFILE
$U^+ - U_1^+ = \frac{1}{0.36} \ln\left(\frac{Y^+}{26}\right)$
U^+
Y^+
30
25
20
15
10
5
20
50
100
500
1000
5000

FIGURE 4·6–1

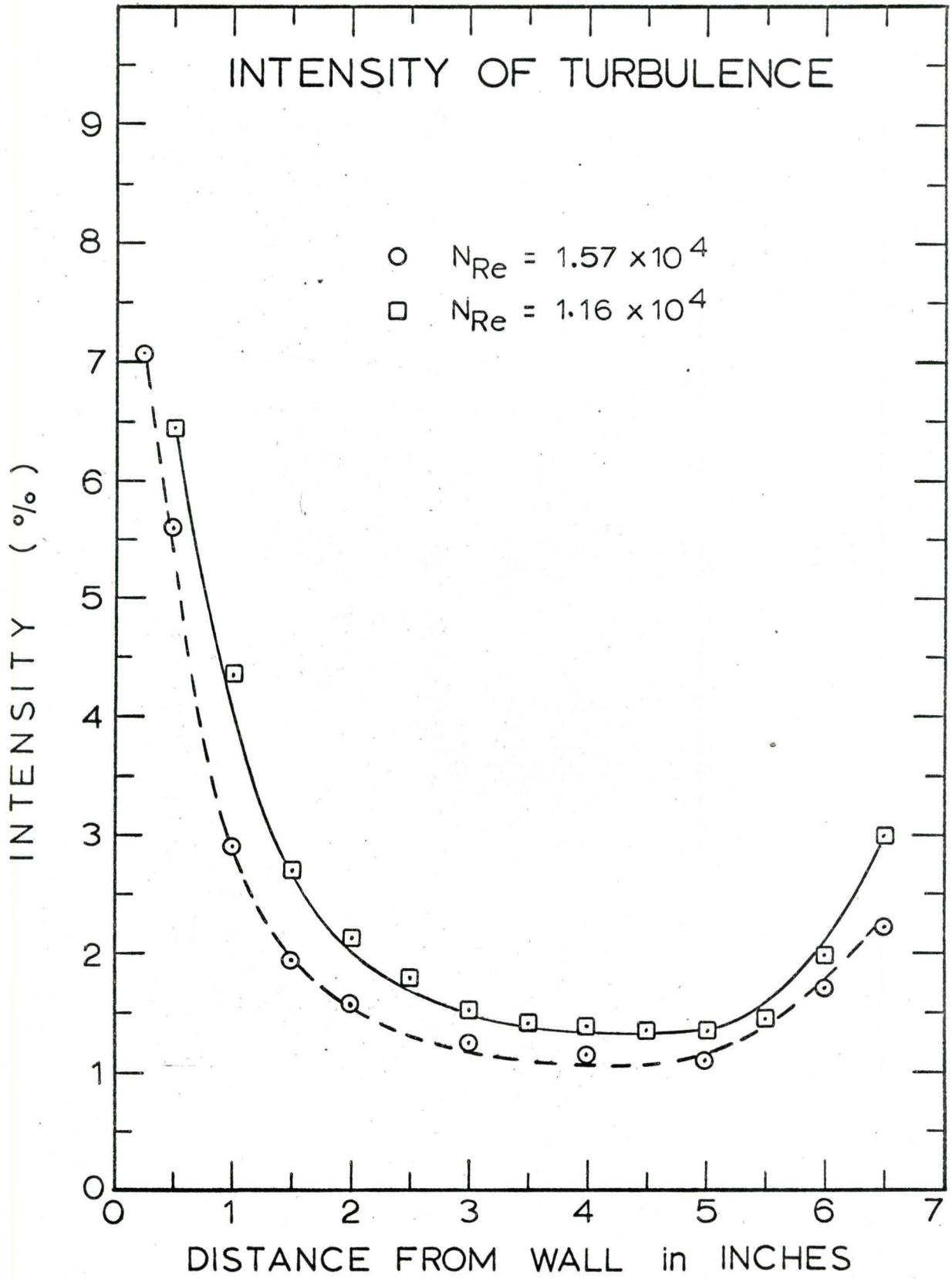
INTENSITY OF TURBULENCE
$N_{Re} = 1.57 \times 10^4$
$N_{Re} = 1.16 \times 10^4$
INTENSITY (%)
DISTANCE FROM WALL in INCHES
0
1
2
3
4
5
6
7
8
9

FIGURE 4·6 −1a

The velocity and intensity measurements indicated that the flow was fully-developed in the evaporator section. The dimensionless velocity profile was not significantly different from that of Deissler and hence Deissler's relationship was used to calculate the point velocities required in the theoretical model described in Section 4.3.

4.6.2 Air Temperatures

(i) Low-Temperature Results

Figure 4.6.2 to 4.6-5 show the experimentally measured temperatures and also indicate the temperatures predicted from the solution of the energy equation at the corresponding axial locations. The notation VP1, VP2, VP4* corresponds to axial distances of 0.5, 3 and 9-in. respectively from the beginning of the "hot-zone". (The "hot-zone" refers to the centre 12-in. of the 14-in. section on which the electrical heaters were wrapped.) The solid line represents the temperatures calculated when the Reynolds number was evaluated at the wall temperature and the broken line represents the temperatures calculated when the Reynolds number was evaluated at the inlet gas temperature.

The calculated temperature profiles are in excellent agreement with the experimentally measured profiles at wall temperatures less than 300^{o}F. This is to be expected since the assumption of constant properties, which was made in the development

---

* This nomenclature corresponds to laboratory notebook numbers referring to Vertical Position 1, 2, etc.

of the energy equation, is valid at these low wall-to-gas temperature differences. Also at these conditions, the heat transfer is not expected to have a significant effect on the velocity profile. Therefore, distortion of the velocity profile and its resultant effect on the heat-transfer rate should be negligible.

It can therefore be concluded that the mathematical model predicts the heat-transfer rate and temperature profiles very well under conditions where the assumptions used in the model are expected to be valid.

(ii) High Temperature Results

Figure 4.6-6 to 4.6-10 show the experimental and predicted temperatures for wall temperatures > 600°F. The results indicate that as the wall temperature increases to a maximum of 1400°F, the measured temperature gradients at the wall become greater than those predicted from the model; or in other words, the model appears to under-estimate the heat-transfer rate at these high temperatures.

These results might suggest that the temperature measuring device was indicating too low a temperature when placed in these high-temperature gradients. Therefore an assessment of the device will be made before drawing any conclusions.

(iii) Assessment of the Temperature-Measuring Device

1. At the commencement of this part of the study, the geometry of the probe-tip was essentially the same as that used in Part I.

GAS TEMPERATURE PROFILES
— AIR · 3C —

---N_{Re} (T_{in}) = 10,240

——N_{Re} (T_{wall}) = 9,460

° MEASURED TEMPERATURES

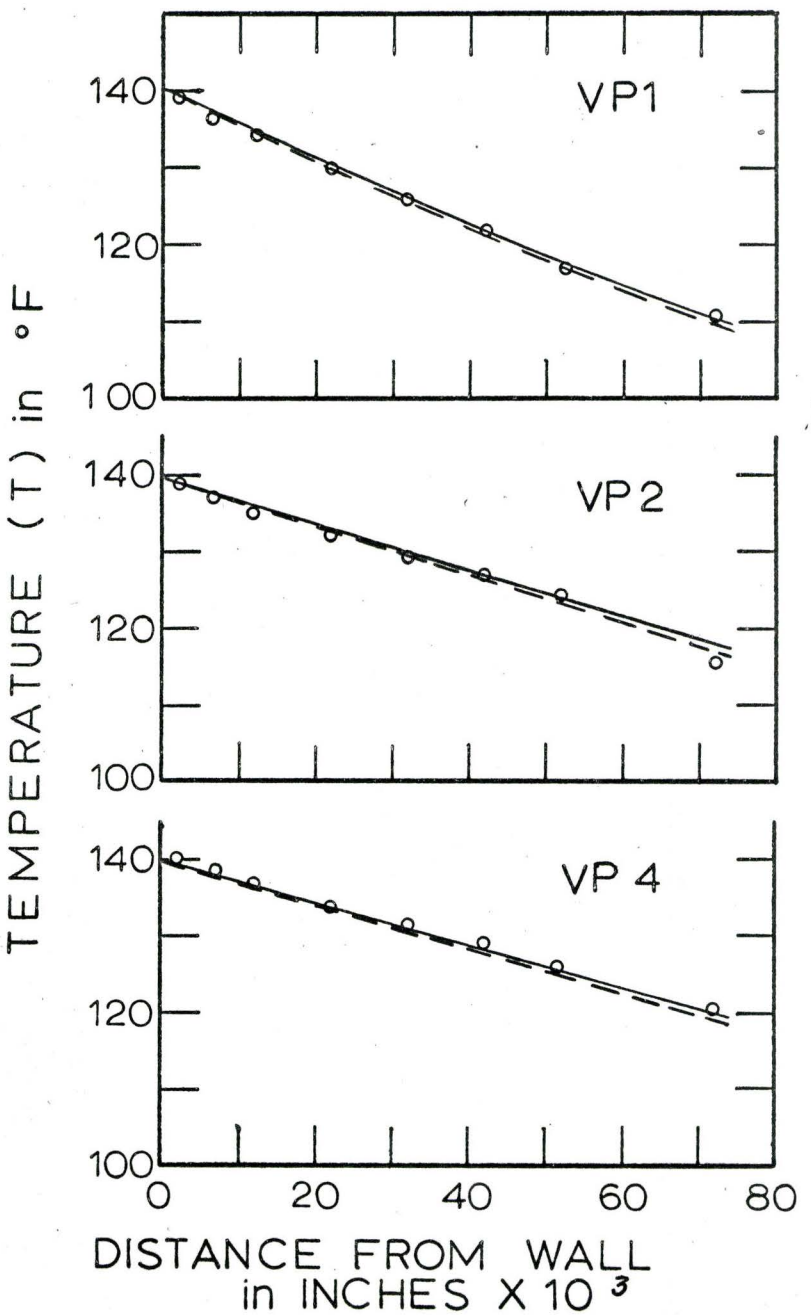

FIGURE 4·6—2

GAS TEMPERATURE PROFILES —AIR 4C—

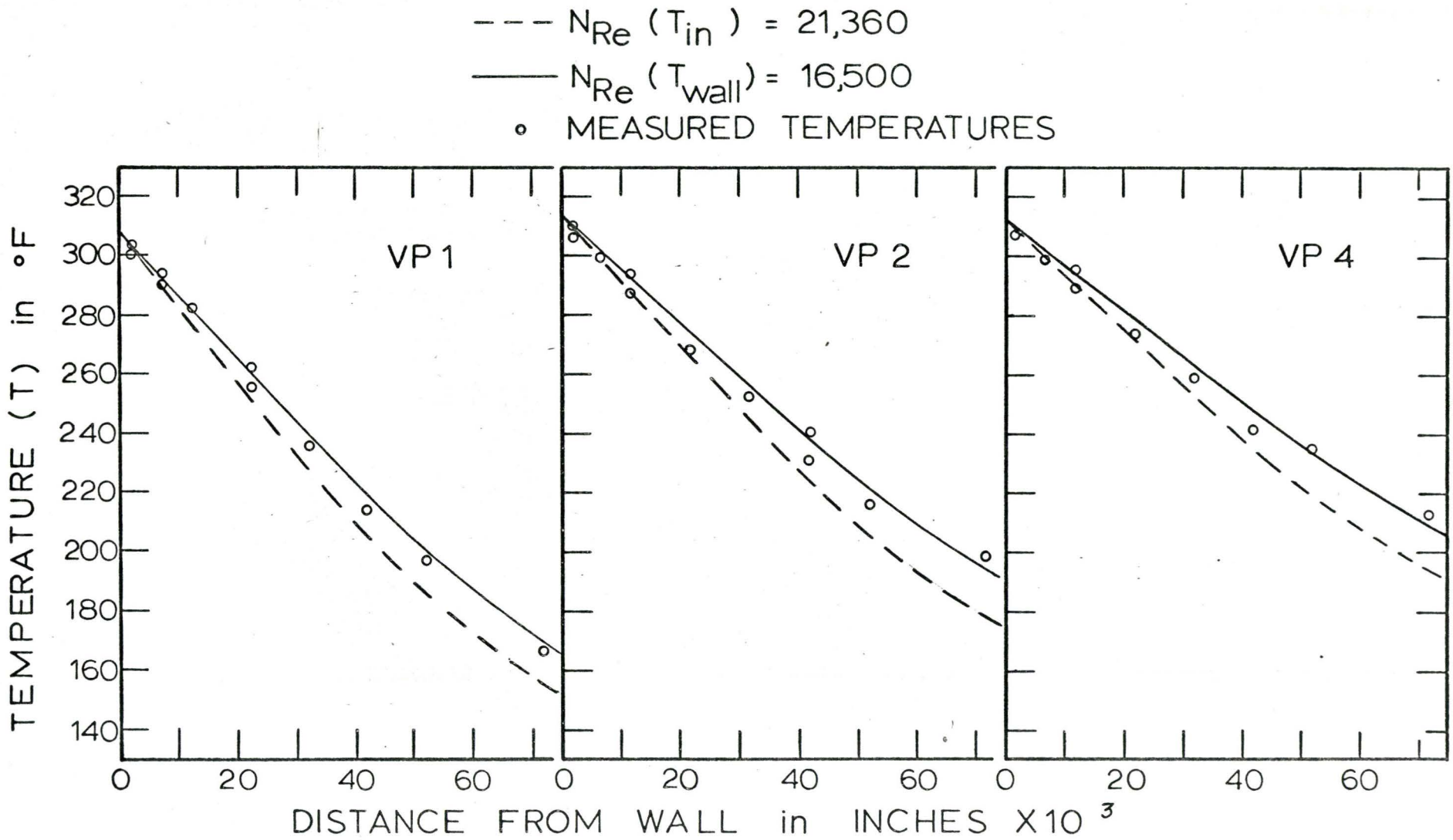

FIGURE 4·6—3

GAS TEMPERATURE PROFILES — AIR 5C —

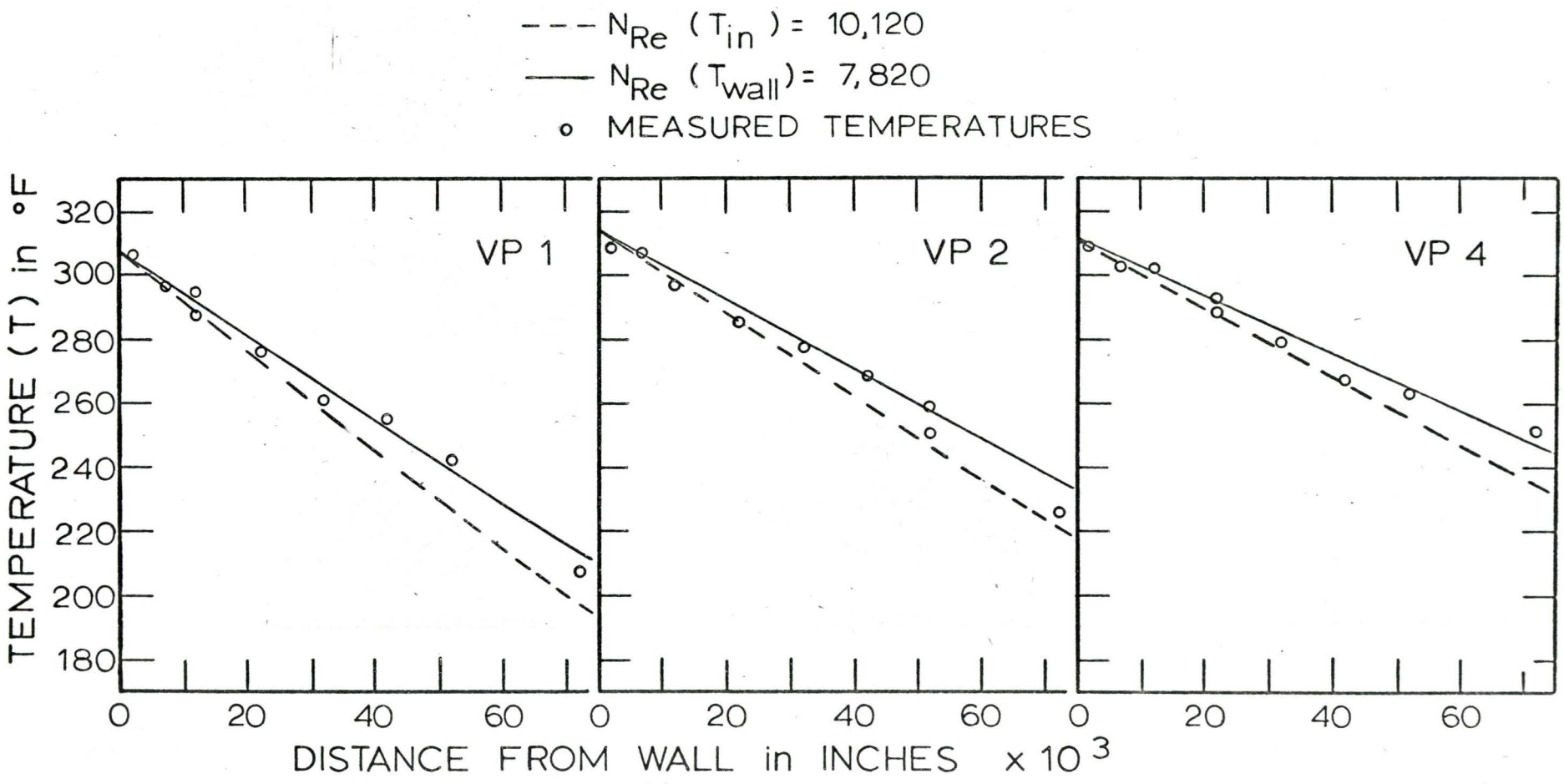

FIGURE 4·6—4

GAS TEMPERATURE PROFILES

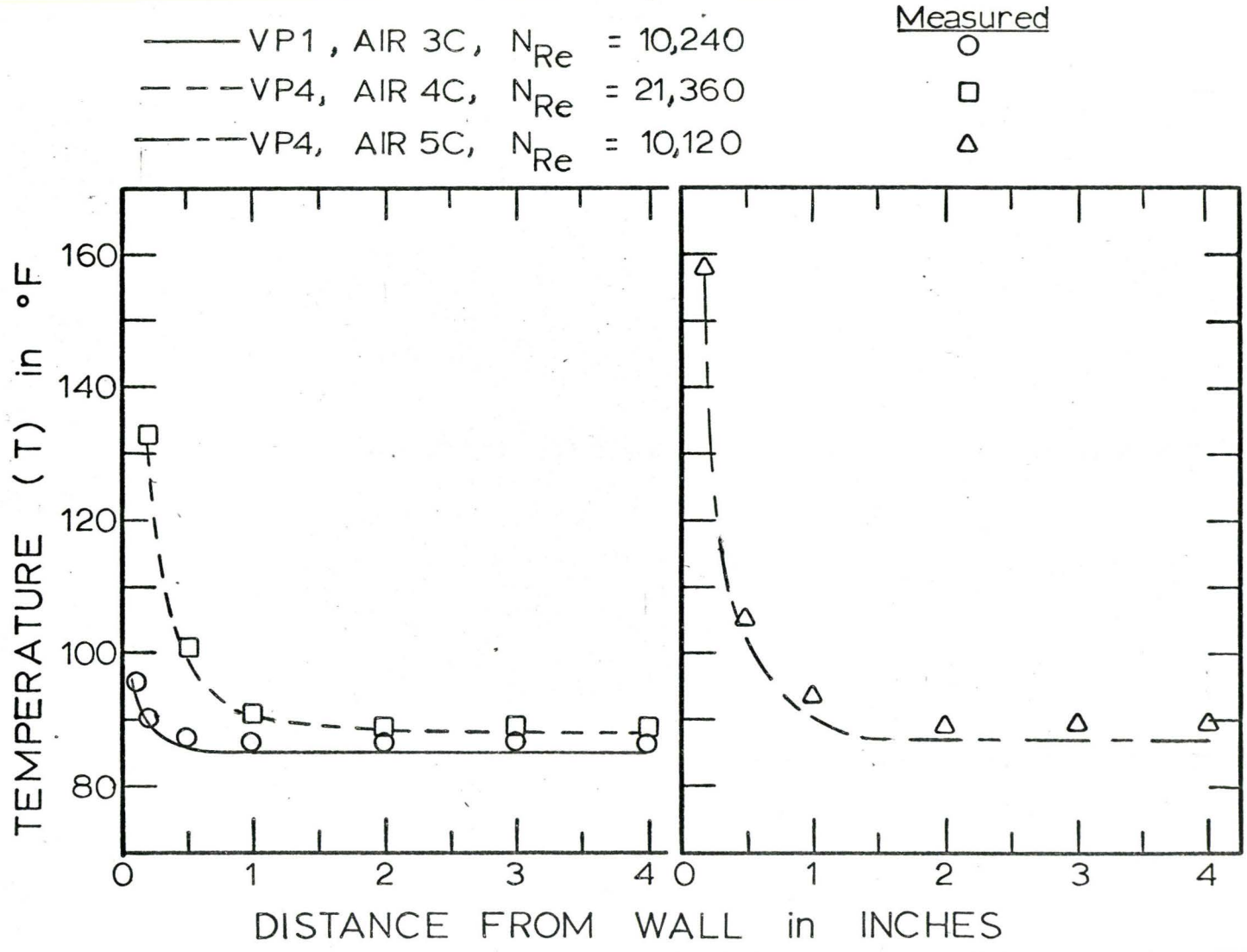

FIGURE 4·6 – 5

GAS TEMPERATURE PROFILES — AIR 6C —

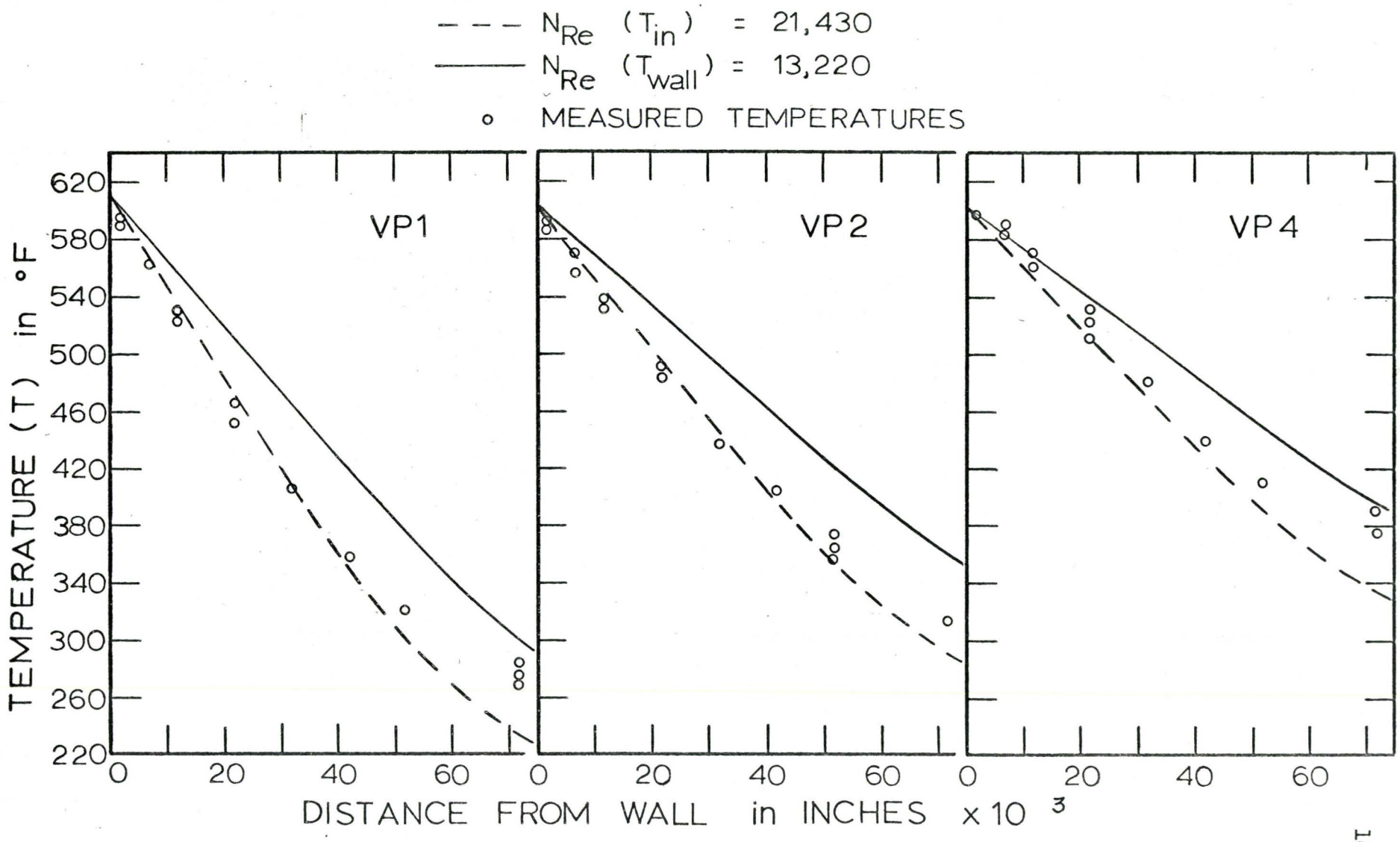

FIGURE 4·6 –6

GAS TEMPERATURE PROFILES — AIR 7C —

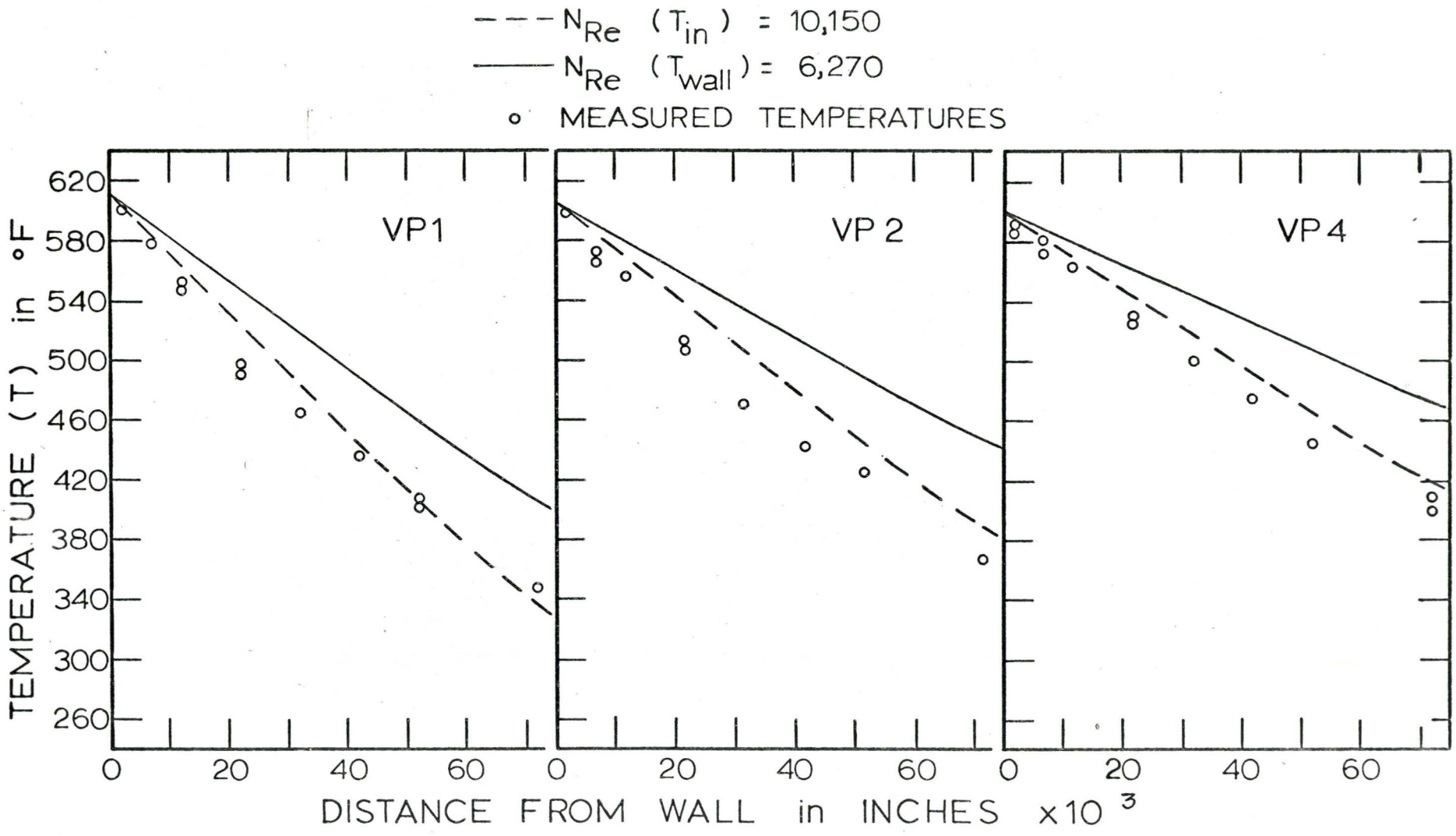

FIGURE 4·6 – 7

GAS TEMPERATURE PROFILES — AIR 8C —

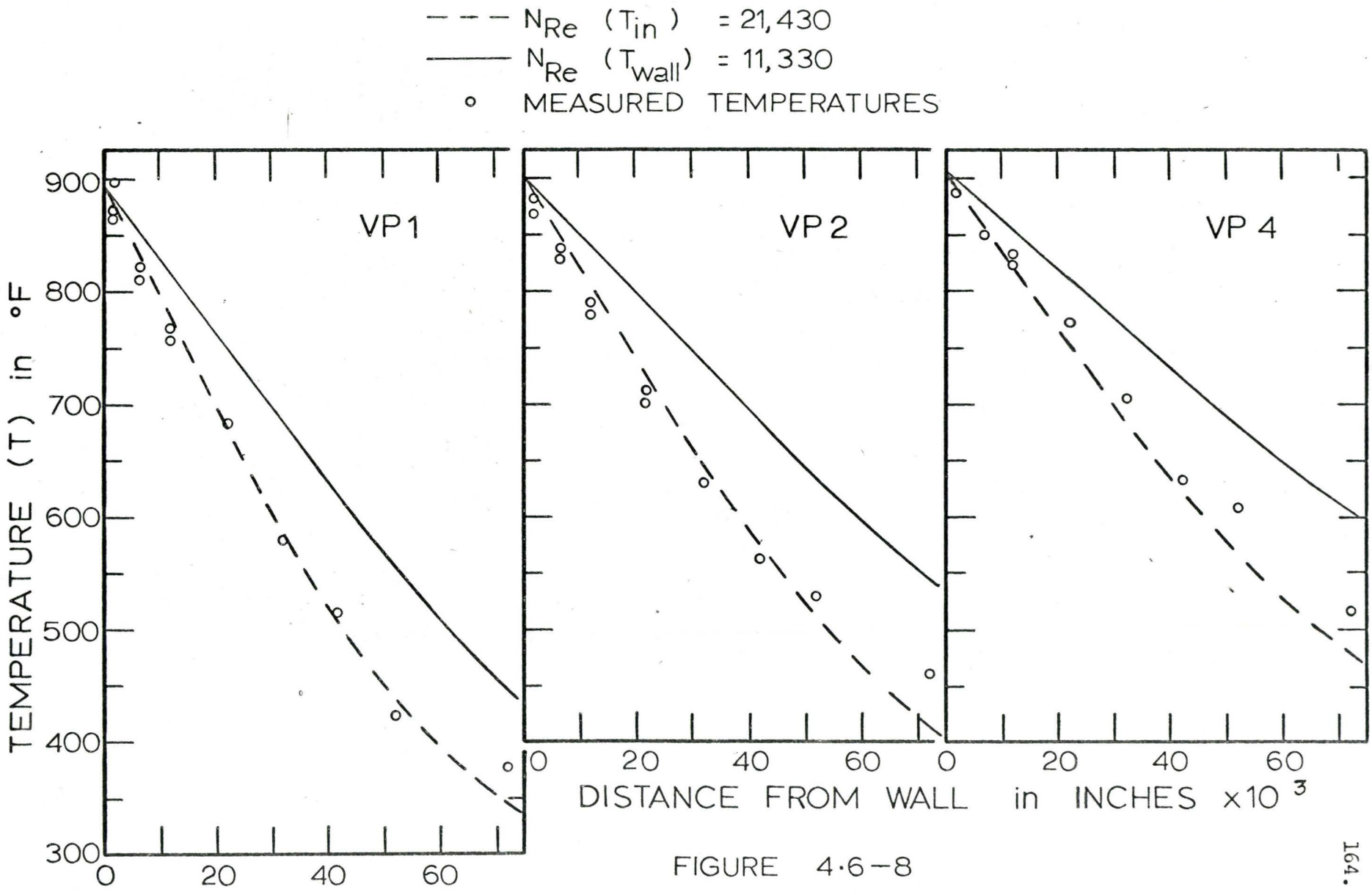

FIGURE 4·6–8

GAS TEMPERATURE PROFILES — AIR 9C —

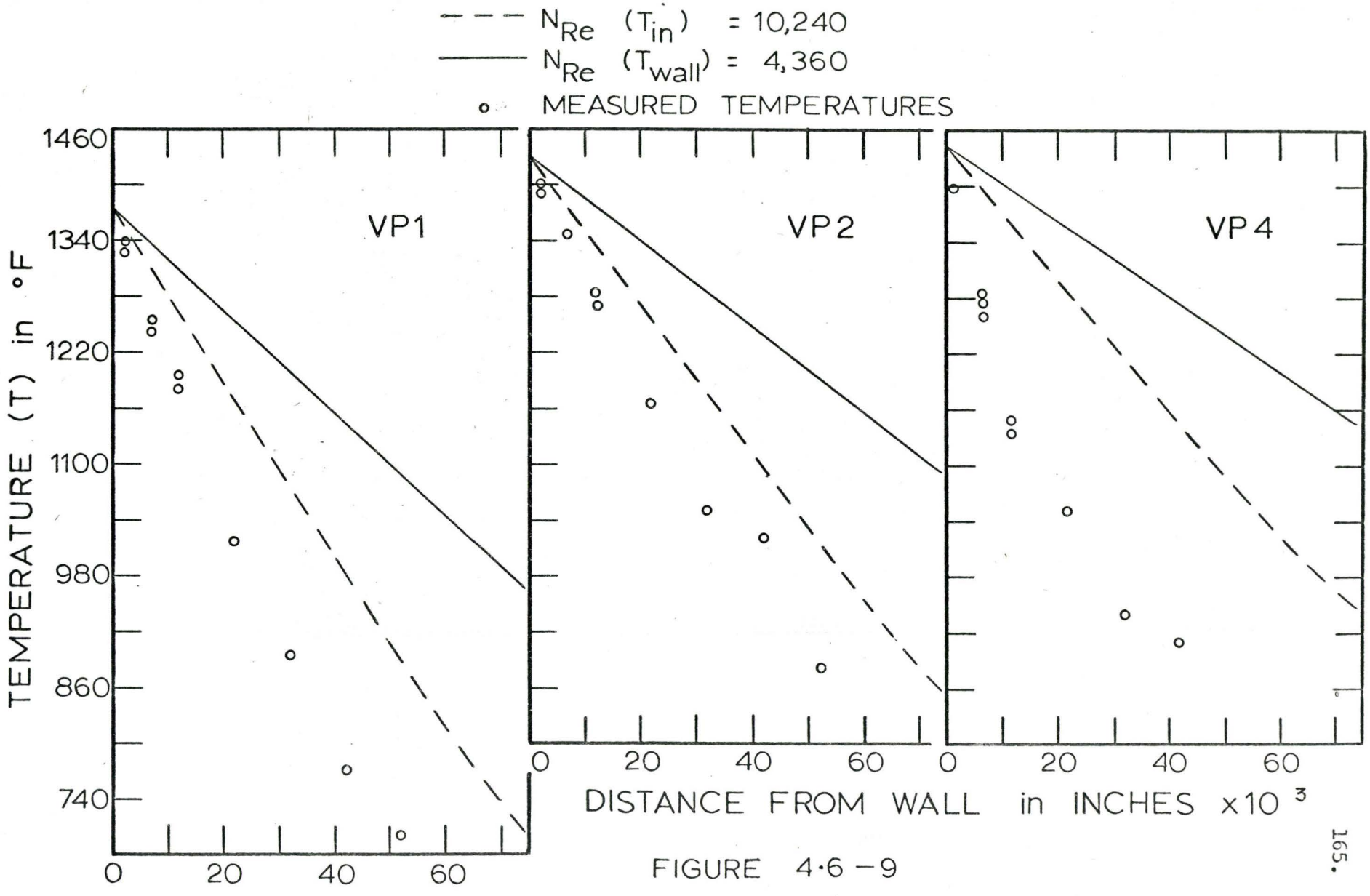

FIGURE 4·6 – 9

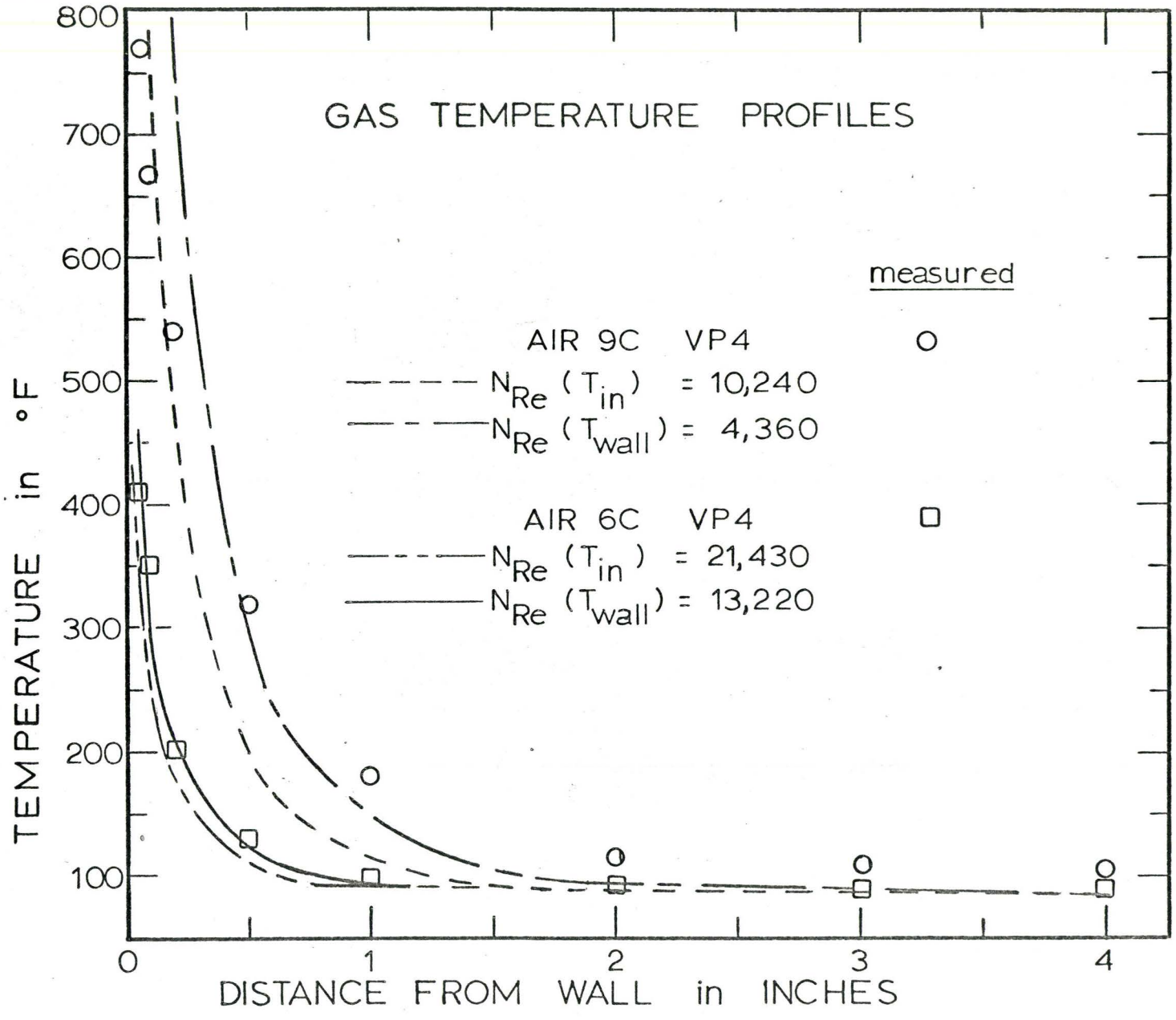
GAS TEMPERATURE PROFILES
measured
AIR 9C VP4
N_{Re} (T_{in}) = 10,240
N_{Re} (T_{wall}) = 4,360
AIR 6C VP4
N_{Re} (T_{in}) = 21,430
N_{Re} (T_{wall}) = 13,220
TEMPERATURE in °F
800
700
600
500
400
300
200
100
0
1
2
3
4
DISTANCE FROM WALL in INCHES

FIGURE 4·6−10

(Described in Section 3.5 and illustrated in Figure 3.3-10). It was noted in Part I that the wall temperature which was obtained by extrapolating the measured gas-temperature profile did not agree with the wall temperature indicated either by the wall-thermocouples or by a two-wavelength pyrometer. The same discrepancy was found also when measuring gas temperatures in the smaller evaporator.

The magnitude of the error caused by conduction of heat along the wires, away from the junction, was found to be negligible[R7]. Thus the junction should have indicated the true gas-temperature; hence it appeared that the entire probe was conducting heat away from, and consequently lowering the temperature of the gas in the vicinity of the junction.

A new probe-tip was constructed with the thermocouple junction located 1¼-in. above the positioning tip rather than ¼-in. as on the original probe. The extrapolated gas-temperature profile now yielded a wall temperature which agreed with the temperature indicated by the wall-thermocouples, (after allowing for the temperature-drop across the wall). A comparison of the profiles obtained with the two probes is shown in Appendix C.3.

It appears that the orientation of the thermocouple junction with respect to the probe-body is very important in the determination of true gas temperatures.

The agreement between the extrapolated and measured wall temperatures indicates that the modified probe used in this work

does allow the true gas temperature to be measured.

2. An analysis of the radiation and conduction error for this fine-wire thermocouple[R7] indicated that under these operating conditions there was a negligible conduction error. In fact, radiation to the larger diameter support wires tends to increase their temperature above that of the gas. Thus if conduction along the fine thermocouple-wire were important it would act in a direction to increase rather than decrease the temperature of the thermocouple junction. Of course these wires would tend also to conduct heat away from the gas since they are located in a steep temperature gradient. However because of their small size this effect would not be very large.

3. To further determine whether the probe acted as a heat-sink, removing heat from the gas in the high temperature gradient present in Run 9c, a comparison can be made between the profiles measured at VP1 - Air 6c (Figure 4.6-6) and VP4 - Air 9c (Figure 4.6-9). At VP1 - Air 6c the steepest predicted gradient is 6,535^{o}F/in. and the measured temperatures are seen to agree quite closely with the predicted profile. However at VP4 - Air 9c, where the steepest predicted gradient is 6,937^{o}F/in. the measured gradient is much greater than that predicted. Since the two predicted gradients are within 6% of one another, the deviation from prediction at the high wall temperature cannot be caused by the probe acting as a heat sink.

4. An evaluation of the validity of the gradients measured with this device could be obtained by integrating the experimentally

determined heat-transfer rates over the entire heat-transfer surface. This calculated total heat transfer could then be compared to the total enthalpy increase of the gas. This was not done in this instance because

(a) of the uncertainty in determining slopes from the temperature data-radius curves. (scattered data)

(b) the velocity profile must be assumed to be the fully-developed velocity profile, i.e. must make the unrealistic assumption that the velocity profile is not distorted by the large temperature gradients.

(c) the gradients would have to be determined at a large number of axial positions as well as in the entrance section preceding the hot zone. With the present device it was not possible to make these measurements in the entrance section.

It would thus appear that the probe was indicating the actual gas temperature in the presence of these high temperature-gradients and that the increased heat-transfer rate was a true phenomenon. The question which must now be answered is - why do these high heat-transfer rates occur when the temperature of the wall is much greater than the bulk temperature of the gas?

(iv) Further Evaluation of the Model

(1) The assumption was made originally that $\varepsilon_h = \varepsilon_m$. To check the sensitivity of the heat-transfer rate to a change in ε_h, the Nusselt numbers were calculated for an arbitrary change in ε_h. When the value of ε_h was increased by 20, 60 and 120% at dimensionless distances from the wall greater than 5, (the actual distance from the wall at a y^+ of 5 was of the order of 0.05-in.; the exact distance was a function of the Reynolds number),

the Nusselt numbers were observed to increase by approximately 8, 23 and 43% respectively. The per cent increase in the heat-transfer rate was approximately 40% of the per cent increase in the value of ε_h. Thus there would have to be a very great difference in the mechanisms of heat and momentum transfer to give an appreciable effect. Consequently it would not appear that the increased heat-transfer rate was caused by an increase in ε_h over ε_m.

2. In the model it was assumed that the physical properties were constant. It is necessary however, to specify the temperature at which the thermal conductivity should be evaluated. Figure 4.6-11 is a plot of the ratio of the molecular conductivity to the total conductivity (molecular + turbulent) versus distance from the wall. The graph indicates that the major effect of molecular transport is restricted to the region very close to the wall and therefore the thermal conductivity evaluated at the wall temperature is expected to be nearer the actual representative value.

3. The predicted temperature gradients at the wall were observed to increase as the Reynolds number was increased, with the total mass-flow kept constant. This increase in the temperature gradient was caused by the velocity profile change, i.e., for a fixed mass-flowrate, if the Reynolds number is increased there is more flow at the wall; therefore the resultant greater heat-sink there causes steeper temperature gradients and hence greater heat

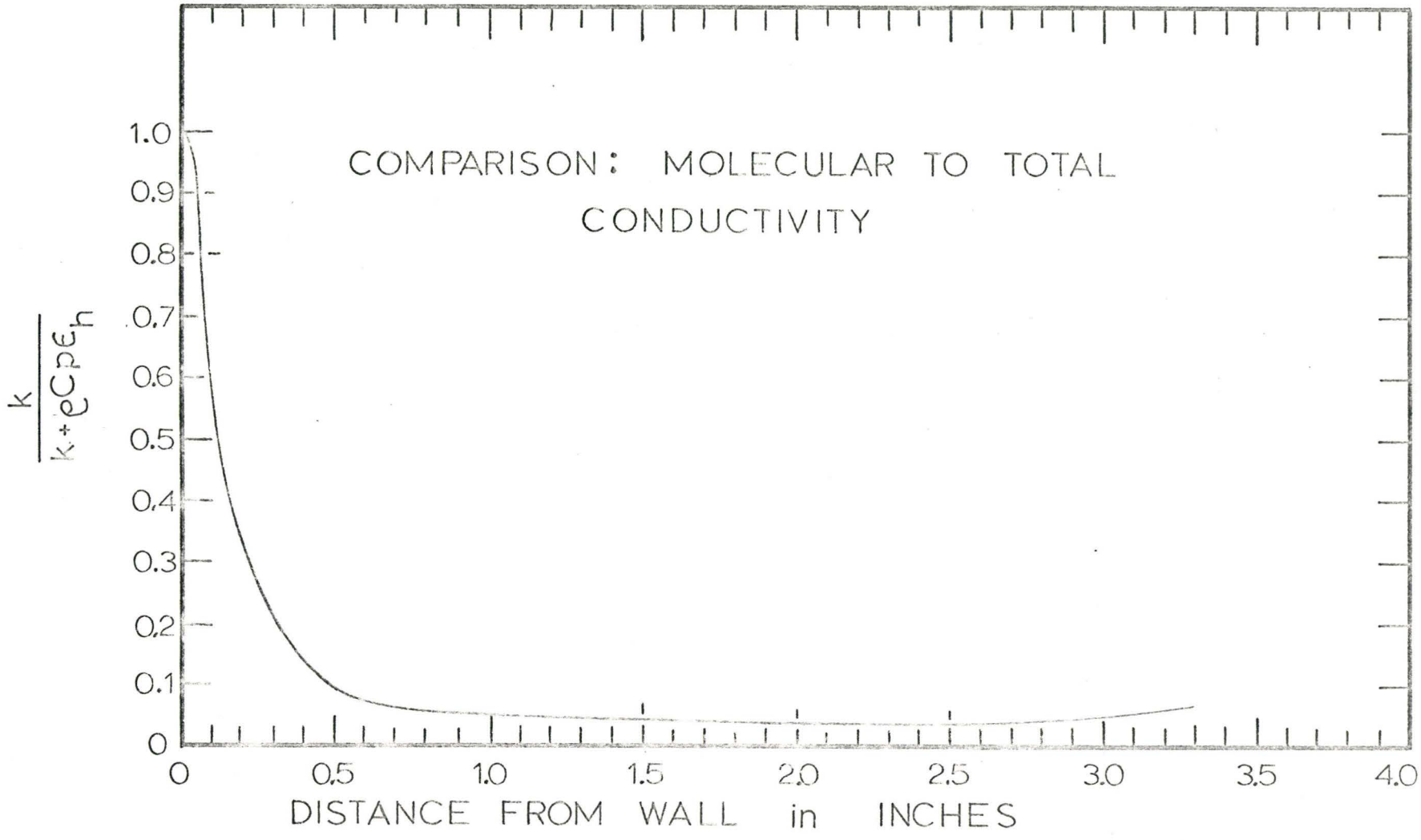
COMPARISON: MOLECULAR TO TOTAL CONDUCTIVITY
$\frac{k}{k+\rho C_p \varepsilon_h}$
1.0
0.9
0.8
0.7
0.6
0.5
0.4
0.3
0.2
0.1
0
0
0.5
1.0
1.5
2.0
2.5
3.0
3.5
4.0
DISTANCE FROM WALL in INCHES

FIGURE 4·6 –11

transfer. (It should be noted that the Reynolds number was changed at a fixed mass-flowrate by virtue of the magnitude of the viscosity which was calculated at either the inlet or the wall temperature.)

4. If the physical properties were allowed to vary with temperature would the predicted gradients agree more closely with the larger, measured gradients? A simple heat-balance analysis (Appendix C.4) indicated that if the change of the thermal conductivity with temperature were accounted for in the model, the predicted gradients would decrease rather than increase. An analagous momentum balance indicated that if the increase of the gas viscosity with temperature were accounted for in the model, the velocity gradient at the wall would decrease. Thus, for a fixed mass-flowrate the flowrate adjacent to the wall would decrease. This reduced flow would reduce the heat sink close to the wall, which would cause the temperature of the gas adjacent to the wall to increase and hence would decrease the gas-temperature gradient.

It is thus seen that the discrepancy between the predicted and measured temperature gradients cannot be caused by the neglect of the property variation in the theoretical model.

5. The velocity profile was assumed to be fully developed and no allowance was made for the effect of natural convection on the profile. The relative magnitude of the natural-convection to the forced-convection forces is usually measured by the parameter

N_{Gr}/N_{Re}^2 (A4, S17). For Air-Run 9c this ratio was found to be 0.8 with the Reynolds number calculated at the inlet conditions. Thus for these conditions, natural convection could be expected to have an influence on the pure forced-flow heat-transfer rate.

In the experiments, the natural-convection forces oppose the forced-convection forces. Consequently the natural-convection or buoyancy forces tend to decrease the forced-convection velocity gradient in the region next to the wall. As explained in the preceding discussion (4), a decreased velocity gradient causes a decreased temperature gradient. Thus if allowance were made in the model for the effect of natural convection on the forced-flow velocity profile, the predicted temperature gradients would be found to decrease.

An evaluation of the model has indicated that if the model were made more realistic by allowing for property variation and natrual-convection effects, the predicted temperature gradients at the wall would decrease compared to those presently predicted; therefore the discrepancy between prediction and experiment would become larger.

It would appear that some phenomenon occurs in the experimental system which increases the rate of heat removal from the gas adjacent to the wall thus causing increased temperature gradients at the wall. Although the natural-convection forces were not excessive in these experiments, they may have been of sufficient magnitude to cause some flow instability and increased

turbulence levels in the forced-convection flow field. This would result in an increased momentum and heat exchange between the relatively cold gas in the core and the hot gas adjacent to the wall; this would tend to increase the temperature gradient at the wall.

A technique for measuring gas velocity in a non-isothermal turbulent flow field had not been perfected at the time of these experiments. Consequently no positive conclusions can be drawn regarding the phenomena which tend to increase the measured temperature gradients and hence rates of heat transfer above those expected.

4.6.3 Steam Temperature

(i) Low-Temperature Results

Figure 4.6-12 and 4.6-13 indicate the experimentally measured and the predicted temperatures for conditions where the assumptions made in the solution of the energy equation are expected to be valid. As in the case of air, the predicted profiles are seen to be in excellent agreement with the measured profiles.

The data for the steam runs corroborate the conclusions drawn from the low-temperature air runs; i.e., the mathematical model is capable of predicting the heat-transfer rate and the temperature profiles in the entrance region of a heated pipe, at low wall-to-bulk temperature ratios.

GAS TEMPERATURE PROFILES —STEAM 1C—

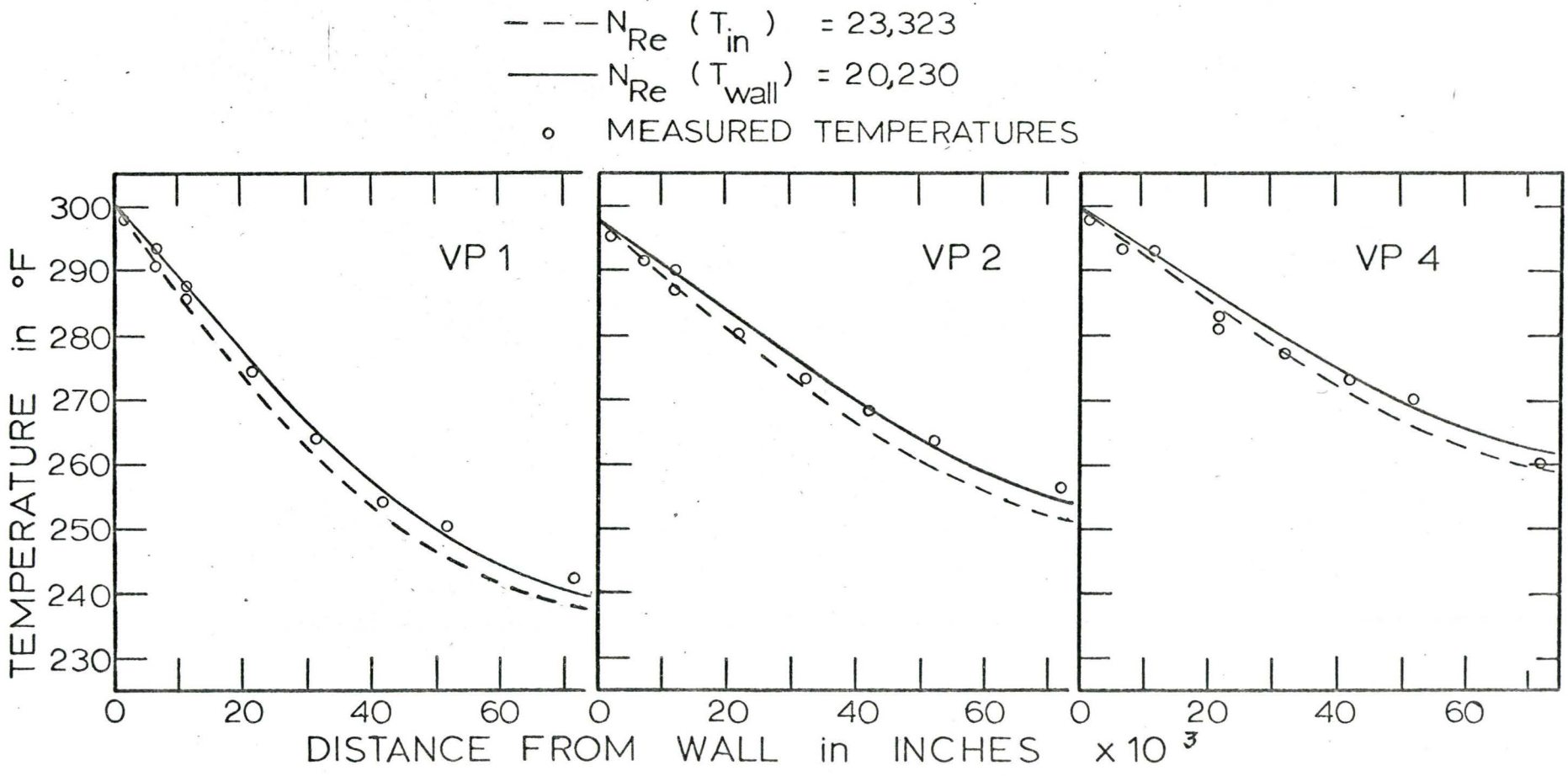

FIGURE 4·6 — 12

GAS TEMPERATURE PROFILES — STEAM 2C —

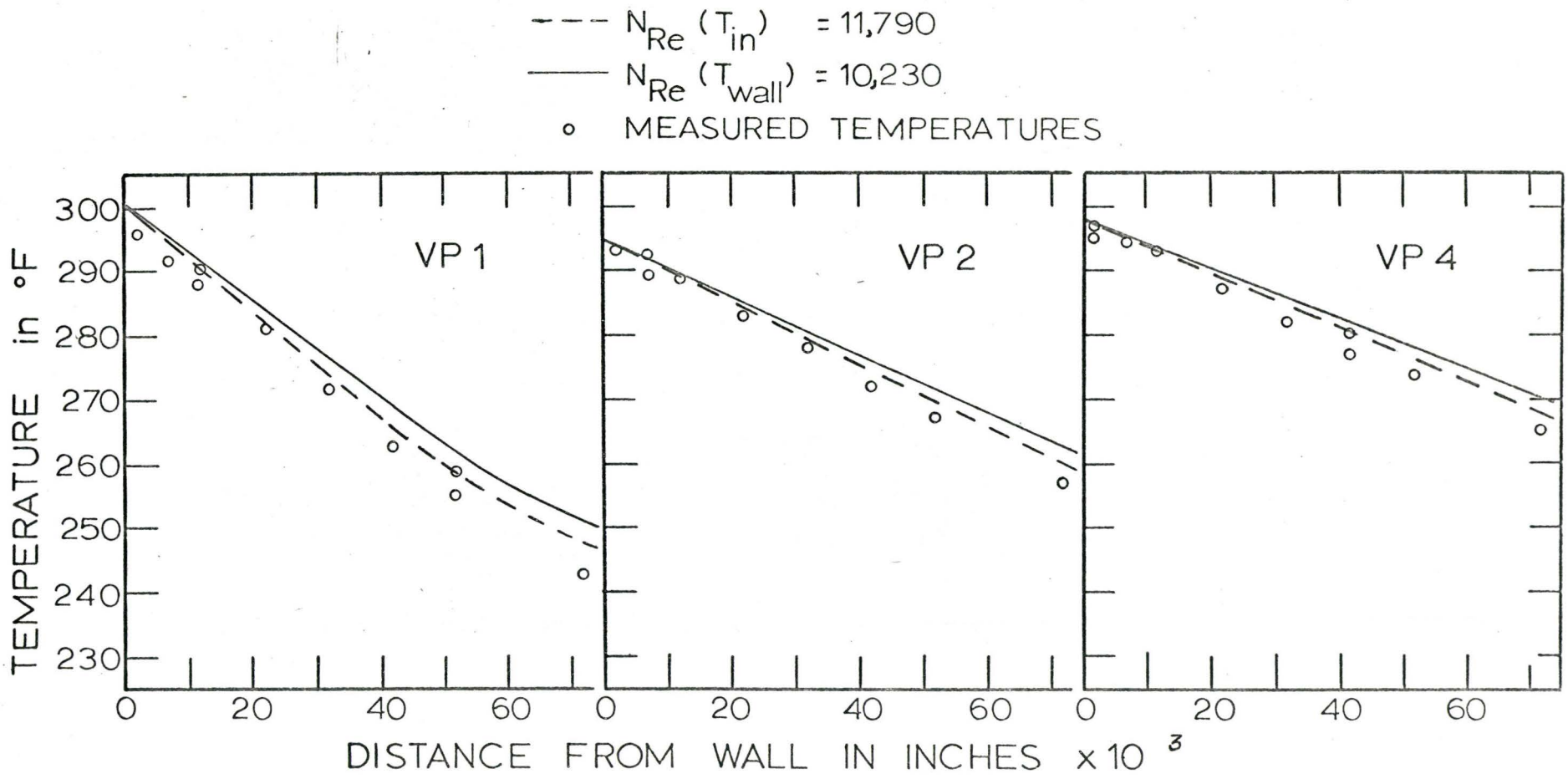

FIGURE 4·6–13

(ii) High-Temperature Results

Figure 4.6-14 to 4.6-17 show the experimental and predicted gas-temperature profiles for wall temperatures of 600 and 1400°F. At a wall temperature of 600°F the measured gradients are observed to exhibit a similar trend to the gradients measured in the air runs, i.e, the measured gradients are steep, i.e., the temperature gradient is much the same as predicted when the velocity profile was evaluated at the inlet Reynolds number.

At a nominal wall temperature of 1400°F the measured gradients at the wall are observed to become less than the predicted gradients; this trend is opposite to that observed for the corresponding air run (9c).

Figure 4.6-18 compares the measured and predicted profiles in the centre region (core) of the column. The measured temperatures are considerably higher than those predicted from the theoretical model. This discrepancy did not exist in the core of the column for the high-temperature air run (9c). (See Figure 4.6-10.)

It should be noted that steam-run 6c was carried out at the same nominal Reynolds number, based on the conditions at the inlet, as air-run 9c. Further, the Grashof number for the steam runs was less than that for the corresponding air run since both the property group, $\frac{g\beta\rho^2}{\mu^2}$, and the ΔT term in the Grashof number were less for steam than for air. Therefore one would expect the velocity profile to be affected in the same way for steam as for air with the same trend towards greater-than-predicted

GAS TEMPERATURE PROFILES —STEAM 3C —

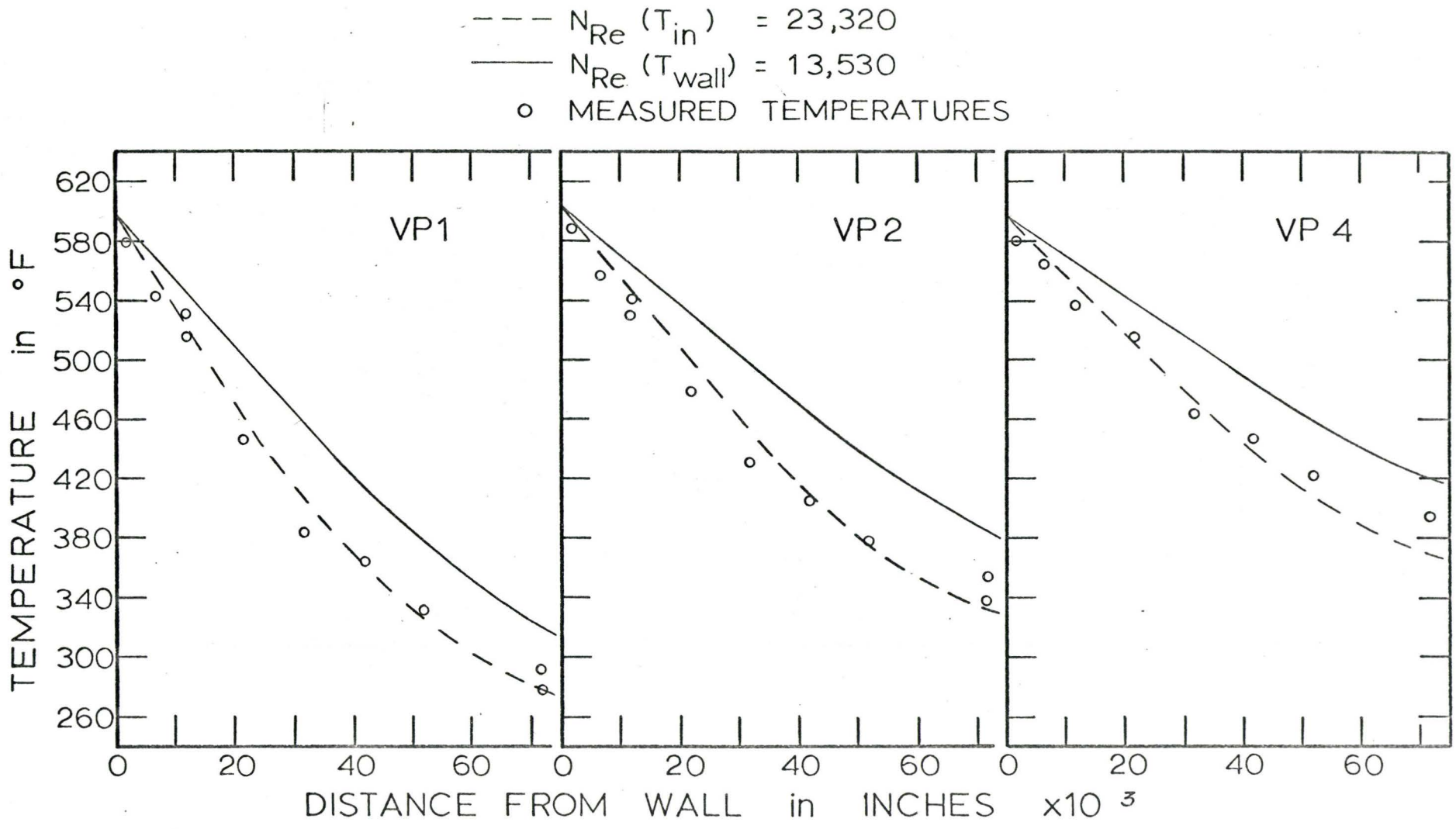

FIGURE 4·6—14

GAS TEMPERATURE PROFILES —STEAM 4C—

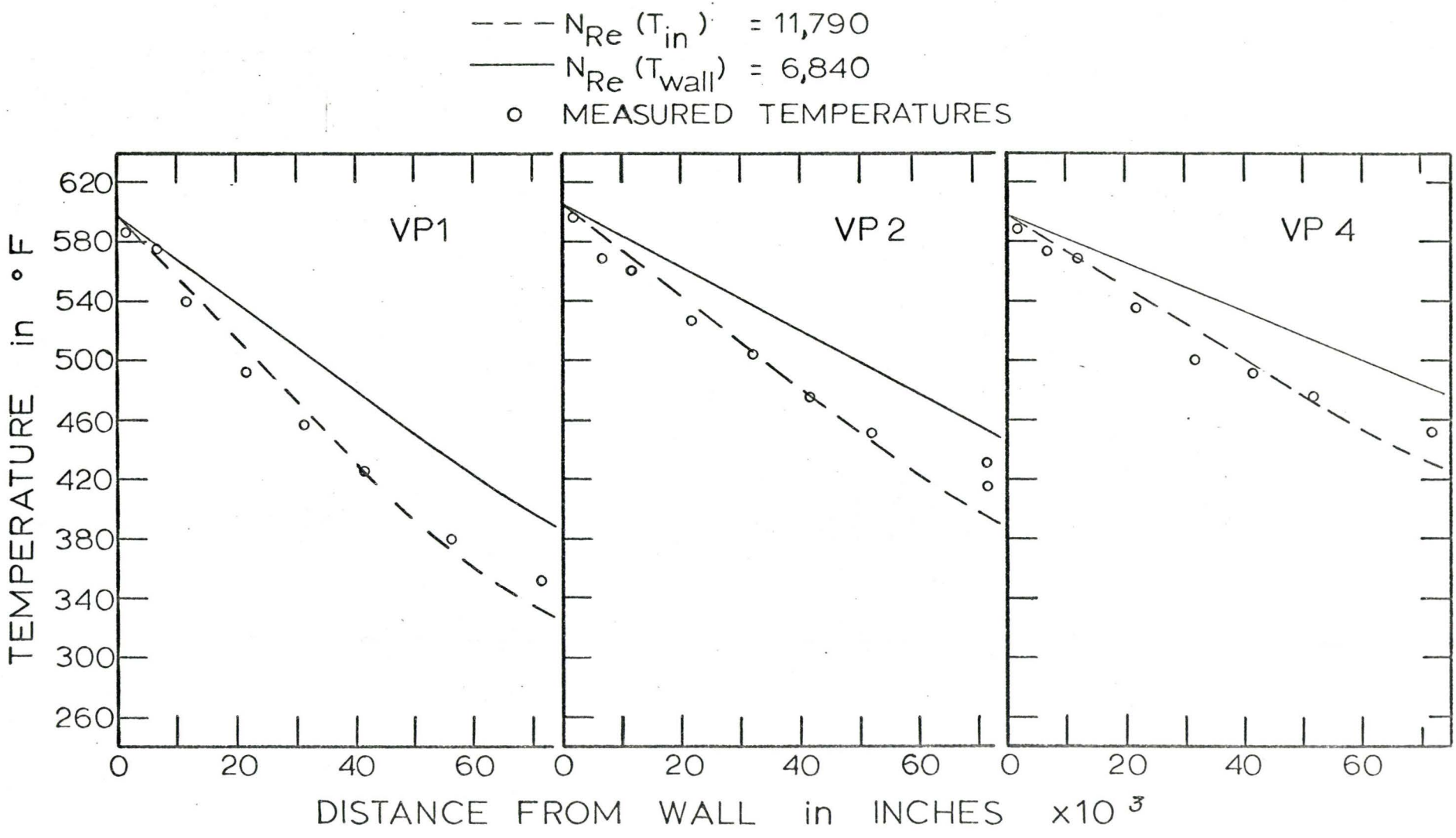

FIGURE 4·6—15

GAS TEMPERATURE PROFILES — STEAM 5C —

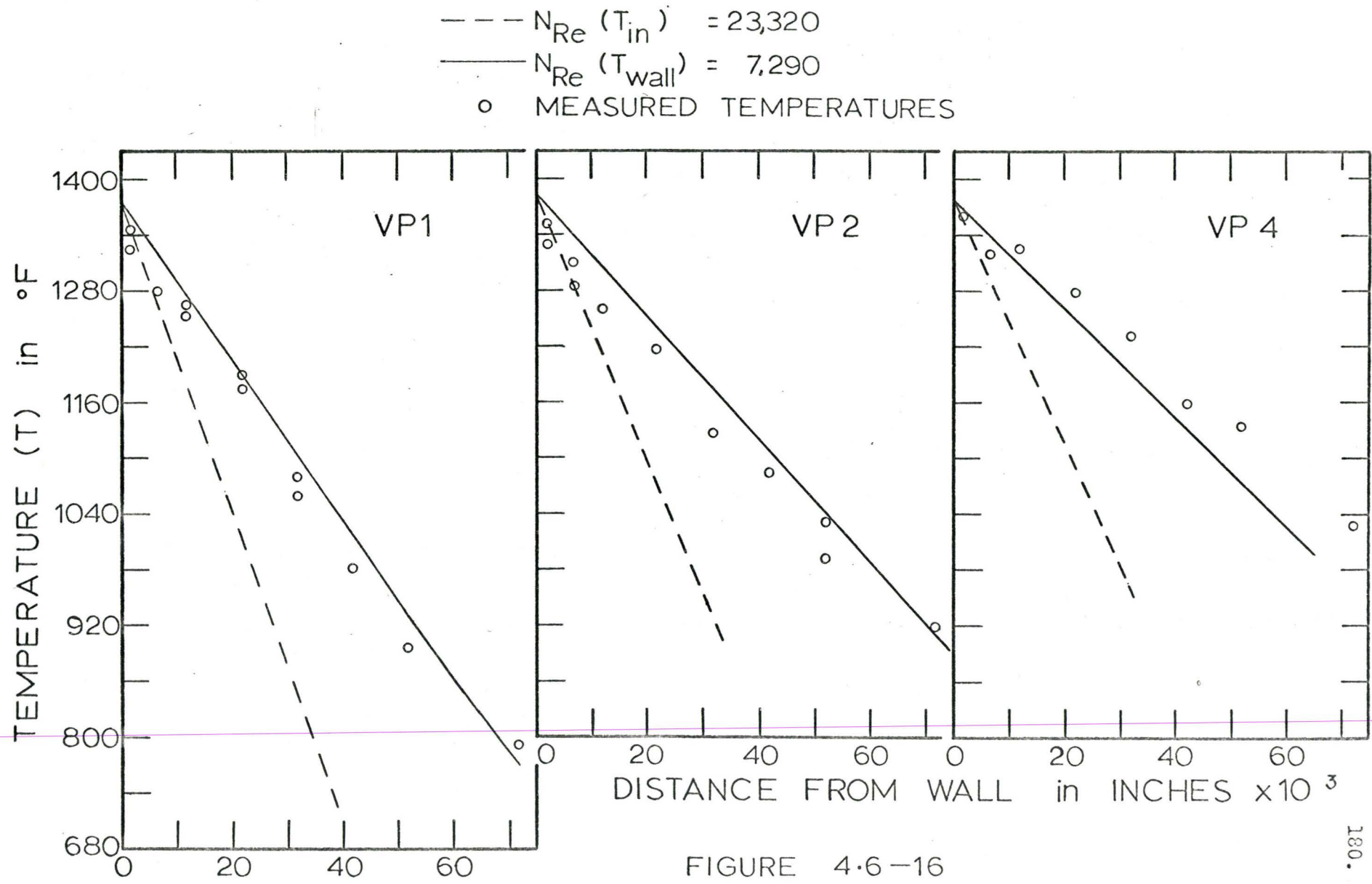

FIGURE 4·6—16

GAS TEMPERATURE PROFILES — STEAM 6C —

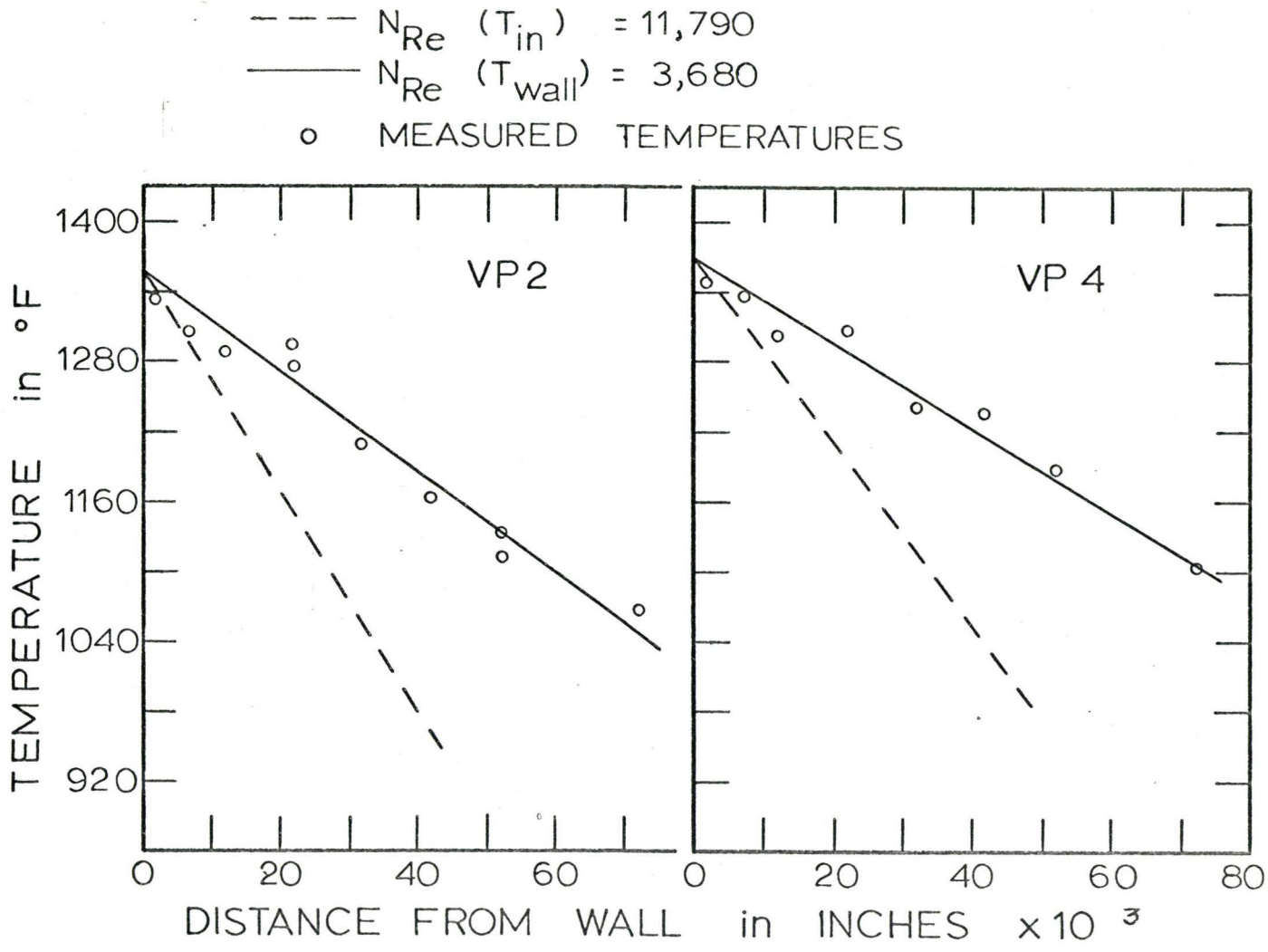

FIGURE 4·6—17

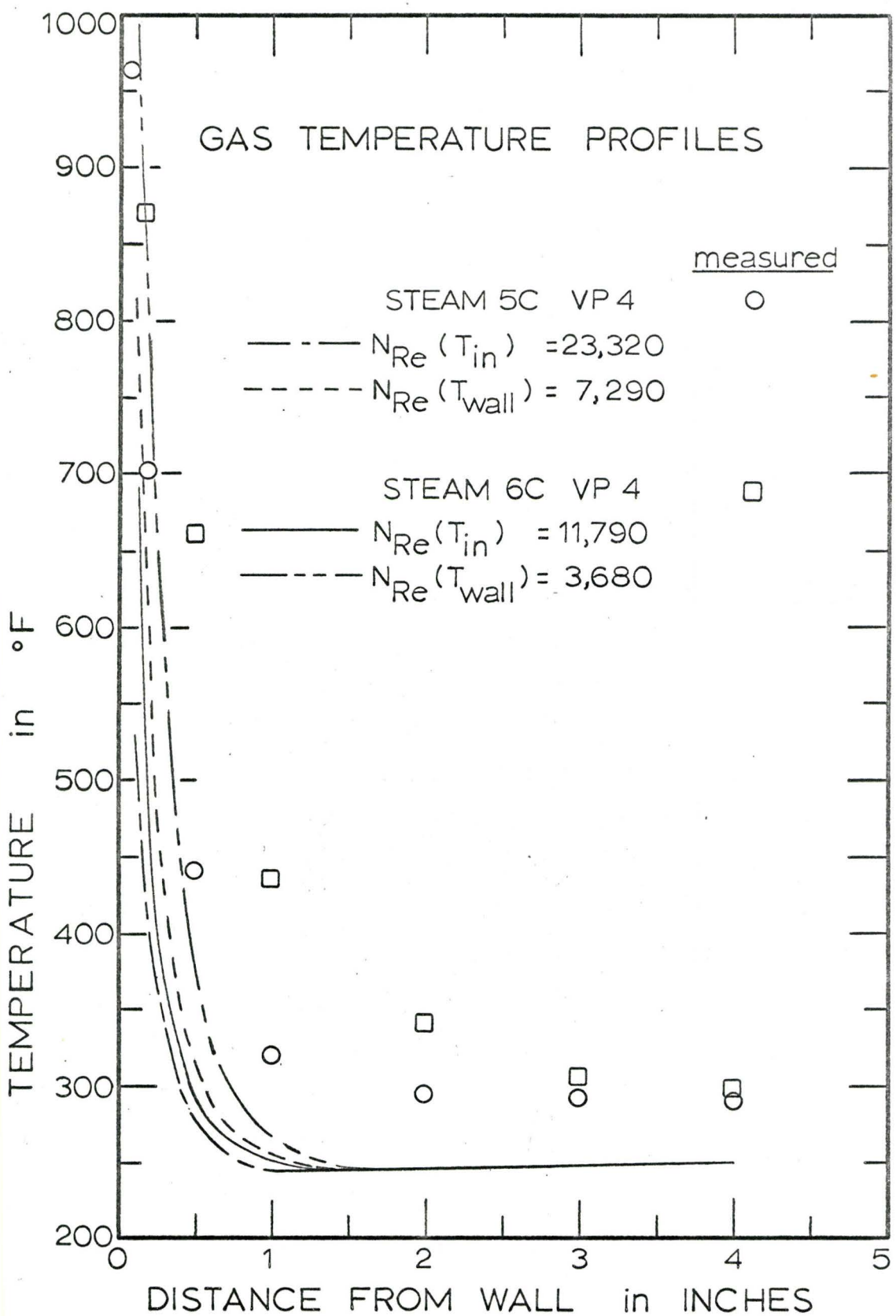
GAS TEMPERATURE PROFILES
measured
STEAM 5C VP 4
$N_{Re}(T_{in})$ =23,320
$N_{Re}(T_{wall})$ = 7,290
STEAM 6C VP 4
$N_{Re}(T_{in})$ = 11,790
$N_{Re}(T_{wall})$ = 3,680
TEMPERATURE in °F
1000
900
800
700
600
500
400
300
200
0
1
2
3
4
5
DISTANCE FROM WALL in INCHES

FIGURE 4·6 —18

temperature gradients. Thus the higher temperatures noted in the steam runs cannot be explained in terms of a natural-convection effect which causes flow reversal and brings hot gases from the lower regions of the pipe.

The higher gas-temperature levels cannot be explained in terms of the hydro-dynamics of the gas flow. It should be recalled that one of the objects of this investigation was to predict the rate of heat transfer by radiation to a flowing, absorbing medium with the contribution of convection included. The experimental runs at this high wall temperature were carried out to experimentally verify the temperatures predicted from a radiation-convection model.

In this discussion it has been established that the profiles measured in steam at high wall temperatures cannot be explained in terms of a flow-phenomenon effect. Consequently the measured temperatures do indicate that the expected effect of radiation was present in the system. Further discussion of the experimental results and the temperatures predicted by a radiation model will be made in the following chapter.

4.7 Conclusions

1. The experimentally measured, isothermal velocity profiles validated the fully-developed flow assumption which was made in the theoretical model.

2. The solution of the finite-difference approximation to the energy equation successfully predicted the temperature profiles and rate of heat-transfer in the immediate entrance region of a cylindrical pipe at low wall-to-bulk temperature ratios where the assumption of constant properties can be considered valid.

3. In the absence of radiation, the mathematical model predicted a lower heat-transfer rate than measured experimentally. The discrepancy could not be explained in terms of a variable physical property effect or in terms of a distortion of the velocity profile due to natural-convection effects.

4. The larger-than-expected heat-transfer rates were hypothesised to be caused by an instability or turbulent phenomenon in the flow field. It was not possible to verify this hypothesis with the present experimental data.

5. To completely understand the heat-transfer phenomena which occur under the flow and high-temperature conditions of these experiments it is imperative that the gas velocities in the system be measured.

6. For steam flows, at high wall temperatures, it was possible to experimentally detect the effect of radiation on gas-temperature

profiles. As expected, radiation was observed to cause the gas-temperature gradients at the wall to be less than those predicted for pure convective heat transfer. Radiation also increased the gas-temperature level across the entire column.

5. RADIATION AND CONVECTION

5.1 Introduction

The experimental temperature profiles presented in Chapter 4, for steam flowing through a cylindrical pipe with walls at 1400°F, indicated that the effect of radiation could be detected in this particular system. Since the prediction of heat transfer by convection in the entrance region of this system has been found to be reasonably satisfactory the next step in the study was to combine the mechanisms of convection and radiation.

The prediction of heat-transfer rates and gas-temperature profiles in a system where radiation and convection both occur, is considered in this chapter. In this analysis the processes of radiation and convection were assumed to be additive. The rate of heat transfer by convection, which was calculated in Chapter 4, was simply added into the radiation model. The rate of heat transfer by radiation was calculated by procedures indicated in the literature.

The ability of the radiation model to predict gas-temperature profiles in the absence of radiation was evaluated; i.e., the temperature profiles predicted with the radiation model were compared to those predicted by the convection model of Chapter 4.

The temperature profiles predicted by the radiation model were then compared to the experimentally measured gas-temperature profiles.

5.2 Analysis

As discussed in Section 2.2.1, the basic idea for the prediction of the radiation interchange in an enclosure is to divide the gas volume and the surfaces into a number of finite, essentially isothermal zones. A heat and material balance is then made on each zone and the unknown zone temperatures can then be determined by solving the resultant set of simultaneous algebraic equations.

For a general zone, the heat and material balance for a steady flow of non-reacting gases can be written as:

Heat into the zone as the result of

(1) the convection/conduction from adjacent wall and gas zones

(2) the enthalpy of the gas flowing into the zone

(3) the absorption of radiation streaming into the zone from all other zones in the system

must be equal to

Heat out of the zone as the result of

(1) the convection/conduction to the adjacent wall and gas zones

(2) the enthalpy of the gas flowing out of the zone

(3) the emission of radiation streaming out of the zone to all other zones in the system.

5.2.1 Radiation

The emission of radiation from each gas and surface zone must be calculated along with the radiant interchange between all pairs of such zones, making due allowance for attenuation of the radiation by the absorbing medium between the zones

and for diffuse reflection from the surfaces of the enclosure. The geometrical portion of the problem can be solved independently of the temperature distribution once a specific zone-geometry has been selected. Because of the requirement that the zones be essentially isothermal, and because the experimental temperature measurements indicated that radial temperature gradients existed across the column, the cylindrical column was zoned by dividing the column into a number of annular rings of square cross-section as shown in Figure 5.2-1. (The numbers indicate the zone identification used in the model of the system.) This particular zone-configuration was dictated by the "interchange areas" (explained in the ensuing discussion) which were available in the literature[E1].

The interchange between any two zones in the system is the sum of the direct radiant flux between the two zones and the reflected flux from the walls of the enclosure due to energy originating at either of the zones under consideration. The direct interchange between two zones, i.e., the interchange in a black-walled* system, will be considered first.

(i) Direct-Interchange Areas

The direct interchange between two finite zones, gray gas (k independent of wavelength and temperature) and/or black surface of any shape and relative disposition and with gray absorbing gas intervening, is proportional to the difference in black emissive power, E ($\equiv \sigma T^4$), of the zones.

* A black-wall or perfect radiator is a surface which emits the maximum radiation possible at a given temperature; i.e., the surface emissivity, ε, has the value, one.

ZONE SYSTEM FOR CYLINDRICAL COLUMN

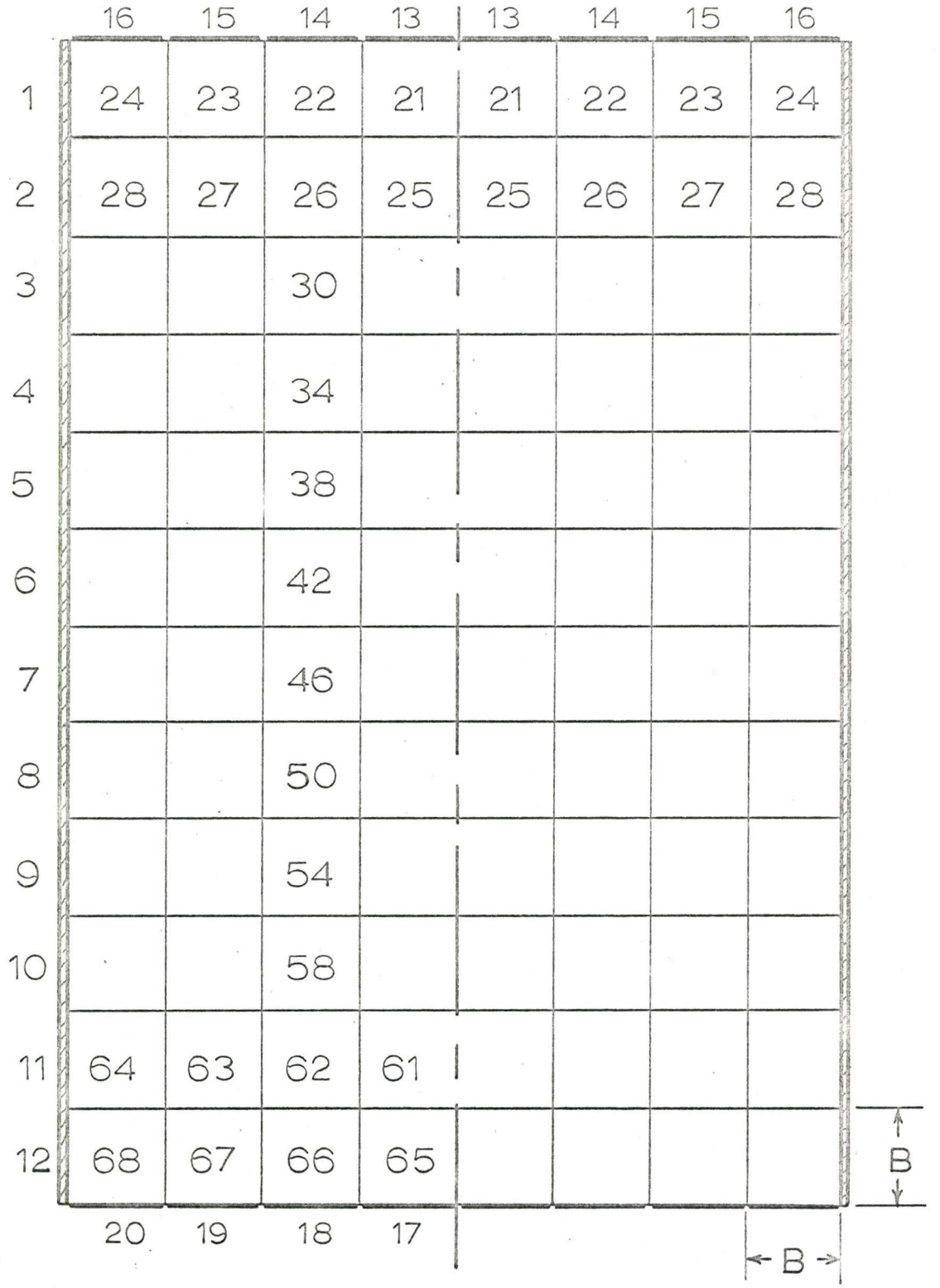

FIGURE 5·2 –1

The proportionality constant, which has the dimensions of area, is a function only of the system shape and of kL where L is a characteristic dimension of the system. This constant, designated by $\overline{ss}$, $\overline{sg}$, or $\overline{gg}$ for surface to surface, surface to gas, or gas to gas radiant interchange respectively, is called the direct-interchange area[H7].

The direct-interchange area may be thought of as the product of two terms. The first, having the dimensions of area, is the actual area for a surface zone and (4) (gas-zone volume) (absorption coefficient) for a gas zone. The second is the "reception factor", f, where f is defined as the fraction of the energy originating in any one zone in a black-walled enclosure which reaches and is absorbed by any other zone in the enclosure. (This factor takes into account the attenuation of the radiation by the absorbing medium between the zones; it is a function of the absorption coefficient of the gas.)

The direct-interchange areas for the interchange between zones of the configuration shown in Figure 5.2-1 are available in the literature[E1] as a function of the product of the absorption coefficient of the gas, k, and the zone size, B.

As discussed in Section 2.2.1, a real gas can be considered as being made up of a number of gray gases, each with a constant absorption coefficient, k. When analyzing the radiation interchange in an enclosure it is necessary to calculate the direct-interchange areas for each of the gray gases which

contribute to make up the real gas. The total interchange for the real gas is then calculated from the sum of the interchanges for each of the gray, plus one clear gas (k = 0).

(ii) Total-Interchange Areas

Radiation from one zone may reach a second zone both directly and after one or more reflections at the enclosure surfaces. Allowance for multiple reflections can be made by the methods of Hottel[H7]. For a gray gas the total flux between two zones i and j must be proportional to $\sigma(T_i^4 - T_j^4)$. The proportionality constant, called the total-interchange area is designated by $\overline{SS}$, $\overline{GS}$, or $\overline{GG}$ with subscripts to identify the zone number. The total-interchange areas between all zone pairs are evaluated from direct-interchange areas for each gray-gas component. When the product of the absorption coefficient and the zone size, kB is larger than 0.4, temperature gradients within the zone can no longer be neglected; i.e., the assumption of an isothermal zone is no longer valid*. For such cases the direct-interchange areas can be modified by the techniques given by Hottel and Sarofim[H12]. When kB is greater than 3, the total-interchange areas between contiguous zone pairs are calculated using the Rosseland diffusion equation[H2, S11, R9]. Details of the calculation of total-interchange areas from direct-interchange areas are given in Appendix E.

In the heat and material balance equation the total-interchange areas are coefficients of the zone temperatures.

---

* In this investigation kB was always less than 0.4

They can be determined prior to solving the heat and material balance by

(1) assuming a representative gas and surface temperature

(2) calculating the absorption coefficient and weighting factor "a_i" for each gray-gas component of the real gas [1] from gas emissivity data as discussed in Section 2.2.1

(3) determining the direct-interchange areas for each of the gray gases plus one clear gas.

(4) calculating the total-interchange areas as shown in Appendix E.

(iii) Present Investigation

In this investigation the 12-in. long "hot-zone" of the column was divided into 12 1-in. long surface zones and 48 1-in by 1-in. annular-ring gas zones. The ends were considered as black porous plugs at the temperature of the inlet gas; they were divided into 4 rings of 1-in. width. The configuration is shown in Figure 5.2-1.

The real gas was assumed to be composed of one gray gas of absorption coefficient, k, and one clear gas (k = 0). Hottel has shown [H7], that for the one clear, one gray-gas assumption the absorption coefficient and weighting factor can be determined from the gas emissivity (or absorptivity), evaluated at path length, L, and a path length of 2L, by the following relationships

$$a = \varepsilon_L^2/(2\varepsilon_L - \varepsilon_{2L}) \qquad (5.2\text{-}1)$$

$$kL = \ell n \, (\varepsilon_L / \varepsilon_{2L} - \varepsilon_L) \qquad (5.2\text{-}2)$$

For this system, with high wall temperatures and relatively low gas temperatures, the process of gas absorption of surface emission predominates over the process of gas emission to the surface. Consequently the "a" and "k" were determined from gas absorptivities rather than emissivities.

A representative gas and wall temperature were selected and the gas emissivity was calculated from Bevan's correlations[B3], (given in Section 2.2.1 as equations 2.2-5 to 2.2-7) at modified pressure-path length products, PwL (T_w/T_G), Pw2L (T_w/T_G) as suggested by Hottel[H8]. Since the correlations were obtained from emissivity data at zero partial pressure of water vapour, it was necessary to apply a correction factor[H8] to the calculated emissivity to account for the actual partial pressure of the water vapour. The absorptivities were determined from the emissivities by multiplying the corrected emissivities by $(T_G/T_w)^{0.45}$ as Hottel suggests. The "a" and "k" were then determined as indicated above.

The calculated value of "k" was multiplied by the zone size "B" and the direct-interchange areas were calculated from Erkku's tabulations[E1].* The total-interchange areas were then calculated as indicated in Appendix E.

---

* Erkku's tabluations of "interchange area" versus kB were regressed to give third order polynomials, one for each pair of zone configurations. Values calculated from the regression equation never differed from the tabulated value by more than 1%.

5.2.2 Convection/Conduction

Gas zones adjacent to enclosure surfaces receive heat ($t_{wall} > t_{gas}$) by convection from the contiguous surface zones. Consequently it is necessary to have a knowledge of the convective heat transfer which occurs in the particular system. The rate of convective heat transfer is proportional to some temperature difference which is characteristic of the system; the proportionality constant is usually referred to as the heat-transfer coefficient, h.

The heat-transfer coefficient is included in the heat and material balance equation as a coefficient of the appropriate zone temperatures. The heat-transfer coefficient is considered to be a coefficient of the wall-zone temperatures and the contiguous gas-zone temperature. Consequently the heat-transfer coefficient must be defined in terms of the temperature difference between the wall temperature and the gas temperature taken at a distance from the wall equal to ½ the zone size; i.e., h must be defined by

$$q/A = -k \left(\frac{\partial t}{\partial r}\right)_{wall} = h \left(t_{wall} - t_{wall + B/2}\right) \qquad (5.2.-3)$$

rather than the more familiar

$$q/A = -k \left(\frac{\partial t}{\partial r}\right)_{wall} = h \left(t_{wall} - t_{bulk}\right) \qquad (5.2-4)$$

In this investigation, the heat-transfer coefficients were determined from the Nusselt numbers ($\frac{hD}{k}$) which were calculated from the temperature profiles predicted by the theoretical convection

model (discussed in Chapter 4). The values of "h" used in the radiation model were fixed for any one surface zone; i.e, they were not allowed to vary with temperature, hence the process of radiation and convection were considered to be additive.

In the radial direction, if the mean value of the radial velocity is zero, heat is transferred between zones by molecular and turbulent diffusion. Thus in the heat and material balance equation the effective thermal conductivity is included as a coefficient of the gas zone temperatures to account for the radial conduction of heat. Since the effective conductivity or diffusivity is a point-function of radial position, some average value must be used when the zones are of finite size. In this analysis the values for the effective diffusivity were taken to be the point values (calculated in the convection model - Chapter 4) which occurred at the boundaries between the gas zones; i.e., the point values which were calculated at r = 1, 2, 3-in. in the convection model were used as temperature coefficients in the radiation model.

Axial diffusion was assumed to be negligible in this model. The calculated results given in Section 4.3.3 indicated the validity of this assumption.

5.2.3 Enthalpy Flux

Energy is transported into and out of each gas zone by bulk transport in the axial direction. ($U'_{ave}\ \rho\ Cp\ t\Pi(r_i^2 - r_j^2)$; where $\Pi(r_i^2 - r_j^2)$ is the cross-sectional area, of the annular gas zone, perpendicular to the direction of flow.) Because of the

relatively coarse grid used in the model it was necessary to determine average velocities over each of the 1-in. annular rings. The velocities were calculated from Pai's expression for the fully-developed turbulent velocity profile for flow in a circular tube[P17],

$$\frac{U'}{U'_{max}} = 1 - 0.351 \left(\frac{r}{r_w}\right)^2 - 0.650 \left(\frac{r}{r_w}\right)^{66}; \qquad (5.2\text{-}5)$$

the coefficients, which are flowrate dependent, were evaluated for a Reynolds number of 25,000.

The average velocity for each zone was calculated in terms of the average velocity over the column cross-section.

The heat-capacity flowrate was included in the heat and material balance equations as a coefficient of the gas-zone temperature.

5.2.4 Heat and Material Balance Equation

The heat and material balance equation, which was previously given in words, can now be written for a general gas-zone.

Since the radiation terms in the energy balance are given as multiples of T^4, the equations were linearized in T^4 by forcing the convection and enthalpy-flux terms into a fourth-power law. A coefficient was defined such that when multiplied by $\sigma T^4(E)$ it yielded the one-way flux between any two zones. With the enthalpy-flux and convective-flux coefficients denoted by η and γ respectively, with a first subscript representing the energy-source zone and a second one the energy-sink zone, they could be written as

$$\eta_{g_1 g_i} = U'_{ave}\ \rho Cp\ A/E_{g_1} \qquad (5.2\text{-}6)$$

$$\gamma_{g_1 g_i} = k_{eff.}\ T_{g_1}\ A/E_{g_1} \qquad (5.2\text{-}7)$$

and

$$\gamma_{s_1 g_i} = h\ T_{s_1}\ A/E_{s_1} \qquad (5.2\text{-}8$$

where A is the area common to zones 1 and i.

With the convention that a positive q represents flux to a zone in question, the energy interchange between gas zone g_1 and all other zones (g_2, g_3 .... g_i, s_1, s_2 .... s_j, those having a common boundary with g_1; g_{10}, g_{11} .... s_{10}, s_{11}, ...; those not touching g_1) was written as

$$E_{g_1}\left(\overline{G_1 G_1} - 4\,k\,a\,V_{g_1} - \sum_i \gamma_{g_1 g_i} - \sum_j \gamma_{g_1 s_j} - \sum_i \eta_{g_1 g_i}\right) + E_{g_2}\left(\overline{G_2 G_1} + \gamma_{g_2 g_1} + \eta_{g_2 g_1}\right) + \ldots$$

$$+ E_{g_{10}}\left(\overline{G_{10} G_1}\right) + \ldots.$$

$$+ E_{s_1}\left(\overline{S_1 G_1} + \gamma_{s_1 g_1}\right) + \ldots.$$

$$+ E_{s_{10}}\left(\overline{S_{10} G_1}\right) + \ldots. = 0 \qquad (5.2\text{-}9)$$

A similar balance was made for each gas and surface zone in the system. The resultant set of simultaneous algebraic equations could be easily solved with the aid of a high-speed digital computer. In this analysis the equations were solved on an IBM 7040 computer by a direct iteration technique; i.e., an

initial gas-temperature distribution was assumed, then each zone temperature was calculated in turn from the existing temperature distribution (assumed and/or previously calculated). This iterative process was repeated until each calculated temperature did not change by more than a pre-determined convergence limit.

The above formulations (5.2-6 to 5.2-9) were taken directly from the analysis of Hottel and Cohen[H7].

Program listings for the solution of heat and material balance equations, with radiation and convection/conduction included, are given in Appendix Z.4.

5.3 Experimental Equipment and Procedure

The apparatus, temperature measuring device and experimental procedure were described in Section 4.4 and 4.5.

5.4 Results and Discussion

5.4.1 Calculated Results

Table 5.4-1 compares the temperatures calculated by the radiation model, when kB was equal to zero, (no radiation to the gas) to those* calculated by the convection model under the same flow conditions and wall temperature distribution. The temperatures

---

* The point temperatures calculated by the convection model were averaged to give the bulk or mixed-cup temperature over 1-in. annular rings corresponding to the gas zone used in the radiation model.

TABLE 5.4-1 : Comparison of Temperatures Predicted by the Convection and Radiation Models

Flowrate 364 lb./hr. - Nominal wall temperature - 1400°F

Axial position (distance from top of hot zone) \ radial boundaries of zones (inches) from centre line	0-1	1-2	2-3	3-4
VP1 (0.5-in.)	249*	247	245	286
	249	247	246	290
VP2 (3.0-in.)	249	247	246	313
	249	247	248	312
VP4 (9.0-in.)	248	247	248	361
	249	248	246	352

Flowrate 184 lb.hr. - Nominal wall temperature - 1400°F

VP1	249	247	246	306
	248	248	246	310
VP2	249	247	246	344
	248	248	249	337
VP4	248	247	252	409
	248	249	258	384

* The top number is the temperature (in °F) calculated by the convection model; the number immediately below is the temperature calculated by the radiation model.

in the table correspond to axial distances along the column where experimental temperature measurements were taken.

The temperatures predicted by the two models are in reasonable agreement, the maximum difference being 7%. At the present stage of development, the calculation of the convection/conduction heat-transfer mechanisms in the radiation model can not be considered to be quantitative; i.e., because it was necessary to use a coarse grid for the radiation analysis, the radial conduction had to be calculated by assuming that point values of the effective eddy diffusivity applied at the zone boundaries.

The present results do indicate though, that the method of allowing for radial conduction in the radiation model is a reasonable one.

5.4.2 Experimental Results

Table 5.4-2 shows the average temperatures calculated from the experimental data for each 1-in. annular ring in the 8-in. diameter column. The calculations were made by assuming that the fully-developed adiabatic velocity profile of Deissler[D13] could be applied to describe the velocity profile in the column. As discussed in Chapter 4, the velocity profile would be distorted under the high temperature gradient conditions of the experiment but since the actual velocity profile was not known Deissler's profile was considered to be a reasonable, rough approximation.

Table 5.4-3 shows the gas-zone temperatures calculated by the radiation model using the experimental wall temperature

TABLE 5.4-2 : Experimental Temperatures (^{o}F)
Averaged over 1-in. Annular Rings

Flowrate 364 lb./hr. - Nominal wall temperature - 1400^{o}F
(steam 5c)

Axial position (distance from top of hot zone) \ Radial Boundaries of zones (inches) from centre line	0-1	1-2	2-3	3-4
VP1 (0.5-in)	263*	263	263	282
	263	263	263	278
VP2 (3.0-in)	276	276	279	312
	276	276	279	307
VP4 (9.0-in)	293	296	306	400
	293	296	306	393

Flowrate 184 lb./hr. - Nominal wall temperature - 1400^{o}F
(steam 6c)

VP2	291	298	323	465
	291	298	323	452
VP4	300	318	370	553
	300	318	369	539

---

* The top number was calculated with velocity profile evaluated at inlet temperature. Lower number corresponds to velocity profile evaluated at wall temperature.

TABLE 5.4-3 : Gas Zone Temperatures (^{o}F) Calculated by Radiation Model

Flowrate 364 lb./hr. - Nominal Wall Temperature - 1400^{o}F
Wall emissivity 0.9

Axial position (distance from top of hot zone) \ Radial Boundaries of zones (inches) from centre-line	0-1	1-2	2-3	3-4
VP1 (0.5-in.)	264*	265	266	295
	264	265	266	307
VP2 (3.0-in.)	269	270	276	334
	269	271	281	363
VP4 (9.0-in.)	282	287	308	412
	284	292	325	476

Flowrate 184 lb./hr. - Nominal Wall Temperature - 1400^{o}F
Wall emissivity 0.9

VP2	303	311	340	522
	304	314	352	548
VP4	334	352	405	630
	340	365	439	673

---

* The upper number was calculated using the heat-transfer coefficients and eddy diffusivities calculated from the convection model with the Reynolds evaluated at the wall temperature. The lower number uses the same parameters from the convection model with the Reynolds number evaluated at the inlet temperature.

distribution. The calculated temperatures did not differ by more than $4^{\circ}F$ when a wall emissivity of 0.8 rather than 0.9 was used. The total-interchange areas were evaluated with kB = 0.306 and a = 0.354. The values of kB and a were determined for an average wall temperature of $1400^{\circ}F$ and an average gas temperature of $300^{\circ}F$. by the methods shown in Appendix E. The temperature distribution was obtained by direct iteration. The solution was assumed to have converged when the gas-zone emissive powers did not change in value from iteration n to iteration n+1 by more than 0.1%. With this convergence criterion the solution converged after 11 iterations. (Computation time : 20 sec.). The rate of convergence was accelerated by using a "relaxation factor" of 3. If the relaxation factor was not used (i.e., had the value of 1) the number of iterations required for convergence was 73. As the value of the relaxation factor was increased beyond 3, the number of iterations required for convergence began to increase.

A comparison of the temperatures presented in Table 5.4-2 and 5.4-3 indicates that the radiation model predicts temperatures which are in reasonable agreement with the measured temperatures. The agreement is seen to be best for the zones in the centre of the column. The predicted temperatures for the zone adjacent to the wall are all greater than the temperatures calculated from the experimental data for this zone. This is to be expected in the light of the results obtained for the air runs. It will be recalled that the experimental gas temperatures, for air, adjacent to the wall were

all less than the temperatures predicted from the convection model (steeper gradient). The experimental temperatures for steam, under the same flow conditions and wall temperature distribution were found to be much closer to, and in some cases greater than, the temperatures predicted by the convection model. This trend was expected since the absorption of thermal radiation by the steam (not accounted for in the convection model) causes the gas-temperature to increase; i.e., the enthalpy content of the gas is increased by both convection and radiation heat-transfer mechanisms. Thus, if radiation is not accounted for in the prediction of the gas temperature profiles, and the same hydrodynamic mechanisms which tend to decrease the gas temperatures adjacent to the wall are active for both steam and air flows, the calculated temperatures would be expected to be closer to the measured temperatures.

When radiation is included in the model the predicted temperatures should now be greater than the measured temperatures adjacent to the wall, as in fact observed.

Sarofim[S11] has shown that the one-gray-plus-clear gas approximation to the real gas gives too small a weighting to the absorption by the gas adjacent to, and far from a surface, but too large a weighting to the absorption in the intermediate regions. He shows how the strong absorption bands which are important at small path lengths cause the temperature of the gas to bend towards the wall temperature in the regions adjacent to the surface. He compared the gas temperature profile predicted by a three-gray-plus-

one-clear gas approximation to those predicted by a one-gray-plus clear gas approximation fitted at mean beam lengths of 1 and 2 and fitted at mean beam lengths of ½ and 1. The temperatures calculated for a one-gray-plus-clear gas, fitted at mean beam lengths of ½ and 1, were in much better agreement (12%) with the temperatures calculated by the more exact approximation (three-gray-one-clear) than those calculated for a one-gray-plus-clear gas fitted at mean beam lengths of 1 and 2 (22%).

The temperatures shown in Table 5.2-3 were calculated for a one-gray-plus-one-clear gas fitted at mean beam lengths of 1 and 2. When the fit was made at mean beam lengths of ½ and 1 the calculated temperature in the zone adjacent to the wall was found to increase by $2^{o}F$ at the entrance to the column and by $11^{o}F$ at the exit. Thus if more weight were given to the absorption by the gas adjacent to the wall, the calculated temperatures would be even higher than the measured temperatures in the gas zone adjacent to the wall.

When the fit was made at mean beam lengths of ½ and 1, kB was found to have a value of 0.514 and a was found to be 0.305. Thus, according to Hottel and Sarofim[H2] it is not realistic to assume an isothermal zone under these conditions and a correction must be applied to account for the temperature gradient across the zone. This was not done in this work but should be considered in future developments of the radiation model.

5.5 CONCLUSIONS

It is obvious that more experimental measurements must be made under a wider range of conditions, and that the model must be further developed before it is possible to quantitatively evaluate the ability of the model to accurately predict gas temperatures in an absorbing medium. The present investigation has indicated however that the temperatures predicted by the model are in qualitative agreement with the measured temperatures and that the deviation between predicted and measured results is in the direction expected when one considers the effects noticed in the air runs.

In particular, the method of handling the radial conduction and convective heat transfer from the wall should be studied and improved upon. Also, the more exact, three-gray-plus-one-clear gas approximation to a real gas should be included in the model.

Because of the high temperature gradients adjacent to the wall, the grid size should be reduced to obtain a better description of the temperature profile close to the wall. A reduction in grid size will necessitate the evaluation of more direct-interchange areas for a cylindrical geometry.

As in the case of the convection model, it is obvious that a complete and accurate radiation model must incorporate a realistic velocity profile. Thus it is emphasized once again that experimental techniques must be developed to permit the determination of gas velocity profiles in turbulent-flow systems in the presence of large temperature gradients.

6. RADIATION TO SPRAYS EVAPORATING IN A HIGH-TEMPERATURE ENVIRONMENT

6.1 Introduction

This chapter discusses briefly the theoretical analysis of radiation to sprays in a high-temperature environment. The simplifying assumptions and methods of calculation are also discussed.

The experimental work, which was begun to check the model and assumptions contained therein, is presented. The preliminary development of an in situ photographic technique is also presented.

6.2 Analysis

The analysis of radiation to sprays evaporating in a high-temperature environment represents an extension of the radiation model discussed in Chapter 5; i.e., the enclosure is divided into a number of isothermal gas and surface zones of finite size and a heat and material balance is performed on each zone.

For a cloud or spray of volatile droplets transported in an absorbing, non-reacting gas under steady-flow conditions, the heat and material balance on a general gas zone can be written as:

Heat into the zone as the result of

(1) the convection/conduction from adjacent wall and gas zones.

(2) the sensible heat content of the gas and droplets flowing into the zone

(3) the absorption of thermal radiation streaming into the zone from all zones in the system

must be equal to

Heat out of the zone as the result of

(1) the convection/conduction to adjacent wall and surface zones

(2) the sensible heat content of the gas and droplets flowing out of the zone

(3) the emission of thermal radiation streaming out of the zone to all other zones in the system

(4) the latent head load within the zone due to evaporation of the spray.

This energy balance is identical to that presented in Section 5.2 except for the additional latent heat load term. The latent heat required for evaporation of a spray in a high-temperature environment is supplied to the droplets by

(1) conduction/convection from the gas

(2) thermal radiation from the absorbing-emitting gas

and(3) thermal radiation from the surfaces of the system

6.2.1 Conduction/Convection

Droplets less than 50 microns in diameter have a terminal velocity which is much less than the gas velocities of 3 to 8 ft./sec. which were used in this study. Dlouhy[D2] and Kessler[K1] found that for small droplets which were flowing with essentially zero velocity relative to the transporting gas, the droplets followed the turbulent eddies of the gas stream and consequently heat was transferred to the droplets by conduction only; i.e, the droplets could be considered to be suspended in a stagnant atmosphere. Theoretical calculation of the rate of heat transfer by conduction

to a sphere immersed in an infinite stagnant fluid environment indicates that the Nusselt number for pure heat transfer would be equal to 2.0.

When a temperature difference exists between the sphere and the fluid, natural-convection effects arise by virtue of the varying buoyancy forces around the sphere, and the heat-transfer rate is increased accordingly.

The above considerations hold for the case of pure heat-transfer. For an evaporating droplet the processes of heat and mass transfer occur simultaneously and the evolution of vapour from the surface of the drop will cause a reduction in the rate of conductive/convective heat transfer[H1]. In a high-temperature environment, any radiation absorbed by the droplet will increase the rate of vapourization over that expected for conduction/convection only. The increased mass flux from the droplet will further reduce the convective/conductive heat-transfer to the droplet.

Hoffman[H1] measured evaporation rates of stationary droplets (0.4 to 1.44 mm) evaporating in a high-temperature environment. The results suggested that the evaporation process was governed by the effect of the evolved vapours on the boundary layer flow. Since the rate of vapour evolution depends upon the total heat transferred to the droplet, both by convection and radiation, the effect of the evolved vapours on the convection process cannot be determined without a knowledge of the radiation absorbed by the droplet. Hoffman found that his results could be correlated by the equation

$$\dot{m}\ Cp/\Pi dk_f = 2.9\ B^{0.93} \qquad (6.2\text{-}1)$$

or, alternatively, by

$$(N_{Nu})_{actual} - B' = 2.9\ B^{0.93} \qquad (6.2\text{-}2)$$

where B is the Spalding transport number ($Cp\Delta t/\lambda$),

B' is a modified transport number which includes the effect of radiation ($Cp\ \Delta t/[\lambda - q_R/\dot{m}]$)

q_R is the radiant energy absorbed by the drop.

$\dot{m}$ is the evaporation rate of the drop ($dm/d\theta$).

As the drop-diameter increases beyond 50 microns the relative velocity between the transporting gas and suspended droplets increases and the droplets become subjected to a forced-convection flow field. (Decelerating droplets in the nozzle zone are also evaporating in a forced-convection flow field.) Ross[R7] studied, both theoretically and experimentally, the effect of vapour evolution on the convective heat-transfer process to a stationary droplet suspended in a flowing medium. The rate of vapour evolution was controlled by means of the radiation heat transfer to the droplet from the surfaces of the system.

Ross[R7] found that his results were well correlated by an equation of the form

$$N_{Nu} = N_{Nu_o}\ \xi\ (B') \qquad (6.2\text{-}3)$$

where N_{Nu_o} is the Nusselt number in the absence of surface flux and $\xi\ (B')$ is a so-called shielding function which is a function of the Spalding number.

Any one of four correlating equations was found to fit the data equally well. As an example, one of the correlations was

given as

$$N_{Nu} = \frac{\ell n(1+B')}{B'} (2.0 + 0.355\, N_{Pr}^{1/3}\, N_{Re}^{0.59}) \qquad (6.2\text{-}4)$$

The studies of Hoffman[H1] and Ross[R7] indicate that the prediction of the rate of convective/conductive heat transfer to droplets evaporating in a high-temperature environment requires a knowledge of the radiant flux incident on and absorbed by the droplet.

6.2.2 Radiation

The evaporation rate of droplets explosed to a high-temperature environment depends upon the radiation incident on the surface of the droplets. If the droplets are suspended in an absorbing medium, and are themselves capable of absorbing thermal radiation, the radiation emitted from the surfaces of the system will be attenuated by the gas and the cloud. The problem of evaluating the attenuation by the gas was discussed in Chapter 5. The problem of determining the attenuation of thermal radiation by a cloud of droplets was discussed in Section 2.2.2. A brief summary is presented here.

A cloud of absorbing droplets attenuates a beam of radiation traversing it by the processes of scattering and absorption. Hoffman[H1] has indicated that the exact Mie equations for the prediction of scattering and absorption by particles cannot be applied to dense clouds of droplets (normally encountered in practice) because the equations do not allow for "shielding" or multiple scattering effects; i.e., the Mie equations assume

that each particle or droplet is exposed to the same intensity of incident radiation. Furthermore, the attenuation predicted by the Mie equations is a function of droplet size, wavelength and index of refraction; hence the drop-size distribution in the cloud, the full spectrum of thermal radiation wavelengths, and the variable refractive index would have to be considered.

The problem is further complicated if one attempts to account for the fact that the droplets are contained in an absorbing medium and enclosed by surfaces of finite dimensions.

Hoffman has pointed out that, if the ratio of the droplet circumference to the wavelength of the radiation is of the order of 100, diffraction can be neglected and the attenuation due to reflection and absorption can be calculated by geometric optics techniques; i.e., the asymptotic relationships of the exact Mie equations can be applied. If the phase shifts are neglected, it is possible to calculate the absorptivity of a droplet as a function of the product of drop-size and absorption coefficient, using the ray tracing techniques suggested by Thomas[T2] and Simpson[S15]. These techniques account for refraction and reflection at the gas-liquid interfaces.

As the product, kr, becomes larger by virtue of either large k or large r, the absorption process predominates as the principal mechanism of attenuation; under these circumstances, reflection and refraction can be neglected. For sprays it is unlikely that this product would be large and reflection/refraction effects should really be considered. Hoffman[H1] has indicated

however that the analysis is greatly simplified if only the process of absorption is considered. The errors involved in making this simplification must be determined experimentally.

As discussed in Section 2.2.2, the absorptivity of a droplet or thin film of water is a strong function of wavelength. The bands over which absorption occurs are almost identical with the absorption bands in the vapour phase. Consequently the concept of band absorption, as discussed for the gas phase, could be applied also to the analysis of the two phase system. The method of determining α_λ from transmissivity measurements was discussed in Section 2.2.2.

A further simplification is possible if one considers the liquid to be a gray-liquid in an analagous manner to the gray-gas approximation. Thus for the simplest case of a "gray" and "clear" liquid an average absorption coefficient and weighting fraction are calculated from transmissivity data taken at two film thicknesses. Once the absorption coefficient and weighting fraction have been determined it is possible to calculate the absorptivity for a droplet of any size in the spray or cloud.

The absorption coefficient for the cloud can be calculated from a knowledge of the drop-size distribution, absorptivity of the drops in each size interval, and the cloud density. The relationship can be written in terms of an average absorptivity, α_{ave}; volume-to-surface mean diameter, d_{vs}; gas density, ρ_s; liquid density, ρ_L; and fraction of the feed evaporated, E_f;

$$k_{CLOUD} = \tfrac{3}{2} (\alpha_{ave}) \left(\frac{\rho_s}{\rho_L}\right) \left(\frac{1}{d_{vs}}\right) \left(\frac{1 - E_f}{E_f}\right) \qquad (6.2\text{-}5)$$

The processes of attenuation of thermal radiation by the cloud and the gas can be considered to act in parallel and as such the absorption coefficients may be added together to yield an effective absorption coefficient to be used for the evaluation of total-interchange areas. However, since the absorption coefficient of the cloud will vary, by virtue of the changes in α_{ave}, ρ_s, d_{vs} and E_f as the spray evaporates, the total-interchange areas must be altered to account for the variation. Hoffman[H1] has suggested a suitable averaging technique which accounts for the variation by weighting the direct-interchange areas obtained at an average kB according to

$$\overline{g_1 g_2}\Big|_{\text{variable kB}} = \overline{g_1 g_2}\Big|_{\text{average kB}} \left\{ \frac{k_1 k_2}{k_{ave}^2} \right\} \qquad (6.2\text{-}6)$$

When the total-interchange areas have been evaluated, the set of heat and material balance equations, one for each gas zone, can be solved by iterative techniques with a high speed digital computer[H1].

The overall radiation model as well as the simplifications which were made in arriving at equation (6.2-5) for the calculation of the absorption coefficient of the cloud must be evaluated experimentally. This can be done by measuring the gas-temperature distribution and drop-size distribution and comparing the results with those predicted by the model. Consequently, before building the particle-radiation model into the existing gas-radiation model (Chapter 5), an experimental program was begun to determine whether drop-size distributions could be obtained with sufficient accuracy

to permit evaluation of the model.

6.3 Experimental Equipment

The majority of the equipment and measuring devices have been described earlier in this dissertation and consequently only a reference to the previous descriptions is given here.

6.3.1 Evaporator

The evaporator section of the column used in this work was described in Section 4.4.2.

6.3.2 Spray Generator and Calming Sections

The spray generator and calming sections which were mounted above the evaporator were previously described in Section 3.3.2. For this part of the investigation a pneumatic nozzle (Spraying Systems Company, No.12A, ¼JN Round Spray Nozzle) was used to atomize the liquid feed.

6.3.3 Drop Sampling Probe

The drop sampling probe was described in Section 3.3.4. For the present investigation it was necessary to control the probe and cell temperature more carefully than was done in Part I of this investigation. To effect this improved temperature control, heat-transfer oil (Sun Oil Company, Sun 21 Heat Transfer Oil) was circulated through the probe by a high pressure, rotary vane pump (Vickers). The oil was supplied from, and returned to a heated, thermostatted reservoir (Haake Ultra Thermostat bath, Model N Be, 1800 va) in which the oil temperature was controlled to within ± 1°C.

The pump was connected to the probe with braided, high pressure, flexible rubber tubing (Aeroquip, MP3Q652, Size 5).

6.3.4 Gas Temperature Probe

The aspiration probe used in this system was shown in Figure 4.4-6. The probe had the same tip-geometry as the probe which was described in Section 3.3.5 for measuring gas temperature in a particulate system.

6.3.5 Photographic Equipment

High speed photographs were taken of the surface of the immersion fluid during the sampling process. The photographs were taken with a "Fastax" 16 m.m. rotating prism camera (WF4ST) operating at 4600 frames per second. Light was supplied from a high-pressure xenon, quartz flash-lamp (Ernest Turner Electrical Instruments Limited) which was charged and synchronized to the Fastax camera by a specially designed charging circuit[H20].

6.4 Experimental Procedure

The general operating procedure for the column was described in Chapter 4. The drop sampling procedure was described in Section 3.4.2.

As well as taking samples in the column, samples were also taken from a spray which was generated in the open laboratory by a small air-driven glass nozzle.

High-speed photographs were taken of the surface of the immersion fluid in the cell when it was exposed to the spray from the glass nozzle. The nozzle was mounted 16 to 35 inches above the top of the cell which was filled with either varsol (Imperial Oil) or silicone oil (Dow Corning 200). The photographs were taken at approximately 5 x magnification at

a speed of 4600 frames per second, for a duration of 0.1 seconds. The surface of the cell was illuminated from the back by focusing a flash-lamp on a ground glass screen close to the cell; i.e., the camera, cell, ground glass screen, and flash lamp were all mounted in a direct line.

No gas temperatures were measured in the particulate system.

6.5 Results and Discussion

Drop samples taken in the colum with air as the transporting gas were obtained with cell exposure times of < 0.7 sec. The samples were consistent in apparent drop-size distribution and contained more than 300 droplets. For these samples, the cell, probe, immersion fluid and microscope cell holder were at ambient temperatures.

Samples were taken from the column with steam as the transporting gas; the nozzle feed-conditions were maintained the same as for the air flow. The microscope cell holder was maintained at 140^{o}F and the immersion fluid was saturated with water at 160^{o}F for 2 to 3 hours prior to sampling. It was necessary to maintain the oil bath at 105^{o}C to avoid condensation in the cell during sampling. Under these conditions it was not possible to obtain consistent samples containing a large number of drops (> 200) even when the cell exposure time was increased to 2 seconds.

The drastic change in the required sampling times and the inconsistency of the samples taken in the steam environment with the same nozzle conditions suggested that perhaps the sampling procedure was affecting the collected samples.

The sampling technique was further studied by sampling from a spray generated by a small glass nozzle in the open laboratory. Samples were taken at distances of 6 to 12 inches below the nozzle. When the

entire sampling procedure was carried out under ambient temperature conditions, large numbers of droplets (>200) were collected with cell exposure times of 0.02 sec. The sample densities were judged to be the same whether silicone oil or varsol was used as the immersion fluid. However, when silicone oil (Dow Corning 200) was used the drops were observed to coalesce in the cell; coalescence was seldom observed with the varsol medium. (The interfacial tension of the silicone oil-water system (2 x 10 dynes/cm.) was found to be approximately ½ that of the varsol-water system (4 x 10 dynes/cm.). Interfacial tensions were determined by a standard "pendant drop" technique.)

When the same procedures were carried out with the cell, probe, immersion fluid, and microscope cell holder maintained at 140^{o}F, the cell exposure time had to be increased to 0.1 to 0.2 sec. to obtain samples of the same density as those taken under ambient conditions. These observations suggested that some surface phenomena were occurring at the immersion fluid surface during the sampling process. Consequently it was decided to photograph the surface of the cell, when exposed to the spray, with a high-speed camera.

The analysis of the film (available in the Chemical Engineering Department of McMaster University) indicated that several of the droplets which came into the field of view in the short time of exposure (< 0.1 sec.) did not penetrate the surface of the immersion fluid. Droplets were observed to approach the surface with velocities in the range of 2 (20 micron droplets) to 9 ft/sec (60 micron drops). Many droplets of 20 to 30 microns diameter were observed to approach the surface with a velocity component tangential to the surface. Some of these drops

remained in focus (depth of field was approximately 300 microns) long enough to permit them to be observed "skating" across the surface. In one case the droplet was observed to reverse its direction of travel while on the surface. While these observations are not quantitative, they do indicate that samples taken under low velocity conditions are subject to bias because of the failure of at least some of drops (as large as 30 microns) to penetrate the surface of the collection medium. The same phenomena were observed to occur regardless of the temperature of the immersion fluid.

Because of the failure of the immersion cell technique to give consistent samples, the possibility of using an in situ photographic technique (similar to that used by Ostrowski [04] and other workers at the University of Michigan) was investigated. With this technique, a spatial distribution of the spray is obtained from the photographs. Some technique such as double-flash photography must be used to determine the droplet velocities and hence permit the spatial distribution to be converted to a temporal distribution. An electronic single-flash system was designed, (Appendix F) built and tested. The preliminary photographs of a spray generated in the open laboratory, were of the same quality as those which Ostrowski [04] used for purposes of analysis. A 5-ft. long camera was constructed and the sampling ports were modified to permit pictures to be taken of the spray inside the column. Further development and evaluation of this photographic technique were considered to be beyond the scope of this thesis.

6.6 Conclusions

Immersion cell drop-sampling techniques cannot be used with any confidence when sampling from sprays moving at relatively low velocities.

Further investigation is required to determine the droplet velocity range over which the immersion cell technique will yield unbiased distributions.

An evaluation of the model and simplifications contained therein was not possible at this point in the experimental program.

An in situ photographic technique appears to be the most feasible way to obtain drop-size distributions in the column. Further development of this technique is necessary.

7. SUMMARY AND RECOMMENDATIONS

7.1 Conclusions and Contributions

The results from Part I of this study indicated that the large natural-convection forces which occur in A.S.T. systems interact with the forced flow and cause increased turbulence and complicated flow patterns. These effects increase immensely the difficulty of the analysis of the system, in fact a comprehensive analysis is not possible until the flow patterns and turbulence level have been quantitatively determined.

In the second part of this investigation an attempt was made to divide the overall problem into a number of separate idealized studies.

The rates of convective heat transfer in the entrance region ($x/D < 2$) of a cylindrical tube were successfully predicted by employing finite-difference techniques to solve the parabolic form of the energy equation. The particular model which was developed enabled the solution to be obtained for any wall temperature distribution. The temperatures predicted by this convection model, at low temperature levels where the constant property assumptions are valid, were found to be in agreement with the experimentally measured gas temperatures for both air and steam flows.

The energy equation was solved in the elliptic form, i.e., with the axial diffusion terms included. The calculated results indicated that axial diffusion was not important at values of $x/D > 0.01$ for the $N_{Pr}\, N_{Re}$ range studied in this work.

A radiation model was developed, employing the zoning technique of Hottel[H7], to predict gas temperatures in a flowing absorbing medium.

The processes of convection from the wall and radial conduction through the gas were included in the model. The predicted temperatures were found to be in reasonable agreement with the experimentally measured gas temperatures.

The actual volume of the liquid feed which entered the evaporator as a cloud of droplets was successfully determined by employing a tracer-colorimetric-analysis technique.

An aspiration temperature probe for measuring gas temperatures in a particulate system was built and tested.

A temperature probe was constructed and measuring techniques were developed for the determination of gas temperatures in steep temperature gradients in the immediate vicinity of a hot wall.

A careful investigation of the technique of immersion sampling, which has been used by experimentalists for over two decades, revealed that reliable results could not be obtained in low-velocity systems.

Preliminary tests with a short duration high intensity flash technique indicated that this was a feasible method for the determination of drop-size distributions which could be readily adapted for use in the existing experimental apparatus.

7.2 Recommendations for Future Work

Techniques must be developed for the measurement of velocities in a turbulent gas stream in the presence of large temperature gradients. Accurate velocity measurements would permit a more complete analysis of the heat-transfer phenomena occurring in such systems.

The radiation-convection model should be further evaluated by comparing the predicted results with experimental results obtained over a wider range of experimental conditions.

Investigation is required to assess further the feasibility of employing in situ flash photographic techniques for the determination of drop-size distributions in the experimental system.

The immersion cell drop sampling technique should be studied to determine quantiatively the error in the drop-size distributions obtained with this method. Such a study might also indicate the range of conditions for which the technique could be expected to yield reliable results.

The present radiation-convection model should be extended to handle the problem of thermal radiation to clouds of particles flowing through a system of finite size. Such a model, when compared to experimental results, should permit an evaluation of the simplifying assumptions made in the proposed method[H1] of determining the absorption coefficient for the cloud. The model could be checked by measuring the actual gas temperature distribution and drop-size distribution occurrring in the experimental system. A further check might be made by determining the actual evaporation of the spray in the system with some form of tracer technique, (e.g. activation analysis).

The present convection model could be improved by (1) allowing for variable property effects and (2) utilizing a more realistic velocity profile for conditions where large temperature gradients exist adjacent to the surface. The predicted heat-transfer coefficients for small values of x/D (less than 2) should be correlated in a form which allows for the dependency on temperature and distance (as done by other investigators at larger values of x/D).

The present radiation model could be improved by (1) using a smaller zone size (this requires the determination of new direct-interchange areas), (2) including a heat-transfer coefficient which is temperature dependent, thus allowing for the interaction of radiation and convection, (3) approximating the real gas by a three-gray-plus-clear gas formulation rather than the one-gray-plus-clear gas formulation used in the present model.

When the various models have been perfected, it will be possible to predict the evaporative-load distribution in the column and the heat-flux distribution on the walls. These predictions should then be extended to the analysis of industrial A.S.T. systems.

NOMENCLATURE

a, a_i	weighting factor for gray gas component of a real gas.
a	thermal diffusivity, $ft^2/sec.$ (Equation (4.2-1)).
A	area common to two zones in radiation model, ft^2
A_s	area of surface zone (Appendix E), ft^2
A_i	coefficient in finite-difference equation (D-12).
B	characteristic dimension of zone in radiation analysis, ft.
B	Spalding transport number (Equation (6.2-1) and (6.2-2))
B'	Modified Spalding transport number (Equation (6.2-2) and (6.2-3).
B_i	coefficient in finite-difference equation (D-12).
C_i	coefficient in finite-difference equation (D-12).
Cp	heat capacity, B.T.U./lb.^oF.
Cp'	heat capacity, cal./gm. ^oC equation (6.2-1).
C_w	emissivity correction factor for self-broadening effects (Equation (E.1-5)).
d	diameter of drop, cm.
d_i	average diameter of drop in size interval i, ft.
d_{vs}	volume-to-surface mean diameter of spray, ft.
D	diameter of cylindrical column, ft.
D_i	coefficient in finite-difference equation (D-12).
Dx	dimensionless distance in finite-difference equation (D-12).

E	black-body emissive power (σT^4), B.T.U./hr. ft^2.
E_i	coefficient in finite-difference equation (D-12).
E_f	fractional evaporation of spray
f	friction factor (von Karman-Nikaradse)
f	frequency, cycles/sec. (Section C.2.2)
f_λ	fraction of incident energy absorbed by drop.
F1, F2, F3, F4	dimensionless variables in finite-difference equation (D-11).
$\overline{gg}$	direct-interchange area (gas-to-gas) ft^2.
$\overline{gs}$	direct-interchange area (gas-to-surface) ft^2.
G	dimensionless total diffusivity (molecular + turbulent) (defined in Equation (4.3-6)).
$\overline{GG}$	total-interchange area (gas-to-gas), ft^2.
$\overline{GS}$	total-interchange area (gas-to-surface) ft^2.
h	heat-transfer coefficient, B.T.U./hr. ft^2 ^oF.
H1, H2, H3, H4	dimensionless variables in finite-difference equation (D-24).
I	intensity of radiation, B.T.U./hr. ft^2
I_ν	intensity of radiation at frequency ν, B.T.U./hr. ft^2
I	current, (Appendix A.6) milliamperes.
k	absorption coefficient, cm^{-1} or ft^{-1}
k	thermal conductivity, B.T.U./hr. ft. ^oF. (Equations (4.2-3), (4.3-1), (5.2-3), (5.2-4)) (Appendices B and C.4).
k_{eff}	effective thermal conductivity, B.T.U./hr. ft. ^oF.
k_f	thermal conductivity of gas at average film temperature, (Equation (6.2-1)), cal./sec. cm. ^oC.

k_{CLOUD} absorption coefficient of cloud of droplets, ft^{-1}.

K_1, K_2, K_3, K_4, K_5, K_6, K_7 constants in Bevans' ε versus $p\ell$ correlations (B3).

ℓ path length, ft. or cm.

L mean beam length (Equation (2.2-9)), ft.

L^o geometric mean beam length (Equation (2.2-8)) ft.

L/D dimensionless axial distance

$\dot{m}$ evaporation rate, gm./sec.

N_{Gr} Grashof number based on length. $\frac{g\beta\rho^2 L^3 \Delta t}{\mu^2}$

N_{Gr_D} Grashof number based on diameter. $\frac{g\beta\rho^2 D^3 \Delta t}{\mu^2}$

N_{Nu} Nusselt number, hD/k

N_{Pr} Prandtl number, $C_p\mu/k$

N_{Re} Reynolds number, $DU'\rho/\mu$

p pressure, atmospheres

q heat flux, B.T.U./hr.

q_R radiant heat-transfer rate to droplet, cal./sec.

r radial distance in cylindrical column, ft.

r radius of drop, ft. (Equation (2.2-11)).

r_s radius of circular nozzle, ft.

r_w radius of cylindrical duct, ft.

R dimensionless radial distance, r/r_w

RO dimensionless radius of cylinder. $r_w \sqrt{T_w/\rho_w}/\mu_w/\rho_w$

$g_i \; R_{s_i}$ reflective flux density B.T.U./hr. ft^2

$\overline{ss}$ direct-interchange area (surface-to-surface), ft^2.

$\overline{SS}$ total-interchange area (surface-to-surface), ft^2.

$s^2(\hat{y})$ standard error of estimate, squared (Appendix B)

t temperature, ^oF.

T temperature, ^oR (Equation (4.2-3) and Chapter 5)

T dimensionless temperature (Chapter 4, Appendix D).

T_G temperature of gas zone, ^oR.

T_w temperature at wall, ^oR.

U' velocity, ft./sec.

V dimensionless velocity

U_s uniform nozzle velocity, ft./sec.

U_k velocity, ft./sec. (defined by Equation (2.5-2)).

V_g volume of gas zone, ft^3.

w flowrate, lb./hr.

w' flowrate, lb./sec.

x dimensionless axial distance, x'/r_w.

x' axial distance, ft.

y radial distance from wall, ft.

y^+ dimensionless distance from wall, $y \sqrt{T_w/\rho_w}/\mu_w/\rho_w$

z constant greater than unity (Equation (D-9)).

Greek Letters

α	absorptivity
α_p	absorptivity of particle
β	constant (Equation (2.2-11)).
γ	convective flux, B.T.U./hr. ft^2 (Equation (5.2-7)).
γ_λ	smoothed absorption coefficient (Equation (2.2-12)).
δ	column diameter, ft.
ε	emissivity
ε_h	eddy diffusivity for heat transfer, ft^2/sec.
ε_m	eddy diffusivity for momentum transfer, ft^2/sec.
λ	latent heat of vapourization (Chapter 6) cal./gm.
λ	wavelength, microns
ρ	density, lb./ft^3.
ρ_s	density of gas, lb./ft^3.
ρ_L	density of liquid, lb./ft^3.
ρ'	surface reflectivity
τ	transmissivity
τ	time constant, seconds (Appendix C.2.2)
η	enthalpy flux, B.T.U./hr. ft^2 (Equation (5.2-6)).
μ	viscosity, lb./ft. sec.
ξ	dimensionless shielding function (Equation (6.2-3)).

Subscripts

b	bulk (temperature)
b	black-body (radiation analysis)
w	wall
i,j	mesh point or zone identification
ν	frequency

BIBLIOGRAPHY

A1 Adams, R.M., J.J. Katz,
J. Opt. Soc. Amer. 46, 895 (1956).

A2 Arni Venkata, R.S.,
Ph.D. Thesis, University of Washington (1959).

A3 Adler, C.R., W.R. Marshall, Jr.,
Chem.Eng.Prog., 47, 515 (1951).

A4 Acrivos, A.,
A.I.Ch.E., 4, 285 (1958).

A5 Altman, M., F.W. Stubb,
Chem.Eng.Prog., Symposium Series, No.29, 55, 121 (1959).

A6. Adrianov, V.N., S.N. Shorin,
AEC - tr - 3928 (1960).

B1 Becker, H.A., H. Hottel, G.C. Williams,
Ninth Symposium (International) on Combustion,
pp 7-19, Reinhold Publ. Corp., New York (1960).

B2 Bevans, J.T., R.V. Dunkle,
J. Heat Transfer, 82, 1 (1960).

B3 Bevans, J.T.,
ASME preprint 60-WA-175, Winter Annual Meeting,
New York (1960).

B4 Bevans, J.T., J.T. Gier, R.V. Dunkle,
Trans. ASME, 80, 1405 (1958).

B5 Bevans, J.T.,
ASME preprint 60-HT-12, Heat Transfer Conference,
Buffalo (1960).

B6 Burch, D.E., E.B. Singleton, W. France, D. Williams,
Appl. Opt., 1, 359 (1962).

B7 ibid,
2, 585 (1963).

B8 Burch, D.E., D.A. Gryunak,
J.Q.S.R.T., 6, 224 (1966).

B9 Blout, E.R., H. Lenormant,
J. Opt. Soc. Amer., 43, 1093 (1953).

B10 Buckhan, J.A., R.W. Warlton,
Chem.Eng.Prog. 51, 126 (1955).

B11 Becker, H.A.,
Sc.D. Thesis, Massachusetts Institute of Technology (1961).

B12 Becker, H.A., H.C. Hottel, G.C. Williams,
Tenth Symposium (International) on Combustion,
pp 1253, Reinhold Publ. Corp. (1965).

B13 Brown, C.K.,
Ph.D. Thesis, McGill University (1963).

B14 Brown, C.K., W.H. Gauvin,
Can.J.Chem.Engin., 43, 313 (1965).

B15 Brown, W.G.,
VDI-Forschungsheft 480, 26, 32 pp.(1960)
cited in reference B13.

B16 Bird, R.B., W.E. Stewart, E.N. Lightfoot,
Transport Phenomena, p.157,
John Wiley & Sons, New York (1960).

C1 Cliffen, E., A. Muraszew,
The Atomization of Liquid Fuels
Chapman & Hall Limited, London (1953).

C2 Chin, J.H., S.W. Churchill,
Chem.Eng.Prog. Symposium Series, 56, No.30, 117 (1960).

C3 Churchill, S.W., C. Chiao-Min, L.P. Evans, L. Tien, S. Pang,
DASA-1257 (1962).

C4 Chin, J.H., S.W. Churchill,
Quart. Appl. Math., 18, 93 (1960).

C5 *Curtet, R.,
Compt. rend. 244, 1450 (1957).

---

* reference C5, C6, C7 cited in reference B1.

C6 *Curtet, R.,
Combustion and Flame, 2, 383 (1958).

C7 *Craya, A., R. Curtet,
Compt. rend. 241, 621 (1955).

C8 Cess, R.D.,
J. Heat Transfer, 86, 469 (1964).

C9 Chandrasekhar, S.,
Radiative Transfer, Oxford Univ. Press, London (1950).

C10 Colburn, A.P., O.A. Hougen,
Ind. Eng. Chem., 22, 522 (1930)
cited in reference B13.

D1 DeJuhasz, K.J.,
Spray Literature Abstracts
Druckerei Winter, Heidelberg, Vol I (1959), Vol II (1964).

D2 Dlouhy, J.,
Ph.D. Thesis, McGill University (1957).

D3 Dlouhy, J., W.H. Gauvin,
A.I.Ch.E., 6, 29 (1960).

D4 Deirmendjian, D., R. Clasen, W. Viezee.,
J.Opt.Soc. Amer., 51, 620 (1961).

D5 Dlouhy, J., W.H. Gauvin,
Can.J.Chem.Eng., 38, 115 (1960).

D6 Darnell, W.H., W.R. Marshall, Jr.,
University of Wisconsin (1958).
cited in reference T4.

D7 De Corso, S.M., R.L. Coit,
Trans. ASME., 77, 1189 (1955)

D8 Dobbins, R.A.,
A.I.A.A., 1, 1940 (1963).

D9 Dunkle, R.V.,
J.Heat Transfer, 86, 75 (1964).

D10 Dunkle, R.V.,
ASME paper 62-WA-120, New York (1962).

D11 Deissler, R.G.,
N.A.C.A., TN 3145 (1954).

D12 Davenport, M.E., P.M. Magee, G. Leppert,
Stanford University, TID-13485, May (1961).

D13 Deissler, R.G.
Recent Advances in Heat and Mass Transfers,
(Hartnett - ed.), McGraw Hill, New York, (1961), pp.253.

D14 Dittus, F.W., M.K. Boelter,
University of California, Pubs. Eng., 2, 443 (1930),
cited in reference M7.

D15 Deissler, R.G.,
N.A.C.A., TN 2138, (1950).

E1 Erkku, H.,
Sc.D. Thesis, Massachusetts Institute of Technology (1959).

E2 Elsasser, W.M.
Harvard Meteorological Studies, No.6 (1947),
cited in reference B2.

E3 Eckert, E.R.G.,
Heat and Mass Transfer, Ch.13, 14,
McGraw Hill, New York (1959).

E4 Edwards, D.K., W.A. Menard,
Appl. Opt., 3, 621 (1964).

E5 Edwards, D.K., K.E. Nelson,
Paper No. 61-WA-175,
ASME Winter Annual Meeting, New York (1961).

E6 Edwards, D.K., B.J. Flornes, L.K. Glasen, W. Sun,
Appl. Opt., 4, 715 (1965).

E7 Eckert, E.R.G., A.J. Diaguila, A.N. Curren,
N.A.C.A. TN 2974, July (1953).

E8 Einstein, T.H.,
N.A.S.A., TR R-154, (1963).

E9 Einstein, T.H.,
N.A.S.A., TR R-156, (1963).

E10 Same reference as E7.

E11 Engineering Materials Handbook (Mantell),
Mcraw Hill, New York, (1958).

F1 Flornes, B.J.,
M.S. Thesis, University of California, L.A., (1962).

F2 Ferriso, C.C., C.B. Ludwig,
J.Q.S.R.T., 4, 215 (1964).

F3 Friedman, H.M., S.W. Churchill,
A.I.Ch.E. preprint 30,
A.I.Ch.E - ASME Heat Transfer Conf., Boston (1963).

F4 Ferriso, C.C., C.B. Ludwig, A.L. Thompson,
J.Q.S.R.T., 6, 241 (1966).

F5 Fischer-Porter, Instruction Bulletin 10A9020,
Correction Factor Curves for Flowrator Meters.

G1 Gauvin, W.H.,
Thermal Treatment of Finely Divided Substances,
Canadian Patent No. 522789, February 4, 1958.
U.S. Patent No. 2,889,874, June 9, 1959.

G2 Gauvin, W.H.,
Chemistry in Canada, Sept. 1955, p.1.

G3 Gauvin, W.H.,
TAPPI, 40, 866 (1957).

G4 Goody, R.M.,
Quart. Journ. Roy. Meteor. Soc., 78, 165 (1952).

G5 Greif, R.
Int. J. Heat Mass Transfer, 7, 891 (1964).

G6 Goldstein, R.,
J.Q.S.R.T., 4, 343 (1964).

G7 Goody, R.M.
The Physics of the Stratosphere,
Univ. Press, Cambridge (1954).
cited in reference G8.

G8 Goldman, A., U.P. Oppenheim,
J.Opt.Soc.Amer., 55, 794 (1965).

G9 Gore, R.C.,
Senior Spectroscopist, Perkin-Elmer Corp.,
Personal communication.

G10 Gretzinger, J., W.R. Marshall, Jr.,
A.I.Ch.E., 7, 312 (1961).

G11 Gordon, A.R.,
J. Chem. Phys., 2, 65 (1934).

G12 ibid., 549.

H1 Hoffman, T.W.,
Ph.D. Thesis, McGill University (1959).

H2 Hottel, H., A. Sarofim,
Int. J. Heat Mass Transfer, 8, 1153 (1965).

H3 Hottel, H.,
Fourth Symposium (International) on Combustion,
p.97, Reinhold Publ. Corp., New York (1953).

H4 Hoffman, T.W., W.H. Gauvin,
Can.J.Chem.Eng., 40, 110 (1962).

H5 ibid,
43, 325 (1965).

H6 ibid,
39, 179 (1961).

H7 Hottel, H.C., E. Cohen,
A.I.Ch.E., 4, 3 (1958).

H8 Hottel, H.C.,
Heat Transmission - 3rd edition by McAdams
Chp. Iv, Mcgraw Hill, New York (1954).

H9 Howard, J.N., D.C. Burch, D. Williams,
J.Opt.Soc.Amer., 46, 186, 237, 242, 334, 542 (1956).

H10 Herschenson, H.M.,
Infra-Red Absorption Spectra,
Academic Press, New York. yrs 1945-1957 (1959).
yrs 1958-1962 (1964).

H11 Hjelmfelt, A.T., L.F. Mockros,
Appl.Sci.Res., A16, 149,(1966).

H12 Hottel, H.C., A.F. Sarofim,
pp 139, Theory and Fundamental Research in Heat Transfer - (Clark - editor), MacMillan Co., New York (1963).

H13 Hasson, D., J. Mizrahi,
Trans.Inst.Chem.Engrs., 39, 415 (1961).

H14 Howell, J.R., M. Perlmutter,
ASME paper 63-AHGT-1, Los Angeles (1963).

H15 ibid,
63-HT-39, Boston (1963).

H16 Hitchcock, J.E.,
Ph.D. Thesis, Purdue University (1963).

H17 Hubbard, P.G.,
Operating Manual for the IHR Hot-Wire and Hot-Film Anemometers, Bulletin 37, No.432,
State University of Iowa.

H18 Hall, W.B., P.H. Price,
Int. Devel. in Heat Transfer,
ASME, New York, 607 (1961).

H19 Houghton, W.T.,
Ph.D. Thesis, McMaster University (1966).

H20 Harvey, D.M., Ph.D. Thesis, McMaster University (1967).

J1 Johnstone, H.F., R.L. Pigford, J.H. Chaplin,
University of Illinois, Eng. Exp. Sta., Bull. 330, (1941).

J2 Jaffe, J.H., W.S. Benedict,
J.Q.S.R.T., 3, 87 (1963).

J3 Johnk, R.E., T.J. Hanratty,
Chem.Eng.Sci., 17, 881 (1962).

K1 Kesler, G.H.,
Sc.D. Thesis, Massachusetts Institute of Technology (1952).

K2 Kroll, H.E.,
Chem.Eng.Prog., 43, No.2; 21 (1947).

K3 Kerker, M., (Edit.)
Electromagnetic Scattering,
Macmillan Company, New York (1963).

K4 Krascella, N.L.,
J.Q.S.R.T., 5, 245 (1965).

K5 Kourganoff, V.,
Basic Methods in Transfer Problems,
Oxford Univ. Press, London (1962).

K6 Krascella, N.L.,
Research Lab., United Aircraft Corporation, C-910092-1 (1964).

K7 Kreith, F.,
Principles of Heat Transfer, 2nd edition,
International Textbook Co., Scranton, Penn. (1965).

L1 Lee, G., N.J. Themelis, W.H. Gauvin,
Pulp and Paper Mag. Canada, 59, 140 (1958).

L2 Lee, G., W.H. Gauvin,
TAPPI, 41, 65 (1958).

L3 Longwell, J.P., N.A. Weiss,
Ind.Eng.Chem., 45, 667 (1953).

L4 Ludwig, C.B., C.C. Ferriso, C.N. Abeyata,
J.Q.S.R.T., 5, 281 (1965).

L5 Ludwig, C.B., C.C. Ferriso, W. Malkmus, F.P .Boynton,
J.Q.S.R.T., 5, 697 (1965).

L6 Ludwig, C.B., C.C. Ferriso,
J.Q.S.R.T., 7, 7 (1967).

L7 Lippincott, E.R., C.E. Weir, A. Van Valkenburg,
J.Chem.Phys., 32, 612 (1960).

L8 Love, T.J., Jr.,
A.R.L. 63-3, January 1963.

L9 Latto, B.,
Int.J. Heat Mass Transfer, 8, 689 (1965).

L10 Lapidus, L.,
Digital Computation for Chemical Engineers,
McGraw-Hill New York (1962), pp.158.

L11 Laufer, J.,
NACA, TN 2954, (1953).

M1 Marshall, W.R., Jr.,
Chem.Eng.Prog., Monograph Sci., 50, No.2 (1954).

M2 Marshall, W.R., Jr.,
Trans. ASME, 77 1377 (1955).

M3 May, K.R.
J.Sci.Inst., 22, 187 (1945).

M4 Merrington, A.C., E.C. Richardson,
Proc. Roy. Soc., 59, 1 (1947).

M5 Manning, W.P., W.H. Gauvin,
A.I.Ch.E., 6, 184 (1960).

M6 McAlister, J.A., E.Y.H. Keng,
Orr. Jr. C., NASA CR-54441 (1965).

M7 McAdams, W.H.
Heat Transmission, 3rd edition,
McGraw Hill, New York (1954).

M8 Magee, P.M.,
Ph.D. Thesis, Stanford University (1965).

N1 Nichols, L.,
Ph.D. Thesis, Case Institute of Technology (1963).

N2 Nichols, L.,
Int. J. Heat Mass Transfer, 8, 589 (1965).

N3 Nelson, K.E.,
M.S. Thesis, University of California, Berkeley (1959).

O1 Oppenheim, A.K.,
Trans. ASME, 78, 725 (1956).

O2 Oppenheim, U.P., Y. Ben-Aryeh,
J.Opt.Soc.Amer., 53, 344 (1963).

O3 Olfe, D.B.,
J.Q.S.R.T., 1, 169,(1961).

O4 Ostrowski, H.S.
University of Michigan, Personal Communication.

P1 Paetkau, T.R.,
M.Eng. Thesis, McMaster University (1966).

P2 Pinder, K.L., W.H. Gauvin,
Industrial Wastes, Nov. (1958).

P3 ibid, Jan. (1959).

P4 ibid, March (1959).

P5 Pinder, K.L.,
M.Eng. Thesis, McGill University (1952)
cited in reference G2.

P6 Putnam, A.A., F. Benington, H. Einbinder, H.R. Hazard,
J.D. Kettelle, A. Levy, C.C. Miesse, J.M. Pilcher,
R.E. Thomas, A.E. Weller, and B.A. Landry,
Injection and Combustion of Liquid Fuels;
WADC Tech. Rept. 56-344, Battelle Memorial Institute (1957).

P7 Penner, S.S.
Quantitative Molecular Spectroscopy & Gas Emissivities,
Addison-Wesley, London (1959).

P8 Penndorf, R.
J.Phys.Chem., 62, 1537 (1958).

P9 Patch, R.W.,
J.Q.S.R.T., 5, 137 (1965).

P10 Plyler, E.K., N. Acquista,
J.Opt.Soc.Amer., 44, 505 (1954).

P11 Potts, W.J., N. Wright,
Anal. Chem., 28, 1255 (1956).

P12 Parker, F.S., D.M. Kirschenbaum,
Spectrochimica Acta, 16,910 (1960).

P13 Pollock, G.G.,
McMaster University, personal communication.

P14 Perry, J.H. (Editor),
Chemical Engineering Handbook - 3rd Edition,
McGraw Hill, New York (1951).

P15 Perkins, H.C., P. Worsoe-Schmidt,
Int. J. Heat Mass Transfer, 8, 1011 (1965).

P16 Pollock, G.G.,
Ph.D. Thesis, McMaster University (1967).

P17 Pai, S.I.,
Viscous Flow Theory, Vol II, Van Nostrand, Princeton, (1957) p41.

R1 Rabinovitch, W.R., P. Luner, R.W.H. James,
W.H. Gauvin,
Pulp Paper Mag., Canada, 57, 123 (1956).

R2 Ranz, W.E.,
Bulletin No.65, Dept. of Eng. Res., Pennsylvania State Univ. (1956).

R3 Ricou, F.P., D.B. Spalding,
J. Fluid Mech., 11, 21 (1961).

R4 Rosensweig, R.E., H.C. Hottel, G.C. Williams,
Chem.Eng.Sci., 15, 111 (1961).

R5 Rupe, J.H.,
Third Symposium (International) on Combustion, pp 680 (1949).

R6 Rupe, J.H.,
Prog. Report No. 4-80, Jet Propulsion Lab.,
California Institute of Technology (1950),
cited in reference T4.

R7 Ross, L.L.,
Ph.D. Thesis, McMaster University (1966).

R8 Ranz, W.E., J.B. Wong,
Ind.Eng.Chem., 44, 1371 (1952).

R9 Rosseland, S.,
Astrophysik und Atom-Theoretisches Grundlage,
P41, Springer Verlag, Berlin (1931),
cited in reference H2.

S1 Short, W.L.,
Ph.D. Thesis, University of Michigan (1962).

S2 Spalding, D.B.
Some Fundamentals of Combustion,
p25, Butterworth Scientific Publ., London (1955).

S3 Sleicher, C.A., S.W. Churchill,
Ind.Eng.Chem., 48, 1819 (1956).

S4 Schack, A.,
Industrial Heat Transfer,
John Wiley & Sons, New York (1933),
cited in reference B3.

S5 Sampson, D.H.,
J.Q.S.R.T., 3, 211 (1965).

S6 Sidorov, E.A.,
translated from Vaprocy Teploobmena, p49 (1959),
by Purdue University, Radiative Transfer Project,
Translation TT-3, June 1961.

S7 Smart, C., V. Vand,
J.Opt.Soc.Amer., 54, 1232 (1964).

S8 Smart, C., R. Jacobsen, M. Kerker, J.P. Kratohuil,
E. Matijević,
J.Opt.Soc.Amer., 55, 947 (1965).

S9 Sternglanz, H.,
Appl. Spectros., 10, 2 (1956).

S10 Soo, S.L.,
Chem.Eng.Sci., 5, 57 (1956).

S11 Sarofim, A.F.,
Sc.D. Thesis, Massachusetts Institute of Technology (1962).

S12 Snyder, N.W., J.T. Gier, R.V. Dunkle,
Trans ASME, 77, 1011 (1955).

S13 Scheele, G.F., T.J. Hanratty,
A.I.Ch.E., 9, 183 (1963).

S14 Scheele, G.F., E.M. Rosen, T.J. Hanratty,
Can.J.Chem.Eng., 38, 67 (1960).

S15 Simpson, H.C.,
Sc.D. Thesis, Massachusetts Institute of Technology (1964).

S16 Short, W.W., B.H. Sage,
A.I.Ch.E., 6, 163 (1960).

S17 Schlichting, H.
Boundary Layer Thoery,
Translated by J. Kestin, McGraw Hill, New York (1955) p.254.

S18 Sparrow, E.M., C.M. Usiskin, H.A. Hubbard,
J. Heat Transfer, 83, 199 (1961).

S19 Sparrow, E.M., T.M. Hallman, R. Siegel,
Appl.Sci.Res., 7A, 37 (1956).

S20 Sleicher, C.A., Jr., M. Tribus,
Trans. ASME, 79, 789 (1957).

S21 Siegel, R., E.M. Sparrow,
J.Heat Transfer, 82, 152 (1960).

S22 Schneider, P.J.
Trans. ASME, 79, 765 (1957).

S23 Streeter, U.L., (editor),
Handbook of Fluid Dynamics, p10-14,
McGraw Hill, New York (1961).

T1 Thring, M.W., M.P. Newby,
Fourth Symposium (International) on Combustion,
p789, Reinhold Publ. Corp., New York (1953).

T2 Thomas, P.H.,
Brit. J. Appl. Phys., 3, 385 (1952).

T3 Thordarson, R.,
M.S. Thesis, University of Wisconsin (1952),
cited in reference A2.

T4 Tate, R.W.,
A.I.Ch.E., 7, 574 (1961).

T5 Tate, R.W., W.R. Marshall, Jr.,
Chem.Eng.Prog., 49, 169 (1953).

T6 Tien, C.L., L.S. Wang,
J.Q.S.R.T., 5, 453 (1965).

T7 Thompson, B.J., J.H. Ward, W.R. Zinky,
Appl. Opt., 6, 519 (1967).

T8 Themelis, N.J., W.H. Gauvin,
Can.J.Chem.Eng. 41, 1 (1963).

T9 Taylor Instrument Company (Toronto),
Technical Data Manual No.27.

U1 Usiskin, C.M., E.M. Sparrow,
Int. J. Heat Mass Transfer, 1, 28 (1960).

V1 Viskanta, R.,
Ph.D. Thesis, University of Chicago (1960); ANL-6170.

V2 Viskanta, R., R.J. Grosh,
Int. J. Heat Mass Transfer, 5, 795 (1962).

V3 Van de Hulst, H.C.,
Light Scattering by Small Particles,
John Wiley & Sons, Inc., New York (1957).

V4 Viskanta, R.,
ASME paper 62-WA-189, New York (1962).

V5 Viskanta, R., R.J. Grosh,
App. Mech. Rev. 17 91 (1964).

V6 Viskanta, R.,
Advances in Heat Transfer, 3, 176 (1966).

W1 Weil, N.A.,
Preprint 45, 54th Annual Meeting A.I.Ch.E., New York (1961).

W2 Wadleigh, K.R., R.A. Oman,
Jet Propulsion, 27, 769 (1957).

W3 Wagman, D.D., J.E. Kilpatrick, W.J. Taylor,
K.S. Petzer, F.D. Rossini,
J. Res. Nat. Bur. Stand., 34, 143 (1945).

W4 Wolf, H.,
J. Heat Transfer, 81, 267 (1959).

W5 Wolf, H.
Ph.D. Thesis, Purdue University (1958).

APPENDIX A : CALIBRATIONS

A.1 Thermocouple Calibration

The aspirated and unshielded probes* both used Pt-Pt 10% Rh thermocouples. The thermocouple junction in the aspiration probe was formed from 0.001-in. diameter wire and was approximately 0.004-in. in diameter. The junction of the unshielded probe was formed from 0.0005-in. diameter wire and had a maximum diameter of 0.002-in. Both probes had these fine thermocouple wires welded to heavier support wires of the same material (0.010-in. diameter). These heavier wires were the conductors in standard "Ceramo" - Ce316 (Thermo Electric Limited) stainless-steel sheathed, thermocouple wire.

The stainless steel sheath was removed for a short distance at the wire ends by de-plating the metal in an electrolyte solution.

The thermocouples were calibrated against a standard iron-constantan thermocouple (8049J, master NBS TEC102). The standard and uncalibrated thermocouples were inserted into two adjacent 7-in. long holes which were drilled into an 8-in. x 2½-in. aluminum cylinder. The cylinder and thermocouples were inserted into a controlled constant temperature oven which was set at different temperature levels. The steady-state thermocouple millivolt signals were recorded at each temperature level by a Honeywell Model 2733 portable potentiometer which had an estimated

---

* Only the straight probes used in the large furnace were calibrated against the standard.

precision of 0.002 millivolts corresponding to approximately 0.4°F for the Pt - Pt 10% Rh thermocouple and 0.07°F for the iron-constantan thermocouple. The cold junctions were immersed in an ice bath. Table A-1 shows the results of the calibrations.

Note that all millivolt readings were converted to degrees Fahrenheit using tables based on the International Temperature Scale of 1948.

TABLE A-1

Thermocouple Calibration

ASPIRATION PROBE		UNSHIELDED PROBE	
Probe	Standard	Probe	Standard
261.5	259.0	430.4	426.6
312.5	310.3	489.8	486.0
355.4	353.3	349.4	346.0
357.8	355.5		

A.2 Probe Calibration

It was not only necessary to ensure that the thermocouples themselves recorded true temperatures but it was also necessary to ensure that the probe geometry and/or aspiration rate would permit true gas temperatures to be measured in the column.

Traverses were made with the unshielded probe at Ports* 4 and 8 in the large column as described in the procedure, Section 3.4.3. The aspiration probe was then placed in position and several traverses made with different suction rates applied to the innermost tube of the probe.

The best agreement was obtained when a vacuum of 4 cm. of mercury was applied to the probe assembly. Table A-2 and Figure A-1 illustrate the agreement between the average temperatures recorded with the two probes. This agreement was considered quite good since under the operating conditions at which these comparisons were made (Wall temperature 1300°F, steam flowrate 200 lb./hr.) the r.m.s. temperature fluctuations** were always greater than 25°F and in some locations as large as 50°F.

At a vacuum of 4 cm. of mercury the mass flowrate of gas through the probe was of the order of 0.1 gm./min. As the mass flowrate was decreased, the temperature recorded by the aspiration probe increased

---

* Numbering from the top.

** At these temperature levels it was found that the peak-to-peak variation measured on the single pen recorder (undamped) was approximately 3 times the magnitude of the r.m.s. reading. Depending upon the frequency of the fluctuations the recorder would only follow the thermocouple millivolt signal within 80 - 90%. Thus at an r.m.s. reading of 25°F, the gas temperature fluctuation at a point was at least 75°F.

above that recorded by the unshielded probe. At higher mass flow rates some droplets were drawn into the probe when measurements were made with the spray flowing.

TABLE A-2

Comparison of Aspiration and Unshielded Probe
(^{o}F)

Distance from Furnace Wall (inches)	PORT 4		PORT 8	
	Aspiration Probe	Unshielded Probe	Aspiration Probe	Unshielded Probe
0.50	855	872	958	954
0.75	795	-	921	-
1.00	-	765	-	892
1.25	735	-	870	-
1.50	-	704	-	847
1.75	670	-	836	-
2.00	-	651	-	821
2.25	612	-	810	-
2.50	-	600	-	788
2.75	565	-	780	-
3.00	-	525	-	765
3.25	509	-	767	-
3.50	-	501	-	746
3.75	480	-	746	-
4.00	-	468	-	746
4.25	447	-	746	-
4.50	-	460	-	750
4.75	447	-	746	-
5.00	-	468	-	754
5.25	472	-	760	-
5.50	-	509	-	769
5.75	517	-	788	-
6.00	-	573	-	803
6.25	597	-	810	-
6.50	-	647	-	851
6.75	662			
7.00				

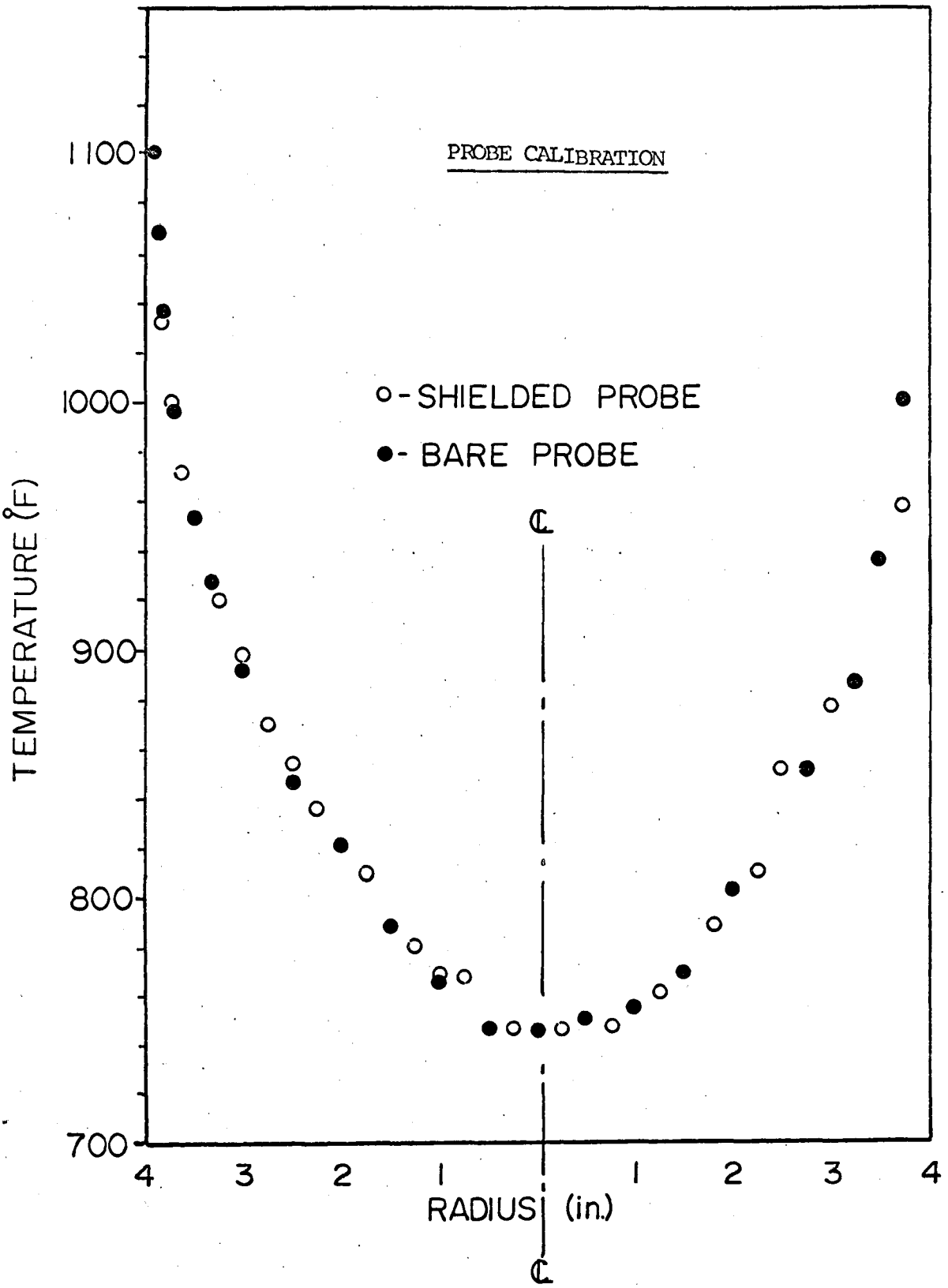
PROBE CALIBRATION
o - SHIELDED PROBE
● - BARE PROBE
TEMPERATURE (°F)
1100
1000
900
800
700
4
3
2
1
1
2
3
4
RADIUS (in.)
℄
℄

FIGURE A-1

A.3 Orifice Calibrations

(a) Orifice B* - 0.636-in. diameter bore
Pipe I.D. - 1.049-in.

The standard formula (P14) was used to calculate the weight rate of discharge

$$w' = CYS_2 \sqrt{\frac{2\, g\, d_1^{\,2}\, \Delta H'}{1-B^4}} \qquad \text{(A.3-1)}$$

where

w' = flow rate (lb./sec.)

C = coefficient of discharge

Y = expansion factor

S_2 = cross-sectional area of discharge opening (sq./ft.)

g = local acceleration due to gravity (ft./sec^2)

d_1 = density at upstream temperature and pressure (lbs./cu.ft.)

$\Delta H'$ = orifice differential - ft. of fluid of density d_1

B = ratio orifice diameter/pipe diameter

After evaluating the various geometric factors, expressing the density in terms of the ideal gas law, and converting the orifice differential to inches of mercury one obtains the following simplified equation

$$w' = 0.159 \sqrt{\frac{P_1 \Delta H}{T_1}} \qquad \text{(A.3-2)}$$

---

* B refers to the equipment designation given in Table 3.3-1 of Section 1.

where

w' = lb./sec.

P_1 = upstream pressure in p.s.i.a.

ΔH = orifice differential (in. - Hg.)

T_1 = upstream temperatures (^{o}R)

with the flow in lb./hr (A.3-2) becomes

$$w = 572 \sqrt{\frac{P_1 \Delta H}{T_1}} \qquad \text{(A.3-2a)}$$

The orifice was then calibrated against two Fischer Porter rotameters connected in parallel.

The rotameters used were

(1) FP-1-35-10 with a 1-GSVT-64 s.s. float

(2) FP-B6-35-250 with a BSVT-64 s.s. float

Flow rates were obtained from the respective calibration curves supplied with the units and corrected for pressure and temperature according to the Fischer-Porter manual[F5]. Before calibrating the orifice the rotameters were connected in series and checked against one another. At the lowest flow rate of 15 S.C.F.M. the corrected flows from the two rotameters agreed within 1%. At all higher flows (31, 49, 59 S.C.F.M.) the agreement was better than 0.4%.

Table A-3 compares the corrected, measured flow rate with the flow rate calculated from equation A.3-2. It will be noted that in every case the predicted flow is less than the measured flow. The coefficient on the orifice equation was thus changed to give a new equation,

$$w' = 0.162 \sqrt{\frac{P_1 \Delta H}{T_1}} \qquad \text{(A.3-3)}$$

or with the flow in lb./hr.

$$w = 584 \sqrt{\frac{P_1 \Delta H}{T_1}} \qquad \text{(A.3-3a)}$$

which predicts the measured flow within 0.5% at all flow rates.

TABLE A-3 : ORIFICE B CALIBRATION

Measured* Flow	Flow Calc'd From A.3-2a	Flow Calc'd From A.3-3a
270	265	271
316	312	317
362	354	361
399	389	400
428	417	427
535	520	533

* All flows in lb./hr.

(b) Orifice D - 0.370-in. diameter bore
Pipe I.D. - 1.049-in.

This orifice was calibrated for both steam and air flows. The calibration with steam as the flowing medium was made by collecting

condensate from the condenser. For air as the flowing medium the orifice was calibrated simultaneously with orifice B since the two orifices were connected in series.

This orifice exhausts to essentially an atmospheric pressure environment and hence at the higher upstream pressures the throat velocity approaches the limiting acoustic velocity. It should be noted however that since the orifice is a square-edged orifice, the normal relationships for predicting the critical throat pressure do not apply, i.e., the discharge will continue to increase as the ratio of downstream to upstream pressure (P_2/P_1) decreases below r_c as calculated from A.3-4.

$$r_c = \left[\frac{2}{\kappa+1}\right]^{\kappa/(\kappa-1)} \qquad \text{(A.3-4)}$$

where $\kappa = Cp/Cv$ = 0.53 for air; 0.58 for saturated steam[P14]

Consequently for purposes of calibration the downstream pressure was always taken as 14.7 p.s.i.a.

For flow in pipes of less than 2-in. I.D. it is recommended[T9] that the discharge equation be expressed in the form

$$w' \text{ (lb./sec.)} = KYD_2^2 \, \Delta P^n \, \rho^{1-n} \qquad \text{(A.3-5)}$$

where

K = overall constant (includes discharge coefficient)

Y = compressibility factor

D_2 = throat diameter in inches

ΔP = orifice differential (p.s.i.)

ρ = gas density (lb./ft^3) at upstream T and P

n = constant to be determined empirically

Rearranging the above equation and grouping KYD_2^2 as one constant one can write

$$w'/\rho = C(\Delta P/\rho)^n \qquad \text{(A.3-6)}$$

In logarithmic form equation (A.3-6) becomes

$$\log (w'/\rho) = \log C + n \log (\Delta P/\rho) \qquad \text{(A.3-7)}$$

Thus if log C remains constant (not a function of flow rate) a plot of w'/ρ vs. $\Delta P/\rho$ on log-log paper will be a straight line of slope n. For steam n was found to be 0.582 and C was calculated as 67.15 thus the flow equation becomes

$$w' = (67.15)\ (\Delta P)^{0.582}\ (\rho^{0.418}) \qquad \text{(A.3-8)}$$

which applies for

$$139.5 < w \text{ (lb./hr.)} < 285.3$$

$$271 < T_{upstream}(^{o}F) < 298$$

$$20 < \Delta P \text{ (p.s.i.)} < 48$$

At mass flows greater than 177 lb./hr. Equation (A.3-8) predicts flows with less than 1% error. At lower flow rates the error increases to 4%.

For air n was found to be 0.32 and C was calculated as 267 and thus the flow equation becomes

$$w' = (267)\ (\Delta P)^{0.32}\ (\rho)^{0.68} \qquad \text{(A.3-9)}$$

which applies for

$$270 < w(\text{lb./hr}) < 535$$

$$28 < \Delta P \text{ (p.s.i.)} < 65$$

$$80 < T_{Upstream} \ (^{o}F) < 90$$

Using the ideal gas law and converting the flow rate to lb./hr. Equation (A.3-9) becomes

$$w = (525) \ (\Delta P)^{0.32} \ \left(\frac{P_{Upstream}}{T_{Upstream}}\right)^{0.68} \qquad \text{(A.3-10)}$$

where

$P_{Upstream}$ is in p.s.i.a.

and $T_{Upstream}$ is in degrees Rankine

A.4 Rotameter Calibration Curves

Figure A4-1 is the calibration curve for Fischer-Porter rotameter FP - ¼ - 25 - G - 5/81 - sapphire float.

Figure A4-2 is the calibration curve for Fischer-Porter rotameter FP - ½ - 21 - G - 10/80 with stainless steel float No.16 USVT-40.

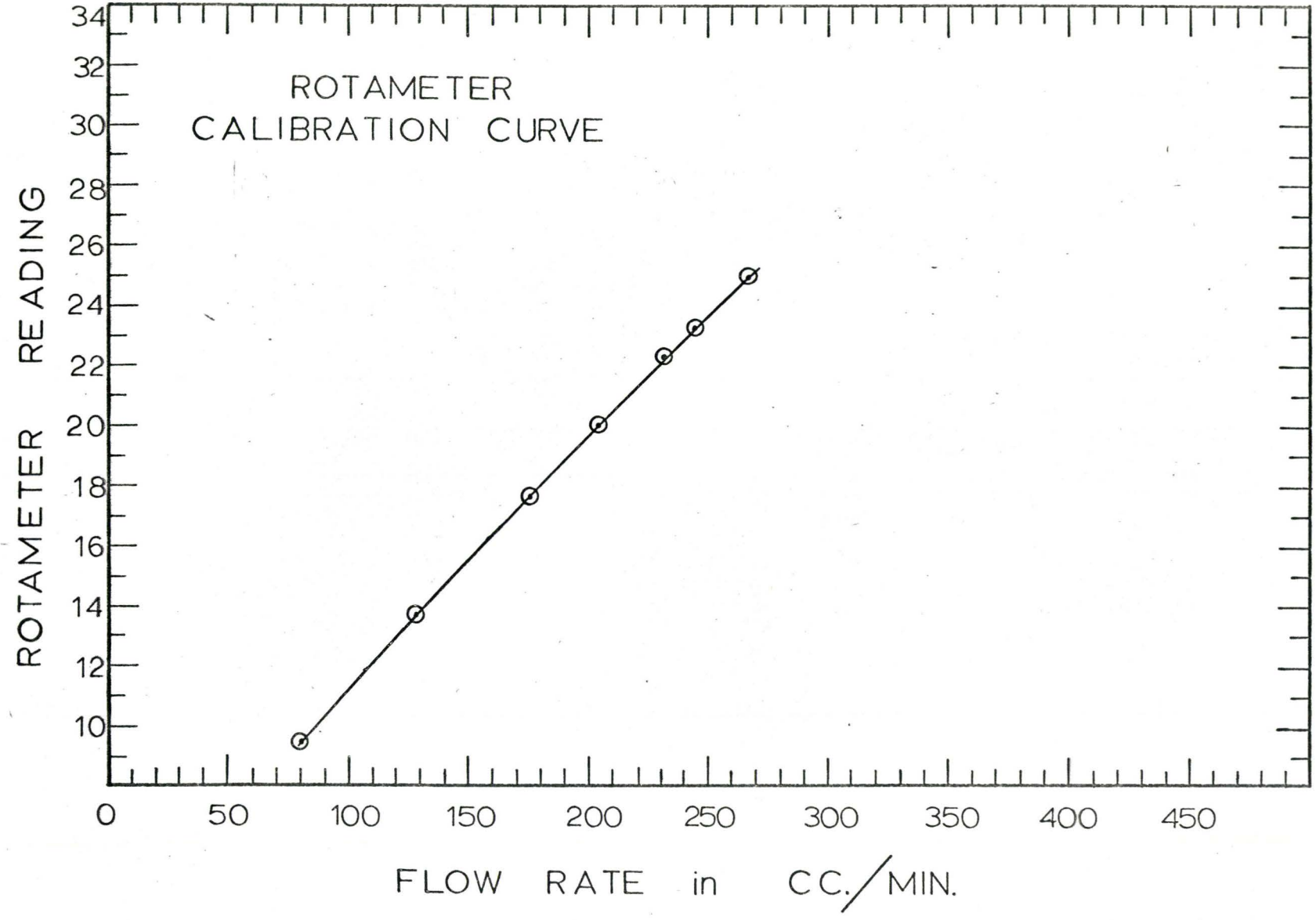
ROTAMETER
CALIBRATION CURVE
ROTAMETER READING
34
32
30
28
26
24
22
20
18
16
14
12
10
0
50
100
150
200
250
300
350
400
450
FLOW RATE in CC./MIN.

FIGURE A·4-1

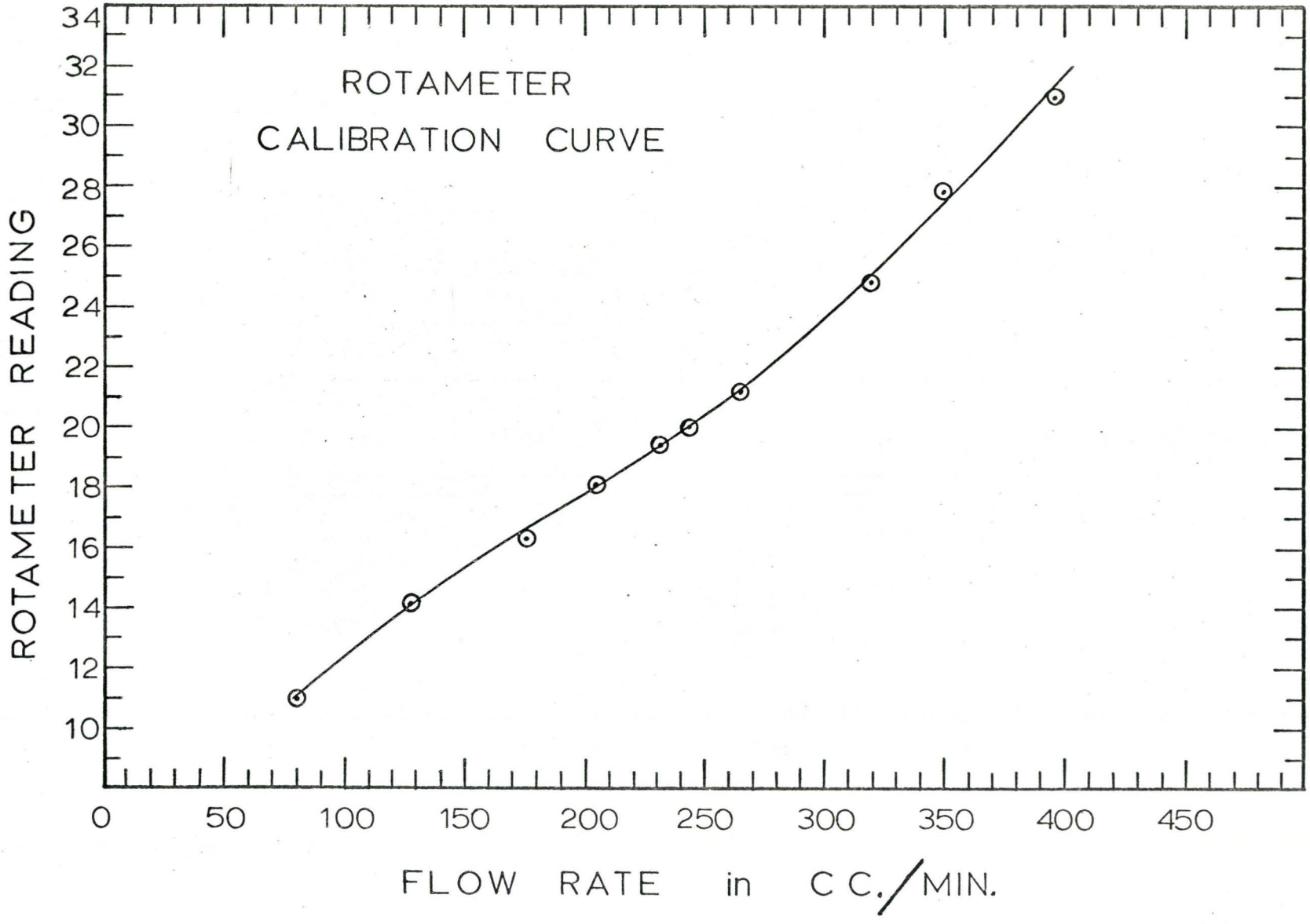
ROTAMETER
CALIBRATION CURVE
ROTAMETER READING
34
32
30
28
26
24
22
20
18
16
14
12
10
0
50
100
150
200
250
300
350
400
450
FLOW RATE in C C./MIN.

FIGURE A·4—2

A.5 Electrophotometer Calibration

The Fisher Model AC Electrophotometer was calibrated by measuring the transmittance of a number of solutions of known $KMnO_4$ concentrations on the logarithmic scale of the instrument. The solutions were prepared by diluting a N/10 stock solution of BDH potassium permanganate. All solutions were buffered with 10 ml. of 85% phosphoric acid.

Figure A5-1 is the calibration curve. It covers a concentration range of 4 to 36 mg./litre. $KMnO_4$ solutions of known concentration* were used to check the calibration. In all cases the indicated and actual concentrations differed by less than 1.5%.

---

* Supplied by the Chemistry Department (Analytical Group) of McMaster University; concentrations known to ± 0.2%.

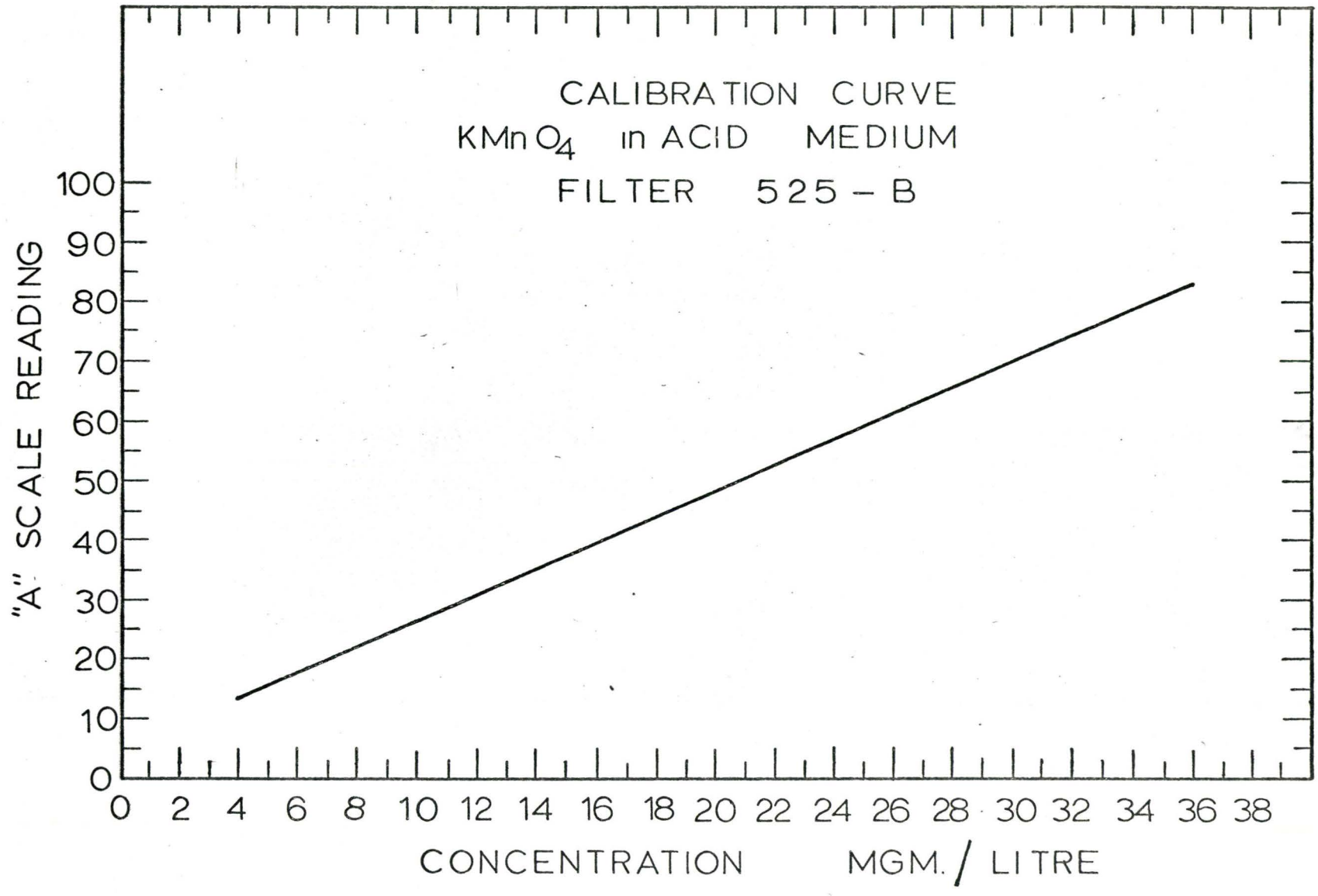
CALIBRATION CURVE
KMnO4 in ACID MEDIUM
FILTER 525 – B
"A" SCALE READING
0
10
20
30
40
50
60
70
80
90
100
0 2 4 6 8 10 12 14 16 18 20 22 24 26 28 30 32 34 36 38
CONCENTRATION MGM./ LITRE

FIGURE A·5 –1

A.6 Hot-Wire Calibration

A 0.00014-in. diameter 8 ohm tungsten wire probe* was used in conjuction with a Hubbard Model IHR constant temperature anemometer. The linearizing circuits of this instrument gave an amplified milliamp read-out which was directly proportional to the gas velocity at the wire (H17).

To calibrate the wire, the probe was placed at the centre-line and two inches above a carefully calibrated flow nozzle (R7) through which air at 80°F was flowing.

Figure A6-1 is the calibration curve. $\Delta\bar{I}$ on the abscissa is the difference between the average milliamp reading at velocity V and at zero velocity, i.e. $(\bar{I} - \bar{I}_o)$. It can be seen that over this velocity range the relationship is linear. The least-squares straight line through the points has a slope of 22.2

---

* The procedure followed in making this probe is described in reference (R7).

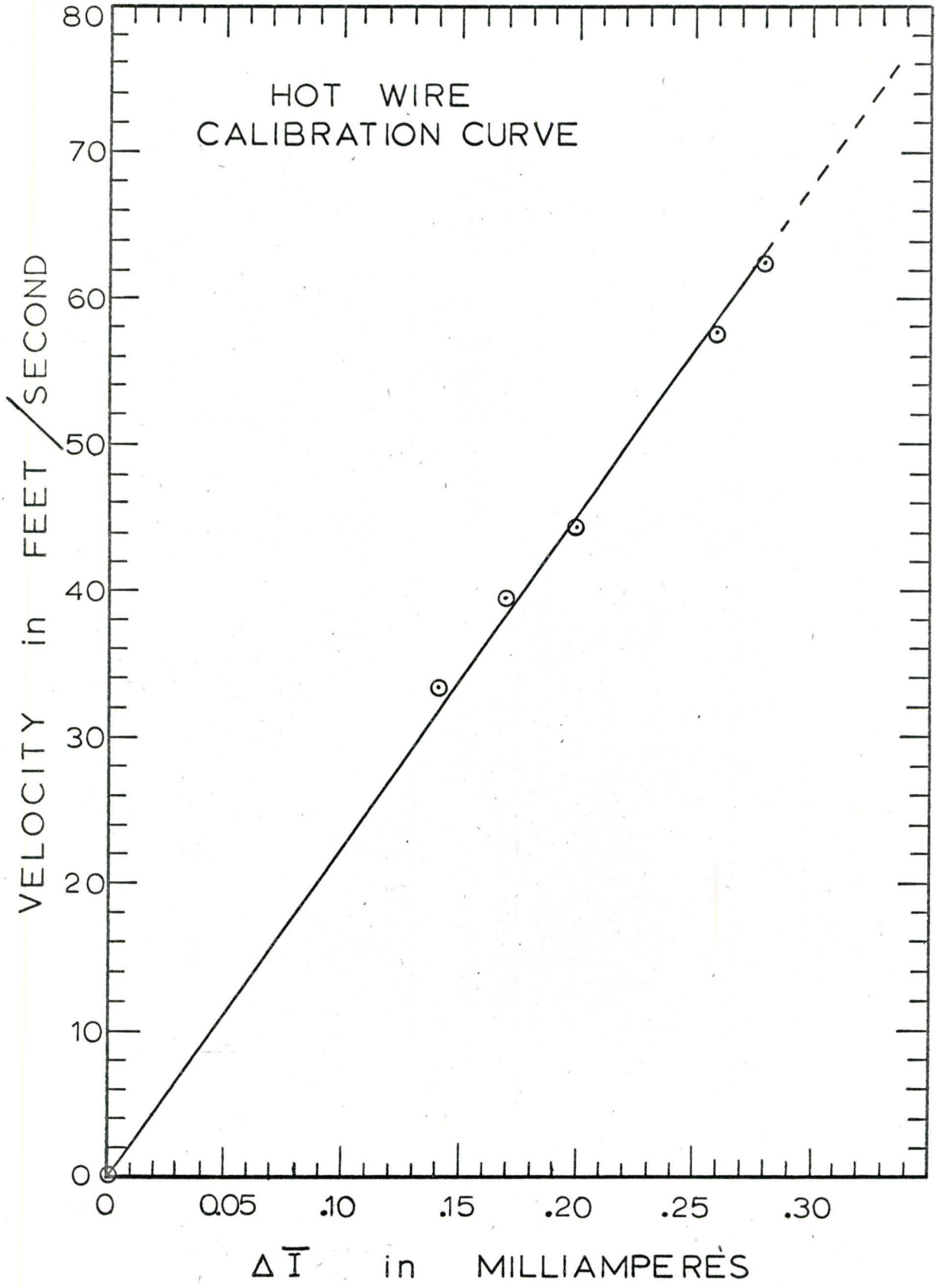
HOT WIRE
CALIBRATION CURVE
VELOCITY in FEET / SECOND
80
70
60
50
40
30
20
10
0
0
0.05
.10
.15
.20
.25
.30
Δ Ī in MILLIAMPERES

FIGURE A·6 — 1

APPENDIX B : PHYSICAL PROPERTIES

B.1. General

The majority of the physical properties of both steam and air at atmospheric pressure were taken from the tabulations presented in National Bureau of Standards Circular 564. The viscosity of steam was determined from the correlation given by Latto[L9]. The heat capacity of steam was also taken from the NBS tables although the values for Cp reported therein are not in agreement with those of Gordon[G11, G12] and Wagman et. al.[W3] especially at steam temperatures less than 500°F The NBS data were chosen because the tabulated heat capacities were calculated from experimental enthalpy measurements whereas Gordon's values (corrected for rotational stretching by Wagman) were obtained from spectroscopic measurements assuming that steam was an ideal gas.

Since the theoretical development and most of the analysis of experimental data involved the use of a digital computer it was necessary to convert the tabulated data into a convenient analytic form. The expressions which follow were obtained by least-squares analysis of the tabulated data over the indicated temperature ranges.

B.2 Physical Properties of Air

All temperatures are in degrees Rankine. The correlations for heat capacity, viscosity and thermal conductivity cover the range 450 to 1980°R. The correlation for density covers the range 540 to 1800°R.

(i) Density, lb./cu.ft.

$$\rho = 0.20738 - 0.41492 \times 10^{-3}T + 0.39657 \times 10^{-6}T^2$$
$$-0.18148 \times 10^{-9}T^3 + 0.31925 \times 10^{-13}T^4$$
$$S^2(\hat{y}) = 0.97789 \times 10^{-7} \text{ on 11 degrees of freedom}$$

(ii) Heat capacity, B.T.U./lb. °R.

$$Cp = 0.24688 - 0.35554 \times 10^{-4}T + 0.49476 \times 10^{-7}T^2$$
$$-0.12047 \times 10^{-10}T^3$$
$$S^2(\hat{y}) = 0.13419 \times 10^{-6} \text{ on 14 degrees of freedom}$$

(iii) Thermal Conductivity, B.T.U./hr.-ft.-°F

$$k = 0.28670 \times 10^{-3} + 0.32778 \times 10^{-4}T - 0.84398 \times 10^{-8}T^2$$
$$+ 0.13190 \times 10^{-11}T^3$$
$$S^2(\hat{y}) = 0.51112 \times 10^{-9} \text{ on 14 degrees of freedom}$$

(iv) Viscosity, lb./ft.-sec.)

$$\mu = 0.28967 \times 10^{-6} + 0.28330 \times 10^{-7}T - 0.13157 \times 10^{-10}T^2$$
$$+ 0.44536 \times 10^{-14}T^3 - 0.63962 \times 10^{-18}T^4$$
$$S^2(\hat{y}) = 0.21966 \times 10^{-15} \text{ on 13 degrees of freedom}$$

B.3 Physical Properties of Steam

All temperatures are in degrees Rankine except for the viscosity correlation where the temperature is in degrees Kelvin. This latter correlation covers the temperature range 373 to 1373 ^{o}K. All other correlations cover the range 684 to 1890 ^{o}R.

(i) Density, lb./cu.ft.

$$\rho = 0.11678 - 0.20820 \times 10^{-3}T + 0.17673 \times 10^{-6}T^2 - 0.71973 \times 10^{-10}T^3 + 0.11322 \times 10^{-13}T^4$$

$$S^2(\hat{y}) = 0.76594 \times 10^{-8} \text{ on 11 degrees of freedom}$$

(ii) Heat Capacity, B.T.U./lb.-^{o}R

$$Cp = 0.10765 \times 10^{1} - 0.19007 \times 10^{-2}T + 0.21208 \times 10^{-5}T^2 - 0.99145 \times 10^{-9}T^3 + 0.17177 \times 10^{-12}T^4$$

$$S^2(\hat{y}) = 0.35893 \times 10^{-5} \text{ on 11 degrees of freedom}$$

(iii) Thermal Conductivity, B.T.U./hr.-ft.-^{o}F.

$$k = 0.18361 \times 10^{-2} + 0.21871 \times 10^{-4}T + 0.22099 \times 10^{-8}T^2$$

$$S^2(\hat{y}) - 0.81157 \times 10^{-8} \text{ on 13 degrees of freedom}$$

(iv) Viscosity, poise (^{o}K)

$$\mu = -0.65634 \times 10^{-5} + 0.26700 \times 10^{-6}T + 0.25500 \times 10^{-9}T^2 - 0.13303 \times 10^{-12}T^3 - 0.22475 \times 10^{-6}T^4 + 0.18488 \times 10^{-19}T^5$$

Latto[L9] reports a standard deviation from the experimental points of ± 1.22%.

APPENDIX C : CALCULATIONS

C.1 Determination of Droplet Sample Size

This calculation was made for the following conditions;

(1) a flow rate of x lb./hr. of water (density - 60.1 lb./cu.ft.)

(2) volume mean diameter of spray is d microns

(3) cross-sectional area of the 8-in. I.D. column, A, is 0.349 sq.ft.

(4) area of collection cell, Ae, is 1.92×10^{-4} sq.ft.

(5) velocity of spray, is, v, ft./sec.

(6) target efficiency is 100%

(7) exposure time of cell is t seconds

Since a flow rate of 1 lb./hr. represents a volume flow rate of 4.62×10^{-6} cu.ft./sec. and the volume of a 1 micron drop is 1.84×10^{-17} cu.ft., the number of drops generated per second is

$$N = (2.52 \times 10^{11})\ (x)/d^3 \qquad \text{(C.1-1)}$$

and the droplet concentrations (drops/unit volume) is given by

$$\frac{N}{V} = (2.52 \times 10^{11})\ (x)/(A)\ (d^3)\ (v) \qquad \text{(C.1-2)}$$

The volume swept by the cell when open for t seconds is

$$(A_c)\ (v)\ (t) = V_c$$

From equation (C.1-2) the number of drops collected is therefore

$$N_c = \frac{N}{V} \cdot V_c = (2.52 \times 10^{11})\ (x)\ (t)\ (A_c)/(A)(d^3)$$

which for this particular system becomes

$$N_c = (1.39 \times 10^{8})\ (x)\ (t)/d^3 \qquad \text{(C.1-3)}$$

Example : For 5 lb./hr. with a d of 50 microns and t of 1 second

$$N_c = (1.39 \times 10^8)\ (5)\ (1)/(5 \times 10)^3 = 5{,}500 \text{ drops}$$

if d is 80 microns, N_c = 1,350 drops

It should be noted that while the number of drops collected decreases as the volume mean diameter increases, a greater fraction of the calculated theoretical maximum number of drops will be collected because the overall target efficiency of the cell increases with increasing drop size.

The relationships developed by Ranz and Wang[R8] for a disc-shaped collector indicate that for 5 micron diameter water droplets, flowing in steam at 4 ft./sec., being intercepted by a 0.76 cm. diameter disc, the target efficiency is approximately 0.40. For 10 micron droplets the efficiency increases to 0.81 while for 20 micron droplets the efficiency is > 0.95. At a velocity of 8 ft./sec. the target efficiencies for the 5 and 10 micron drops become 0.62 and 0.90 respectively.

C.2 Thermocouple Response

The following calculations were made assuming that the thermocouples were measuring the temperature of steam at 400°F. The properties used were taken from tables (K7). It was also assumed that the thermocouple junction was formed by butt-welding the two wires thus giving a junction of the same diameter as the wire.

C.2.1. Calculation of Thermocouple Time Constant

Hoffman (H1) used a thermocouple constructed of 0.010-in. Pt - Pt 10% Rh thermocouple wire. The suction applied to the thermocouple probe was such as to give velocities of the order of 100 ft./sec. at the thermocouple junction. This velocity corresponds to a Reynolds number for the wire of 211.

Using a standard correlation for flow over wires (p.411, K7) the Nusselt number is calculated to be 7.45 which corresponds to a heat transfer coefficient, h, of 179 for this steam flow.

Using a density of 1334 lb./cu.ft. and a heat capacity of 0.0326 B.T.U./lb.°F (E11) for platinum and neglecting the effect of rhodium, the time constant of the wire is calculated as:

$$\frac{C_p \rho V}{h A} = \frac{(0.326)(1334)(\cdot 010)(3600)}{(179)\qquad (12)\ (6)} = 0.121 \text{ sec.}$$

where $\frac{V}{A}$ is assumed to be $(\frac{V}{A})_{\text{sphere}} = \frac{D}{6}$

Similarly for a 0.0005-in. diameter wire at a gas velocity of 5 ft./sec. the Reynolds number, Nusselt number and heat transfer coefficient are found to be 0.527, 0.721, 346 respectively.

The time constant is thus

$$(0.121)\ (0.0005/0.010)\ (179/346) = 0.00314 \text{ sec.}$$

For the same sized wire Brown[B13] reports a time constant of 0.0037 seconds.

C.2.2 Calculation of Magnitude Ratio

The magnitude ratio, in frequency response studies, represents the ratio of the magnitude of an output signal to an input signal. If the output signal from a system is a linear function of the input signal the magnitude ratio (M.R.) can be calculated from[P13]

$$M.R. = 1/(1 + (2\pi fT)^2)^{\frac{1}{2}} \qquad (C.2\text{-}1)$$

where

f is the frequency of the input signal in cycles/sec.

T is the time constant of the system in sec.

For a thermocouple, if the millivolt fluctuation which corresponds to a temperature fluctuation in the medium being monitored is considered as the input signal, then the millivolt signal which is transmitted to the measuring circuit can be considered as the output signal. Thus the M.R. gives a measure of the ability of the thermocouple to follow temperature fluctuations.

For a frequency of 10 c.p.s. the M.R. for Hoffman's thermocouple is

$$M.R. = 1/(1 + (2\pi \cdot 10 \cdot 0 \cdot 121)^2)^{\frac{1}{2}} = 0.13$$

For the unshielded 0.0005-in. thermocouple

$$M.R. = 1/(1 + (2\pi \cdot 10 \cdot 0 \cdot 00314)^2)^{\frac{1}{2}} = 0.98$$

Thus the small thermocouple can be expected to follow the gas temperature fluctuations approximately 8 times better than the large thermocouple employed by Hoffman.

C.3 Comparison of Thermocouple Probes

Figure C.3-1 compares the gas-temperature profile which was measured with the original probe (thermocouple junction ¼-in. above the stop-rod) to that which was measured with the modified probe (thermocouple junction 1¼-in. above the stop-rod). The profiles were measured in an air flow, (N_{Re} = 10,100) at a nominal wall temperature of 600°F, at an axial distance of 3-in. from the start of the "hot zone". It can be readily seen from the figure, that the extrapolated wall-temperatures differ by approximately 50°F. The gradient measured with the original probe is also seen to be steeper (approximately 60% steeper), than the gradient measured with the modified probe. Consequently, the rate of heat transfer calculated from the data taken with the original probe would be higher than that calculated from the data taken with the modified probe.

The geometry of the original probe-tip (junction ¼-in. above the stop-rod) was identical to the probe-tip geometry employed by

Brown[B13]. Brown found that the heat-transfer rates which were calculated from his experimentally measured temperature profiles were 20 to 45% higher than those of other workers[B15, C10, E7]. Since Brown's probe was the same as the original probe used in this work it would appear that his apparent high heat-transfer rates were caused by the effect of the probe on the gas-temperature profiles.

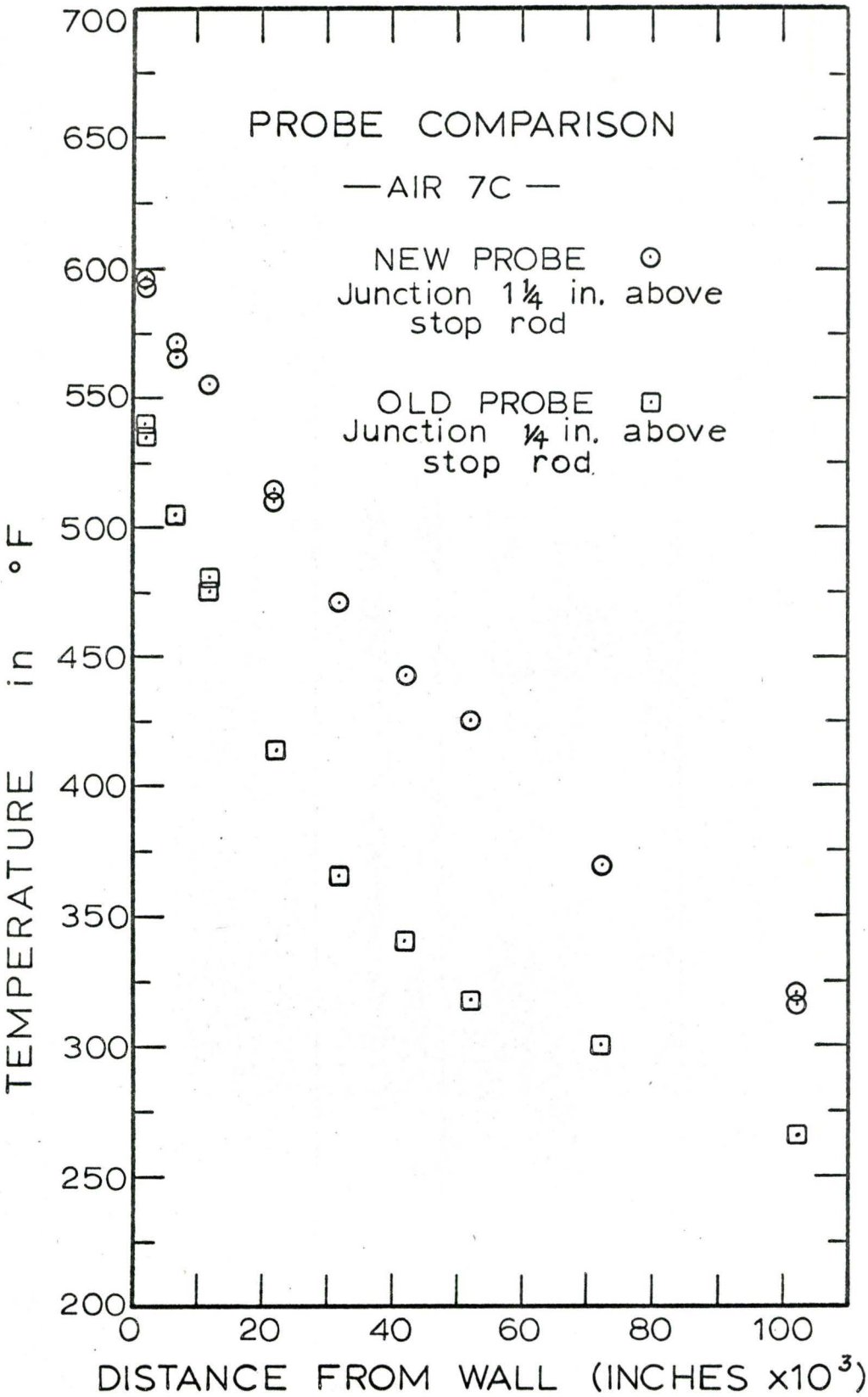
PROBE COMPARISON
—AIR 7C —
NEW PROBE ⊙
Junction 1¼ in. above stop rod
OLD PROBE ⊡
Junction ¼ in. above stop rod
TEMPERATURE in °F
700
650
600
550
500
450
400
350
300
250
200
0
20
40
60
80
100
DISTANCE FROM WALL (INCHES x10³)

FIGURE C.3-1

C.4 Effect of Variable Thermal Conductivity on the Temperature Gradient at the Wall

For purposes of illustration, consider a narrow slab of gas adjacent to a hot wall ($t_{wall} > t_{gas}$) as shown in the Figure below.

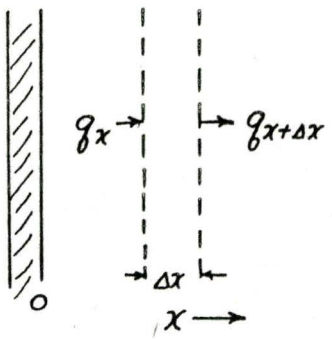

If the assumption is made that a heat-sink, Q' (B.T.U./hr. ft.^{3}), exists in the gas (analogous to the heat transported away by the flowing gas in the real system), a steady-state one-dimensional heat balance on a slab of thickness Δx can be written as

$$q_x A - q_{x+\Delta x} A - Q' \Delta x A = 0 \qquad \text{(C.4-1)}$$

where q is the heat flux, B.T.U./hr. ft^2

A is the area of the slab perpendicular to the direction of the heat flux, ft^2.

Dividing equation (C.4-1) by $\Delta x A$ and taking the limit as Δx goes to zero gives

$$\lim_{\Delta x \to 0} \left[\frac{q_x - q_{x+\Delta x}}{\Delta x} \right] - Q' = 0 \qquad \text{(C.4-2)}$$

The first term of this equation is just the first derivative of q with

respect to x and so the equation becomes

$$-\frac{dq}{dx} - Q' = 0 \qquad \text{(C.4-3)}$$

Fourier's law in the form, $q = -\frac{kdt}{dx}$ is now substituted into equation (C.4-3) to obtain

$$-\frac{d}{dx}\left(-\frac{kdt}{dx}\right) - Q' = 0 \qquad \text{(C.4-4)}$$

(i) Constant Thermal Conductivity

When the thermal conductivity is constant, equation (C.4-4) can be written as

$$\frac{d^2t}{dx^2} = Q'/k \qquad \text{(C.4-5)}$$

This equation indicates, as expected, that the temperature gradient increases as the wall is approached. It is obvious from equation (C.4-5) that if k is evaluated at t_{wall} (k increases with temperature for gases) with Q' kept constant, the temperature gradient at the wall is not as large as when k is evaluated at t_{gas}.

(ii) Variable Thermal Conductivity

If k is considered now to be a function of t in equation (C.4-4), the indicated differentiation yields

$$\frac{\partial k}{\partial x}\frac{\partial t}{\partial x} + k\frac{\partial^2 t}{\partial x^2} = Q' \qquad \text{(C.4-6)}$$

If k is only a function of t and t is only a function of x, the above equation can be written as

$$\frac{d^2t}{dx^2} = \frac{Q'}{k} - \frac{1}{k}\frac{dk}{dt}\left(\frac{dt}{dx}\right)^2 \qquad \text{(C.4-7)}$$

Since in this case $\frac{dk}{dt}$ is known to be positive, the second term on the right side of equation (C.4-7) is always positive; therefore a comparison of equations (C.4-7) and (C.4-5) indicates that allowance for a variable thermal conductivity will result in a decreased temperature gradient at the wall.

APPENDIX D : FINITE-DIFFERENCE APPROXIMATIONS

D.1 Parabolic Equation (no axial diffusion)

(i) Dimensionless Energy Equation

The dimensionless energy equation (4.3-3) will be rewritten here for ease of reference

$$RO{\cdot}U \frac{\partial T}{\partial x} = \frac{1}{R} G \frac{\partial T}{\partial T} + \frac{\partial G}{\partial R} \frac{\partial T}{\partial R} + G \frac{\partial^2 T}{\partial R^2} \qquad (D\text{-}1)$$

where the dimensionless variables have the same definition as given in Section 4.3.2. The mesh system to be used was given in Figure 4.3-3.

(ii) Derivative Approximations

(a) Axial direction - a standard forward-difference approximation was used

$$\frac{\partial T}{\partial x} = \frac{T_{i,j+1} - T_{i,j}}{x_{j+1} - x_j} \qquad (D\text{-}2)$$

(b) Radial direction - using the Crank-Nicholson approximation for the radial temperature gradients the derivatives can be represented as

$$\frac{\partial T}{\partial R} = \frac{1}{2} \left[\frac{T_{i+1,j} - T_{i-1,j}}{R_{i+1} - R_{i-1}} + \frac{T_{i+1,j+1} - T_{i-1,j+1}}{R_{i+1} - R_{i-1}} \right] \qquad (D\text{-}3)$$

$$\frac{\partial^2 T}{\partial R^2} = \frac{1}{2}\left[\frac{2\,T_{i+1,j}}{(R_{i+1} - R_i)(R_{i+1} - R_{i-1})} - \frac{2\,T_{i,j}}{(R_i - R_{i-1})(R_{i+1} - R_i)}\right.$$

$$+ \frac{2\,T_{i-1,j}}{(R_i - R_{i-1})(R_{i+1} - R_{i-1})} + \frac{2\,T_{i+1,j+1}}{(R_{i+1} - R_i)(R_{i+1} - R_{i-1})}$$

$$\left. - \frac{2\,T_{i,j+1}}{(R_i - R_{i-1})(R_{i+1} - R_i)} + \frac{2\,T_{i-1,j+1}}{(R_i - R_{i-1})(R_{i+1} - R_{i-1})}\right] \quad \text{(D-4)}$$

Equations (D-3) and (D-4) approximate the derivatives by using the average of the derivatives at axial locations j and j+1. The expression for the second derivative at any one axial location j is found from a Taylor's series expansion for a variable step size[H19]. If the step size is constant, equation (D-4) reduces to the more familiar form

$$\frac{\partial^2 T}{\partial R^2} = \frac{1}{2}\left[\frac{T_{i+1,j} - 2\,T_{i,j} + T_{i-1,j}}{(R_{i+1} - R_i)^2} + \frac{T_{i+1,j+1} - 2\,T_{i,j+1} + T_{i-1,j+1}}{(R_{i+1} - R_i)^2}\right] \quad \text{(D-5)}$$

Equation (D-3) is the standard central-difference form of the first derivative for a constant radial step size. The more exact expression which is derived from a Taylor's series for a variable step-size could not be used because it was found[H19] that the solution was always unstable. Equation (D-3) was found to yield stable solutions under all conditions. This equation has a truncation error of order

$$\left[(R_{i+1} - R_i)^2 - (R_{i-1} - R_i)^2\right] \frac{\partial^2 T}{\partial R^2}$$

whereas the more exact expression (analogous to equation (D-4) for the second derivative) has a truncation error of order

$$(R_{i+1} - R_{i-1})^3 \frac{\partial^3 T}{\partial R^3} \quad .$$

Thus although equation (D-3) has a higher truncation error than the more accurate expression, the magnitude of the error is still very small.

Similarly, the first derivative of the eddy diffusivity equation was evaluated by a constant step-size central difference expression. The derivatives were not averaged as in the case of the temperature derivatives because the diffusivity was assumed to be independent of axial distance. The resulting expression is

$$\frac{\partial G}{\partial R} = \frac{G_{i+1} - G_{i-1}}{R_{i+1} - R_{i-1}} \qquad \text{(D-6)}$$

(iii) Boundary Conditions

(1) at $x = 0$, $T_{i,1} = T_{inlet}(R)$ (initial temperature distribution is known)

(2) at $R = 1$, $T_{N,j+1} = T_{wall}(x)$ (wall temperature is known)

(3) at $R = 0$, $\frac{\partial T}{\partial R}(i,j) = 0$ (axial symmetry)

When boundary condition (3) is applied to (D-1) the term $\frac{1}{R} G \frac{\partial T}{\partial R}$ becomes indeterminate. Applying L'Hopital's rule this term becomes

$$\frac{G \frac{\partial}{\partial R} (\partial T/\partial R)}{\frac{\partial}{\partial R}(R)} = G \frac{\partial^2 T}{\partial R^2} \qquad \text{(D-7)}$$

and the energy equation at the centre line becomes

$$RO \cdot U \frac{\partial T}{\partial x} = 2G \frac{\partial^2 T}{\partial R^2} \qquad (D\text{-}8)$$

The expressions for approximating these derivatives have already been given.

(iv) Determination of Radial mesh-points

The radial step-sizes were calculated from a formula similar to that used by Houghton[H19]

$$\Delta R_p = \left[\frac{Z^{p-1} - 1}{Z-1}\right] \Big/ \sum_{p=1}^{N-1} \Delta R_p \qquad (D\text{-}9)$$

where N is the number of radial mesh points, including the wall. The larger the value of Z the more rapid the increase in step-size, as p increases.

Since the mesh-points were numbered from the centre-line to the wall, each radial mesh point was calculated as shown in equation (D-10).

$$\text{for } i = 1 \;,\quad R_i = 0$$

$$\text{for } i \geq 2 \;,\quad R_i = R_{i-1} + \Delta R_{N+1-i} \qquad (D\text{-}10)$$

(v) Finite-Difference Equation

The following new variables were defined to avoid the manipulation of cumbersome equations.

$$F1 = 1/(R_{i+1} - R_{i-1})$$

$$F2 = 2/(R_{i+1} - R_i)\,(R_{i+1} - R_{i-1})$$

$$F3 = 2/(R_i - R_{i-1})\,(R_{i+1} - R_i)$$

$$F4 = 2/(R_i - R_{i-1})\,(R_{i+1} - R_{i-1})$$

$$Dx = x_{j+1} - x_j$$

$$DiF_i = \left(\frac{\partial G}{\partial R}\right)_i = \frac{G_{i+1} - G_{i-1}}{R_{i+1} - R_{i-1}}$$

$$A_i = \frac{F1}{2}\left[\frac{G_i}{R_i} + DiF_i\right] - \frac{F4}{2} G_i$$

$$B_i = \frac{F3}{2} G_i - \frac{RO \cdot U_i}{DX}$$

$$C_i = -\frac{F1}{2}\left[\frac{G_i}{R_i} + DiF_i\right] - \frac{F2}{2} G_i$$

$$D_i = \frac{F3}{2} G_i + \frac{RO \cdot U_i}{DX} \qquad \text{(D-11)}$$

The following equation is the finite-difference equation for the solution of the energy equation at mesh points i = 3 to i = N-1.

$$C_i T_{i+1,j+1} + D_i T_{i,j+1} + A_i T_{i-1,j+1} =$$

$$-C_i T_{i+1,j} - B_i T_{i,j} - A_i T_{i-1,j} \qquad \text{(D-12)}$$

where the temperatures on the L.H.S. are all unknown and the temperatures on the R.H.S. are known.

At the centre line, i = 1, and symmetry dictates that

$$T_{i+1,j} \equiv T_{i-1,j} \qquad \text{(D-13)}$$

$$T_{i+1,j+1} \equiv T_{i-1,j+1}$$

and the coefficients have the following form

$$A_1 + C_1 = -G_1 [F2 + F4]$$

$$B_1 = F3\ G_1 - \frac{RO \cdot U_2}{DX}$$

$$D_1 = F_3\ G_1 - \frac{RO \cdot U_1}{DX} \qquad \text{(D-14)}$$

The finite-difference equation is thus written as

$$T_{i,j+1} = \frac{-B_1}{D_1} T_{1,j} - \frac{(A_1 + C_1)}{D_1} T_{2,j} - \frac{(A_1 + C_1)}{D_1} T_{2,j+1} \qquad (D\text{-}15)$$

Thus where $i = 2$, the value for $T_{1,j+1}$ from (D-15) is substituted into equation (D-12) to yield

$$\left[1 - \frac{A_2}{D_1 D_2} (A_1 + C_1) \right] T_{2,j+1} + \frac{C_2}{D_2} T_{3,j+1} =$$

$$\left[- \frac{A_2}{D_2} + \frac{B_1 A_2}{D_1 D_2} \right] \cdot T_{1,j} + \left[- \frac{B_2}{D_2} + \frac{(A_1 + C_1) A_2}{D_1 D_2} \right] T_{2,j}$$

$$- \frac{C_2}{D_2} T_{3,j} \qquad (D\text{-}16)$$

The temperatures at each axial-step were determined by inverting the tri-diagonal matrix of coefficients given in equations (D-12) and (D-16). The inversion was performed by a standard library routine which used a Gaussian elimination technique (BNDSOL on the McMaster IBM 7040 computer). Thus the temperatures were determined for mesh points $i = 2$ to $i = N-1$ after inversion. The centre line temperature, $T_{1,j+1}$, was then determined from equation (D-15).

(vi) Determination of U_i

The equation for the dimensionless velocity profile (4.3-4) was numerically integrated with the MIDAS library routine (5th order Predictor-Corrector). The results were then regressed using a least-squares, orthogonal polynomial analysis[P16]. A ninth order polynomial gave results which differed from Deissler's velocity profile[D13] by no more than 0.5% at all values of y^+ up to 26.

(vii) Program Listing

The program listing for the solution of the finite difference equation is given in Appendix Z.1.

D.2 Elliptic Equation (axial diffusion)

The dimensionless energy equation with the axial diffusion term included, equation (4.3-10) is rewritten here as equation (D-17).

$$RO{\cdot}U\ \frac{\partial T}{\partial x} = \frac{G}{R}\ \frac{\partial T}{\partial R} + \frac{\partial G}{\partial R}\ \frac{\partial T}{\partial R} + G\ \frac{\partial^2 T}{\partial R^2} + G\ \frac{\partial^2 T}{\partial x^2} \qquad (D\text{-}17)$$

where the dimensionless variables have the same definition as given in Section 4.3.2. The assumptions are the same as those employed in the solution of the parabolic form of the energy equation with the exception that axial diffusion is not neglected. The additional assumption was made that the eddy diffusivity at a point is assumed to be the same in the axial and radial directions.

All the derivatives in this analysis were written in terms of a central-difference approximation. As in the case of the parabolic form, the first derivatives were expressed in standard form without allowance for a variable step size. As explained in Appendix D.1 this leads to a larger truncation error than is obtained with approximations which account for the variable step-size but the solution remains stable under all conditions. The expressions for the second derivatives reduce to

the standard form when the step size remains constant.

(i) Derivative Approximations

(a) Axial Direction

$$\frac{\partial T}{\partial x} = \frac{T_{i,j+1} - T_{i,j}}{x_{j+1} - x_{j-1}} \qquad \text{(D-18)}$$

$$\frac{\partial^2 T}{\partial x^2} = \frac{2\,T_{i,j+1}}{(x_{j+1} - x_j)(x_{j+1} - x_{j-1})} - \frac{2\,T_{i,j}}{(x_{j+1} - x_j)(x_j - x_{j-1})}$$

$$+ \frac{2\,T_{i,j-1}}{(x_j - x_{j-1})(x_{j+1} - x_{j-1})} \qquad \text{(D-19)}$$

(b) Radial direction

$$\frac{\partial G}{\partial R} = \frac{G_{i+1} - G_{i-1}}{R_{i+1} - R_{i-1}} \qquad \text{(D-20)}$$

$$\frac{\partial T}{\partial R} = \frac{T_{i+1,j} - T_{i-1,j}}{R_{i+1} - R_{i-1}} \qquad \text{(D-21)}$$

$$\frac{\partial^2 T}{\partial R^2} = \frac{2\,T_{i+1,j}}{(R_{i+1} - R_i)(R_{i+1} - R_{i-1})} - \frac{2\,T_{i,j}}{(R_{i+1} - R_i)(R_i - R_{i-1})}$$

$$+ \frac{2\,T_{i-1,j}}{(R_i - R_{i-1})(R_{i+1} - R_{i-1})} \qquad \text{(D-22)}$$

(ii) Boundary Conditions

(1) at $R = 1$, $T_{N,j+1} = T_{wall}(x)$ (wall temperature is known)

(2) at $R = 0$ $\frac{\partial T}{\partial R}(1,j) = 0$

(3) at $x = 0$ $T_{i,1} = T_{inlet}(R)$ (initial temperature distribution is known)

(4) at $x = x'$ $T_{i,j} = T_{x'}(R)$ (temperature distribution from parabolic equation is used at $x = x'$)

As discussed in Appendix D.1, at the centre-line the term $\frac{G}{R}\frac{\partial T}{\partial R}$ is indeterminate. When L'Hopital's rule is applied, the energy equation at the centre-line has the form

$$RO \cdot U \frac{\partial T}{\partial x} = G\left(2\frac{\partial^2 T}{\partial x^2} + \frac{\partial^2 T}{\partial x^2}\right) \qquad \text{(D-23)}$$

(iii) Determination of Mesh Points

The radial mesh-points are determined as in the parabolic case and can be found from equations (D-9) and (D-10). The axial mesh-size is constant except in the entrance region where the initial step is further subdivided because of the large axial temperature gradients existing there.

(iv) Finite-Difference Equation

The following new variables were defined to avoid the manipulation of cumbersome equations.

$$F1 = 1/(R_{i+1} - R_{i-1})$$

$$F2 = 2/(R_{i+1} - R_i)\ (R_{i+1} - R_{i-1})$$

$$F3 = 2/(R_i - R_{i-1})\ (R_{i+1} - R_i)$$

$$F4 = 2/(R_i - R_{i-1})\ (R_{i+1} - R_{i-1})$$

$$H1 = 1/(x_j - x_{j-1})$$

$$H2 = 2/(x_{j+1} - x_j)\ (x_{j+1} - x_{j-1})$$

$$H3 = 2/(x_j - x_{j-1})\ (x_{j+1} - x_j)$$

$$H4 = 2/(x_j - x_{j-1})\ (x_{j+1} - x_{j-1})$$

$$DlF_i = \left(\frac{\partial G}{\partial R}\right)_i = \frac{G_{i+1} - G_{i-1}}{R_{i+1} - R_{i-1}}$$

$$A_i = F1\ \left(DlF_i + \frac{G_i}{R_i}\right) = F4G_i$$

$$B_i = (F3 + H3)\ G_i$$

$$C_i = -F1\ \left(DlF_i + \frac{G_i}{R_i}\right) - F2G_i$$

$$D_i = RO \cdot U_i\ H1 - H2G_i$$

$$E_i = RO \cdot U_i\ H1 - H4G_i \qquad \text{(D-24)}$$

The following equation is the finite-difference equation for the solution of the elliptic form of the energy equation at all mesh points where the temperature is unknown except at the centre-line mesh point, (i=1).

$$B_i\ T_{i,j} + C_i\ T_{i+1,j} + A_i\ T_{i-1,j} + D_i\ T_{i,j+1} + E_i\ T_{i,j-1} = 0 \qquad \text{(D-25)}$$

At the centre-line where i = 1

$$T_{i+1,j} \equiv T_{i-1,j}, \text{ because of symmetry,}$$

and the coefficients A_i, B_i, C_i become

$$A_1 + C_1 = -(2F4 + 2F2)\ G_1$$

$$B_1 = (2F3 + H3)\ G_1 \qquad \text{(D-26)}$$

The finite-difference equation at the centre-line is thus written as

$$B_1 T_{1,j} + (A_1 + C_1) T_{2,j} + D_1 T_{1,j+1} + E_1 T_{1,j-1} = 0 \qquad \text{(D-27)}$$

The temperature coefficients in equations (D-25) and (D-27) are inserted as the elements in a banded matrix which was inverted by a standard library routine (BNDSOL). This routine also performs the appropriate multiplications with the inverted matrix which are necessary for the determination of the unknown temperatures.

(v) Program Listing

The program listing for the solution of the finite-difference approximation to the elliptic partial-differential equation is given in Appendix Z.2.

APPENDIX E RADIATION ANALYSIS

E.1 Gas Emissivity

The gas emissivity was calculated from the following correlations of Bevans [B3]

$$\varepsilon = K_1 (p\ell) + (K_2 p\ell)^{\frac{1}{2}} \qquad \text{(E.1-1)}$$

$$0.01 \leq p\ell \leq 0.1 \quad \text{atm.-ft.} \qquad \text{(E.1-1)}$$

$$\varepsilon = (K_3 p\ell)^{\frac{1}{2}} + K_4 \log(K_5 p\ell)$$

$$0.1 < p\ell \leq 1 \quad \text{atm.-ft.} \qquad \text{(E.1-2)}$$

$$\varepsilon = K_6 \log (K_7 p\ell)$$

$$1.0 < p\ell \leq 20 \quad \text{atm.-ft} \qquad \text{(E.1-3)}$$

The coefficients K are functions of temperature. The tabulated values of K given by Bevans were regressed to yield K as a quadratic function of temperature. ($K = a_o + a_1 T + a_2 T^2$). The calculated values of K never differed from the tabulated values by more than 0.8%. The K's were fitted over two temperature ranges; Table E.1-1 gives the coefficients of the quadratic equation.

The emissivity data of Hottel [H8] were fitted by a third-order polynomial at 600°R, for $0.005 \leq p\ell \leq 20$ atm.-ft. The calculated emissivity never differed from Hottel's values by more than 0.9%. The equation used to calculated ε was

$$\varepsilon = -1.1463 + 0.33723\ (p\ell) - 0.37953 \times 10^{-1}\ (p\ell)^2 + 0.78059 \times 10^{-3}\ (p\ell)^3 \qquad \text{(E.1-4)}$$

TABLE E.1-1 : Temperature Coefficients

(i) Temperature Range 800 to 1399°R

K	$a_o \times 10$	$a_1 \times 10^2$	$a_2 \times 10^6$
K_1	- 0.25874	0.20647	- 0.67997
K_2	- 0.15806	- 0.11528	- 0.42670
K_3	- 0.55392	0.25207	- 0.84426
K_4	- 0.17307	- 0.06902	0.01824
K_5	0.33601	0.09476	- 0.77771
K_6	- 0.17335	0.06512	- 0.24112
K_7	00.37366	- 0.17653	0.45636

(ii) Temperature Range 1400 to 2000°R

K_1	- 0.15737	0.07146	- 0.23242
K_2	- 0.21956	- 0.04953	- 0.58523
K_3	- 0.46312	0.12027	- 0.36588
K_4	- 0.20928	- 0.02076	- 0.14210
K_5	0.40372	- 0.02445	- 0.27222
K_6	- 0.12568	0.00529	- 0.05695
K_7	0.32675	- 0.10382	0.17586

A linear interpolation was used to obtain gas emissivities at temperatures between 600 and 800^{o}R.

The correction factor, C_w, given by Hottel[H8], to allow for a non-zero partial pressure of the water vapour (Hottel's data are given for a zero partial pressure of water vapour.) was regressed to yield the equation

$$C_w = 1.3633 - 0.86801 \times 10^{-1} \, (\ell n(p\ell) - 0.45815) \qquad \text{(E.1-5)}$$

for a total pressure of 1 atmosphere and pure steam (vapour pressure = 1 atmosphere)

E.2 Direct-Interchange Areas

Erkku's[E1] modified interchange areas were tabulated at values of kB of 0.0, 0.10, 0.25, 0.50, 0.75, 1.00, 1.25, using the following relationships

EW = Interchange Area, End-to-Wall/B^2

EE - Interchange Area, End-to-End /B^2

WW = Interchange Area, Wall-to-Wall/B^2

EG = Interchange Area, End-to-Gas/$(kB)B^2$

GG = Interchange Area, Gas-to-Gas$((kB)^2B^2$

GW = Interchange Area, Gas-to-Wall/$(kB)B^2$ (E.2-1)

Each interchange area was identified by three numbers, e.g., GG 324.

The first number is the maximum axial distance, measured in B units, between points in the two zones under consideration.

The second number is the maximum radial distance, in B units, from the centre-line to the furthest point in the zone closest to the centre-line.

The third is the maximum radial distance to the furthest point in the other zone. For example, the designation GG 324 would be the modified interchange area for the cross-hatched zones shown in the following diagram, or any other pair of zones with this particular orientation.

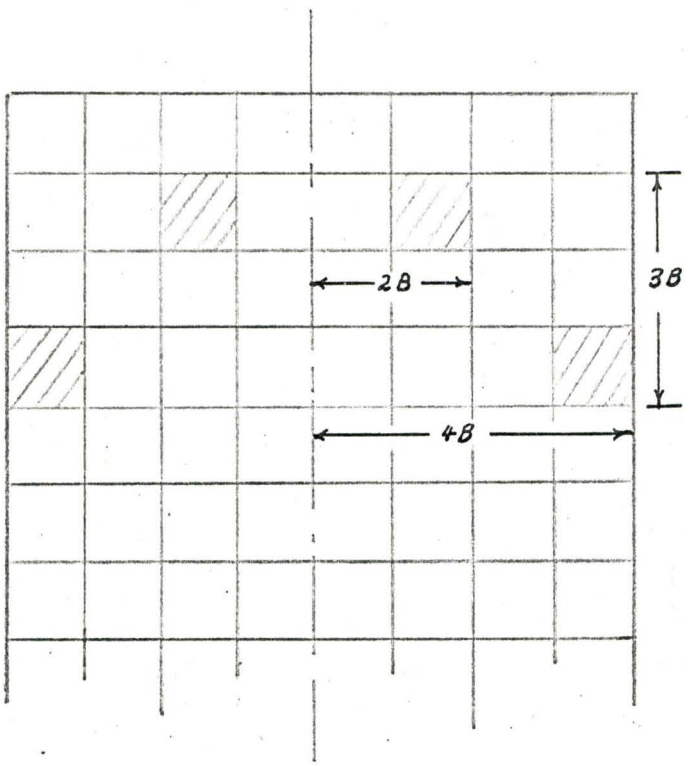

Interchange Area Illustration

Figure E.2-1

Erkku's tabulations were all regressed to third-order polynomials. (Since there are a total of 960 interchange areas, each having 4 coefficients,

they are not listed here. A listing of the coefficients, as well as a binary card-deck, is available in the Chemical Engineering Department of McMaster University.) In only 39 of the possible 960 interchange-area equations did the calculated values differ by more than 0.5% from the tabulated values. Of these 39, only 9 differed by 1 to 2%, the remainder differed by 0.5 to 1%.

(i) Characterstics of Direct-Interchange Areas

Since the net flux between two zones is equal to the difference in the two one-way flux terms, it follows that when the two zones are at the same temperature, the net flux must be zero and hence

$$\overline{g_1 s_2} = \overline{s_2 g_1}, \quad \overline{g_1 g_2} = \overline{g_2 g_1} \quad \text{etc.}$$

These reciprocal relationships are true only if the absorption coefficient is the same in the two one-way terms, regardless of temperature. This requirement is realized if the absorption coefficient is evaluated from the gas emissivity or absorptivity at some average gas and surface temperatures (Equation 5.2-2) rather than at the temperature of each zone. Evaluation of k and the direct-interchange area at the temperature of each zone is a more rigorous approach but the added calculational complexity is not warranted in most engineering applications.

The total of all the interchange "areas" representing flux from any one zone to each of the others in the enclosure, including itself, must be equal to the energy originating from that zone, per unit emissive power, i.e.,

$$\sum_i \overline{s_1 s_i} + \sum_i \overline{s_1 g_i} = A_{s_1} \qquad \text{(E.2-2)}$$

and similarly

$$\sum_i \overline{g_1 g_i} + \sum_i \overline{g_1 s_i} = 4 k V_{g_1} \qquad \text{(E.2-3)}$$

The direct-interchange areas apply only in a black enclosure, i.e., no radiation is reflected from the walls of the enclosure. If the walls are not black, reflection must be taken into account; this is done through total-interchange areas which are derived from direct-interchange areas as described in Section E.3

E.3 Total-Interchange Areas

Most surfaces of industrial importance are partial reflectors, i.e., non-black; they also approximate diffuse, rather than specular, reflectors for which incident radiation is reflected almost uniformly in all directions. The reflected radiation is distributed among all the gas and all the surfaces in the enclosure in accordance with the geometrical configuration of all the various surfaces and the absorbing power of the gas. The reflected radiation which in turn is incident on the surfaces of the enclosure is again partially absorbed and partially reflected and the process is repeated ad infinitum. Consequently a calculation of the total-interchange area applicable to any two zones will require a knowledge of all zones they can "see" either directly or by wall reflection.

As Hottel and Cohen[H7] indicate, the interchange area between any two zones in the enclosure cannot be a function of temperature as

long as the emissivity and absorptivity are not considered to be functions of temperature. Consequently the total-interchange terms can be evaluated at any convenient temperature. Hottel and Cohen show that the evaluation of the total-interchange areas can be simplified by assuming that all surface and gas zones in the enclosure except one are at a temperature of absolute zero; hence all such zones have an emissive power of zero. The one emitting zone can then be assigned a temperature such that it has a black emissive power ($E=\sigma T^4$) of one. As a result of this particular arbitrary temperature distribution there will be a radiant flux at and toward every surface in the system, and at and away from it as well, owing solely to original emission from the one zone and to the multiple reflections within the enclosure. The terminology[H7] to describe this outgoing flux density is R, with a presubscript designating the original source of the energy and a postsubscript designating the reflecting surface.

(i) Original Emitter is a Gas Zone

If, for example, gas zone g_i is the sole emitter, then the total radiant flux at and away from any surface, s_j, in the enclosure is designated as ${}_{g_i}R_{s_i}\,A_{s_j}$. Since this is the reflected flux, multiplication by the ratio of absorptivity (equal to emissivity) of the surface to the reflectivity of the surface ($\rho' = 1-\varepsilon$) yields the rate of energy absorption at the surface. Since the original emitter was assigned an emissive power of one, this rate of energy absorption must be, by definition, identical with the desired total-interchange area G_iS_j; or

$$\overline{G_iS_j} = \overline{S_jG_i} = {}_{g_i}R_{s_j}\,A_{s_j}\,\varepsilon_{s_j}/\rho'_{s_j} \qquad \text{(E.3-1)}$$

The problem of finding $\overline{G_i S_j}$ has thus been reduced to one of determining the reflected flux ${}_{g_i}R_{s_j}$. To do this one must solve the system of simultaneous equations which result from writing a radiant energy balance on each surface. The total rate of energy impingement on surface s_1 is equal to the contributions from all the surfaces in the system, including itself, plus the energy it receives from the single emitting gas zone. If the sum of all these terms is then multiplied by the surface reflectivity, the result, which is the reflected flux, must be equal to ${}_{g_i}R_{s_1} A_{s_1}$; or

$$(\overline{s_1 s_1}\ {}_{g_i}R_{s_1} + \overline{s_1 s_2}\ {}_{g_i}R_{s_2} + .. + \overline{g_i s_1})\ \rho'_{s_1} = {}_{g_i}R_{s_1} A_{s_1} \qquad \text{(E.3-2)}$$

This summation can be carried out for every surface in the enclosure, yielding a set of linear equations, one for each surface, which can be expressed in a more compact form as

$$\sum_j s_1 s_j\ {}_{g_i}R_{s_j} - A_{s_1}\ {}_{g_i}R_{s_1}/\rho'_{s_1} = -\overline{g_i s_1}$$

for surface 1, and

$$\sum_j s_2 s_j\ {}_{g_i}R_{s_j} - A_{s_2}\ {}_{g_i}R_{s_2}/\rho'_{s_2} = -\overline{g_i s_2} \qquad \text{(E.3-3)}$$

for surface 2, and so on.

This simultaneous set of linear algebraic equations, with the direct-interchange areas as coefficients, can be solved for the unknown reflected fluxes, R, with the aid of a high speed digital computer, utilizying standard matrix-inversion techniques. The appropriate total-interchange areas are then calculated from the relationship given previously (E.3-1).

If gas zone g_m is the original emitter, then the total reception at any other gas zone, g_n, is equal to the direct radiation from g_m to g_n, $\overline{g_m g_n}$, plus the sum of the products of the reflected flux at each surface in the enclosure multiplied by the fraction of that flux which reaches and is absorbed by gas zone g_n. Since the emissive power of zone g_m has been set equal to one, the sum represents the desired $\overline{G_m G_n}$; i.e.,

$$\overline{G_m G_n} = \overline{g_m g_n} + \sum_i g_m R_{s_i} \overline{s_i g_n} \qquad \text{(E.3-4)}$$

(ii) Original emitter is a Surface Zone

To obtain the total-interchange areas between surfaces ($\overline{SS}$), a surface zone is considered to be the sole emitter, with an emissive power of one. A radiant energy balance is again written for each surface, e.g.,

$$(\overline{s_1 s_1}\ (_{s_1}R_{s_1} + \varepsilon_{s_1}) + \overline{s_1 s_2}\ {}_{s_1}R_{s_2} + \ldots.)\rho'_{s_1}$$

$$= A_{s_1}\ {}_{s_1}R_{s_1}, \qquad \text{(E.3-5)}$$

and the resultant set of simultaneous algebraic equations is solved for the unknown R's

The total-interchange areas are then calculated from

$$\overline{S_i S_j} = A_{s_j}\ \varepsilon_{s_j}\ {}_{s_i}R_{s_j}/\rho'_{s_j} = \overline{S_j S_i} \qquad \text{(E.3-6)}$$

The total-interchange areas obey the following relationships (analagous to equations E.2-2 and E.2-3 for direct-interchange areas)

$$\sum_j \overline{S_j S_i} + \sum_i \overline{S_j G_i} = \varepsilon_{s_j} A_{s_j} \qquad \text{(E.3-7)}$$

$$\sum_j \overline{G_i G_j} + \sum_j \overline{G_i S_j} = 4 k V_{g_j} \qquad \text{(E.3-8)}$$

Equations E.2-2, E.2-3, E.3-7, and E.3-8 can be used to check that the interchange areas have been properly evaluated.

The preceding discussion applies to a gray gas with an absorption coefficient, k. For a real gas, the total-interchange area is the sum of the products of the total-interchange area and the appropriate weighting factor "a_i" of each gray gas component; e.g., for the one gray, one clear gas approximation

$$S_i S_j = a\, S_i S_j\big|_k + (1-a)\, S_i S_j\big|_{k=0},$$

$$G_i S_j = a\, G_i S_j\big|_k,$$

and

$$G_i G_j = a\, G_i G_j\big|_k \qquad \text{(E.3-9)}$$

The computer program listings for the calculation of the total-interchange areas, for the present cylindrical system, are given in Appendix Z.3.

APPENDIX F : FLASH PHOTOGRAPHY

The discovery that the immersion cell technique was not a suitable method for drop sampling at low velocities necessitated the development of another technique for the determination of drop-size distributions in sprays. The technique which appeared most amenable to this work was the in situ flash photographic technique which Ostrowski [O4] and earlier workers at the University of Michigan have employed for determining drop-size distributions in conventional sprays and flashing liquid jets.

A single-flash electronic circuit as shown in Figure F-1 was designed, built, and tested. The flash lamp (Ernest Turner Electrical Instruments Limited, England) was a quartz tube, high pressure Xenon lamp designed to yield a flash duration of 2 to 3 microseconds. The lamp was rated at 4 kilowatt seconds per flash.

The 0.1 μf, 15 k.v. capacitor (Dubilier, Nitrogol Non-Inductive) was charged by a 0-18 k.v. portable high voltage power supply (Universal Voltronics Corp.).

The physical lay-out of the components was arranged to permit installation of a second capacitor and timing circuit for double-flash photography. A double-flash technique is required to determine droplet velocities and hence permit the spatial distribution on the photographs to be converted to a temporal distribution.

Preliminary tests were made using a 100 mm. focal length lens and a 4 x 5 film holder (Graphlex) mounted 5 ft. from the lens. The droplet images were recorded on Kodak Ortho Process film.

SCHEMATIC OF FLASH CIRCUIT

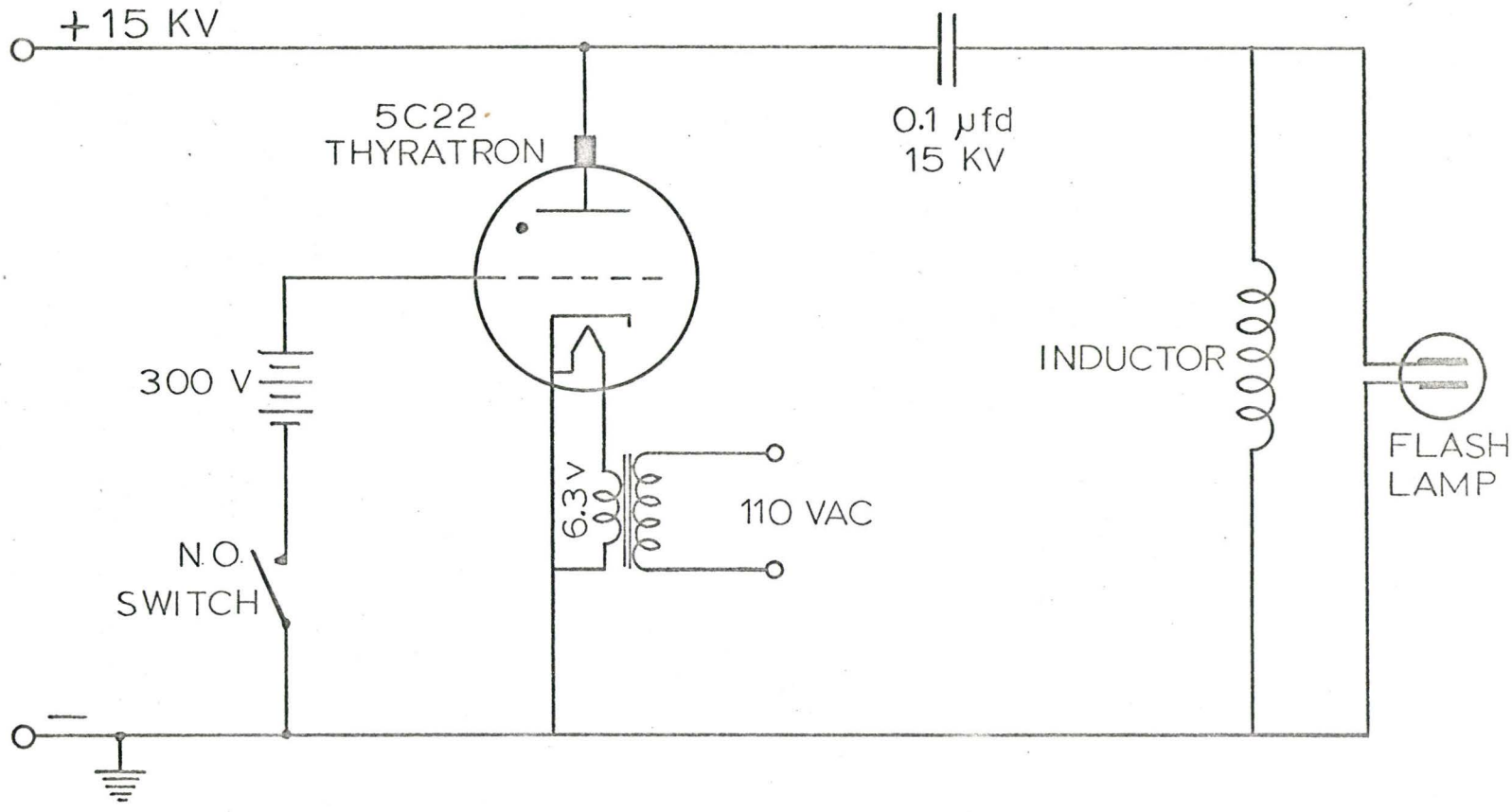

FIGURE F-1

APPENDIX G : EXPERIMENTAL DATA

Temperatures in ^{o}F. Flowrates in lb./hr.

VP1 corresponds to 0.5-in. from the start of the hot zone

VP2 corresponds to 3.0-in. from the start of the hot zone

VP4 corresponds to 9.0-in. from the start of the hot zone

Radial distances from the wall are given in thousandths of an inch up to a distance of 0.502-in. The radial distances from 0.502-in. to the centre line of the column (4-in.) are given in inches.

AIR 3c : Flowrate 241 lb./hr. Inlet Temperature 85°F
- Nominal Wall Temperature 145°F

	VP1	VP2	VP4
2	139	140	140
7	136	137	139
12	134	135	137
22	128	132	134
32	126	130	131
42	122	128	130
52	117	124	126
72	111	116	120
102	102	107	111
202	92	95	100
502	88	88	92
1	87	87	88
2	87	87	88
3	87	87	88
4	87	87	88

AIR 4c : Flowrate 503 lb./hr. Inlet Temperature 85°F
- Nominal Wall Temperature 300°F

2	303, 300	306, 310	307
7	294, 290	299	299
12	282	293, 287	295, 288
22	263, 256	268	274
32	235	233	259
42	215	240, 231	242
52	197	216	235
72	167	198	213
102	130	140	170
202	102	115	133
502	92	94	101
1	89	90	91
2	89	90	89
3	89	90	89
4	89	90	89

AIR 5c : Flowrate 238 lb./hr. Inlet Temperature 85°F
- Nominal Wall Temperature 300°F

	VP1	VP2	VP4
2	306	308	309, 307
7	296	306	303, 305
12	287, 294	296	301, 297
22	276	285	293, 289
32	261	277	279
42	255	268	267
52	241	259, 250	263
72	207	226	251
102	165	193	213, 210, 207
202	117	138	158
502	94	101	105
1	90	93	96
2	87	88	89
3	87	88	89
4	86	88	89

AIR 6c : Flowrate 504 lb./hr. Inlet Temperature 86°F
- Nominal Wall Temperature 600°F

2	590, 595	590, 585	596
7	563	569, 555	590, 584
12	524, 532	536, 530	560, 570
22	453, 461	482, 490	511, 522, 530
32	407	436	481
42	360	405	439
52	322	374, 366, 358	411
72	286, 278, 272	315	376, 390
102	235, 245	290, 286, 272	350, 344
202	147	176	227
502	100	108	130
1	89	90	99
2	88	88	94
3	88	88	92
4	88	88	92

AIR 7c : Flowrate 239 lb./hr. Inlet Temperatures 86°F
- Nominal Wall Temperature 600°F

	VP1	VP2	VP4
2	602, 600	597, 595	586, 590
7	578	565, 572	580, 572
12	546, 552	555	563
22	490, 496	509, 513	525, 531
32	465	472	501
42	436	443	476
52	402, 408	426	446
72	348	368	401, 410
102	301, 291	316, 320	348
202	174	218	247
502	124	143	172
1	103	110	140
2	98	99	113
3	98	99	102
4	98	99	99

AIR 8c : Flowrate 504 lb./hr. Inlet Temperature 85°F
- Nominal Wall Temperature 900°F

2	864, 869	878, 868	885, 879
7	820, 808	836, 828	848
12	766, 755	788, 780	823, 830
22	683	701, 712	772
32	577	632	703
42	514	564	632
52	421, 425	532	607
72	377	463	516
102	322, 312, 304	400, 412	443
202	159	229	291
502	112	128	172
1	99	102	112
2	95	96	102
3	95	96	98
4	95	96	98

AIR 9c : Flowrate 241 lb./hr. Inlet Temperature 88°F
- Nominal Wall Temperature 1450°F

	VP1	VP2	VP4
2	1327, 1338	1380, 1388	1357, 1366
7	1241, 1254	1348	1256, 1267, 1285
12	1195, 1182	1286, 1271	1133, 1150
222	1016	1167	1035, 1051
32	895	1054	941
42	771	1024	913
52	702	886	825
72	659	705	769
102	523, 541	611, 634	666, 689
202	311	402	541
502	174	221	320
1	131	151	181
2	102	104	116
3	102	102	111
4	102	104	106

STEAM 1c : Flowrate 364 lb./hr. Inlet Temperature 250°F - Nominal Wall Temperature 300°F

	VP1	VP2	VP4
2	298	295	298
7	291, 293	291	293
12	285, 287	290, 287	293
22	274	280	281, 283
32	264	273	277
42	254	268	273
52	251	264	270
72	243	256	260
102	232	242	253
202	236	238	245
502	243	243	242
1	247	246	245
2	250	250	248
3	251	252	249
4	251	252	249

STEAM 2c : Flowrate 184 lb./hr. Inlet Temperature 250°F - Nominal Wall Temperature 300°F

2	296	293	295, 297
7	292	289, 292	294
12	290, 288	288	293
22	281	283	287
32	272	278	282
42	263	272	280, 277
52	255, 259	267	274
72	243	257	265
102	233	246	256
202	232	235	248
502	236	237	239
1	239	238	240
2	245	244	241
3	245	244	243
4	245	244	243

STEAM 3c : Flowrate 364 lb./hr. Inlet Temperature 250°F - Nominal Wall Temperature 600°F

	VP1	VP2	VP4
2	578	588	580
7	543	556	565
12	530, 516	540, 531	537
22	445	479	516
32	382	433	463
42	364	407	447
52	332	380	422
72	280, 292	356, 340	394
102	255	301	337
202	245	261	298
502	248	246	260
1	249	248	254
2	252	251	256
3	252	253	256
4	252	253	256

STEAM 4c : Flowrate 184 lb./hr. Inlet Temperature 255°F - Nominal Wall Temperature 600°F

	VP1	VP2	VP4
2	585	595	589
7	573	568	574
12	538	560	568
22	492	527	535
32	459	505	501
42	426	476	472
52	379	451	477
72	352	416, 431	452
102	302	361	401
202	245	285	326
502	241	242	268
1	244	243	249
2	244	246	247
3	244	245	247
4	244	246	247

STEAM 5c : Flowrate 364 lb./hr. Inlet Temperature 247°F
- Nominal Wall Temperature 1400°F

	VP1	VP2	VP4
2	1327, 1345	1351, 1320	1360
7	1278	1309, 1285	1321
12	1265, 1251	1269	1325
22	1190, 1176	1219	1278
32	1060, 1079	1128	1231
42	983	1087	1159
52	896	1023, 995	1135
72	794	921	1029
102	605,633	780, 750, 731	964
202	403	502	701
502	276	300	442
1	263	287	321
2	263	276	299
3	263	276	295
4	263	276	292

STEAM 6c : Flowrate 184 lb./hr. Inlet Temperature 252°F
- Nominal Wall Temperature 1400°F

	VP2	VP4
2	1335	1348
7	1307	1325
12	1289	1300
22	1295, 1275	1307
32	1209	1241
42	1164	1237
52	1134, 1103	1188
72	1069	1104
102	968, 925	1039
202	775	868
502	551	659
1	362	436
2	306	340
3	293	305
4	290	296

Wall Temperature Distribution

Axial distances are given in inches.

The indicated temperatures were obtained by interpolation between the actual measured wall temperatures. The data were converted to this form for ease of computation in the theoretical model.

Axial distance	Air 3c	Air 4c & 5c	Air 6c & 7c
0	113	237	393
0.5	125	269	496
1.0	136	300	598
1.5	140	307	613
2.0	142	309	616
2.5	142	311	610
3.0	142	313	606
4.0	140	314	604
5.0	138	314	605
6.0	135	313	607
7.0	133	311	608
8.0	134	310	608
9.0	137	310	607
10.0	140	311	603
11.0	142	311	603
12.0	145	309	608
13.0	140	302	598

	Air 8c	Air 9c
0	575	871
0.5	735	1117
1.0	895	1363
1.5	906	1384
2.0	910	1396
2.5	909	1413
3.0	906	1430
4.0	902	1446
5.0	902	1456
6.0	903	1452
7.0	906	1440
8.0	906	1425
9.0	903	1432
10.0	903	1462
11.0	908	1494
12.0	909	1484
13.0	898	1380

Axial distance	Steam 1c & 2c	Steam 3c & 4c	Steam 5c & 6c
0	240	346	856
0.5	266	459	1112
1.0	292	575	1368
1.5	301	597	1376
2.0	304	605	1384
2.5	304	608	1389
3.0	301	607	1394
4.0	298	605	1398
5.0	298	602	1382
6.0	298	600	1350
7.0	298	598	1334
8.0	298	597	1348
9.0	298	597	1380
10.0	300	597	1406
11.0	303	599	1416
12.0	304	603	1408
13.0	296	591	1320

Velocity Measurements (Hot Wire Probe)

Symbols after the run identification number refer to the identification used in Figure 4.6-1.

Run 3 ○ $N_{Re} = 1.2 \times 10^4$

y^+	U^+
23	12.2
46	14.1
92	15.7
138	16.6
184	17.4
276	18.4
322	19.2
368	19.7
414	20.1
460	19.7

Run 4 □ $N_{Re} = 2.1 \times 10^4$

y^+	U^+
72	15.9
109	17.0
217	18.7
289	19.8
362	21.0
433	21.5
506	21.8
578	22.1
651	22.3
723	22.6

Run 5 ⬭ $N_{Re} = 2.1 \times 10^4$

y^+	U^+
37	13.0
147	17.8
220	19.5
293	20.6
440	21.6
586	22.2
880	22.2

Run 6 △ $N_{Re} = 2.1 \times 10^4$

y^+	U^+
37	14.4
110	16.6
220	18.8
293	20.4
367	20.9
440	21.4
587	22.2
735	22.2

Run 7 ▽ $N_{Re} = 1.6 \times 10^4$

y^+	U^+
58	15.2
87	16.3
144	18.0
202	19.0
231	19.6
347	20.7
462	21.3
577	21.3
694	20.1

Run 8 ◇ $N_{Re} = 1.6 \times 10^4$

y^+	U^+
29	13.3
58	15.2
116	17.4
173	18.6
231	19.3
347	20.6
462	21.3
577	21.3
694	21.0

APPENDIX Z COMPUTER PROGRAM LISTINGS

The operations performed in the programs listed here have been documented rather extensively by "comment cards" inserted throughout the program listings. Consequently, only a brief summary of the calculational procedure precedes each of the separate listings. The times indicated for each program are those required by an IBM 7040 computer.

Z.1 Solution of the Parabolic Form of the Energy Equation by Finite-Difference Techniques

This program was used to solve equations (D-12) and (D-16).

The program has a number of optional features which are controlled by information on the first 7 data cards read in at the time of execution.

The remaining data input is arranged as follows,

(1) wall temperature distribution

(2) coefficients for dimensionless velocity correlation

(3) coefficients for physical property correlations

(4) cylinder radius and selection of mesh size

(5) number of mesh points in the radial and axial directions

(6) identifier (alphameric)

(7) average inlet temperature, representative wall temperature, mass flowrate

(8) inlet gas-temperature distribution.

The calculation proceeds as follows,

(1) Calculate Reynolds and Prandtl numbers.

(2) Calculate friction factor, f (Subroutine FRFAC)

(3) Calculate dimensionless, radial mesh-point locations

(4) Calculate dimensionless velocity at each radial mesh point (if $y^+ < 26$, U is calculated from Subroutine UPLUS)

(5) Calculate dimensionless effective diffusivity at each radial mesh point

(6) Calculate wall temperature from initial input distribution (Subroutine INTERP)

(7) Calculate coefficients for finite-difference equation

(8) Load and invert tri-diagonal matrix (BNDSOL Library Routine) to obtain temperature profile at one axial location

(9) Calculate Nusselt number (Subroutine NUSS) and bulk temperature

(10) Move to next axial location and repeat steps 6, 7, 8, 9.

(11) Repeat step 10 until desired axial distance has been traversed.

Source Program - Compilation time	:	4 min. 14 sec.
Object Program - Load time	:	1 min. 3 sec.
Execution time per case	:	2 to 3 min. (depending on mesh size)

```
$IBFTC EN007
C
C      SOL'N OF ENERGY EQU'N BY FINITE DIFFERENCES
C      ******************************************
C
       COMMON ALPHA(15), BETA(15), BEE(15),
      1 PRTW(200),PRTB(200),PRNU1(200),PRNU2(200),PRNU3(200),PRNU4(200),
      2 PRNU5(200),PRNU6(200),PRGRAD(200),PRREW1(200),PRREW2(200),
      3 PRREB(200),PRREF(200),PRPRW(200),PRPRB(200),PRPRF(200),PRX(200),
      4 PRXD(200),PRTWTB(200)
       COMMON /ONE/ GRADW2,H,CEPT,SSLOPE
       DIMENSION  GAS(1), DUMR(60), R(60), Y(60), YPLUS(60), U(60),
      1  G(60), DIF(60), T(60,5),  X(60), A(60), B(60), C(60), D(60),
      2  TRI(3,60), RHS(60), XW(150), TW(150),  TT(60), GG(60),YTHOU(60)
       DATA CORYPL,CORU,CAPPA,EN / 26.0, 12.849, 0.36, 0.124 /
       DATA SECHR,CONVER,PI / 3600.0, 0.0672, 3.14159 /
       KPR = 0
       IPRINT = 0
       ENSQ = EN*EN
C
       READ(5,8) FTEMP
C      FTEMP CONTROLS THE TEMP. BETWEEN TIN AND TWALL AT WHICH THE
C      REYNOLDS NO. AND PRANDTL NO. ARE EVALUATED
C      IF FTEMP IS 0  TIN = TWALL
C      IF FTEMP IS 1  TIN = TIN
C
       READ(5,2) INUSS, NENT
C      IF INUSS IS 0  CORRELATE ON TBULK
C      IF INUSS IS 1 CORRELATE ON TT AT RADIAL LOCATION 'NENT'
C
C      IF ADIFUS LT 1  NORMAL EVALUATION OF G(I)
C      IF ADIFUS IS 1  ADD GFAC*G(I) TO G(I) IF Y+ LT YL2 (26)
C      IF ADIFUS IS 2  ADD GFAC*G(I) TO G(I) IF Y+ GT YL1 (5)
       READ(5,8) ADIFUS, YL1, YL2, GFAC
C
       READ(5,2) KIKOUT,KTEST
C
C      IF KTEST = 1 THEN KIKOUT WILL CONTROL THE PROGRAM TERMINATION
C      IF KTEST = 0 PROGRAM OPERATED UNDER NORMAL CONTROL PROCEDURE
C
C
C      ZERO OUT MATRICES
C
       DO 70 I=1,60
       DUMR(I) = 0.0
       R(I) = 0.0
       Y(I) = 0.0
       YPLUS(I) = 0.0
       YTHOU(I) = 0.0
       U(I) = 0.0
       G(I) = 0.0
       GG(I) = 0.0
       DIF(I) = 0.0
       X(I) = 0.0
       A(I) = 0.0
       B(I) = 0.0
       C(I) = 0.0
       D(I) = 0.0
```

```
      RHS(I) = 0.0
      TT(I) = 0.0
      DO 75 J=1,5
   75 T(I,J) = 0.0
   70 CONTINUE
      DO 80 I=1,15
      ALPHA(I) = 0.0
      BETA(I) = 0.0
      BEE(I) = 0.0
   80 CONTINUE
      DO 90 I=1,3
      DO 90 J=1,60
   90 TRI(I,J) = 0.0
C
C     READ PRINT CONTROL VARIABLES AND  WALL TEMP.
C
      READ(5,2) NPRCON,NDUMP
C     NPRCON = 0 NO PRINT UNTIL XINCH.GT.XLIM
C     NPRCON = 1 PRINT CONTROLLED ENTIRELY BY NPRIN1,NPRIN2,NPRIN3
C     NDUMP = 0 DON'T CALL PRINTO
C     NDUMP = 1 CALL PRINTO - DUMP NU COMPARISONS
      READ(5,6) XLIM
      READ(5,2) NPRIN3,NPRIN1,NPRIN2
      READ(5,2) KEN
C     KEN  NO. OF WALL TEMP. DATA POINTS
      READ(5,7) (XW(I),TW(I),I=1,KEN)
C
C     READ CONSTANTS FOR LOPF FIT OF U+ VS Y+
C
      READ(5,4) (ALPHA(I),I=2,14)
      READ(5,4) (BETA(I),I=2,14)
      READ(5,4) (BEE(I),I=2,14)
C     CONSTANTS FOR PROPERTY VALUE CORRELATIONS
C
      READ(5,3) VISCCT, VISCA, VISCB, VISCC, VISCD, VISCE
      READ(5,3) TCONCT, TCONA, TCONB, TCONC
      READ(5,3) CPCT, CPA, CPB, CPC, CPD
      READ(5,3) DENSCT, DENSA, DENSB, DENSC, DENSD
      VISC(Z) = VISCCT + Z*(VISCA + Z*(VISCB + Z*(VISCC + Z*(VISCD +
     1  Z*VISCE))))
      TCON(Z) = TCONCT + Z*(TCONA + Z*(TCONB + Z*TCONC))
      CP(Z) = CPCT + Z*(CPA + Z*(CPB + Z*(CPC + Z*CPD)))
      DENS(Z) = DENSCT + Z*(DENSA + Z*(DENSB + Z*(DENSC + Z*DENSD)))
C     READ IN GEOMETRY CONDITIONS
C
      READ(5,1) RADIUS, DRNOTI, H, DXI
      READ(5,2) N, M, MEXTRA, IGAS
C     IGAS = 0 AIR IS THE FLOWING MEDIUM
C     IGAS = 1 STEAM IS THE FLOWING MEDIUM
      READ(5,5) GAS(1)
C
C
C     INITIAL TEMP CONDITIONS AND MASS FLOWRATE   (T IN DEG.F.)
C
      READ(5,1) TINF, TWALLF, WFLOW
      TIN = TINF + 460.0
      TWALL = TWALLF + 460.0
C
```

```
C     CALCULATE INITIAL INLET PARAMETERS
C
      TNORM = TWALL - TIN
      AREA = PI*RADIUS*RADIUS/144.0
      GFLOW = WFLOW/AREA
      UAVE = GFLOW/(DENS(TIN)*SECHR)
C
      TIN = TWALL - (TWALL - TIN)*FTEMP
C
C     FTEMP CONTROLS THE TEMP. BETWEEN TIN AND TWALL AT WHICH THE
C     REYNOLDS NO. AND PRANDTL NO. ARE EVALUATED
C     IF FTEMP IS 0  TIN = TWALL
C     IF FTEMP IS 1  TIN = TIN
C
      TQ = TIN
      IF(IGAS.GE.1) TQ = TQ/1.8
      RE = (RADIUS/6.0)*GFLOW/(SECHR*VISC(TQ))
      IF(IGAS.GE.1) RE = RE/CONVER
      PR = CP(TIN)*VISC(TQ)*SECHR/TCON(TIN)
      IF(IGAS.GE.1) PR = PR*CONVER
      CALL FRFAC(RE,FFAC)
      ROOTF = SQRT(FFAC/2.0)
      RO = ROOTF*RE/2.0
      DRNOT = DRNOTI/RADIUS
      DX = DXI/RADIUS
C
C     CALC'N OF RADIAL MESH POINT LOCATIONS
C
      NMINUS = N - 1
      DO 10 II=1,NMINUS
      DUMR(II) = DRNOT*(H**II - 1.0)/(H - 1.0)
   10 SUM = SUM + DUMR(II)
C     NORMALIZING
      DO 20 II=1,NMINUS
      DUMR(II) = DUMR(II)/SUM
   20 SUMX = SUMX + DUMR(II)
C     RADIAL STEPS
      R(1) = 0.0
      Y(1) = 1.0
      YTHOU(1) = RADIUS*1000.0
      DO 30 I=2,N
      NX = N + 1 - I
      R(I) = R(I-1) + DUMR(NX)
      Y(I) = 1.0 - R(I)
      YTHOU(I) = Y(I)*RADIUS*1000.0
   30 CONTINUE
C
C     CALCULATE DIMENSIONLESS Y+(YPLUS) AND U+(U) AND DIFFUSIVITY(G)
C
      DO 35 I=1,N
      YPLUS(I) = Y(I)*ROOTF*RE/2.0
      IF(YPLUS(I).LE.CORYPL) CALL UPLUS(YPLUS(I),U(I))
      IF(YPLUS(I).GT.CORYPL) U(I) = ALOG(YPLUS(I)/CORYPL)/CAPPA + CORU
      IF(I.EQ.N) U(I) = 0.0
      IF(YPLUS(I).LE.CORYPL) G(I) = 1.0/PR + ENSQ*U(I)*YPLUS(I)*(1.0 -
     1 EXP(-ENSQ*U(I)*YPLUS(I)))
      IF(YPLUS(I).GE.CORYPL) GG(I) = 1.0/PR + CAPPA*YPLUS(I)*(1.0 -
     1 YPLUS(I)/RO) - 1.0
```

```
      IF(YPLUS(I).EQ.CORYPL) GO TO 1000
      IF(YPLUS(I).GT.CORYPL) G(I) = GG(I)
      IF(YPLUS(I).GT.CORYPL.AND.YPLUS(I).GT.(RO/2.0)) G(I) = G(I) + 1.0
      GO TO 36
 1000 G(I) = (G(I) + GG(I))/2.0
C
C     IF ADIFUS LT 1  NORMAL EVALUATION OF G(I)
C     IF ADIFUS IS 1  ADD GFAC*G(I) TO G(I) IF Y+ LT YL2 (26)
C     IF ADIFUS IS 2  ADD GFAC*G(I) TO G(I) IF Y+ GT YL1 (5)
C
   36 IF(ADIFUS.LT.0.5) GO TO 35
      IF(ADIFUS.GT.1.5) GO TO 37
      IF(YPLUS(I).GT.YL2) GO TO 35
      GO TO 38
   37 IF(YPLUS(I).LE.YL1) GO TO 35
   38 G(I) = G(I) + GFAC*G(I)
C
   35 CONTINUE
C
C     CALCULATE DIFFERENTIAL DIFFUSIVITY
C
      DO 45 I=2,NMINUS
      DIF(I) = (G(I+1) - G(I-1))/(R(I+1) - R(I-1))
   45 CONTINUE
      DX1 = DX
      DX2 = DX/(FLOAT(MEXTRA))
      MXTR = DX2/DRNOT + 0.01
      MARK = MEXTRA + MXTR
      KEV = MXTR
      MMAX = MXTR + MEXTRA
C
C     OUTPUT OF RUN CONDITIONS
C
      WRITE(6,999) GAS(1)
      TIN1 = TIN - 460.0
      WRITE(6,983) TIN1, INUSS, NENT, ADIFUS
      WRITE(6,998) TINF,TWALLF,WFLOW,GFLOW,UAVE,RE,PR,FFAC,RADIUS,RO
      WRITE(6,997) DRNOTI, DRNOT, DXI, DX, H
      WRITE(6,996) N,M,MXTR,MEXTRA
      WRITE(6,995) SUMX
      WRITE(6,994)
      WRITE(6,993) (I,R(I),Y(I),YPLUS(I),U(I),G(I),YTHOU(I),I=1,N)
C
C     READ INITIAL GAS TEMPERATURES
C
      M = M + MEXTRA + MXTR
      READ(5,6) (T(I,1),I=1,NMINUS)
      DO 41 I=1,NMINUS
   41 T(I,1) = (T(I,1) - TINF)/TNORM
C
C     CALCULATE AXIAL POS'NS AND COMMENCE MARCH IN AXIAL DIRECTION
C
      J = 1
      X(1) = 0.0
      XINCH = 0.0
      CALL INTERP(KEN,XW,TW,XINCH,T(N,1))
      T(N,J) = (T(N,J) - TINF)/TNORM
      DO 100 KGP =1,M
```

```
      DX = DX1
      IF(X(J).LT.DX1) DX = DX2
      IF(X(J).LT.DX2) DX = DRNOT
      X(J+1) = X(J) + DX
      XINCH = X(J+1)*RADIUS
      CALL INTERP(KEN,XW,TW,XINCH,T(N,J+1))
      T(N,J+1) = (T(N,J+1) - TINF)/TNORM
      IF(KGP.EQ.1) T(N,J)   = (T(N,J) + T(NMINUS,J))/2.0
      JJ = KGP + 1
C
C     CALCULATE COEFF. FOR I = 1
C
      DR1 = R(2) - R(1)
      DR2 = R(2) - R(1)
      DR3 = 2.0*DR2
      F2 = 2.0/(DR2*DR3)
      F3 = 2.0/(DR1*DR2)
      F4 = 2.0/(DR1*DR3)
      A(1) = -G(1)*F4
      B(1) = -RO*U(1)/DX + G(1)*F3
      C(1) = -G(1)*F2
      D(1) = RO*U(1)/DX + F3*G(1)
C
C     CALCULATE COEFF. FOR I GT 1
C
      DO 200 I=2,NMINUS
      DR1 = R(I) - R(I-1)
      DR2 = R(I+1) - R(I)
      DR3 = R(I+1) - R(I-1)
      F1 = 1.0/DR3
      F2 = 2.0/(DR2*DR3)
      F3 = 2.0/(DR1*DR2)
      F4 = 2.0/(DR1*DR3)
      ODD1 = F1*(G(I)/R(I) + DIF(I))/2.0
      ODD2 = G(I)*F4/2.0
      ODD3 = RO*U(I)/DX
      ODD4 = G(I)*F3/2.0
      ODD5 = G(I)*F2/2.0
      A(I) = ODD1 - ODD2
      B(I) = -ODD3 + ODD4
      C(I) = -ODD1 - ODD5
  200 D(I) = ODD3 + ODD4
C
C     SOL'N OF SIMULTANEOUS EQ'NS BY INVERSION OF TRIDIAGONAL MATRIX
C
      DO 300 I=2,NMINUS
      TRI(2,I-1) = 1.0
      IF(I.EQ.2) TRI(2,1) = TRI(2,1) - A(2)*(A(1) + C(1))/(D(1)*D(2))
      IF(I.EQ.2) GO TO 301
      TRI(1,I-1) = A(I)/D(I)
      IF(I.EQ.NMINUS) GO TO 302
  301 TRI(3,I-1) = C(I)/D(I)
  302 RHS(I-1) = -A(I)*T(I-1,J)/D(I) - B(I)*T(I,J)/D(I) - C(I)*
     1  T(I+1,J)/D(I)
      IF(I.EQ.2) RHS(1) = RHS(1) + B(1)*A(2)*T(1,J)/(D(1)*D(2)) +
     1  (A(1) + C(1))*A(2)*T(2,J)/(D(2)*D(1))
      IF(I.EQ.NMINUS) RHS(I-1) = RHS(I-1) - C(NMINUS)*T(NMINUS+1,J+1)/
     1  D(NMINUS)
```

```
  300 CONTINUE
      NN = NMINUS - 1
C
      CALL BNDSOL(TRI,RHS,3,1,NN)
C
      IND = 0
      DO 400 I=2,NMINUS
      T(I,J+1) = RHS(I-1)
      IF(T(I,J+1).GT.2.0.OR.T(I,J+1).LT.(-0.5)) IND = 1
  400 CONTINUE
      IF(IND.EQ.1) GO TO 3000
      T(1,J+1) = -B(1)*T(1,J)/D(1) - (A(1) + C(1))*T(2,J)/D(1) -
     1  (A(1) + C(1))*T(2,J+1)/D(1)
      IF(IPRINT.EQ.1) GO TO 4500
      IF(NPRCON.EQ.1) GO TO 8000
      IF(XINCH.LT.XLIM) GO TO 110
      IPRINT = 1
      GO TO 6000
 8000 IF(KGP.GT.MMAX) GO TO 4500
      IF(KGP.GT.MXTR) GO TO 6500
      IF(KGP.EQ.1) GO TO 5500
      LIM = KGP - IL
      IF(LIM.EQ.NPRIN3) GO TO 5500
      GO TO 110
 5500 IL = KGP
      GO TO 3500
 6500 LIM = KGP - KEV
      IF(LIM.EQ.NPRIN1) GO TO 7000
      GO TO 110
 7000 KEV = KGP
      GO TO 3500
 4500 LIM = KGP - MARK
      IF(LIM.EQ.NPRIN2) GO TO 6000
      GO TO 110
 6000 MARK = KGP
C
C     CALCULATE LOCAL NUSSELT NO. AND WALL GRADIENT AND BULK TEMP.
C     USE TRAPEZOIDAL RULE FOR BULK TEMP. CALC'N
C
 3500 KPR = KPR + 1
      TVR = 0.0
      VR = 0.0
      DO 155 I=1,NMINUS
      TVR = TVR + (R(I+1) - R(I))*(U(I+1)*T(I+1,J+1)*R(I+1) +
     1  U(I)*T(I,J+1)*R(I))/2.0
      VR = VR + (R(I+1) - R(I))*(U(I+1)*R(I+1) + U(I)*R(I))/2.0
  155 CONTINUE
      TBULK = TVR/VR
      TBULKF = TBULK*TNORM + TINF
      DO 55 I=1,N
   55 TT(I) = T(I,J+1)*TNORM + TINF
      GRADW1 = (T(N,J+1) - T(N-4,J+1))*TNORM* 3.0/(R(N) - R(N-4))
      SNUSS1 = (T(N,J+1) - T(N-4,J+1))/2.0 *RADIUS/((R(N) - R(N-4))*
     1  (T(N,J+1) - TBULK))
      CALL NUSS(YTHOU,TT,N)
      SNUSS2 = -GRADW2*RADIUS/((TT(N) - TBULKF)*6.0)
C
C     IF INUSS IS 0  CORRELATE ON TBULK
```

```
C     IF INUSS IS 1 CORRELATE ON TT AT RADIAL LOCATION 'NENT'
C
      IF(INUSS.EQ.0) GO TO 3001
      SNUSS2 = SNUSS2*(TT(N) - TBULKF)/(TT(N) - TT(NENT))
 3001 CONTINUE
C
      XX = X(J+1)/2.0
      WRITE(6,992) JJ,XX,XINCH,SNUSS1,GRADW1,SNUSS2,GRADW2
 3000 WRITE(6,991)
      WRITE(6,990) (T(I,J+1),I=1,N)
      WRITE(6,988) SSLOPE,CEPT,TBULKF,TBULK
      WRITE(6,987) (TT(I),I=1,N)
      WRITE(6,985)
      WRITE(7,984) JJ,XX,XINCH,SNUSS2,GRADW2,TBULKF,TT(N),GAS(1)
      IF(IND.EQ.1) GO TO 4000
C     ALL VARIABLES BEGINNING WITH 'PR' ARE PRINTED OUT AT END OF CALC'N
      PRTB(KPR) = TBULKF
      PRTW(KPR) = TT(N)
      PRX(KPR) = XINCH
      PRXD(KPR) = XX
      PRNU1(KPR) = SNUSS2
      PRGRAD(KPR) = GRADW2
      RCONST = (RADIUS/6.0)*GFLOW/SECHR
      WALLT = TT(N) + 460.0
      BULKT = TBULKF + 460.0
      FILMT = (WALLT + BULKT)/2.0
      T1 = WALLT
      T2 = BULKT
      T3 = FILMT
      IF(IGAS.LT.1) GO TO 8500
      T1 = T1/1.8
      T2 = T2/1.8
      T3 = T3/1.8
 8500 PRREW1(KPR) = RCONST/VISC(T1)
      PRREW2(KPR) = PRREW1(KPR)*BULKT/WALLT
      PRREB(KPR) = RCONST/VISC(T2)
      PRREF(KPR) = RCONST/VISC(T3)
      PRPRW(KPR) = CP(WALLT)*VISC(T1)*SECHR/TCON(WALLT)
      PRPRB(KPR) = CP(BULKT)*VISC(T2)*SECHR/TCON(BULKT)
      PRPRF(KPR) = CP(FILMT)*VISC(T3)*SECHR/TCON(FILMT)
      IF(IGAS.LT.1) GO TO 9000
      PRREW1(KPR) = PRREW1(KPR)/CONVER
      PRREW2(KPR) = PRREW2(KPR)/CONVER
      PRREB (KPR) = PRREB (KPR)/CONVER
      PRREF (KPR) = PRREF (KPR)/CONVER
      PRPRW(KPR) = PRPRW(KPR)*CONVER
      PRPRB(KPR) = PRPRB(KPR)*CONVER
      PRPRF(KPR) = PRPRF(KPR)*CONVER
 9000 PRTWTB(KPR) = WALLT/BULKT
  110 DO 85 I=1,N
   85 T(I,J) = T(I,J+1)
      IF(KTEST.EQ.0) GO TO 100
      IF(KGP.GE.KIKOUT) GO TO 5000
  100 X(J) = X(J+1)
      GO TO 5000
 4000 WRITE(6,989)
 5000 IF(NDUMP.EQ.1) CALL PRINTO(KPR)
      WRITE(6,986)
```

```
      Q1 = 1.0
      Q2 = 2.0
      STOP
    1 FORMAT(6E12.5)
    2 FORMAT(16I5)
    3 FORMAT(6E13.6)
    4 FORMAT(1X,5E15.7)
    5 FORMAT(10A6)
    6 FORMAT(13F6.1)
    7 FORMAT(2F10.5)
    8 FORMAT(8F10.1)
  983 FORMAT(10X,23HPROPERTIES EVUALATED AT, F7.1, 7H DEG.F.,5X,
     1 8HINUSS = , I2,5X,7HNENT = , I3,5X,8HADIFUS =, F5.1/10X,37(1H-)/)
  984 FORMAT(1X,I5,2F9.3,F10.2,F10.1,F10.2,F10.1,9X,A6)
  985 FORMAT(3X,125(1H-))
  986 FORMAT(////)
  987 FORMAT(10X,10F11.4)
  988 FORMAT(1H0,4X,4HSDEV, E12.4,4X, 11HTWALL(CALC), F9.2,5X,
     1 22HTEMPERATURES IN DEG.F., 10X,16HBULK TEMPERATURE, F10.2,2X,
     2 1H(,F10.7,2H )/25X,5(1H-), 20X,22(1H-),10X,16(1H-)/)
  989 FORMAT(1H0///10X,89HSOLUTION TERMINATED BECAUSE ONE OR MORE TEMPER
     1ATURES ARE LESS THAN -0.5 OR GREATER THAN 2/10X,89(1H*)/)
  990 FORMAT(10X,10F11.7)
  991 FORMAT(50X,26HDIMENSIONLESS TEMPERATURES/50X,25(1H-)/)
  992 FORMAT(1H0/5X,11HAXIAL POS'N,I5, 5X,3HX/D,F9.4, 5X,8HX (INCH),
     1  F9.4, 5X,11HNUSSELT NO.,F9.2, 5X,25HWALL GRADIENT (DEG.F./FT),
     2 F9.1/76X,F9.2,30X,F9.1/)
  993 FORMAT(I11,F12.8,F13.7,3E14.4,F15.2)
  994 FORMAT(10X,1HI,7X,1HR,13X, 1HY,11X,2HY+,12X, 2HU+,10X,6HDIFFUS,
     1  9X,12HY(INCH*E-03)//)
  995 FORMAT(11X,43HSUMX = TOTAL OF NORMALIZED RADIAL DIVISIONS,F9.4//)
  996 FORMAT(11X,17HNO. RADIAL POS'NS,I5, 9X,16HNO. AXIAL POS'NS,I5,
     2 10X,23HEXTRA INITIAL DIVISIONS,I5/96X,I5/)
  997 FORMAT(6X,13HDRNOTI (INCH),E11.4, 5X,5HDRNOT,E12.4, 5X,
     2  10HDXI (INCH),F9.4, 7X,2HDX,E11.4, 10X,1HH,F11.3//)
  998 FORMAT(10X,10HINLET TEMP,F7.1, 5X,9HWALL TEMP,F8.1, 5X,
     1  12HFLOW (LB/HR),F7.1, 5X,9HMASS VEL.,F10.2,5X,13HVEL. (FT/SEC),
     2  F8.2//16X,2HRE,F10.1, 11X,2HPR,F8.2, 5X,12HFAN FRIC FAC,F9.5,
     3  4X,6HRADIUS,F7.1, 13X,2HRO,F18.6//)
  999 FORMAT(1H0/50X,20(1H=)//57X,A6//50X,20(1H=)///)
      END
```

```
$IBFTC FRFAC
      SUBROUTINE FRFAC(RE,FFAC)
C
C     EVALUATE ADIABATIC K-N FRICTION FACTOR
C
      DATA EPS, FTRY / 0.00003, 0.007 /
      FLHS = 1.0/SQRT(FTRY)
 2000 FRHS = 4.0*ALOG10(RE/FLHS) - 0.40
      IF(ABS((FRHS - FLHS)/FRHS).LT.EPS) GO TO 1000
      FLHS = FRHS
      GO TO 2000
 1000 FFAC = 1.0/(FRHS*FRHS)
      RETURN
      END



$IBFTC UPLUS
      SUBROUTINE UPLUS(Y,U)
C
C     CALCULATE U+ FOR A GIVEN VALUE OF Y+
C
      COMMON  ALPHA(15), BETA(15), BEE(15)
      DIMENSION P(20)
      IF(Y.LE.0.80) GO TO 101
      P(1) = 0.0
      P(2) = 1.0
      DO 100 KK=2,14
      P(KK+1) = (Y - ALPHA(KK+1))*P(KK) - BETA(KK)*P(KK-1)
  100 U = U + BEE(KK)*P(KK)
      GO TO 102
  101 U = Y
  102 RETURN
      END
```

```
$IBFTC INTRP
      SUBROUTINE INTERP(JK,X,Y,XA,YA)
      DIMENSION X(150),Y(150)
      IF(XA.GE.X(JK)) GO TO 811
      YA=0.0
      IF((X(1)-X(2)).GT.0.0) GO TO 804
      DO 805 II=1,JK
      IF((XA-X(II)).LE.0.0) GO TO 806
  805 CONTINUE
  804 DO 809 II=1,JK
      IF((X(II)-XA).LE.0.0) GO TO 806
  809 CONTINUE
  806 IF(II.LE.3) GO TO 807
      IF(II.GE.(JK-2)) GO TO 808
      MM=II-3
      MMM=II+2
      GO TO 810
  807 MM=1
      MMM=6
      GO TO 810
  808 MM=JK-5
      MMM=JK
  810 DO 801 I=MM,MMM
      PROD=Y(I)
      DO 800 J=MM,MMM
      IF(J.EQ.I) GO TO 800
      PROD=PROD*(XA-X(J))/(X(I)-X(J))
  800 CONTINUE
  801 YA=YA+PROD
      GO TO 812
  811 YA = Y(JK)
  812 RETURN
      END
```

```
$IBFTC NUSSLT
      SUBROUTINE NUSS(XX,YY,NN)
C
C     THIS ROUTINE EVALUATES THE TEMPERATURE GRADIENT AT THE WALL BY
C     PERFORMING A LINEAR LEAST SQUARES FIT OVER THE MESH POINTS WHICH
C     ARE ADJACENT TO THE WALL.......THE NUMBER OF POINTS TAKEN DEPENDS
C     UPON THE NO. OF RADIAL MESH POINTS USED .
C
      COMMON /ONE/ GRADW2,H,CEPT,SSLOPE
      DIMENSION XX(60), YY(60), Y(35), X(35)
      DATA THOU,FT/ 1000.0, 12.0/
      IF(NN.EQ.20) N = 11
      AN = NN
      IF(AN.EQ.20.0.AND.H.LE.1.6) N = 8
      IF(NN.EQ.25) N = 10
      IF(NN.EQ.40) N = 13
      IF(NN.EQ.60) N = 30
      DO 50 I=1,N
      L = NN + 1 -I
      Y(I) = YY(L)
   50 X(I) = XX(L)/THOU
      SUMX = 0.0
      SUMY = 0.0
      SUMX2 = 0.0
      SUMY2 = 0.0
      SUMXY = 0.0
      DO 100 I=1,N
      SUMX = SUMX + X(I)
      SUMY = SUMY + Y(I)
      SUMX2 = SUMX2 + X(I)*X(I)
      SUMY2 = SUMY2 + Y(I)*Y(I)
  100 SUMXY = SUMXY + X(I)*Y(I)
      DATA = N
      XP2 = SUMX2 - SUMX*SUMX/DATA
      YP2 = SUMY2 - SUMY*SUMY/DATA
      XYP = SUMXY - SUMX*SUMY/DATA
      XAV = SUMX/DATA
      YAV = SUMY/DATA
      SLOPE = XYP/XP2
      CEPT = YAV - SLOPE*XAV
      R2 = XYP*XYP/(XP2*YP2)
      VARY = (1.0 - R2)*YP2/(DATA - 2.0)
      SSLOPE = SQRT(VARY/XP2)
      GRADW2 = SLOPE*FT
      RETURN
      END
```

```
$IBFTC PRIN
      SUBROUTINE PRINTO(KPR)
C
C     CALCULATES NUSSELT NO. AND PRINTS OUT FOR COMPARISON
C
      COMMON ALPHA(15), BETA(15), BEE(15),
     1 PRTW(200),PRTB(200),PRNU1(200),PRNU2(200),PRNU3(200),PRNU4(200),
     2 PRNU5(200),PRNU6(200),PRGRAD(200),PRREW1(200),PRREW2(200),
     3 PRREB(200),PRREF(200),PRPRW(200),PRPRB(200),PRPRF(200),PRX(200),
     4 PRXD(200),PRTWTB(200)
      DATA C1,C2,C3,C4,HUN / .024,.023,0.7,.0205,100.0 /
      WRITE(6,981)
      WRITE(6,980) (I,I=1,12)
      WRITE(6,983) (I,I=1,12)
      DO 400 I=1,KPR
  400 WRITE(6,982) I,PRXD(I),PRX(I), PRTW(I),PRTB(I),PRGRAD(I),
     1 PRREW1(I),PRREW2(I),PRREB(I),PRREF(I), PRPRW(I),PRPRB(I),
     2 PRPRF(I),I
      WRITE(6,981)
      WRITE(6,978) (I,I=1,7)
      WRITE(6,977) (I,I=1,7)
      DO 455 I=1,KPR
      PRNU2(I) = C2*(PRREW1(I)**0.8)*(PRPRW(I)**0.4)*(1.0 +
     1 (1.0/PRXD(I))**C3*PRTWTB(I)**C3)
      PRNU3(I) = PRNU2(I)/PRTWTB(I)
      PRNU4(I) = C1*(PRREB(I)**0.8)*(PRPRB(I)**0.4)*((1.0/PRTWTB(I))
     1 **C3)*(1.0 + (1.0/PRXD(I))**C3*PRTWTB(I)**C3)
      PRNU5(I) = C4*(PRREF(I)**0.8)*(PRPRF(I)**0.4)*(1.0 +
     1 (1.0/PRXD(I))**C3*PRTWTB(I)**C3)
      PRNU6(I) = PRNU5(I)*PRTB(I)/((PRTB(I) + PRTW(I))/2.0)
      DIF2 = (PRNU2(I) - PRNU1(I))/PRNU1(I)*HUN
      DIF3 = (PRNU3(I) - PRNU1(I))/PRNU1(I)*HUN
      DIF4 = (PRNU4(I) - PRNU1(I))/PRNU1(I)*HUN
      DIF5 = (PRNU5(I) - PRNU1(I))/PRNU1(I)*HUN
      DIF6 = (PRNU6(I) - PRNU1(I))/PRNU1(I)*HUN
  455 WRITE(6,979) I,PRXD(I),PRNU1(I), PRNU2(I),DIF2, PRNU3(I),DIF3,
     1 PRNU4(I),DIF4, PRNU5(I),DIF5, PRNU6(I),DIF6
      RETURN
  977 FORMAT(1H0,21X,I2,I8,I13,4I17/)
  978 FORMAT(25X,I3,43H...X/D  (COL. 3-7 ARE NU AND PERCENT DIFF.)/25X,
     1 I3,36H...CALC'D NU FROM FINITE DIFF. SOL'N/25X,I3,50H...NU BASED
     2ON P+W EQU'N 11 (NO TEMP. RATIO ON RE)/25X,I3,27H...NU BASED ON P+
     3W EQU'N 11/ 25X,I3,27H...NU BASED ON P+W EQU'N 10 /25X,I3,51H...NU
     5 BASED ON DML EQU'N 16 WITH ENTRANCE PARAMETER /25X,I3,44H...NU AS
     6IN (6) EXCEPT HAS TEMP. RATIO ON RE /)
  979 FORMAT(15X,I4,F7.2,F7.1,5(F10.1,F7.1))
  980 FORMAT(25X,I3,22H...X/D   DIMENSIONLESS /25X,I3,30H...X  AXIAL DIS
     1TANCE IN INCHES /25X,I3,23H...WALL TEMP. IN DEG.F. /25X,I3,23H...B
     2ULK TEMP. IN DEG.F. /25X,I3,24H...GRADIENT - DEG.F./FT. /25X,I3,
     3 20H...WALL REYNOLDS NO. /25X,I3,29H...MODIFIED WALL REYNOLDS NO.
     4 /25X,I3,20H...BULK REYNOLDS NO. /25X,I3,20H...FILM REYNOLDS NO.
     5 /25X,I3,19H...PR AT WALL TEMP. /25X,I3,19H...PR AT BULK TEMP. /25
     6X,I3,19H...PR AT FILM TEMP. /)
  981 FORMAT(1H1)
  982 FORMAT(15X,I4,2F7.2,2F7.1,F10.1,4F9.1,3F6.2,I5)
  983 FORMAT(1H0,21X,I2,I7,I8,I7,I10,4I9,I5,2I6/)
      END
```

Z.2 Solution of the Elliptic Form of the Energy Equation by Finite-Difference Techniques.

The program was used to solve equations (D-25) and (D-27).

The program has two optional features which are controlled by information on the first data card.

The remaining data input is arranged as follows

(1) wall temperature distribution

(2) coefficients for dimensionless velocity correlation

(3) coefficients for physical property correlations

(4) cylinder radius and selection of mesh size

(5) number of mesh points in radial and axial directions

(6) identifier (alphameric)

(7) average inlet and wall temperatures, mass flowrate

(8) radial gas-temperature distributions at the beginning and end of the region of interest.

The calculation proceeds as follows

(1) Calculate Reynolds and Prandtl numbers

(2) Calculate friction factor, f, (Subroutine FRFAC)

(3) Calculate dimensionless, radial mesh-point locations

(4) Calculate dimensionless velocity at each radial mesh point (if $y^+ < 26$, U is calculated from Subroutine UPLUS)

(5) Calculate dimensionless effective diffusivity at each radial mesh point.

(6) Calculate dimensionless axial mesh-point locations.

(7) Calculate wall temperatures at each axial location (Subroutine INTERP)

(8) Calculate coefficients for finite-difference equation.

(9) Load and invert banded matrix (BNDSOL Library Routine) to obtain temperature distribution over entire region of interest.

Source Program - Compilation time	:	3 min. 16 sec.
Object Program - Load time	:	57 sec.
Execution time per case	:	34 sec.

```
$IBFTC EN21
C
C      SOLUTION OF ENERGY EQU'N IN ELLIPTIC FORM USING CENTRAL
C      DIFFERENCES IN BOTH DIRECTIONS
C      ****************************************
C
       COMMON ALPHA(15), BETA(15), BEE(15)
C
C      A TO E MATRICES ALLOW A MAX'M OF 40 RADIAL POINTS
C      T MATRIX MUST BE CHANGED AS NO. OF MESH POINTS CHANGE
C      T MATRIX IS DIMENSIONED FOR TOTAL NO. OF MESH POINTS
C      ABC MATRIX CHANGES AS NO. OF MESH POINTS CHANGE
C      IN ABC THE FIRST NO. IS NO. OF COLUMNS = 2*(NO. OF AXIAL POSITIONS
C       - 3
C      SECOND NO. IS THE PRODUCT OF (NO. OF RADIAL POS'NS - 1)*
C      (NO. OF AXIAL POS'NS - 2)
C      RHS MATRIX IS ALSO DIMENSIONED FOR THIS PRODUCT
C      THIS PRODUCT REPRESENTS THE TOTAL NO. OF UNKNOWN TEMPS.
C      X AND XINCH MATRICES CHANGE DIMENSIONS AS NO. OF AXIAL POS'NS
C      CHANGE
C      N = NO. OF RADIAL NODES INCLUDING WALL AND CENTRE LINE
C      M = NO. OF AXIAL NODES INCLUDING BOTH BOUNDARIES
C      NOTE - IN THIS PROGRAM M IS NOT CHANGED FROM IT'S INITIAL READ IN
C             VALUE AS IT IS IN THE PARABOLIC SOL'N  (EN15 OR EN16)
C             I.E.  NO. OF AXIAL NODES IS FIXED EVEN THO' THE SIZE OF
C             THE MESH MAY CHANGE CLOSE TO THE ENTRANCE
C
       DIMENSION GAS(1), DUMR(30), R(30), Y(30), YPLUS(30),
      1 U(30), G(30), DIF(30), A(30), B(30), C(30), D(30), E(30),
      2 XW(50 ), TW(50 ), TT(30), GG(30), YTHOU(30),
      3X(20), XINCH(20),T(25,20), ABC(37,432), RHS(432)
       DATA CORYPL,CORU,CAPPA,EN / 26.0, 12.849, 0.36, 0.124 /
       DATA SECHR,CONVER,PI / 3600.0, 0.0672, 3.14159 /
       ENSQ = EN*EN
C
C      CORYPL, CORY, CAPPA, EN ARE CONSTANTS USED IN DIMENSIONLESS
C      VELOCITY CORRELATION
C
       READ(5,2) KPRIN,INZ
C
C      INZ = 0  STANDARD CALC'N
C      INZ = 1 CALC'N STARTS PART WAY THRU THE COLUMN AT XW(1)
C      KPRIN CONTROLS INTERMEDIATE PRINT OUT OF ABC AND RHS MATRICES
C      ...0...NO PRINT OUT
C      ...1...PRINT OUT ABC AND RHS JUST BEFORE INVERSION
C      ...2...PRINT OUT RAW COEFFICIENTS A,B,C,D,E AS WELL AS ABOVE CASE
C
C      READ WALL TEMPERATURES
C
       READ(5,2) KEN
C
C      KEN  NO. OF WALL TEMP. DATA POINTS
C
       READ(5,7) (XW(I),TW(I),I=1,KEN)
C
C      READ CONSTANTS FOR LOPF FIT OF U+ VS Y+
C
       DO 80 I=1,15
       ALPHA(I) = 0.0
```

```
      BETA(I) = 0.0
      BEE(I) = 0.0
   80 CONTINUE
      READ(5,4) (ALPHA(I),I=2,14)
      READ(5,4) (BETA(I),I=2,14)
      READ(5,4) (BEE(I),I=2,14)
C     CONSTANTS FOR PROPERTY VALUE CORRELATIONS
C
      READ(5,3) VISCCT, VISCA, VISCB, VISCC, VISCD, VISCE
      READ(5,3) TCONCT, TCONA, TCONB, TCONC
      READ(5,3) CPCT, CPA, CPB, CPC, CPD
      READ(5,3) DENSCT, DENSA, DENSB, DENSC, DENSD
      VISC(Z) = VISCCT + Z*(VISCA + Z*(VISCB + Z*(VISCC + Z*(VISCD +
     1  Z*VISCE))))
      TCON(Z) = TCONCT + Z*(TCONA + Z*(TCONB + Z*TCONC))
      CP(Z) = CPCT + Z*(CPA + Z*(CPB + Z*(CPC + Z*CPD)))
      DENS(Z) = DENSCT + Z*(DENSA + Z*(DENSB + Z*(DENSC + Z*DENSD)))
C
C     READ IN GEOMETRY CONDITIONS
C
      READ(5,1) RADIUS, DRNOTI, H, DXI
      READ(5,2) N, M, MEXTRA, IGAS
C
C     IGAS = 0 AIR IS THE FLOWING MEDIUM
C     IGAS = 1 STEAM IS THE FLOWING MEDIUM
C
      READ(5,5) GAS(1)
C
C     INITIAL TEMP CONDITIONS AND MASS FLOWRATE   (T IN DEG.F.)
C
      READ(5,1) TINF, TWALLF, WFLOW
      TIN = TINF + 460.0
      TWALL = TWALLF + 460.0
C
C     VARIABLES TO CONTROL COLUMN SELECTION IN ABC MATRIX
C
      IUN = N - 1
      JUN = M - 2
      KOL1 = 1
      KOL2 = JUN
      KOL3 = M - 1
      KOL4 = M
      KOL5 = 2*M - 3
      LAST = IUN*JUN
      LBF = LAST - JUN
C
C     ZERO OUT MATRICES
C
      DO 70 I =1,30
      DUMR(I) = 0.0
      R(I) = 0.0
      Y(I) = 0.0
      YPLUS(I) = 0.0
      YTHOU(I) = 0.0
      U(I) = 0.0
      G(I) = 0.0
      GG(I) = 0.0
      DIF(I) = 0.0
```

```
      A(I) = 0.0
      B(I) = 0.0
      C(I) = 0.0
      D(I) = 0.0
      E(I) = 0.0
      TT(I) = 0.0
   70 CONTINUE
      DO 75 I=1,N
      DO 75 J = 1,M
   75 T(I,J) = 0.0
      DO 85 J=1,LAST
      RHS(J) = 0.0
      DO 85 I=1,KOL5
   85 ABC(I,J) = 0.0
C
C     CALCULATE INITIAL INLET PARAMETERS
C
      TNORM = TWALL - TIN
      AREA = PI*RADIUS*RADIUS/144.0
      GFLOW = WFLOW/AREA
      UAVE = GFLOW/(DENS(TIN)*SECHR)
      TQ = TIN
      IF(IGAS.GE.1) TQ = TQ/1.8
      RE = (RADIUS/6.0)*GFLOW/(SECHR*VISC(TQ))
      IF(IGAS.GE.1) RE = RE/CONVER
      PR = CP(TIN)*VISC(TQ)*SECHR/TCON(TIN)
      IF(IGAS.GE.1) PR = PR*CONVER
      CALL FRFAC(RE,FFAC)
      ROOTF = SQRT(FFAC/2.0)
      RO = ROOTF*RE/2.0
      DRNOT = DRNOTI/RADIUS
      DX = DXI/RADIUS
      DX1 = DX
      DX2 = DX/(FLOAT(MEXTRA))
      MXTR = DX2/DRNOT + 0.01
C
C     CALC'N OF RADIAL MESH POINT LOCATIONS
C
      NMINUS = N - 1
      DO 10 II=1,NMINUS
      DUMR(II) = DRNOT*(H**II - 1.0)/(H - 1.0)
   10 SUM = SUM + DUMR(II)
C     NORMALIZING
      DO 20 II=1,NMINUS
      DUMR(II) = DUMR(II)/SUM
   20 SUMX = SUMX + DUMR(II)
C
C     RADIAL STEPS
C
      R(1) = 0.0
      Y(1) = 1.0
      YTHOU(1) = RADIUS*1000.0
      DO 30 I=2,N
      NX = N + 1 - I
      R(I) = R(I-1) + DUMR(NX)
      Y(I) = 1.0 - R(I)
      YTHOU(I) = Y(I)*RADIUS*1000.0
   30 CONTINUE
```

```
C
C     CALCULATE DIMENSIONLESS Y+(YPLUS) AND U+(U) AND DIFFUSIVITY(G)
C
      DO 35 I=1,N
      YPLUS(I) = Y(I)*ROOTF*RE/2.0
      IF(YPLUS(I).LE.CORYPL) CALL UPLUS(YPLUS(I),U(I))
      IF(YPLUS(I).GT.CORYPL) U(I) = ALOG(YPLUS(I)/CORYPL)/CAPPA + CORU
      IF(I.EQ.N) U(I) = 0.0
      IF(YPLUS(I).LE.CORYPL) G(I) = 1.0/PR + ENSQ*U(I)*YPLUS(I)*(1.0 -
     1 EXP(-ENSQ*U(I)*YPLUS(I)))
      IF(YPLUS(I).GE.CORYPL) GG(I) = 1.0/PR + CAPPA*YPLUS(I)*(1.0 -
     1 YPLUS(I)/RO) - 1.0
      IF(YPLUS(I).EQ.CORYPL) GO TO 1000
      IF(YPLUS(I).GT.CORYPL) G(I) = GG(I)
      IF(YPLUS(I).GT.CORYPL.AND.YPLUS(I).GT.(RO/2.0)) G(I) = G(I) + 1.0
      GO TO 35
 1000 G(I) = (G(I) + GG(I))/2.0
   35 CONTINUE
C
C     CALCULATE DIFFERENTIAL DIFFUSIVITY
C
      DO 45 I=2,NMINUS
      DIF(I) = (G(I+1) - G(I-1))/(R(I+1) - R(I-1))
   45 CONTINUE
C
C     OUTPUT OF RUN CONDITIONS
C
      WRITE(6,999) GAS(1)
      WRITE(6,998) TINF,TWALLF,WFLOW,GFLOW,UAVE,RE,PR,FFAC,RADIUS,RO
      WRITE(6,997) DRNOTI, DRNOT, DXI, DX, H
      WRITE(6,996) N,M,MXTR,MEXTRA
      WRITE(6,995) SUMX
      WRITE(6,994)
      WRITE(6,993) (I,R(I),Y(I),YPLUS(I),U(I),G(I),YTHOU(I),I=1,N)
C
C     READ INITIAL AND FINAL KNOWN GAS TEMPERATURES
C
      READ(5,8) (T(I,1),I=1,NMINUS)
      READ(5,8) (T(I,M),I=1,NMINUS)
      DO 41 I=1,NMINUS
      T(I,M) = (T(I,M) - TINF)/TNORM
   41 T(I,1) = (T(I,1) - TINF)/TNORM
C
      J = 1
      XINCH(1) = XW(1)
      X(1) = XINCH(1)/RADIUS
   42 CALL INTERP(KEN,XW,TW,XINCH(1),T(N,1))
      T(N,J) = (T(N,J) - TINF)/TNORM
      DO 100 J=1,KOL3
      DX = DX1
      IF(X(J).LT.DX1) DX = DX2
      IF(X(J).LT.DX2) DX = DRNOT
      X(J+1) = X(J) + DX
      XINCH(J+1) = X(J+1)*RADIUS
      CALL INTERP(KEN,XW,TW,XINCH(J+1),T(N,J+1))
      T(N,J+1) = (T(N,J+1) - TINF)/TNORM
      IF(INZ.EQ.1) GO TO 100
      IF(J.EQ.1) T(N,J) = 0.0
```

```
  100 CONTINUE
C
      L = 0
      DO 500 I=1,IUN
      K = I
      IF(I.EQ.1) GO TO 2002
      DR1 = R(K) - R(K-1)
      DR2 = R(K+1) - R(K)
      DR3 = R(K+1) - R(K-1)
      F1 = 1.0/DR3
      F2 = 2.0/(DR2*DR3)
      F3 = 2.0/(DR1*DR2)
      F4 = 2.0/(DR1*DR3)
      GO TO 2003
 2002 CONTINUE
      DR1 = R(2) - R(1)
      DR2 = R(2) - R(1)
      DR3 = 2.0*DR2
      F2 = 2.0/(DR2*DR3)
      F3 = 2.0/(DR1*DR2)
      F4 = 2.0/(DR1*DR3)
 2003 CONTINUE
      DO 500 J=2,KOL3
      L = L + 1
      AX1 = X(J) - X(J-1)
      AX2 = X(J+1) - X(J)
      AX3 = X(J+1) - X(J-1)
      H1 = 1.0/AX3
      H2 = 2.0/AX2/AX3
      H3 = 2.0/AX1/AX2
      H4 = 2.0/AX1/AX3
      IF(I.EQ.1) GO TO 2000
C
C     CALCULATE COEFF. FOR I GT 1
C
      ODD1 = F1*(DIF(K) + G(K)/R(K))
      ODD2 = RO*U(K)*H1
      A(K) = ODD1 - G(K)*F4
      B(K) = G(K)*(F3 + H3)
      C(K) = -ODD1 - G(K)*F2
      D(K) = ODD2 - G(K)*H2
  200 E(K) = -ODD2 - G(K)*H4
      GO TO 1500
C
C     CALCULATE COEFF. FOR I = 1
C
 2000 CONTINUE
      A(1) = -G(1)*2.0*F4
      B(1) = G(1)*(2.0*F3 + H3)
      C(1) = -G(1)*2.0*F2
      D(1) = RO*U(1)*H1 - G(1)*H2
      E(1) = -RO*U(1)*H1 - G(1)*H4
C
C     LOAD COEFFICIENTS INTO ABC MATRIX
C
 1500 IF(KPRIN.LT.2) GO TO 605
      WRITE(6,991) L
      WRITE(6,992) (A(K),K=1,24)
```

```
      WRITE(6,992) (B(K),K=1,24)
      WRITE(6,992) (C(K),K=1,24)
      WRITE(6,992) (D(K),K=1,24)
      WRITE(6,992) (E(K),K=1,24)
  605 CONTINUE
      IF(L.LT.KOL3) GO TO 801
      ABC(KOL1,L) = A(I)/B(I)
  801 IF(J.EQ.2) GO TO 820
      ABC(KOL2,L) = E(I)/B(I)
      GO TO 802
  820 RHS(L) = -(E(I)/B(I))*T(I,1)
  802 ABC(KOL3,L) = 1.0
      IF(J.EQ.KOL3) GO TO 840
      ABC(KOL4,L) = D(I)/B(I)
      GO TO 804
  840 RHS(L) = -(D(I)/B(I))*T(I,M)
  804 IF(L.LE.KOL2) GO TO 806
      IF(L.GT.LBF) GO TO 805
      ABC(KOL5,L) = C(I)/B(I)
      GO TO 500
  806 ABC(KOL5,L) = (C(1) + A(1))/B(1)
      GO TO 500
  805 RHS(L) = RHS(L) - C(IUN)*T(N,J)/B(IUN)
C
  500 CONTINUE
C
      IF(KPRIN.LT.1) GO TO 505
      WRITE(6,991) KOL1
      WRITE(6,992) (ABC(KOL1,L),L=1,LAST)
      WRITE(6,991) KOL2
      WRITE(6,992) (ABC(KOL2,L),L=1,LAST)
      WRITE(6,991) KOL3
      WRITE(6,992) (ABC(KOL3,L),L=1,LAST)
      WRITE(6,991) KOL4
      WRITE(6,992) (ABC(KOL4,L),L=1,LAST)
      WRITE(6,991) KOL5
      WRITE(6,992) (ABC(KOL5,L),L=1,LAST)
      WRITE(6,986)
      WRITE(6,992) (RHS(L),L=1,LAST)
      WRITE(6,986)
  505 CONTINUE
C
      CALL BNDSOL(ABC,RHS,37,18,LAST)
C
C     DIMENSIONS IN BNDSOL MUST BE CHANGED IF NO. OF MESH PTS. CHANGED
C
C     LOAD T MATRIX FROM RHS MATRIX
C
      L = 0
      DO 550 I=1,IUN
      DO 550 J=2,KOL3
      L = L + 1
  550 T(I,J) = RHS(L)
C
C     WRITE OUT TEMPERATURES IN SAME FORM AS PARABOLIC SOLUTIONS
C
      DO 551 J=1,M
      WRITE(6,989) J,XINCH(J)
```

```
      WRITE(6,992) (T(I,J),I=1,N)
      DO 552 I=1,N
  552 TT(I) = T(I,J)*TNORM + TINF
      WRITE(6,988)
      WRITE(6,987) (TT(I),I=1,N)
  551 WRITE(6,985)
C
      WRITE(6,986)
      Q1 = 1.0
      Q2 = 2.0
      STOP
    1 FORMAT(6E12.5)
    2 FORMAT(16I5)
    3 FORMAT(6E13.6)
    4 FORMAT(1X,5E15.7)
    5 FORMAT(10A6)
    6 FORMAT(13F6.1)
    7 FORMAT(2F10.5)
    8 FORMAT(8F10.4)
  985 FORMAT(3X,125(1H-))
  986 FORMAT(////)
  987 FORMAT(10X,10F11.4)
  988 FORMAT(1H0)
  989 FORMAT(1H0/10X,I5,F10.4/)
  990 FORMAT(10X,10F11.7)
  991 FORMAT(1H0/10X,I4/)
  992 FORMAT(8X,10E12.4)
  993 FORMAT(I11,F12.8,F13.7,3E14.4,F15.2)
  994 FORMAT(10X,1HI,7X,1HR,13X, 1HY,11X,2HY+,12X, 2HU+,10X,6HDIFFUS,
     1  9X,12HY(INCH*E-03)//)
  995 FORMAT(11X,43HSUMX = TOTAL OF NORMALIZED RADIAL DIVISIONS,F9.4//)
  996 FORMAT(11X,17HNO. RADIAL POS'NS,I5, 9X,16HNO. AXIAL POS'NS,I5,
     2 10X,23HEXTRA INITIAL DIVISIONS,I5/96X,I5/)
  997 FORMAT(6X,13HDRNOTI (INCH),E11.4, 5X,5HDRNOT,E12.4, 5X,
     2  10HDXI (INCH),F9.4, 7X,2HDX,E11.4, 10X,1HH,F11.3//)
  998 FORMAT(10X,10HINLET TEMP,F7.1, 5X,9HWALL TEMP,F8.1, 5X,
     1  12HFLOW (LB/HR),F7.1, 5X,9HMASS VEL.,F10.2,5X,13HVEL. (FT/SEC),
     2  F8.2//16X,2HRE,F10.1, 11X,2HPR,F8.2, 5X,12HFAN FRIC FAC,F9.5,
     3  4X,6HRADIUS,F7.1, 13X,2HRO,F18.6//)
  999 FORMAT(1H0/50X,20(1H=)//10X,15HELLIPTIC EQU'NS, 32X,A6//10X,
     1 15(1H*),25X,20(1H=)///)
      END
```

```
$IBFTC FRFAC
      SUBROUTINE FRFAC(RE,FFAC)
C
C     EVALUATE ADIABATIC K-N FRICTION FACTOR
C
      DATA EPS, FTRY / 0.00003, 0.007 /
      FLHS = 1.0/SQRT(FTRY)
 2000 FRHS = 4.0*ALOG10(RE/FLHS) - 0.40
      IF(ABS((FRHS - FLHS)/FRHS).LT.EPS) GO TO 1000
      FLHS = FRHS
      GO TO 2000
 1000 FFAC = 1.0/(FRHS*FRHS)
      RETURN
      END
```

```
$IBFTC UPLUS
      SUBROUTINE UPLUS(Y,U)
C
C     CALCULATE U+ FOR A GIVEN VALUE OF Y+
C
      COMMON  ALPHA(15), BETA(15), BEE(15)
      DIMENSION P(20)
      IF(Y.LE.0.80) GO TO 101
      P(1) = 0.0
      P(2) = 1.0
      DO 100 KK=2,14
      P(KK+1) = (Y - ALPHA(KK+1))*P(KK) - BETA(KK)*P(KK-1)
  100 U = U + BEE(KK)*P(KK)
      GO TO 102
  101 U = Y
  102 RETURN
      END
```

```
$IBFTC INTRP
      SUBROUTINE INTERP(JK,X,Y,XA,YA)
C
C     INTERPOLATES WALL TEMPERATURES IN REGION WHERE WALL TEMPERATURE
C     IS NOT CONSTANT
C
      DIMENSION X(50), Y(50)
      IF(XA.GE.X(JK)) GO TO 811
      YA=0.0
      IF((X(1)-X(2)).GT.0.0) GO TO 804
      DO 805 II=1,JK
      IF((XA-X(II)).LE.0.0) GO TO 806
  805 CONTINUE
  804 DO 809 II=1,JK
      IF((X(II)-XA).LE.0.0) GO TO 806
  809 CONTINUE
  806 IF(II.LE.3) GO TO 807
      IF(II.GE.(JK-2)) GO TO 808
      MM=II-3
      MMM=II+2
      GO TO 810
  807 MM=1
      MMM=6
      GO TO 810
  808 MM=JK-5
      MMM=JK
  810 DO 801 I=MM,MMM
      PROD=Y(I)
      DO 800 J=MM,MMM
      IF(J.EQ.I) GO TO 800
      PROD=PROD*(XA-X(J))/(X(I)-X(J))
  800 CONTINUE
  801 YA=YA+PROD
      GO TO 812
  811 YA = Y(JK)
  812 RETURN
      END
```

Z.3 Calculation of Total-Interchange Areas

This program was used to calculate the total-interchange areas, described in Section E.3, from the modified direct-interchange areas evaluated by Erkku[E1].

The program has several optional features which are controlled by information on the first 4 data cards.

The remaining data input is arranged as follows

(1) column dimensions (inches) and shape factor

(2) average gas and surface temperatures

(3) emissivity of surfaces

(4) coefficients for determination of Bevans' K values[B3]

(5) coefficients for C_w versus $p\ell$ correlation

(6) matrix of coefficients (6, 180, 4) for direct-interchange area versus kB correlations

The calculation proceeds as follows

(1) Load zone-identification matrices

(2) Calculate gas absorptivities at P_wL and $2P_wL$, (Subroutine ABCALC).

(3) Calculate absorption coefficient and weighting factor for gray-gas component of the real gas.

(4) Calculate total-interchange areas (Subroutine LOAD) for clear-gas fraction ($k = 0$).

(5) Calculate total-interchange areas (Subroutine LOAD) for gray-gas fraction.

Subroutine LOAD calculates the direct-interchange areas for each zone-pair in the system from the modified direct-interchange areas of Erkku (Subroutine FACT and Function EQN). The total

interchange area calculation involves (1) loading a matrix of coefficients (direct-interchange areas) of the reflected fluxes, R, (2) solving for the various R's by inverting the matrix (INVMAT Library Routine) and (3) evaluating the total-interchange areas by the relationships given in Section E.3

The total-interchange areas are obtained as a binary-output card deck.

Source Program - Compilation time	:	4 min. 10 sec.
Object Program - Load time	:	50 sec.
Execution time per case	:	1 min. 10 sec.

```
$IBFTC TIA
C
C    TOTAL INTERCHANGE AREAS  -  (TIA)
C
C   IAF    .....INDICATOR - IF IAF = 0, AF IS SET = 0.  (I.E. NO RADIATION
C          .....EFFECT ON THE GAS TEMPERATURE)
C    NTEST..........1 - BLACK BODY SYSTEM.  BY-PASS TOTAL INTERCHANGE
C                   AREA CALC'N
C              ......0 - GRAY SURFACES.  CALC. TOTAL INTERCHANGE AREAS
C    NPRINT.........PRINT CONTROL VARIABLE
C                   IF NPRINT = 1  PRINT OUT 'HBAL' ARRAY
C                   IF NPRINT = 0  NO PRINT OUT
C    RADIUS.........RADIUS OF COLUMN IN INCHES
C    HEIGHT.........HEIGHT OF COLUMN IN INCHES
C    RZ.............NUMBER OF RADIAL ZONES
C    NR.............NUMBER OF RADIAL ZONES
C    NW.............NUMBER OF WALL ZONES
C    NG.............NUMBER OF GAS ZONES
C    NE.............NUMBER OF END ZONES
C    NNTOT..........TOTAL NUMBER OF SURFACE ZONES - CONSIDERING ENDS AS
C                   SURFACE ZONES
C    NTOT...........TOTAL NUMBER OF ZONES IN COLUMN  (NR + NW + NG)
C    MATSIZ.........SIZE OF MATRIX CONTAINING DIRECT VIEW FACTORS
C                   I.E. (NTOT)**2,  MAXIMUM SIZE OF 82 X 82 CORRESPONDS
C                   TO A 12 WALL ZONE, 5 RADIAL ZONE SYSTEM
C    KB.............(ABSORPTION COEFF.)*(ZONE SIZE IN FEET)
C    A..............MATRIX OF COEFFICIENTS IN BINARY MODE FOR CALC'N
C                   OF DIRECT VIEW FACTORS AT VARIOUS ''KB'S''
C                   COEFFICIENTS CALC'D ASSUMING A CUBIC FIT OF DATA
C    IDEN...........MATRIX CONTAINING GEOMETRICAL IDENTIFIERS
C    IDEN2..........GEOM. IDENTIFIERS FOR WALL TO WALL SYSTEM
C    NA.............IDENTIFIER CALC'D FROM RELATIVE POSITIONING OF THE
C                   ZONES. - COMPARED WITH IDEN OR IDEN2 IN ORDER TO
C                   SELECT THE CORRECT POSITION IN THE 'A' MATRIX
C    FLXDNO.........OUTGOING FLUX DENSITY  (HOTTEL'S NOMENCLATURE)
C    AVETW..........AVERAGE WALL TEMP. IN DEG.F.
C    AVETG..........AVERAGE GAS TEMP. IN DEG.F.
C    PHI............SHAPE FACTOR FOR CYLINDER
C    PW.............PARTIAL PRESSURE OF WATER VAPOR
C                   PROBLEM ASSUMES STEAM ATMOSPHERE AT 1 ATM.  (PW =1)
C    EMGAS..........GAS EMISSIVITY
C    ABGAS..........GAS ABSORPTIVITY
C    CORECT.........CORRECTION REQUIRED SINCE PWL IS NOT ZERO  (HOTTEL)
C    EMSURF.........STORES SURFACE EMISSIVITIES
C    AA.............CONTAINS VALUES OF 4KV AND ZONE AREA
C    HBAL...........CONTAINS TOTAL OR DIRECT INTERCHANGE AREAS
C    COEF...........COEFF. FOR K VS T OVER THREE PL RANGES (BEVANS DATA)
C                   K'S FITTED OVER TWO TEMP. RANGES  800 - 1399 DEG.R.
C                   AND 1399 - 2000 DEG.R.    (QUADRATIC FIT)
C    COR600.........COEFF. FOR EMISSIVITY VS PL AT 600 DEG.R.
C    SS.............SURFACE TO SURFACE DIRECT INTERCHANGE AREAS.  'SS'
C                   MATRIX IS INVERTED TO CALC. TOTAL INTERCHANGE AREAS
C    FACT...........SUBROUTINE TO EVALUATE THE DIRECT VIEW FACTOR
C    ABCALC.........SUBROUTINE TO EVALUATE GAS ABSORPTIVITIES
C    LOAD...........SUBROUTINE TO EVALUATE TOTAL INTERCHANGE AREAS
C
      REAL KB,KL,LNGTH
C
      DIMENSION CC(13)
```

```
      DIMENSION NOS(6), GRP(69)
      DIMENSION COEF(14,3)
      COMMON  II,PI,TW,TG,CORECT,INDIC,NPRINT,NTEST,IDEN(180),IDEN2(60),
     1 AAA(82), A(6,180,4), SSEXTR(22,22), ACOEF(7,3), PWL(2), COR600(4)
     2 ,SS(22,22), NR,NW,NG,NE,NTOT,NNTOT,RZ,HEIGHT,RADIUS,AVETW,
     3 AVETG,PHI,B,KB,AF,EMSURF(22), REFL(22),EMGAS(2),ABGAS(2),
     4 AA(12), HBAL(82,82)
      EQUIVALENCE (NOS(1),NR), (NOS(2),NW), (NOS(3),NG), (NOS(4),NE),
     1 (NOS(5),NTOT), (NOS(6),NNTOT)
      EQUIVALENCE  (GRP(1),RZ), (GRP(2),HEIGHT), (GRP(3),RADIUS),
     1 (GRP(4),AVETW), (GRP(5),AVETG), (GRP(6),PHI), (GRP(7),B),
     2 (GRP(8),KB), (GRP(9),AF), (GRP(10),EMSURF(1)),(GRP(32),REFL(1)),
     3 (GRP(54),EMGAS(1)),(GRP(56),ABGAS(1)),(GRP(58),AA(1))
      DO 50 I=1,82
      DO 50 J=1,82
   50 HBAL(I,J) = 0.0
      DO 55 I=1,22
      DO 55 J=1,22
   55 SSEXTR(I,J) = 0.0
      READ(5,1) IAF
      READ(5,2) IPW, PWRDIN
      READ(5,14) CC
      READ(5,1) NPRINT, NTEST
      READ(5,6) RZ,RADIUS,HEIGHT,PHI
      READ(5,6) AVETW,AVETG
      B = RADIUS/RZ/12.0
      NR = RZ
      NW = HEIGHT/12.0/B
      NG = NR*NW
      NE = 2*NR
      NTOT = NG + NW + NR*2
      NNTOT = NE + NW
      MATSIZ = NTOT*NTOT
      PI=3.1415927
      WRITE(6,998) RZ,RADIUS,HEIGHT,PHI,B,AVETW,AVETG
      READ(5,13)(EMSURF(I),I=1,NNTOT)
      READ(5,16)((COEF(I,J),J=1,3),I=1,14)
      READ(5,15) (COR600(I),I=1,4)
      READ(5) A
      IF(NW.GT.12)  GO TO 99
      DO 35 I=1,NNTOT
   35 REFL(I) = 1.0 - EMSURF(I)
      WRITE(6,11)
      WRITE(6,9) (I,EMSURF(I),REFL(I),I=1,NNTOT)
 2000 KK=1
C
C    LOAD IDEN AND IDEN2 MATRICES
C
      DO 20 I=1,12
      DO 20 J=1,5
      NN=(I-1)*5 + J
      IDEN2(NN)=100*I + 10*J
      DO 25 K=J,5
      IDEN(KK)=I*100+10*J+K
   25 KK=KK+1
   20 CONTINUE
      INDIC = 0
      IF(IAF.EQ.0) GO TO 101
```

```
      PW = 1.0
      IF(IPW.EQ.1) PW = PWRDIN
      LNGTH = PHI*2.0*RADIUS/12.0
      PWL1 = PW*LNGTH
      TW = AVETW + 460.0
      TG = AVETG + 460.0
      PWL(1) = PWL1*(TW/TG)
      PWL(2) = 2.0*PWL(1)
      IF(TG.GE.1400.0) GO TO 1000
      DO 100 I=1,7
      DO 100 J=1,3
  100 ACOEF(I,J) = COEF(I,J)
      GO TO 1500
 1000 DO 150 I=8,14
      DO 150 J=1,3
  150 ACOEF(I-7,J) = COEF(I,J)
 1500 CALL ABCALC
      IF(INDIC.EQ.1) GO TO 2222
C
C    CALCULATE KL AND WEIGHTING FACTOR 'AF' ASSUMING ONE CLEAR AND ONE
C    GRAY GAS WITH ABSORPTION COEFFICIENT 'K'
C
      KL = ALOG(ABGAS(1)/(ABGAS(2) - ABGAS(1)))
      AF = ABGAS(1)*ABGAS(1)/(2.0*ABGAS(1) - ABGAS(2))
  101 IF(IAF.EQ.0) AF = 0.0
      KB = 0.0
      CALL LOAD
      IF(IAF.EQ.0) GO TO 102
      KB = KL/LNGTH*B
  102 CONTINUE
      WRITE(6,997) PWL(1),PWL(2),EMGAS(1),EMGAS(2),ABGAS(1),ABGAS(2),
     1 KL,AF,KB
      IF(IAF.EQ.0) GO TO 103
      CALL LOAD
  103 CONTINUE
      IF(NPRINT.EQ.0) GO TO 500
      DO 45 I=1,NTOT
      WRITE(6,4)
   45 WRITE(6,5) (HBAL(I,J),J=1,NTOT)
  500 WRITE(7) NOS
      WRITE(7) GRP
      WRITE(7,14) CC
      WRITE(7) ((HBAL(I,J),J=1,NTOT),I=1,NTOT)
      GO TO 2222
   99 WRITE(6,10) NW
 2222 WRITE(6,7)
      XX = 1.0
      XX = 1.0
      STOP
    1 FORMAT(16I5)
    2 FORMAT(I5,F10.1)
    4 FORMAT(/)
    5 FORMAT(8X,10E12.5)
    6 FORMAT(8F10.5)
    7 FORMAT(///)
    9 FORMAT(1H0,I19,2F10.4,I10,2F10.4,I10,2F10.4)
   10 FORMAT(1H-,35X,47HTOO MANY WALL ZONES ** NUMBER OF WALL ZONES IS ,
     1  I3)
```

```
   11 FORMAT(1H0,31X,35HSURFACE EMISSIVITY AND REFLECTIVITY/29X,37(1H-))
   13 FORMAT(13F6.3)
   14 FORMAT(1X,13A6)
   15 FORMAT(4E15.8)
   16 FORMAT(3E15.8)
   17 FORMAT(1H0,23HHBAL READY TO BE DUMPED//)
  998 FORMAT(1H0,17X,2HRZ,4X,6HRADIUS,4X,6HHEIGHT,7X,3HPHI,6X,1HB,8X,
     1 5HAVETW,5X,5HAVETG/10X,3F10.1,2F10.4,2F10.1//)
  997 FORMAT(1H0,18X,6HPWL(I),12X,8HEMGAS(I),12X,8HABGAS(I),12X,2HKL,
     1 8X,2HAF,8X,2HKB/10X,2F10.2,7F10.4)
      END


$IBFTC AB
      SUBROUTINE ABCALC
      COMMON  II,PI,TW,TG,CORECT,INDIC,NPRINT,NTEST,IDEN(180),IDEN2(60),
     1 AAA(82), A(6,180,4), SSEXTR(22,22), ACOEF(7,3), PWL(2), COR600(4)
     2 ,SS(22,22), NR,NW,NG,NE,NTOT,NNTOT,RZ,HEIGHT,RADIUS,AVETW,
     3 AVETG,PHI,B,KB,AF,EMSURF(22), REFL(22),EMGAS(2),ABGAS(2),
     4 AA(12), HBAL(82,82)
      DIMENSION CORRK(7)
      TT = TG
      IF(TG.LT.800.0) TT = 800.0
      DO 100 I=1,7
  100 CORRK(I) = EXP(ACOEF(I,1) + TT*(ACOEF(I,2) + TT*ACOEF(I,3)))
      DO 150 I=1,2
      KOUNT = 0
      IF(PWL(I).GE.0.01.AND.PWL(I).LE.0.10) KOUNT =1
      IF(PWL(I).GT.0.10.AND.PWL(I).LE.1.00) KOUNT =2
      IF(PWL(I).GT.1.00.AND.PWL(I).LE.20.0) KOUNT =3
      IF(PWL(I).LT.0.01. OR.PWL(I).GT.20.0) GO TO 1000
      GO TO (2000,2500,3000),KOUNT
 2000 EMGAS(I) = CORRK(1)*PWL(I) + SQRT(CORRK(2)*PWL(I))
      GO TO 150
 2500 EMGAS(I) = SQRT(CORRK(3)*PWL(I)) + CORRK(4)*ALOG10(CORRK(5)*
     1 PWL(I))
      GO TO 150
 3000 EMGAS(I) = CORRK(6)*ALOG10(CORRK(7)*PWL(I))
  150 CONTINUE
      IF(TG.GE.800.0) GO TO 4000
      DO 200 K=1,2
      PWLLN = ALOG(PWL(K))
      EM600 = EXP(COR600(1) + PWLLN*(COR600(2) + PWLLN*(COR600(3) +
     1 PWLLN*COR600(4))))
  200 EMGAS(K) = (EM600 - EMGAS(K))*(800.0 - TG)/200.0 + EMGAS(K)
 4000 DO 250 K=1,2
      CORECT = 0.13633333E 01 - 0.86801048E-01*(ALOG(PWL(K)) -
     1 0.45814537E 00)
      EMGAS(K) = EMGAS(K)*CORECT
  250 ABGAS(K) = EMGAS(K)*((TG/TW)**0.45)
      GO TO 1500
 1000 WRITE(6,99) PWL(I)
      INDIC = 1
   99 FORMAT(1H0,20X,6HPWL = ,F8.3,31H - OUTSIDE RANGE OF CORRELATION//)
 1500 RETURN
      END
```

```
$IBFTC LOAD
      SUBROUTINE LOAD
      REAL KB
      COMMON  II,PI,TW,TG,CORECT,INDIC,NPRINT,NTEST,IDEN(180),IDEN2(60),
     1 AAA(82), A(6,180,4), SSEXTR(22,22), ACOEF(7,3), PWL(2), COR600(4)
     2 ,SS(22,22), NR,NW,NG,NE,NTOT,NNTOT,RZ,HEIGHT,RADIUS,AVETW,
     3 AVETG,PHI,B,KB,AF,EMSURF(22), REFL(22),EMGAS(2),ABGAS(2),
     4 AA(12), HBAL(82,82)
      DIMENSION SF(484), ICOMP(60), STORE(60), NI(82), WORK(82),
     1  FLXDNO(82,82), HH(6724)
      EQUIVALENCE (HH(1),HBAL(1),FLXDNO(1))
      EQUIVALENCE (SS(1),SF(1))
C
C   II SELECTS THE PARTICULAR SYSTEM
C   THERE ARE SIX SYSTEMS  EW  EE  GE  GG  GW  WW
C
C   EACH OF THE SIX SECTIONS CORRESPONDING TO THE APPROPRIATE SYSTEM
C   PERFORMS THE FOLLOWING OPERATIONS ....
C   (1) ... DETERMINE AXIAL AND RADIAL SEPARATING DISTANCES LR, LA
C           IF NECESSARY
C   (2) ... CALCULATE THE IDENTIFIER 'NA' AND CHECK, IF NECESSARY, TO
C        SEE IF THE 3RD DIGIT OF 'NA' IS LESS THAN THE 2ND DIGIT.
C        IF IT IS, REVERSE THE ORDER OF THESE TWO DIGITS.  THIS IS DONE
C        BECAUSE THE ORIGINAL COEFFICIENTS ARE IDENTIFIED WITH THE LAST
C        DIGIT ALWAYS GREATER THAN OR EQUAL TO THE 2ND DIGIT.
C        I.E. 132 = 123  AND THE LATTER IS THE MANNER IN WHICH THE
C        COEFFICIENTS ARE IDENTIFIED.
C   (3) ... CALL SUBROUTINE 'FACT' TO CALCULATE THE APPROPRIATE 'FACTOR'
C   (4) ... STORE THE 'FACTOR' IN THE 'HH' ARRAY
C
      DO 50 I=1,22
      DO 50 J=1,22
   50 SS(I,J) = 0.0
      DO 100 II=1,6
      GO TO (105,110,115,120,125,130), II
C
C        EW
  105 DO 200 I=1,NR
      JI=I + NR
      DO 200 J=1,NW
      NA = J*100 + I*10 + NR
      CALL FACT(NA,EW)
      JJ = NW + 1 - J
      L = 22*(J-1) + NW + I
      LL = 22*(JJ-1) + NW + JI
      SF(L) = EW
      SF(LL) = EW
  200 CONTINUE
      GO TO 100
C
C        EE
  110 DO 250 I=1,NR
      JLOW = 1 + NR
      JUP = NR*2
      DO 250 J=JLOW,JUP
      NA = NW*100 + I*10 + J-NR
      IF((J-NR).LT.I) NA = NW*100 + (J-NR)*10 + I
      CALL FACT(NA,EE)
      L = 22*NW + (I-1)*22 + NW + J
```

```
      SF(L) = EE
  250 CONTINUE
      GO TO 100
C
C        GE
  115 IF(KB.EQ.0.0) GO TO 100
      DO 300 I=1,NR
      JI = I + NR
      DO 300 J=1,NG
      LA = (J-1)/NR + 1
      LR = J - ((J-1)/NR)*NR
      NA=LA*100 + I*10 + LR
      IF(LR.LT.I) NA=LA*100 + LR*10 + I
      CALL FACT(NA,GE)
      GE = GE*KB
      JJ = NR*(NW-LA) + LR
      L = 82*NW + (I-1)*82 + NE + NW + J
      LL = 82*NW + (JI-1)*82 + NE + NW + JJ
      HH(L) = GE
      HH(LL) = GE
  300 CONTINUE
      GO TO 100
C
C        GG
  120 IF(KB.EQ.0.0) GO TO 100
      DO 350 I=1,NR
      LRI = I - ((I-1)/NR)*NR
      DO 350 J=1,NG
      LA = IABS((J-1)/NR - (I-1)/NR + 1)
      LRJ = J - ((J-1)/NR)*NR
      NA=100*LA + 10*LRJ + LRI
      IF(LRI.LT.LRJ) NA=100*LA + 10*LRI + LRJ
      CALL FACT(NA,GG)
      GG=GG*KB*KB
      L = 82*(NE+NW) +(I-1)*82 + NE + NW + J
      HH(L)=GG
      JI = I + NR
      JJ = J + NR
      DO 360 KI=JI,NG,NR
      IF(JJ.GT.NG) GO TO 350
      L = 82*(NE+NW) +(KI-1)*82 + NE + NW + JJ
      HH(L)=GG
  360 JJ = JJ + NR
  350 CONTINUE
      GO TO 100
C
C        GW
  125 IF(KB.EQ.0.0) GO TO 100
      DO 400 I=1,NW
      DO 400 J=1,NG
      LRJ = J - ((J-1)/NR)*NR
      LA = I - (J-1)/NR
      IF(LA.LE.0) LA=IABS(LA)+2
      NA = 100*LA + LRJ*10 + NR
      IF(I.EQ.1) GO TO 3500
      DO 410 K=1,NG
      IF(NA.EQ.ICOMP(K)) GO TO 4000
  410 CONTINUE
```

```
 4000 GW = STORE(K)
      GO TO 3000
 3500 CALL FACT(NA,GW)
      GW = GW*KB
      ICOMP(J)=NA
      STORE(J) = GW
 3000 L = 82*(I-1) + NE + NW + J
      HH(L) = GW
  400 CONTINUE
      GO TO 100
C
C         WW
  130 I=1
      DO 450 J=1,NW
      NA = 100*J + 10*NR
      DO 455 K=1,60
      IF(NA.EQ.IDEN2(K)) GO TO 4500
  455 CONTINUE
 4500 WW=EQN(A(II,K,1),A(II,K,2),A(II,K,3),A(II,K,4),KB)*B*B
      KI=I
      DO 460 KJ=J,NW
      L = 22*(KI-1) + KJ
      SF(L) = WW
  460 KI=KI+1
  450 CONTINUE
  100 CONTINUE
C
C   CALCULATE THEORETICAL '4KV' AND'AREAS' FOR ALL THE COLUMN ZONES
C
      DO 700 I=1,NR
      F=I
  700 AA(I)=4.0*KB*PI*B*B*(F*F - (F-1.0)*(F-1.0))
      NRR = 2*NR
      DO 705 J=I,NRR
      F = J - NR
  705 AA(J)=PI*B*B*(F*F - (F-1.0)*(F-1.0))
      AA(J) = 2.0*PI*FLOAT(NR)*B*B
      WRITE(6,7)
      WRITE(6,2)
      WRITE(6,8) (I,AA(I),I=1,J)
      WRITE(6,7)
      KNG = NE + NW
      DO 710 KK=1,NR
      KNG = KNG + 1
      DO 710 K=KNG,NTOT,NR
  710 AAA(K) = AA(KK)
      DO 715 L=1,NW
  715 AAA(L) = AA(J)
      KNE = NW
      KKNE = NW + NE
      KJ = J - 1
      DO 720 KKK = KK,KJ
      KNE = KNE + 1
      DO 720 K=KNE,KKNE,NR
  720 AAA(K) = AA(KKK)
C
C   GENERATE ENTIRE 'SS' MATRIX
C
```

```
      DO 800 I=1,NNTOT
      DO 800 J=1,NNTOT
  800 SS(I,J) = SS(J,I)
C
C   LOAD 'SS' MATRIX INTO UPPER LEFT CORNER OF 'HBAL' MATRIX FOR
C   ANALYSIS OF BLACK SYSTEM  OR  CALC'N OF TOTAL INTERCHANGE AREAS
C
      DO 805 J=1,NNTOT
      DO 805 I=1,NNTOT
  805 HBAL(I,J) = SS(I,J)
      IF(KB.EQ.0.0) GO TO 510
C
C   HH AND HBAL ARE EQUIVALENT  THEY CONTAIN THE VARIOUS SUB-MATRICES
C   OF DIRECT INTERCHANGE AREAS FORMED FROM EACH OF THE SYSTEMS
C
      NN = NTOT - 1
      DO 500 J=1,NN
      KI=J+1
      DO 500 I=KI,NTOT
  500 HBAL(J,I)=HBAL(I,J)
      IF(NPRINT.EQ.0) GO TO 510
      DO 40 I=1,NTOT
      WRITE(6,4)
   40 WRITE(6,5) (HBAL(I,J),J=1,NTOT)
C
C   SUM EACH ROW OF THE MATRIX 'HBAL' AND COMPARE THE VALUE WITH THE
C   THEORETICAL VALUE STORED IN THE APPROPRIATE 'AAA' LOCATION
C
      IPP = 0
  510 WRITE(6,3)
      DO 550 I=1,NTOT
      TOT=0.0
      DO 555 J=1,NTOT
  555 TOT=TOT + HBAL(I,J)
      PERC=(AAA(I)-TOT)*100.0/AAA(I)
      IF(IPP.EQ.0) GO TO 551
      WRITE(6,11) I, TOT, PERC
      IPP = 0
      GO TO 550
  551 IPP = 1
      WRITE(6,9) I,TOT,PERC
  550 CONTINUE
      ATEST = NTEST
      IF(ATEST.EQ.1.0.AND.KB.EQ.0.0) GO TO 5000
      IF(NTEST.EQ.1) GO TO 5500
C
C   SUBTRACT  AREA/REFLECTIVITY  FROM DIAGONAL ELEMENTS OF 'SS' AND
C   INVERT THE 'SS' MATRIX TO PERMIT CALC'N OF TOTAL INTERCHANGE AREAS
C
      DO 815 I=1,NNTOT
  815 SS(I,I) = SS(I,I) - AAA(I)/REFL(I)
      WRITE(6,7)
      CALL INVMAT(SS,22,NNTOT,0.1E-10,IERR,NI,WORK)
      WRITE(6,1) IERR
      WRITE(6,7)
C
C   CALCULATE TOTAL INTERCHANGE AREAS
C
```

```
      IF(KB.EQ.0.0) GO TO 885
      NN = NNTOT + 1
      DO 820 K=NN,NTOT
      DO 825 I=1,NNTOT
      SUM = 0.0
      DO 830 J=1,NNTOT
  830 SUM = SUM - SS(I,J)*HBAL(K,J)
  825 STORE(I) = SUM
      DO 880 I=1,NNTOT
  880 FLXDNO(K,I) = STORE(I)
      DO 840 I=NN,NTOT
      SUMM = 0.0
      DO 845 J=1,NNTOT
  845 SUMM = SUMM + FLXDNO(K,J)*HBAL(J,I)
  840 HBAL(K,I) = HBAL(K,I) + SUMM
  820 CONTINUE
      DO 850 I=NN,NTOT
      DO 850 J=1,NNTOT
      HBAL(I,J) = FLXDNO(I,J)*AAA(J)*EMSURF(J)/REFL(J)
  850 HBAL(J,I) = HBAL(I,J)
  885 DO 870 K=1,NNTOT
      DO 855 I=1,NNTOT
      SUMS = 0.0
      DO 860 J=1,NNTOT
  860 SUMS = SUMS - SS(I,J)*HBAL(K,J)*EMSURF(K)
  855 STORE(I) = SUMS
      DO 865 I=1,NNTOT
  865 HBAL(K,I) = STORE(I)*AAA(I)*EMSURF(I)/REFL(I)
  870 CONTINUE
      IF(KB.EQ.0.0) GO TO 5000
 5500 DO 895 I=1,NTOT
      DO 895 J =1,NTOT
      HBAL(I,J) = HBAL(I,J)*AF
  895 IF(I.LE.NNTOT.AND.J.LE.NNTOT) HBAL(I,J) = HBAL(I,J) + SSEXTR(I,J)
C
  560 WRITE(6,7)
      IPP = 0
      WRITE(6,3)
      DO 565 I=1,NTOT
      TOT = 0.0
      DO 570 J=1,NTOT
  570 TOT = TOT + HBAL(I,J)
      PERC = (AAA(I)*AF - TOT)*100.0/(AAA(I)*AF)
      IF(I.LE.NNTOT) PERC = (AAA(I)*EMSURF(I) - TOT)*100.0/
     1  (AAA(I)*EMSURF(I))
      IF(IPP.EQ.0) GO TO 571
      WRITE(6,11) I,TOT,PERC
      IPP = 0
      GO TO 565
  571 IPP = 1
      WRITE(6,9) I,TOT,PERC
  565 CONTINUE
      IF(NTEST.EQ.1) GO TO 810
      GO TO 999
 5000 DIF = 1.0 - AF
      DO 890 I=1,NNTOT
      DO 890 J=1,NNTOT
  890 SSEXTR(I,J) = HBAL(I,J)*DIF
```

```
      GO TO 999
 5000 DIF = 1.0 - AF
      DO 890 I=1,NNTOT
      DO 890 J=1,NNTOT
  890 SSEXTR(I,J) = HBAL(I,J)*DIF
      GO TO 999
  810 WRITE(6,14)
  999 RETURN
    1 FORMAT(10X,I5)
    2 FORMAT(34X,23H4KV'S AND SURFACE AREAS/33X,25(1H-))
    3 FORMAT(42X,12HMATRIX CHECK/41X,14(1H-))
    4 FORMAT(/)
    5 FORMAT(8X,10E12.5)
    7 FORMAT(///)
    8 FORMAT(1H0,36X,I5,E15.6)
    9 FORMAT(20X,I5,E15.6,F8.3)
   11 FORMAT(55X,I5, E15.6, F8.3)
   14 FORMAT(1H0,40X,55HBLACK SYSTEM - TOTAL INTERCHANGE AREA ROUTINE BY
     1-PASSED/41X,55(1H-)/)
      END
```

```
$IBFTC FACT
      SUBROUTINE FACT(NNA,Z)
      COMMON  II,PI,TW,TG,CORECT,INDIC,NPRINT,NTEST,IDEN(180),IDEN2(60),
     1 AAA(82), A(6,180,4), SSEXTR(22,22), ACOEF(7,3), PWL(2), COR600(4)
     2 ,SS(22,22), NR,NW,NG,NE,NTOT,NNTOT,RZ,HEIGHT,RADIUS,AVETW,
     3 AVETG,PHI,B,KB,AF,EMSURF(22), REFL(22),EMGAS(2),ABGAS(2),
     4 AA(12), HBAL(82,82)
      DO 50 K=1,180
      IF(NNA.EQ.IDEN(K)) GO TO 1000
   50 CONTINUE
 1000 Z=EQN(A(II,K,1),A(II,K,2),A(II,K,3),A(II,K,4),KB)*B*B
      RETURN
      END
```

```
$IBFTC EQN
      FUNCTION EQN(Z1,Z2,Z3,Z4,ZKB)
      CAL=Z1 + ZKB*(Z2 + ZKB*(Z3 + ZKB*Z4))
      EQN=EXP(CAL)
      RETURN
      END
```

Z.4 Radiation Model for Prediction of Gas-Temperature Profile in Cylindrical Column - Convection Included

This program was used to solve the heat and material balance equations which were written for each gas zone in the system. The solution yields the radial and axial temperature distribution in the column. The overall heat balance is also calculated.

The definition of the program variables, the order of input data, and the calculation procedure are well documented in the program.

Source Program - Compilation time	:	3 min. 34 sec.
Object Program - Load time	:	50 sec.
Execution time per case	:	20 sec.

```
C
C  ***********************************************************************
C   HEAT BALANCE CALCULATIONS WITH BULK CONVECTION (AXIAL) AND
C   CONVECTION FROM THE WALL  (RDCNBK)
C  ***********************************************************************
C
C  DELE.......INCREMENTAL EMISSIVE POWER
C  PREV  .....TEMPORARY STORAGE FOR INCREMENTAL EMISSIVE POWER
C  FLWCOF.....HFLOW*TEMPR/EMISSIVE POWER  -  MAKES EQ'NS PSEUDO LINEAR
C        .....IN EMISSIVE POWER
C  HFLOW .....THERMAL CAPACITY - (WCP) FOR EACH ZONE
C  RESID .....RESIDUAL REMAINING AFTER HEAT BALANCE ON EACH ZONE
C  EMPOWR.....EMISSIVE POWER OF EACH ZONE
C        .....APPROACHES ZERO WITH INCREASING CONVERGENCE
C  TEMPR .....TEMPERATURE OF EACH ZONE
C  SURTEM.....TEMPERATURE OF SURFACE ZONES
C  HTCOEF.....WALL HEAT TRANSFER COEFFICIENTS
C  FLUX  .....RADIANT HEAT FLUX - BTU/HR.FT.**2
C  FLUX  .....RADIANT HEAT FLUX - BTU/HR.FT.**2 FROM SURFACE ZONES
C  TBULK .....AVERAGE GAS TEMPERATURE AT EACH AXIAL POSITION
C  EFFECT.....EFFECTIVENESS OF RADIANT HEAT TRANSFER TO GAS
C  CONDUC.....THERMAL CONDUCTIVITY OF GAS
C  BOLZMN.....BOLTZMAN NUMBER - DIMENSIONLESS ENERGY FLOW RATE (GCP)
C  RADCON.....RADIATION-CONDUCTION PARAMETER - REPRESENTS EFFECT OF
C        .....THERMAL CONDUCTION ON HEAT TRANSFER IN A RADIATION
C        .....-ABSORBING GAS
C  RATIO .....RATIO OF INLET BULK TEMPERATURE TO MAX'M TEMPERATURE
C        .....(TMAX) IN DEG.R.
C  RISRAT.....RATIO OF INLET TO OUTLET BULK TEMPERATURE
C  TEMGAS.....TEMPERATURE OF INLET GAS - NOT NECESSARILY UNIFORM
C  GASPWR.....EMISSIVE POWER OF INLET GAS STREAM
C  TMAX  .....MAX'M POSSIBLE GAS TEMPERATURE, EQUAL TO TEMPERATURE AT
C        .....MIDDLE OF COLUMN
C  ENTHAL.....TOTAL INCREASE IN GAS ENTHALPY  (BTU/HOUR)
C  NOS   .....DUMMY MATRIX CONTAINING ZONE NUMBER INFORMATION
C  GRP   .....DUMMY MATRIX CONTAINING COLUMN GEOMETRY AND GAS PROPERTY
C        .....INFORMATION FROM PRECEEDING PROGRAM
C  HBAL  .....MATRIX CONTAINING TOTAL INTERCHANGE AREAS
C  AVETG .....AVERAGE GAS TEMPERATURE AT WHICH GAS PROPERTIES WERE CALC
C  AVETW .....AVE. WALL TEMPERATURE AT WHICH GAS PROPERTIES WERE CALC.
C  FLXIN .....RADIANT ENERGY FROM WALL ZONES
C  FLXBOT.....RADIANT ENERGY OUT EXIT END ZONES
C  FLXTOP.....RADIANT ENERGY OUT INLET END ZONES
C  GASIN .....HEAT CONTAINED IN INLET GAS
C  GASOUT.....HEAT CONTAINED IN EXIT GAS
C  DATA  .....CONTAINS ALPHAMERIC DESCRIPTION OF THE SYSTEM
C  AA    .....CONTAINS AREA AND 4KV TERMS FOR ALL TYPICAL COLUMN ZONES
C  ITEST .....INDICATOR TO DETERMINE WHETHER SOLUTION HAS CONVERGED
C        .....0 - CONVERGENCE HAS BEEN ATTAINED
C        .....1 - NO CONVERGENCE - ITERATE AGAIN
C  NIT   .....NUMBER OF ITERATIONS
C  EPS   .....INCREMENTAL EMISSIVE POWER USED IN ESTIMATING ORGINAL
C        .....EMISSIVE POWER DISTRIBUTION
C  WF    .....WEIGHTING FACTOR FOR STEP SIZE PER ITERATION
C  X     .....WEIGHTING FACTOR TO DETERMINE INITIAL EMISSIVE POWER DIST
C  MM    .....INDICATOR, EQUALS 0 OR 1
C        .....0 - EXIT END ZONES EMISSIVE POWERS SET EQUAL TO EXIT GAS
C        .....ZONE EMISSIVE POWERS PLUS AN INCREMENTAL EMISSIVE POWER
C        .....EQUAL TO HALF THE DIFFERENCE BETWEEN THE LAST TWO GAS
```

```
C          .....ZONE EMISSIVE POWERS AT THE CORRESPONDING RADIAL POSITION
C          .....1 - EXIT END ZONE EMISSIVE POWER EQUALS INLET END ZONE
C   LIM1   .....NUMBER OF SURFACE TEMPERATURE DIST'NS TO BE CONSIDERED
C   LIM2   .....NUMBER OF MASS FLOW RATES TO BE CONSIDERED FOR ANY ONE
C          .....SURFACE TEMPERATURE DISTRIBUTION
C   WTFLOW.....POUNDS PER HOUR OF GAS
C   G      .....POUNDS PER HOUR SQUARE FOOT OF GAS
C   ATOT   .....COLUMN CROSS-SECTIONAL AREA
C   SNUS   .....NUSSELT NO. BASED ON TEMP. AT WALL AND ZONE ADJ. TO WALL.
C   HTCOEF.....HEAT TRANSFER COEFFICIENT BASED ON TEMP. DIFFERENCE
C          .....BETWEEN WALL AND ADJACENT ZONE - CALC'D FROM SNUS.
C          .....(PROPERTIES AT TWALL)  I.E. SNUS*TCON/DIA.
C   THDIF  .....EFFECTIVE THERMAL DIFFUSIVITY (MOL. AND TURB. TRANSPORT)
C   EFFK   .....EFFECTIVE THERMAL CONDUCTIVITY (FROM THDIF)  AT T-INLET
C   ARAFAC.....AREA FACTOR FOR CYLINDRICAL GEOMETRY
C   RO     .....RADIUS OF ZONE CENTRE
C   TTOL   .....TOLERANCE ON HEAT BALANCE SOLUTION
C
C   ********************************************************************
C
C                        ORDER OF INPUT DATA
C
C       A.  TTOL
C       1.  DATA - (ALWAYS 5 CARDS)
C       1A  IGAS       ('0' FOR AIR  '1' FOR STEAM)
C       1B  CONSTANTS FOR GAS PROPERTIES
C       2.  WF, X
C       3.  MM
C       4.  LIM1
C       5.  NOS - GRP - CC - HBAL
C       5A  FRAC  (WEIGHTING FOR VELOCITY DIST'N)
C       6.  SURTEM, TEMGAS, TMAX
C       7.  LIM2
C       7A  THDIF
C       7B  SNUS
C       8.  WTFLOW, CP, CONDUC.....WTFLOW, CP, CONDUC.....LIM2 TIMES
C       9.  SURTEM, TEMGAS, TMAX
C       10. LIM2
C       10A THDIF
C       10B SNUS
C       11. WTFLOW, CP, CONDUC.....WTFLOW, CP, CONDUC.....LIM2 TIMES
C       LAST THREE STEPS ARE REPEATED LIM1 TIMES
C
C   ********************************************************************
C
C                     CALCULATION PHILOSOPHY
C
C       END ZONES ARE CONSIDERED AS BLACK POROUS PLUGS
C       INLET END ZONE AND WALL ZONE TEMPERATURE ARE FIXED
C       ENTERING GAS TEMPERATURE IS FIXED
C       TEMPERATURE AT CENTRE WALL ZONE IS USED AS TMAX
C       GAS ZONE EMISSIVE POWER GRADIENT ASSUMED LINEAR
C       AFTER ALL INITIAL CONDITIONS ARE CALCULATED ITERATIVE SOLUTION
C       BEGINS
C       ALL EMISSIVE POWERS ASSUMED KNOWN EXCEPT ONE
C       SOLVE FOR THIS TEMPERATURE FROM THE HEAT BALANCE ON THE ZONE
C       IN QUESTION
C       PROCEED TO NEXT ZONE AND USE THE NEW CALCULATED TEMPERATURES OF
```

```
C       ALL PRECEEDING ZONES IN THE HEAT BALANCE
C       AFTER ALL ZONES HAVE BEEN TRAVERSED, IF CONVERGENCE HAS NOT BEEN
C       ATTAINED FOR ALL ZONES BEGIN SOLUTION AGAIN WITH THE NEW
C       TEMPERATURE DISTRIBUTION
C       AFTER CONVERGENCE CALCULATE HEAT FLUX DIST'NS AND OVERALL HEAT
C       BALANCE FOR THE SYSTEM
C
C***********************************************************************
C
      CALL TIME(NOWA)
C***********************************************************************
      DIMENSION FRAC(5)
      DIMENSION THDIF(5), EFFK(5), ARAFAC(5), RO(5), SNUS(12)
      DIMENSION HTCOEF(12)
      DIMENSION DELE(82), PREV(82), HFLOW(82), RESID(82)
      DIMENSION BB(82,82), GRP(69), NOS(6), EMSURF(22), REFL(22),
     1  EMGAS(2), ABGAS(2), AA(12), HBAL(82,82), SURTEM(82), TEMPR(82),
     2 EMPOWR(82), NI(82), WORK(82), AAA(82), FLUX(22), DATA(65)
      DIMENSION CC(13), FLWCOF(82), TBULK(12), TEMGAS(5), GASPWR(5)
      EQUIVALENCE (HBAL(1),BB(1)), (SURTEM(1),TEMPR(1))
      EQUIVALENCE (NOS(1),NR), (NOS(2),NW), (NOS(3),NG), (NOS(4),NE),
     1 (NOS(5),NTOT), (NOS(6),NNTOT)
      EQUIVALENCE  (GRP(1),RZ), (GRP(2),HEIGHT), (GRP(3),RADIUS),
     1 (GRP(4),AVETW), (GRP(5),AVETG), (GRP(6),PHI), (GRP(7),B),
     2 (GRP(8),KB), (GRP(9),AF), (GRP(10),EMSURF(1)),(GRP(32),REFL(1)),
     3 (GRP(54),EMGAS(1)),(GRP(56),ABGAS(1)),(GRP(58),AA(1))
C***********************************************************************
      REAL KB, KD, LD
      ITIME = 0
      INDIC = 0
      DATA STFBLZ, PI / 0.1713E-08, 3.14159 /
      DATA SECHR,  CONVER / 3600.0, 0.0672/
      DO 19 I=1,12
   19 HTCOEF(I) = 0.0
      DO 5 I=1,82
      DELE(I) = 0.0
      RESID(I) = 0.0
      NI(I) = 0
      WORK(I) = 0.0
      DO 5 J=1,82
    5 HBAL(I,J) = 0.0
      DO 10 I=1,22
      EMSURF(I) = 0.0
      REFL(I) = 0.0
   10 FLUX(I) = 0.0
C***********************************************************************
      READ(5,2) TTOL
      READ(5,1) (DATA(I),I=1,65)
      WRITE(6,990) (DATA(I),I=1,65)
      READ(5,3) IGAS
      READ(5,965) VISCCT,VISCA,VISCB,VISCC,VISCD,VISCE
      READ(5,965) TCONCT,TCONA,TCONB,TCONC
      READ(5,965) CPCT,CPA,CPB,CPC,CPD
      READ(5,965) DENSCT,DENSA,DENSB,DENSC,DENSD
      READ(5,2) WF, X
      READ(5,3) MM
      READ(5,3) LIM1
      READ(5) NOS
```

```
      READ(5) GRP
      READ(5,4) CC
      READ(5) ((HBAL(I,J),J=1,NTOT),I=1,NTOT)
      READ(5,2) (FRAC(I),I=1,NR)
C     ***************************************************************
C
C      IF AVETG IS LESS THAN 0.1 - A ''GRAY'' RATHER THAN A ''REAL''
C      GAS IS BEING USED
C
      IF(AVETG.LT.0.1) GO TO 1000
      WRITE(6,998)
      WRITE(6,997) RZ,RADIUS,HEIGHT,PHI,B,AVETW,AVETG
      WRITE(6,996) EMGAS(1),EMGAS(2),ABGAS(1),ABGAS(2),AF,KB
      GO TO 1500
 1000 WRITE(6,995)
      WRITE(6,994) RZ,RADIUS,HEIGHT,KB,B
 1500 WRITE(6,982)
      DO 26 I=1,NNTOT
   26 WRITE(6,981) I,EMSURF(I)
      WRITE(6,992)
      DO 15 I=1,NTOT,4
      TOT = 0.0
      DO 20 J=1,NTOT
   20 TOT = TOT + HBAL(I,J)
   15 WRITE(6,999) I,TOT
      IF(AVETG.LT.0.1) AF = 1.0
      ATOT = PI*RADIUS*RADIUS/144.0
      KD = KB*RADIUS/(6.0*B)
      LD = HEIGHT/(2.0*RADIUS)
      VISC(Z) = VISCCT + Z*(VISCA + Z*(VISCB + Z*(VISCC + Z*(VISCD +
     1  Z*VISCE))))
      TCON(Z) = TCONCT + Z*(TCONA + Z*(TCONB + Z*TCONC))
      CP(Z) = CPCT + Z*(CPA + Z*(CPB + Z*(CPC + Z*CPD)))
      DENS(Z) = DENSCT + Z*(DENSA + Z*(DENSB + Z*(DENSC + Z*DENSD)))
      DO 21 I=1,NR
      F = I
   21 RO(I) = B*(F - 0.5)
C     ***************************************************************
C
C      MAIN LOOP FOR DIFFERENT SURFACE TEMPERATURES
C
      DO 1111 KEN1=1,LIM1
      DO 140 I=1,82
      SURTEM(I) = 0.0
      EMPOWR(I) = 0.0
  140 CONTINUE
      KNOWN = NW + NR
C
C      READ WALL AND INLET END ZONE TEMPERATURES IN DEG.F.
C
      READ(5,2) (SURTEM(I),I=1,KNOWN)
      READ(5,2) (TEMGAS(I),I=1,NR), TMAX
      READ(5,3) LIM2
C     ***************************************************************
C
C      MAIN LOOP FOR DIFFERENT FLOW CONDITIONS
C
      DO 2222 KEN2=1,LIM2
      KNOWN = NW + NR
```

```
      LNR = NR - 1
      READ(5,2) (THDIF(I),I=1,LNR)
      TTT = TEMGAS(1) + 460.0
      DO 22 I=1,LNR
      EFFK(I) = THDIF(I)*DENS(TTT)*CP(TTT)
   22 ARAFAC(I) = 2.0*PI*B*EFFK(I)/ALOG(RO(I+1)/RO(I))
      READ(5,961) (SNUS(I),I=1,NW)
C
C      CHANGE INPUT TEMPERATURES TO DEG.R. AND CALCULATE EMISSIVE POWER
C
      DO 8 I=1,NR
      TEMGAS(I) = TEMGAS(I) + 460.0
    8 GASPWR(I) = STFBLZ*TEMGAS(I)**4
      DO 13 I=1,KNOWN
      SURTEM(I) = SURTEM(I) + 460.0
   13 EMPOWR(I) = STFBLZ*SURTEM(I)**4
      DO 24 I=1,NW
      TTT = SURTEM(I)
   24 HTCOEF(I) = SNUS(I)*TCON(TTT)*6.0/RADIUS
      EPS = X*GASPWR(1)
C
C      SET FIRST GAS ZONES = INLET GAS EMISSIVE POWER + EPS
C
      DO 11 I=1,NR
      II = I + NNTOT
   11 EMPOWR(II) = GASPWR(I) + EPS
C
C      EACH REMAINING GAS ZONE IS SET EQUAL TO PRECEEDING ZONE IN
C      CORRESPONDING RADIAL POSITION + EPS
C
      IL = NNTOT + NR + 1
      DO 12 I=IL,NTOT
      IIN = I - NR
   12 EMPOWR(I) = EMPOWR(IIN) + EPS
C
C      DETERMINE EXIT END ZONES - CALCULATION DEPENDS ON VALUE OF 'MM'
C
      IL = NW + NR + 1
      ILL = NW + NE
      DO 14 I=IL,ILL
      IIN = I + NG
      INX = I - NR
      EMPOWR(I) = EMPOWR(IIN) + EPS/2.0
   14 IF(MM.EQ.1) EMPOWR(I) = EMPOWR(INX)
C
C      CALCULATE ALL ZONE TEMPERATURES IN DEG.R.
C
      DO 106 I=1,NTOT
  106 TEMPR(I) = (EMPOWR(I)/STFBLZ)**0.25
C  ***************************************************************************
      KNOWN = NNTOT
      NIT = 0
      BULKIN = 0.0
      FLXIN = 0.0
      FLXOUT = 0.0
      GASIN = 0.0
      GASOUT = 0.0
      FLXTOP = 0.0
```

```
      FLXBOT = 0.0
      DO 6 I=1,82
      PREV(I) = 0.0
      HFLOW(I) = 0.0
      FLWCOF(I) = 0.0
      AAA(I) = 0.0
    6 CONTINUE
      DO 7 I=1,12
    7 TBULK(I) = 0.0
      DO 18 I=1,22
   18 FLUX(I) = 0.0
C  ***********************************************************************
C
C
C       READ GAS FLOW IN LB./HR.
C
      READ(5,2) WTFLOW,CP
      G = WTFLOW/ATOT
      WRITE(6,969) WTFLOW,G,ATOT
C  ***********************************************************************
C
C       ALLOCATE 'AREA' OR '4KV' VALUES FOR EACH ZONE FROM THE APPROP.
C       VALUES STORED IN 'AA'
C
C       ALLOCATE '4KV' FOR ALL GAS ZONES
C
      KNG = NE + NW
      DO 710 KK=1,NR
      KNG = KNG + 1
      DO 710 K=KNG,NTOT,NR
  710 AAA(K) = AA(KK)
C
C       ALLOCATE 'AREA' FOR EACH WALL ZONE
C
      DO 715 L=1,NW
  715 AAA(L) = AA(NE+1)
C
C       ALLOCATE 'AREA' FOR EACH END ZONE AND CALCULATE INITIAL RADIAL
C       THERMAL CAPACITY DISTRIBUTION.
C
      KNE = NW
      KKNE = NW + NE
      J = 0
      DO 720 KKK=KK,NE
      KNE = KNE + 1
      J = J + 1
      DO 720 K=KNE,KKNE,NR
      HFLOW(K) = G*AA(KKK)*CP*FRAC(J)
  720 AAA(K) = AA(KKK)
C
C       ALLOCATE INITIAL THERMAL CAPACITIES FOR EACH GAS ZONE
C
      DO 725 I=1,NR
      IL = NNTOT + I
      II = NW + I
      DO 725 J=IL,NTOT,NR
  725 HFLOW(J) = HFLOW(II)
C  ***********************************************************************
C
```

```
C       SUBTRACT '4KVA' FROM DIAGONAL GAS ELEMENTS
C
        INDIC = INDIC + 1
        IF(INDIC.GT.1) GO TO 36
        IL = NNTOT + 1
        DO 35 I=IL,NTOT
     35 HBAL(I,I) = HBAL(I,I) - AAA(I)*AF
C
C       CALCULATE FLOW COEFFICIENTS FOR INLET END ZONES BUT NOTE THAT
C       CALC'N IS BASED ON INLET GAS RATHER THAN END ZONE TEMPERATURE
C
     36 IL = NW + 1
        ILL = NW + NR
        II = 1
        DO 80 I=IL,ILL
        FLWCOF(I) = HFLOW(I)*TEMGAS(II)/GASPWR(II)
     80 II = II + 1
C
C       CALCULATE FLOW COEFFICIENTS FOR EACH GAS ZONE
C
        IL = NNTOT + 1
        DO 81 I=IL,NTOT
     81 FLWCOF(I) = HFLOW(I)*TEMPR(I)/EMPOWR(I)
C  ***************************************************************************
C
C       +++++       BEGIN ITERATIVE CONVERGENCE LOOP        +++++
C
C  ***************************************************************************
   4500 IF(NIT.EQ.1.OR.NIT.EQ.25.OR.NIT.EQ.50.OR.NIT.EQ.75)CALL TIME(NOWB)
        ITEST = 0
        IL = 1 + KNOWN
        NN = NNTOT + NR
C
C       KK.....COUNTER TO PICK UP CORRECT VALUE OF HTCOEF.  WILL VARY FROM
C          1 TO NW.
C       KGP.....COUNTER TO INDICATE WHENEVER GAS ZONE IN QUESTION IS AN
C          INTEGRAL MULTIPLE OF NR.  WHEN THIS OCCURS THE GAS ZONE IN
C          QUESTION IS ADJACENT TO A WALL ZONE.
C          IF GAS ZONE IS ADJACENT TO A WALL ZONE - ADD H*A*TWALL TO THE
C          VALUE OF THE RESIDUAL.   ALSO SUBTRACT H*A*TGAS/EMPOWR(GAS)
C          FROM THE COEFFICIENT OF THE GAS EMISSSVE POWER OF THE ZONE
C          IN QUESTION.
C       KEV.....COUNTER TO PICK UP CORRECT VALUE OF ARAFAC
C          WHEN KEV = 1, CENTRE ZONE - NO HEAT OUT
C          WHEN KEV = NR, WALL ZONE - USE HTCOEF FOR CONVECTION INTO ZONE
C          AND ARAFAC FOR CONDUCTION OUT OF ZONE.
C
        KEV = 0
        KK = 0
        KGP = 0
C
C       CALCULATION LOOP FOR EACH UNKNOWN EMISSIVE POWER
C
C  ***************************************************************************
C
        DO 30 I=IL,NTOT
        KEV = KEV + 1
        KGP = KGP + 1
```

```
C
C       SUM ALL RADIATION TERMS EXCEPT FOR THE ZONE IN QUESTION
C
        DO 31 J=1,NTOT
        IF(I.EQ.J) GO TO 31
        RESID(I) = RESID(I) + HBAL(I,J)*EMPOWR(J)
   31 CONTINUE
C
C       IF I.LE.NN FIRST GAS ZONES ARE BEING CONSIDERED
C       IF CONSIDERING FIRST GAS ZONES - FLOW TERMS = INLET END FLOWS
C       FOR REMAINING GAS ZONES, FLOWS ARE THOSE OF ADJACENT GAS ZONES
C
        IF(I.LE.NN) GO TO 5500
        IIN = I - NR
        RESID(I) = RESID(I) + FLWCOF(IIN)*EMPOWR(IIN)
        GO TO 6000
 5500   INX = I - 2*NR
        RESID(I) = RESID(I) + FLWCOF(INX)*EMPOWR(INX)
 6000   IF((NR - KGP).NE.0) GO TO 32
        KK = KK + 1
        KEV = 0
        KGP = 0
        RESID(I) = RESID(I) + HTCOEF(KK)*AAA(KK)*TEMPR(KK) +
       1 ARAFAC(NR-1)*TEMPR(I-1)
        COND = ARAFAC(NR-1)*TEMPR(I)/EMPOWR(I)
        CONVEC = HTCOEF(KK)*AAA(KK)*TEMPR(I)/EMPOWR(I)
        GO TO 37
   32   IF(KEV.EQ.1) GO TO 34
        RESID(I) = RESID(I) + ARAFAC(KEV)*TEMPR(I+1) + ARAFAC(KEV-1)*
       1 TEMPR(I-1)
        CONVEC = 0.0
        COND = (ARAFAC(KEV) + ARAFAC(KEV-1))*TEMPR(I)/EMPOWR(I)
        GO TO 37
   34   RESID(I) = RESID(I) + ARAFAC(KEV)*TEMPR(I+1)
        CONVEC = 0.0
        COND = ARAFAC(KEV)*TEMPR(I)/EMPOWR(I)
C
C       DIVIDE RESIDUAL BY COEFFICIENTS OF EMISSIVE POWER OF ZONE IN
C       QUESTION TO DETERMINE NEW EMISSIVE POWER
C
   37   PREV(I) = -RESID(I)/(HBAL(I,I) - FLWCOF(I) - COND - CONVEC)
   33   DELE(I) = PREV(I) - EMPOWR(I)
        TEST = ABS(DELE(I)/EMPOWR(I))
C
C       TEST TO SEE IF CHANGE IN EMISSIVE POWER IS LESS THAN A PRESET
C       TOLERANCE
C
        IF(TEST.GE.TTOL) ITEST = 1
C
C       DO NOT ALLOW NEW EMISSVE POWER TO BECOME NEGATIVE
C
 2500   IF((EMPOWR(I) + DELE(I)*WF).GT.0.0) GO TO 3000
        DELE(I) = DELE(I)/2.0
        GO TO 2500
C
C       MAGNITUDE OF CALCULATED CHANGE CAN BE MODIFIED BY 'WF'
C
 3000   EMPOWR(I) = EMPOWR(I) + DELE(I)*WF
```

```
      TEMPR(I) = (EMPOWR(I)/STFBLZ)**0.25
      FLWCOF(I) = HFLOW(I)*TEMPR(I)/EMPOWR(I)
   30 CONTINUE
C  ***************************************************************************
C
C       CALCULATE NEW EXIT END ZONE TEMPERATURE IF 'MM' = 0
C
      IF(MM.EQ.1) GO TO 17
      IL = NW + NR + 1
      ILL = NW + NE
      DO 16 I=IL,ILL
      IIN = I + NG
      IINN = IIN - NR
      EPS = (EMPOWR(IIN) - EMPOWR(IINN))/2.0
      EMPOWR(I) = EMPOWR(IIN) + EPS
   16 TEMPR(I) = (EMPOWR(I)/STFBLZ)**0.25
   17 IL = NNTOT + 1
      NIT = NIT + 1
      CALL TIME(NOWC)
C
C       TIME CHECK ON PROGRESS OF SOLUTION
C  ***************************************************************************
      IF(NIT.EQ.2.OR.NIT.EQ.26.OR.NIT.EQ.51.OR.NIT.EQ.76) GO TO 4001
      GO TO 4000
 4001 TIM = FLOAT(NOWB - NOWC)/60.0
      TIM1 = FLOAT(NOWB)/60.0
      TIM2 = FLOAT(NOWA - NOWC)/60.0
      WRITE(6,978) NIT,TIM,TIM1,TIM2
 4000 IF(NOWC.LE.900) ITIME = 1
      IF(ITIME.EQ.1) GO TO 5000
C  ***************************************************************************
      DO 105 I=1,82
      RESID(I) = 0.0
      DELE(I) = 0.0
  105 CONTINUE
C
C       CHECK FOR CONVERGENCE
C
      IF(ITEST.EQ.1) GO TO 4500
      WRITE(6,976) NIT
C
C       CONVERT TEMPERATURES TO DEG.F.
C
      DO 120 I=1,NTOT
  120 TEMPR(I) = TEMPR(I) - 460.0
      DO 121 I=1,NR
  121 TEMGAS(I) = TEMGAS(I) - 460.0
C
C       EVALUATE BULK TEMPERATURE AT EACH AXIAL LEVEL AND CALCULATE
C       DIMENSIONLESS PARAMETERS BASED ON INITIAL CONDITIONS
C  ***************************************************************************
      II = 0
      DO 130 I=IL,NTOT,NR
      II = II + 1
      DO 135 J=1,NR
      INX = I + J - 1
      INXX = NW + J
  135 TBULK(II) = TBULK(II) + TEMPR(INX)*AAA(INXX)
```

```
  130 TBULK(II) = TBULK(II)/ATOT
      DO 131 I=1,NR
      INXX = NW + I
  131 BULKIN = BULKIN + TEMGAS(I)*AAA(INXX)
      BULKIN = BULKIN/ATOT
      TT = BULKIN + 460.0
      IF(IGAS.GE.1) TT = TT/1.8
      RE = (RADIUS/6.0)*G/(SECHR*VISC(TT))
      IF(IGAS.GE.1) RE = RE/CONVER
      BOLZMN = G*CP/(STFBLZ*(TMAX + 460.0)**3)
      RADCON = CONDUC/((RADIUS/6.0)*STFBLZ*(TMAX + 460.0)**3)
      EFFECT = (TBULK(NW) - BULKIN)/(TMAX - BULKIN)
      RATIO = (BULKIN + 460.0)/(TMAX + 460.0)
      RISRAT = (BULKIN + 460.0)/(TBULK(NW) + 460.0)
      WRITE(6,968)
      WRITE(6,967) BULKIN, TBULK(NW), RATIO, RISRAT
      WRITE(6,966) BOLZMN, RADCON, EFFECT, KD, KB, LD
      WRITE(6,964) RE
      WRITE(6,960) (I,THDIF(I),EFFK(I),I=1,LNR)
C
C       WRITE GAS TEMPERATURES AND EMISSIVE POWERS
C   ***************************************************************************
 5000 WRITE(6,993)
      DO 50 I=1,NW
      L = NR*I + NNTOT
      K = L - NR + 1
      GO TO (50,55,60,65,70), NR
   55 WRITE(6,987) I, (TEMPR(J),J=K,L), (EMPOWR(J),J=K,L), I
      GO TO 50
   60 WRITE(6,988) I, (TEMPR(J),J=K,L), (EMPOWR(J),J=K,L), I
      GO TO 50
   65 WRITE(6,989) I, (TEMPR(J),J=K,L), (EMPOWR(J),J=K,L), I
      GO TO 50
   70 WRITE(6,991) I, (TEMPR(J),J=K,L), (EMPOWR(J),J=K,L), I
   50 CONTINUE
C   ***************************************************************************
C
C       WRITE THERMAL CAPACITIES AND BULK TEMPERATURES
C   ***************************************************************************
      WRITE(6,975)
      DO 51 I=1,NW
      L = NR*I + NNTOT
      K = L - NR + 1
      GO TO (51,53,51,52,51), NR
   52 WRITE(6,974) I,(HFLOW(J),J=K,L),TBULK(I),I
      GO TO 51
   53 WRITE(6,973) I,(HFLOW(J),J=K,L),TBULK(I),I
   51 CONTINUE
C   ***************************************************************************
C
C       ASSUMES ALL RADIANT HEAT INTO SYSTEM ORIGINATES AT WALLS AND
C       ALL RADIANT HEAT OUT IS THROUGH END ZONES
C   ***************************************************************************
      DO 75 I=1,NNTOT
      DO 76 J=1,NTOT
   76 FLUX(I) = FLUX(I) + HBAL(I,J)*(EMPOWR(I) - EMPOWR(J))
      IF(FLUX(I).LE.0.0) GO TO 500
      IF(I.GT.NW) GO TO 501
```

```
      IK = I*NR + NNTOT
      FLUX(I) = FLUX(I) + HTCOEF(I)*AAA(I)*(TEMPR(I) - TEMPR(IK))
  501 FLXIN = FLXIN + FLUX(I)
      GO TO 75
  500 IF(I.LE.(NW + NR)) GO TO 74
      FLXBOT = FLXBOT + FLUX(I)
      GO TO 75
   74 FLXTOP = FLXTOP + FLUX(I)
   75 FLUX(I) = FLUX(I)/AAA(I)
      DO 110 I=1,NR
      II = NW + I
  110 GASIN = GASIN + HFLOW(II)*TEMGAS(I)
      IL = NTOT - NR + 1
      ILL = NTOT
      DO 115 I=IL,ILL
  115 GASOUT = GASOUT - HFLOW(I)*TEMPR(I)
C     ***************************************************************
C
C
C        WRITE SURFACE FLUXES,TEMP.S, EMISSIVE POWERS, AND EMISSIVITIES
C     ***************************************************************
      WRITE(6,985)
      WRITE(6,984) (I,FLUX(I),TEMPR(I),EMPOWR(I),EMSURF(I),
     1  HTCOEF(I),I=1,NW)
      WRITE(6,983)
      IL = NW + 1
      WRITE(6,963) (I,FLUX(I),TEMPR(I),EMPOWR(I),EMSURF(I),I=IL,NNTOT)
C     ***************************************************************
C
C
C        WRITE DISTRIBUTION OF HEAT FLOWS
C     ***************************************************************
      WRITE(6,979)
      WRITE(6,971) FLXIN,GASIN,FLXTOP,FLXBOT,GASOUT
      FLXIN = FLXIN + GASIN
      FLXOUT = FLXBOT + FLXTOP + GASOUT
      ENTHAL = -(GASIN + GASOUT)
      DIFF = FLXIN + FLXOUT
      PCENT = DIFF*100.0/FLXIN
C     ***************************************************************
C
C
C        WRITE TOTAL HEAT BALANCE AND ERROR
C
      WRITE(6,970) ENTHAL, FLXIN, FLXOUT, DIFF, PCENT
      IF(ITIME.EQ.1) GO TO 1200
 2222 CONTINUE
 1111 CONTINUE
C     ***************************************************************
      GO TO 1234
 1200 WRITE(6,977) NIT
 1234 WRITE(6,986)
      X = 1.0
      X = 1.0
      STOP
C     ***************************************************************
    1 FORMAT(13A6)
    2 FORMAT(8F10.1)
    3 FORMAT(16I5)
    4 FORMAT(1X,13A6)
  960 FORMAT(1H0,34X,I5,F10.2,F12.4)
```

```
961 FORMAT(13F6.1)
962 FORMAT(I5,F10.1)
963 FORMAT(1X,30X,I2,F15.1,F11.1,F15.1,F11.4)
964 FORMAT(1H0/35X,29HINLET BULK REYNOLDS NUMBER IS,F9.0/35X,29(1H*)//)
965 FORMAT(6E13.6)
966 FORMAT(/10X,15HBOLTZMAN NUMBER,10X, 22HRAD'N-COND'N PARAMETER,
   1 10X,20HRADIATION EFFICIENCY,10X, 2HKD,7X,2HKB,7X,3HL/D/10X,
   2 15(1H-),10X,22(1H-),10X,20(1H-),10X,2H--,7X,2H--,7X,3H---/10X,
   3 F10.2,F28.2,F31.3,F21.2,F9.2,F10.2)
967 FORMAT(/50X,12HTEMPERATURES,7X,39H(IN DEG.F., ALL RATIOS BASED ON
   1DEG.R.)/49X,14(1H-)//22X,10HINLET BULK,10X,11HOUTLET BULK,10X,
   2 17HRATIO INLET/MAX'M,10X,18HRATIO INLET/OUTLET/22X,10(1H-),10X,
   3 11(1H-),10X,17(1H-),10X,18(1H-)/22X,F8.1,F21.1,F23.4,F27.4/)
968 FORMAT(1H0//8X,120(1H=)///25X,66HTHE FOLLOWING PARAMETERS HAVE BEE
   1N CALCULATED FOR THESE CONDITIONS/25X,66(1H-)//)
969 FORMAT(1H1//8X,120(1H=)//10X,12HMASS FLOW IS, F7.1, 8H LB./HR.,
   1 10X,12HMASS FLUX IS, F7.1, 14H LB./HR.FT.**2, 10X,
   2 23HCROSS-SECTIONAL AREA IS, F6.2, 7H FT.**2//8X,120(1H=)//)
970 FORMAT(1H0/15X,21HGAS ENTHALPY INCREASE,10X,13HTOTAL HEAT IN,10X,
   1 14HTOTAL HEAT OUT,10X,10HDIFFERENCE,6X,7HPERCENT/14X,23(1H-),
   2 8X,15(1H-),8X,16(1H-),8X,12(1H-),4X,9(1H-)/15X,F14.1,F26.1,
   4 F23.1,F22.1,F14.2////)
971 FORMAT(10X,15HHEAT FROM WALLS,5X,18HINLET GAS ENTHALPY,9X,
   1 12HHEAT OUT TOP,5X,15HHEAT OUT BOTTOM,5X,19HOUTLET GAS ENTHALPY/
   2 9X,17(1H-),3X,20(1H-), 7X,14(1H-), 3X,17(1H-),3X,21(1H-)/
   3 10X,F11.1,F21.1,F25.1,F17.1,F24.1/)
972 FORMAT(6(5X,10E12.5/),5X,8E12.5/)
973 FORMAT(33X,I2,2F15.1,F36.1,I9)
974 FORMAT(18X,I2,4F15.2,F21.1,I9)
975 FORMAT(1H0//45X,16HTHERMAL CAPACITY,28X,16HBULK TEMPERATURE/
   1 44X,18(1H=),26X,18(1H=)//)
976 FORMAT(1H0,20X,23HNUMBER OF ITERATIONS = ,I5//)
977 FORMAT(1H0,20X,28HSOLUTION NOT CONVERGED AFTER,I4,11H ITERATIONS/
   1 19X,45(1H*))
978 FORMAT(1H0,2X,5HAFTER,I4, 34H ITERATIONS, TIME PER ITERATION IS,
   1 F5.2,8H SECONDS, 6X,14HSTART TIME WAS, F8.2, 8H SECONDS, 6X,
   2 15HELAPSED TIME IS, F8.2, 8H SECONDS)
979 FORMAT(///57X,12HHEAT BALANCE/56X,14(1H=)//)
980 FORMAT(1H0,10X,I3/)
981 FORMAT(1H0,36X,I5,F15.5)
982 FORMAT(1H0,39X,18HSURFACE EMISSIVITY/39X,20(1H-))
983 FORMAT(////61X,4HENDS/60X,6(1H=)//40X,4HFLUX,10X,5HTEMP.,5X,
   1 11HEMIS. POWER,3X,10HEMISSIVITY/39X,6(1H-),8X,7(1H-),3X,13(1H-),
   2 2X,11(1H-)/)
984 FORMAT(1X,30X,I2,F15.1,F11.1,F15.1,F11.4,F12.1)
985 FORMAT(1H1,60X,4HWALL/60X,6(1H=)//40X,4HFLUX,10X,5HTEMP.,5X,
   1 11HEMIS. POWER,3X,10HEMISSIVITY,3X,10HH.T. COEF./39X,6(1H-),
   2 8X,7(1H-),3X,13(1H-),1X,12(1H-),1X,12(1H-)/)
986 FORMAT(////)
987 FORMAT(1X,I2,2F15.1,61X,2F15.1,I4)
988 FORMAT(1X,I2,3F15.1,31X,3F15.1,I4)
989 FORMAT(1X,I2,4F13.1,11X,4F13.1,I5)
990 FORMAT(///  20X,84(1H=)/5(20X,14A6//)/20X,84(1H=))
991 FORMAT(1X,I2,5F15.1, 3X,5F15.1,I3)
992 FORMAT(1H0,42X,12HMATRIX CHECK/42X,14(1H-)/)
993 FORMAT(1H1,14X,28HGAS TEMPERATURE DISTRIBUTION,39X,
   1 31HGAS EMISSIVE POWER DISTRIBUTION/12X,34(1H=),33X,36(1H=)//
   2 38X,48H( CENTRE TO WALL PROCEEDING FROM LEFT TO RIGHT )//)
```

```
  994 FORMAT(1H0,38X,2HRZ,4X,6HRADIUS,4X,6HHEIGHT,7X,2HKB,8X, 1HB/37X,
     1 45(1H-)/31X,3F10.1,2F10.4//)
  995 FORMAT(1H0,19X,84(1H=)/20X,84HTOTAL INTERCHANGE AREAS CALCULATED F
     1OR A ''GRAY'' GAS UNDER THE FOLLOWING CONDITIONS/20X,84(1H=)/)
  996 FORMAT(1H0,33X,8HEMGAS(I),12X,8HABGAS(I),10X,2HAF,8X,2HKB/32X,
     1 54(1H-)/25X,6F10.4//)
  997 FORMAT(1H0,29X,2HRZ,4X,6HRADIUS,4X,6HHEIGHT,7X,3HPHI,6X,1HB,8X,
     1 5HAVETW,5X,5HAVETG/29X,64(1H-)/22X,3F10.1,2F10.4,2F10.1/)
  998 FORMAT(1H0,19X,84(1H=)/20X,84HTOTAL INTERCHANGE AREAS CALCULATED F
     1OR A ''REAL'' GAS UNDER THE FOLLOWING CONDITIONS/20X,84(1H=)/)
  999 FORMAT(1H0,36X,I5,E16.7)
C  ***********************************************************************
      END
$IBLDR TIMER   01/19/65
$CDICT TIMER
*5 X(X 7   8*)X 0 *)P0
$TEXT  TIMER
*T (P(*7V*         74''4 D '7 '9M874 5-
$DKEND TIMER
$IBLDR TIMER   01/19/65
$CDICT TIMER
*5 X(X 7   8*)X 0 *)P0
$TEXT  TIMER
*T (P(*7V*         74''4 D '7 '9M874 5-
$DKEND TIMER
```